Characterising mechanisms of aberrant mutant androgen receptor signalling in advanced prostate cancer

Wenrui Guo

120444241

Supervisors:
Dr. Luke Gaughan
Prof. Craig Robson

Surgical Oncology Research Group
Northern Institute for Cancer Research, Newcastle.
September 2018

Abstract

Prostate cancer (PC) is the most commonly diagnosed disease in the UK which causes approximately 10,000 deaths annually. Although an initially effective response to androgen deprivation therapy (ADT) occurs in most patients, the tumour normally recurs in a more aggressive form of the disease termed castrate resistant PC (CRPC) and is largely untreatable at this stage. In many cases, disease is driven by inappropriate androgen receptor (AR) signalling. It is therefore vital to have better understanding of mechanisms that re-activate AR and promote ADT resistance in the clinic and hence better treatments for advanced tumour.

Activation of AR by testosterone is crucial for prostate growth and transformation. Anti-androgens, the second most common PC therapy after surgery, antagonise ligand binding to the receptor and hence deactivate AR signalling. In 2012, enzalutamide, a more potent agents in terms of availability to block AR was approved by the FDA and ENA as a second-generation anti-androgen for clinical usage. Although it demonstrated several advantages over its pervious counterpart bicalutamide, response rates of just 50% in CRPC patients and subsequent resistance observed in responders has limited its effectiveness. Critically, several lines of evidence from pre-clinical models and patient samples indicate that one particular resistant mechanism is the emergence of AR mutant(s), in part, driven by a specific AR mutation F876L that enables the compound to act as an agonist. Importantly, the same mutant was later detected in metastatic PC patient had been treated with apalutamide. Evidently, novel therapies emerging into clinical treatment of advance disease have the added challenge of being efficacious in the background of mutant AR and thus developing model systems to test this is of paramount importance.

In order to enable more physiological modelling of aberrant ARF876L activity that would highlight potentially distinct mechanisms that could be exploited in future therapies, this project aimed to generate CRISPR-edited LNCaP and CWR22Rv1 cell lines expressing the enzalutamide-activated ARF876L mutant. Meanwhile, a part of project has also focused on generation of a physiologically relevant AR rescue/replacement in vitro cell line model (LNCaP- AR_{F876L} cells) which permits ability for studying ARF876L directly regulated gene expression profiles by effectively knockdown endogenous AR without impacting on the ectopically expressed mutant. Furthermore, by using

Illumina Human HT-12 arrays analysing LNCaP-AR$_{F876L}$ cells revealed a comprehensive transcriptomic data-set to provide an insight into how an enzalutamide-activated AR mutant can drive a distinct gene-set in advanced PC. This is important as it may enable distinct biomarker discovery in enzalutamide-resistance disease and has highlighted interplay between the AR$_{F876L}$ mutation and the glucocorticoid receptor. Lastly, the LNCaP- AR$_{F876L}$ cell lines was utilised to demonstrate that aberrantly-functioning receptor is sensitive to BET inhibitors. In all, the work has shown that the AR$_{F876L}$ mutant drives a distinct transcriptional programme to the endogenous AR in LNCaP cells and the model can be utilised effectively to indicate sensitivities of the receptor to clinically-relevant compounds.

Acknowledgments

Contents

List of Abbreviations

ACTH	Adrenocorticotrphic hormone
ADT	Androgen deprivation therapy
AF-1	Activation function 1
AF-2	Activation function 2
AHR	aryl hydrocarbon receptor
AIS	Androgen insensitivity syndrome
AR	Androgen receptor
ARE	Androgen response element
AR-fl	Androgen receptor full length
AR-V	Androgen receptor variant
ATCC	American Type Culture Collection
BET	BRD and extra- terminal
BETi	BET inhibitors
BPH	Benign prostatic hyperplasia
BRDs	Bromodomains
BSA	Bovine serum albumin
Cas	CRISPR associated
CAT	Chloramphenicol acetyltransferase
CBP	CREB binding protein
CBP/p300	(CREB)-binding protein and p300 histone acetyltransferase
CCAR2	Cell cycle and apoptosis regulator 2
CDK	Cyclin-dependent kinase
cDNA	Complementary DNA
ChIP	Chromatin immunoprecipitation
CPA	Cyproterone acetate
CRISPR/Cas9	clustered regularly interspaced short palindromic repeats/CRISPR-associated
CRPC	Castrate resistant prostate cancer

crRNA	CRISPR RNA
CTCs	Circulating tumour cells
DBD	DNA binding domain
DBS	DNA double stranded break
DCC	Dextran-coated charcoal
DEPC	Diethylpyrocarbonate
DES	Diethylstilbestrol
DHEA	Dehydroepiandrosterone
DHEA-S	DHEA-sulphate
DHT	Dihydrotestosterone
DHX9	DEAH-Box helicase 9
DNA-PKcs	DNA-dependent protein kinase catalytic subunit
DRE	Downstream response elements
DUB	Deubiquitinase
ECL	Enhanced chemi-luminescence
EDTA	Ethylenediaminetetraacetic acid
EGFR	Epidermal growth factor receptor
Enz	Enzalutamide
ER	Estrogen receptor
ERBT	External-beam radiotherapy
ETS	E-twenty six
ETV1	ETS translocation variant 1
FCS	Fetal calf serum
FGFR	Fibroblast growth factor receptor
FRAP	Fluorescence recovery after photobleaching
FSH	Follicle stimulating hormone
FUBP1	FUSE binding protein 1
GR	Glucocorticoid receptor
HAT	Histone acetyltransferase

HAT	histone acetyltransferases
HAT	Histone acetyl-transferases
HDAC	Histone deacetylase
HDR	homology-directed repair
HEPES	4-(2-hydroxyethyl)-1-piperazineethanesulfonic acid
HMT	histone methyltransferases
Indels	small insertions and deletions
iPS	induced pluripotent stem
IR	Insulin-like growth factor receptor
LB	Luria-Bertani
LBD	Ligand binding domain
LBD	Ligand-binding domain
LCPS	Luciferase counts per second
LH	Lutenizing hormone
LHRH	Luteinizing-hormone-releasing-hormone
LHRHR	Leutinizing-hormone release hormone receptor
LNCaP	Lymph node carcinoma of the prostate
MAPK	Mitogen-activated protein kinase
MMLV	Moloney murine leukaemia virus
mRNA	messenger RNA
NDRG1	N-myc downstream regulated 1
NHEJ	non-homologous end-joining
NLS	Nuclear localisation signal
NTC	No template control
NTD	N-terminal domain
OGT	Oxford gene technologies
ONPG	o-nitrophenyl-β-D-galactosidase
PAIS	Parital androgen insensitivity syndrome
PAM	protospacer adjacent motif

PBS	Phosphate buffered saline
PC	Prostate cancer
pCAF	p300/CBP-associating factor
PCR	Polymerase chain reaction
PI	Propidium iodide
PR	Progesterone receptor
PSA	Prostate specific antigen
P-TEFb	positive transcription elongation factor B
PTM	Post translation modification
qPCR	Quantitative polymerase chain reaction
RACE	5' or 3' rapid amplification of cDNA ends
RIN	RNA integrity number
RIPA	Radioimmunoprecipitation assay buffer
RNA	Ribonucleic acid
RNAi	RNA interference
RT	Room temperature or Reverse transcription
RUVBL1	RuvB like AAA ATPase 1
SBMA	Spinal-Bulbar muscular atrophy
SHBG	Sex hormone binding globulin
SNPs	Single Nucleotide Polymorphism
SOC	Super optimal broth
SPOP	speckle-type POZ protein
SRB	Sulforhodamine B
SRC1	steroid receptor coactivator-1
ssODN	single-stranded oligodeoxynucleotides
SUMO	Small ubiquitin-like modifier
TAD	Transactivation domain
TAE	Tris base, acetic acid, EDTA
TALENs	transcription activator-like effector nucleases

TAU	Tris base, acetic acid, EDTA
TBS	Tris buffered saline
TE	Tris-EDTA
TFIIF	Transcription factor II F
TFs	transcription factors
TIDE	Tracing Indel by DEcomposetion
TIF2	transcriptional intermediary factor-2
tracrRNA	trans-activating CRISPR RNA
TSS	transcription start site
TTBS	Tween-20 Tris buffered saline
TURP	Trans-urethral resection of the prostate
UAS	Upstream activation sequence
WB	Western blot
wtAR	wild-type androgen receptor
ZFNs	zinc finger nucleases
β-gal	β-galactosidase

List of Figures

16

List of Tables

Chapter 1: General introduction

1.1.Prostate cancer and treatment.

The first prostate cancer (PC) case was described as 'a very rare disease' in 1853 (Adams J, 1853; Denmeade and Isaacs, 2002). Remarkably, the same disease 150 years later has become the most important health issue among the aging population in the Western world. Globally, PC is the second most common cancer, and the third most common cancer in men in developed countries (Hassanipour-Azgomi et al., 2016). PC today has become the leading cause of cancer-associated deaths in men in the UK and accounts for 13% of all cancer deaths in males with over 10,000 deaths in 2016 (CRUK).

PC incidence is strongly related to age; with the highest mortality rates being in older men (>70 years). In the UK between 2014 and 2016, 74% of PC cases was diagnosed in males over the age of 75 while only 1% in males under 50 (Figure 1.1). Significantly, PC incidence is expected to further increase in the future due to improvements in diagnosis and an increase in the ageing population (Divo et al., 2014).
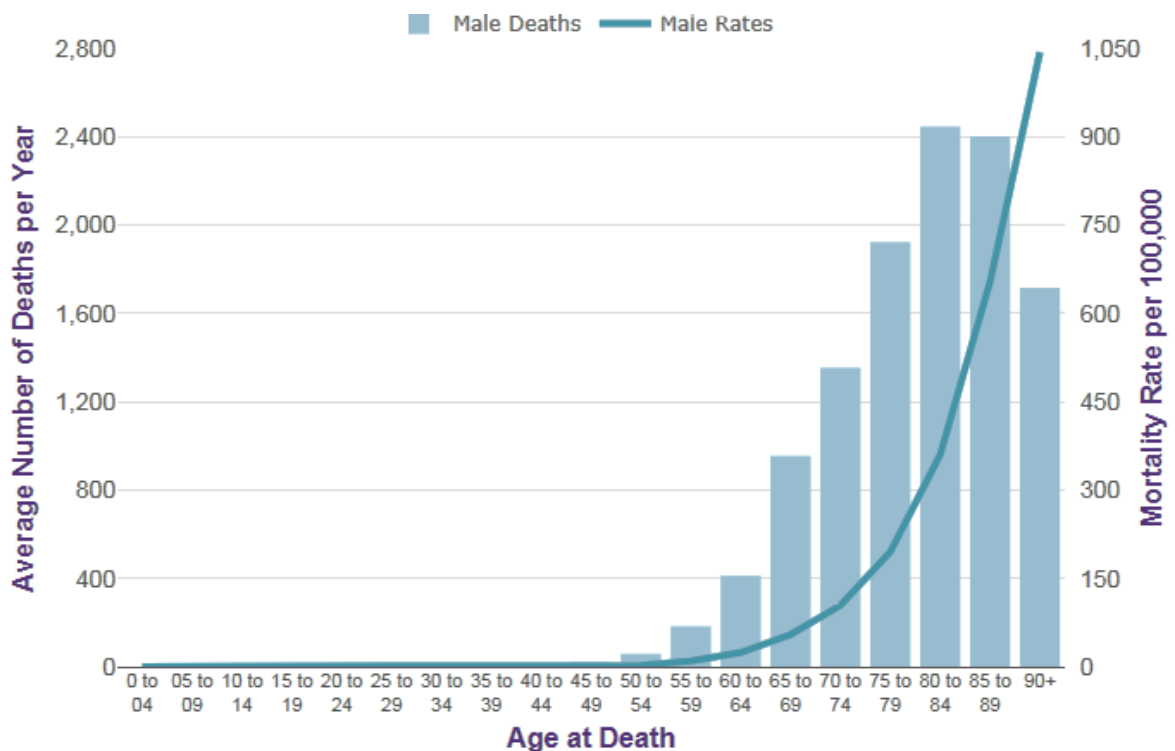
Figure 1.1 Average Number of Deaths per Year and Age-Specific Mortality Rates (per 100,000 Population, 2014-2016, UK). Prostate cancer mortality rates have age specific distribution. Figure taken from CRUK, cancer stats, last updated 10/2017.

Many factors have been suggested that may relate to higher PC risk, including external influences, such as environmental changes and lifestyle (Gann, 2002); and phenotypic factors including age, race/ethnicity, family history and genetic alteration. The inherited factors are estimated to be responsible for 5–9% of incidences. For instance, risk of developing PC is 5 times higher in men with *BRCA2* mutations (Cavanagh and Rogers, 2015). Although with extensive research, no preventable risk factors have been conclusively linked with PC risk.

Many patients with the disease have tumours with slow growth that may never cause a problem. Others can be cured by treating the tumour within the prostate gland. But in some, the cancer spreads to elsewhere in the body, usually to the bones (Yap *et al.*, 2011). Depending on the situation, the treatment options for men with PC include: i) expectant management or active surveillance; ii) surgery; iii) radiation therapy; iv) cryosurgery (cryotherapy); v) hormone therapy; vi) chemotherapy; vii) vaccine treatment and viii) bone-directed treatment (Mohler *et al.*, 2014). Most of these treatments are employed individually, although in some cases they may be combined. Hormone therapy, for example, is often used in combination with radiation therapy. The treatment of choice for PC, however, is more complicated as it takes into account the stage and grade of disease, patents' age and expected life span, or whether patents have other serious health conditions (Carroll *et al.*, 2014).

1.2.Androgen sensitivity in prostate cancer.

Over half a century ago, PC patients diagnosed with local advanced or metastatic disease normally died within 1-2 years (Li *et al.*, 2016a). This changed when the role of androgenic activity in PC was firstly discovered in 1941 (Huggins and Clark, 1940). Two PC research pioneers, Huggins and Hodges (1972) found that PC responded to surgical castration therapies. Initially, they noticed that reducing androgen levels in patients led to growth arrest of the tumour. By monitoring patients' serum acid-phosphatase levels after surgical castration (orchiectomy) or oral estrogen (stilbesterol) administration, they sequentially reported the elimination or down-regulation of androgen levels can inhibit disseminated prostatic carcinoma growth. Thus, PC was concluded as an 'androgen-sensitive' disease for the first time (Huggins and Hodges, 2002). Their

discovery of hormone dependence in PC brought a new era to cancer treatment. 'Endocrine-therapy' therefore firstly entered into PC therapy history, and to this day, androgen ablation remains the most useful PC therapy (Denmeade and Isaacs, 2002).

Following their important discovery, a wave of androgen-ablation treatments emerged during the 1960s, which aimed either to reduce androgen production, or to block androgen functions within the target tissues. Those methods have become the predecessor of modern androgen-deprivation therapy (ADT), that is alternatively known as hormone therapy (Denmeade and Isaacs, 2002).

Today, ADT is the second most common treatment approach, after surgery, for local advanced PC (Canalichio *et al.*, 2015). It has three different hormonal approaches: luteinizing hormone-releasing hormone (LHRH) agonists, orchiectomy, and anti-androgens. Orchiectomy and LHRH agonist aim to lower the levels of testosterone or other androgens; while anti-androgens were designed to block the action of those hormones. ADT is usually used as first line treatment for advanced PC patients where disease is likely extended beyond the prostate gland and into nearby tissues. However, there are numerous other settings in which ADT is used. These include administration in the neoadjuvant or adjuvant setting combined with surgery or radiation therapy or when there is biochemical recurrence after therapy with curative intent (Suzman and Antonarakis, 2014).

In most of cases, ADT is initially effective. Most patients respond favorably with tumour regression and often with reduced expression level of the PC serum biomarker prostate-specific antigen (PSA). Unfortunately, androgen deprivation is not sufficient to completely cure metastatic tumours (Tsao *et al.*, 2012). After a median time of 18 months, up to 40% of patients with definitive local disease and nearly all metastatic patients will eventually have disease relapse.

Tumours re-appear in a more aggressive, androgen-independent form, termed castrate-resistant PC (CRPC). Disease is largely lethal at this stage due to patients pre-treated with ADT no longer responding to conventional hormonal targeting analogue treatment. Hence resurgence of

advanced prostatic tumours represents a major clinical challenge, as therapies for patients at this stage are largely ineffective.

1.3. The androgen-receptor signalling cascade in prostate cancer and castration-resistant prostate cancer

In the human body, the main androgens are testosterone and dihydrotestosterone (DHT), the latter being the most potent endogenous androgen, most of which is produced from the testes, although the adrenal glands also make a small amount. DHT binds to the androgen receptor (AR), a member of the nuclear receptor (NR) superfamily (Brinkmann, 2011); specifically the steroid-hormone receptor family that includes the estrogen receptor (ER), progesterone receptor (PR), glucocorticoid receptor (GR) and mineralocorticoid receptor (MR).

The activation of the androgen-AR signalling pathway is indispensable for the differentiation, growth and support of male primary sexual characteristics. The signalling axis initiates at early stages of embryogenesis (Mateo *et al.*, 2014) to enable development and growth of the prostate, which is especially active in adult male reproductive organs, including the prostate in order to maintain the male phenotype. The AR-mediated signalling axis also plays an essential role in the early stages of PC development: AR is overexpressed in a large number of localised PC patients and leads to an increase in the serum level of PSA (Karantanos *et al.*, 2013). Androgens stimulate PC cells to grow hence ablating serum androgen levels or stopping their function in PC cells causes tumours to initially shrink (Gomella, 2009).
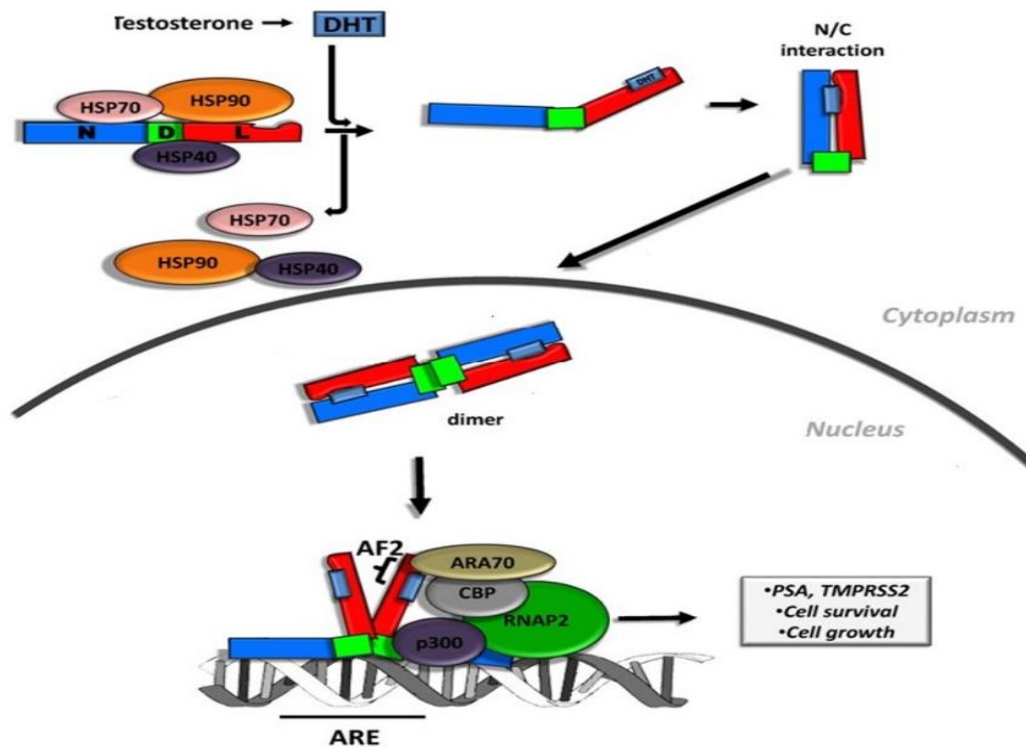
Figure 1.2 The signal transduction pathway of androgen receptor. Graphic representations of AR action. DHT interacts with the AR and releases it from bound heat shock proteins (HSP) enabling N/C-terminal interaction and dimerization of the receptor. This exposes a nuclear localization signal (NLS) required for interaction with importin-α and nuclear translocation. Inside the nucleus, DNA binding to target genes whereby the N/C-terminal interaction is lost (Askew *et al.*, 2012), allowing the recruitment of transcriptional co-regulators, such as CREB binding protein (CBP), and p300 that facilitate the recruitment of RNA-Polymerase II (RNAP2) to transcribe AR-dependent genes (Brooke *et al.*, 2008) (van de Wijngaart *et al.*, 2012). N—N-terminal domain (NTD); D—DNA-binding domain (DBD); L—ligand-binding domain (LBD). ARE-androgen response elements. Image adapted from (Brooke *et al.*, 2008).

In vivo, unliganded AR stays in the cytoplasm as a stable protein complex with molecular chaperones, including heat shock protein 90 (HSP90) and HSP70 (Figure **1.2**). Upon binding its ligand, DHT, the receptor undergoes a conformational rearrangement and consequently disassociates from the HSPs leading to AR dimerisation and an essential intermolecular interaction between the N- and C-termini of the AR. This so called N/C-terminal interaction exposes a bi-partite nuclear localisation signal (NLS), which allows translocation of the AR to the nucleus (Lange *et al.*, 2007). Post-nuclear translocation, the AR homodimerises, via the DNA binding domain (DBD) (Figure **1.2**), and subsequently interacts with specific DNA sequences within chromatin termed androgen response elements (AREs). Co-regulators are recruited that

facilitate the binding of the RNA polymerase II machinery to transcribe AR-dependent genes, including *PSA, KLK2*, and *TMPRSS2* (Brooke et al., 2008).

In addition to androgen-dependent PC, the AR signalling axis remains unexpectedly active in the castration-resistant setting regardless of castrate levels of androgen (Karantanos *et al.*, 2013; de Oliveira Barros *et al.*, 2014). Comprehensive studies over the past decade have shown that the androgen receptor pathway is very often altered in most CRPC samples and promotes the concept that persistent AR signalling occurs in most CRPC (Petrylak, 2013) (Lorente and De Bono, 2014).

Currently, several resistant mechanisms have been implicated in CRPC (Tan *et al.*, 2015b). These include, but are not limited to: *AR* gene amplification and/or overexpression; the acquisition of *AR* mutations during ADT; inappropriate AR activation by interleukins, cytokines and growth factors; intratumoural androgen synthesis, such as up-regulated transcript levels of enzymes involved in androgen synthesis; aberrant AR co-regulator expression, such as cAMP response element binding protein (CREB)-binding protein (CBP)/p300 and steroid receptor coregulator-1 (SRC-1) which facilitate AR binding to DNA. Recently, emerging evidence implicates that therapy-induced selection of novel AR splice forms, termed AR-variants (AR-Vs), that lack the target site of conventional anti-androgen therapies, have a role in CRPC (Dehm and Tindall, 2011).

The reactivation of AR signalling in most CRPC patients indicates that the AR remains a critical factor in treatment-resistant advanced tumours. Most importantly, it suggests that AR remains a suitable therapeutic target for advanced PC. In this regard, deciphering aberrant AR regulation and function in CRPC is essential for the development of more effective therapies for this fatal disease.

1.4. The structure of the androgen receptor

The human *AR* gene is located on the X chromosome at position Xq11-12 consists of eight exons and encodes a 919 amino acid protein (Figure **1.3**). Similar to other steroid receptor family members, the AR protein contains three major functional domains and several activation functional units that control its activity. The AR is composed of an unstructured N-terminal transactivation domain (NTD), a highly conserved DNA-binding domain (DBD), a short hinge region and a C-terminal ligand-binding domain (LBD) (Tan *et al.*, 2015b).

AR structure
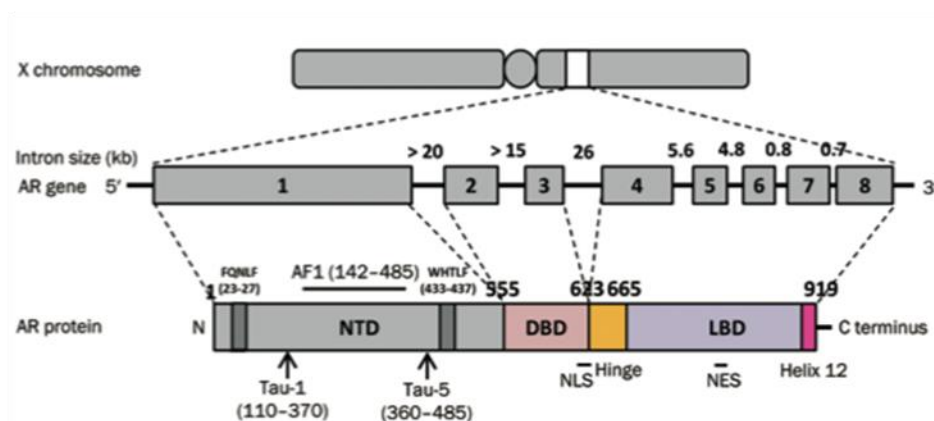
Figure 1.3 Functional domains of the androgen receptor. Scheme of the domain organization of the AR: NTD (N-terminal transactivation domain), DBD (DNA binding domain), hinge region (Hinge) and LBD (ligand binding domain). Residue numbers above the scheme delineate the domain boundaries. Figure adapted from (Tan *et al.*, 2015b).

1.4.1. N-terminal transactivation domain (NTD)

The N-terminal transactivation domain of AR (AR-NTD) is the least conserved region among all NR members (Claessens *et al.*, 2008). AR–NTD corresponds to the first 558 residues encoded by *exon* 1 and spans about 60% of the coding region of the receptor. The activation function 1 (AF-1) region within the NTD contains the majority of inherent transcriptional activity of the receptor. Two overlapping but distinct transcription activation units (TAU), TAU-1 (amino acid residues 110-485) and TAU-5 (amino acid residues 360-528) are located within AF-1. By deleting either

one of the units from AF-1, TAU-1 was revealed to be required for ligand-dependent activation of the full length receptor while TAU-5 is important for ligand-independent activity and is capable of permitting transactivation for the receptor that lacks the LBD or in the absence of ligand (Bevan *et al.*, 1999). In addition, the NTD of AR also harbors an important motif, FQNLF (residues 23–27), that facilitates NTD binding to the LBD, enabling the N/C-interaction of the receptor. Thus, this short motif is vital for the full transcriptional potential of the AR to be elicited (McEwan, 2004).

1.4.2.The DNA-binding Domain (DBD) and hinge region (H)

The DNA binding domain (DBD) is the most conserved functional domain of the AR. Its genomic sequence has up to 80% similarity with corresponding domains in other NR family members, including PR and ER. The AR-DBD consists of three α-helices that are organised into two zinc finger modules and a relatively unstructured C-terminal extension. The α-helix in the first zinc-finger contains 5 amino acid residues (577-GSCKV-581); so-called the proximal (P)-box which confers specific sequence recognition of the receptor to 15-bp palindromic target sites within androgen responsive elements (AREs) that are located in the promoter and enhancer region of androgen-responsive genes. The second and the third α-helix form the second zinc finger, containing a distal (D)-box (596-ASRND-600) that is involved in receptor dimerisation. A direct interaction between the DBD of the receptor and the major groove of DNA is also required for recognition of AREs of ligand-activated AR. Additional contacts with the DNA are made by the C-terminal extension that is adjacent to the ligand-binding domain (LBD). The DBD also contains the first part of a bipartite nuclear localisation signal (NLS) and a non-classical nuclear export signal and has also suggested to be involved in nucleo-cytoplasmic shuttling (Lorente and De Bono, 2014).

A part of *exon* 4 codes for a flexible and poorly conserved hinge region, positioned between residues 624–689. The hinge contains the second part of NLS. It also is a target for several post-translational modifications, including acetylation and methylation, which regulates AR function (Coffey *et al.*, 2012)

1.4.3.The ligand-binding domain (LBD)

The ligand-binding domain (LBD) is the most well studied functional domain in the AR. It is 265 amino acids long (665-919) and encoded by *exon*s 5-8. Unlike the DBD, the AR-LBD shares less sequence homology with other NRs; with almost half of the AR-LBD sequence differing from other family members (Poujol *et al.*, 2000). The LBD is composed of 11 α-helices, one less than other steroid receptors, although the nomenclature remains the same: helices 1-12 with omission of helix 2. Helices 3, 5, 7 and 11 of 12 are of particular importance. Helices 3, 5, 7 and 11 form a barrel-like structure suitable for hormone binding. This ligand-binding pocket has an important role for AR activity in providing a hydrophobic pocket for binding of testosterone and DHT in order to activate the receptor. Upon binding of ligands, the LBD undergoes a conformational change in which helix 12 swings round and closes the ligand-binding pocket. This rearrangement of helix 12 results in a hydrophobic surface groove (also referred to as the coactivator binding pocket) and serves as a docking site for the AF-1 FQNLF motif within the NTD (Bourguet *et al.*, 2000; Greschik and Moras, 2003). In addition, the coactivator binding pocket also plays a role for determining the preference of transcriptome modulation via mediating co-regulatory protein interaction (Greschik and Moras, 2003).

1.5.Direct AR-targeting anti-androgens.

With the recent increasing understanding of the physiology and molecular mechanism of AR function in advanced disease, development of direct or indirect AR targeting agents and androgen analogues has been a major objective in PC research for improved therapies. Many drugs have been developed and are most frequently used in the clinic as daily practice for intermediate- and high-risk diseases whether or not within the context of a LHRH agonists.

Figure 1.4 Schematic of AR activation and anti-androgens mechanism. The diagram illustrates the mechanism of antiandrogen action. AR-LBD target antiandrogens are competing with AR ligand, the endogenous androgens, testosterone or DHT for the same ligand-binding pocket of the receptor and ultimately block the activation of AR signalling. Image taken from (Chen *et al.*, 2009) .

Most anti-androgens are designed to interfere with AR function by competitively inhibiting androgen binding to cognate receptors at the target organ. Two types of anti-androgens have clinically been used (Chen *et al.*, 2009): the steroidal anti-androgens and the non-steroidal anti-androgens. Several steroidal anti-androgens includes cyproterone acetate, megestrol acetate, and medroxyprogesterone acetate are initially used for androgen blockade in patients. However, their clinical use is limited due to severe drawbacks such as hepatotoxicity, interference with libido and impotence, cardiovascular side effects and low efficacy. Non-steroidal anti-androgens were later developed, which including the first-generation anti-androgens, such as hydroxyflutamide, bicalutamide (Casodex), nilutamide, and the second-generation compounds: enzalutamide (MDV3100) and apalutamide (ARN-509). Most of the non-steroidal anti-androgens have been widely used in combined therapies as they avoid the typical constraints of steroidal anti-androgens.

In the *in vivo* scenario, non-steroidal anti-androgens, acting as androgen analogues, compete with endogenous DHT for the same ligand-binding pocket of AR and subsequently block the AR signalling cascade. As illustrated in Figure **1.4**, bicalutamide and enzalutamide disturb the AR signalling pathway by binding to the ligand-binding pocket of the AR, which prevents coactivator recruitment and abrogating AR-DNA interaction. The novel AR antagonist enzalutamide was first introduced in 2009 as a second-generation anti-androgen to patients who had failed first-line hormonal therapy (Semenas et al., 2013) (Figure **1.5**). In comparison with the 'classical' anti-androgens, such as bicalutamide, enzalutamide does not only block androgen binding, but it also inhibits translocation of the AR to the nucleus and impairs AR binding to DNA (Tran et al., 2009). With several advantages over bicalutamide, both the US Food and Drug Administration (FDA) and European Medicines Agency (EMA) approved enzalutamide for clinical use in patients with chemo-resistant CRPC in 2012 (Heck *et al.*, 2012). Another second-generation antiandrogen that is related to enzalutamide called apalutamide, has rapidly progressed into Phase I and Phase II clinical trials due to its lower side effect and higher efficacy than enzalutamide (Schweizer and Antonarakis, 2012).

M. L. Mohler *et al.*
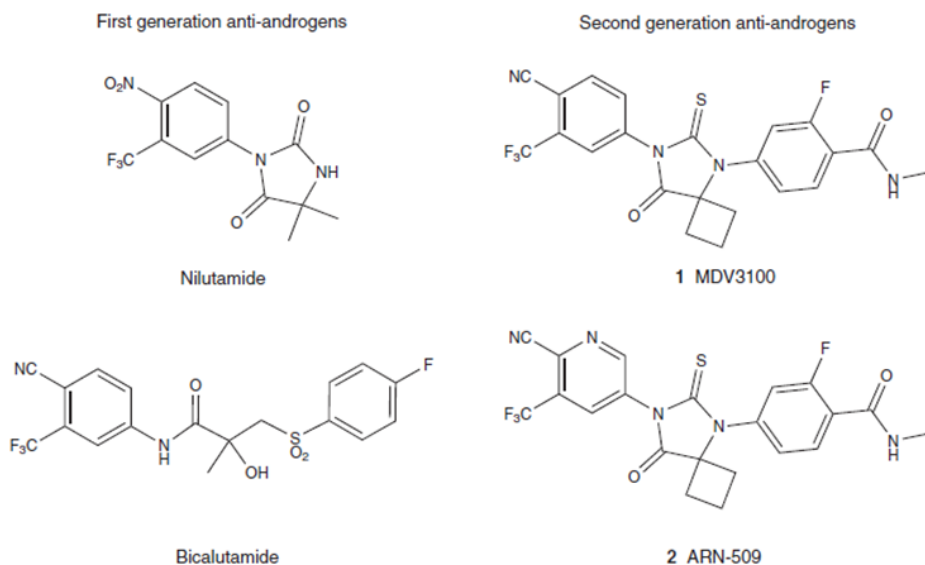
Figure 2. First- and second-generation anti-androgens.

Figure 1.5 The molecule structure of first and second-generation anti-androgens. MDV3100-enzalutamide, ARN-509-apalutamide. Image was taken form (Mohler et al., 2012).

1.6.Acquisition of AR mutation as a mechanism of therapy evasion.

Unfortunately, although initially being sensitive to anti-androgen therapy, most PC patients will relapse; with disease progressing to a refractory, untreatable state. At this stage, tumours either become endocrine-therapy resistant during the course of treatment or possesses a small population of pre-existing hormone-refractory cells that remain viable in spite of castration level of androgen (van de Wijngaart *et al.*, 2012). By selective outgrowth of resistant cells, tumours aggressively progress and eventually claim the life of patients.

Acquisition of genetic changes could contribute to disease progression. In particular, somatic mutations in the *AR* gene is a consistent finding present in metastatic PC, as well as in human PC cell lines and xenograft animal models (Koochekpour, 2010). In the clinic, non-synonymous *AR* mutations are rarely detectable in localized or anti-androgen naive patients, but presents in around 20% of initial CRPC patients (Beltran *et al.*, 2017). Importantly, AR mutation frequency is elevated in androgen-independent PC and are further significantly increased in distant metastases of patients following endocrine therapy, which suggests that treatment failure may result from PC cells adapting resistance from the selective pressure applied by the therapy.

AR gene sequencing of CRPC patients, has identified 159 AR mutations in PC tissue (last update 2015, Tan *et al.* 2015a). Almost 50% of them were found to fall within the LBD (Gottlieb *et al.*, 2012). These included L701H, H874Y and T877A (Figure **1.6**), noticeably, all of which were from patients that had been treated with anti-androgens. Further studies found that most of them resulted in reduced ligand specificity and hence permitted inappropriate receptor activation by binding with adrenal androgens or other steroid metabolites. AR_{L701H} can become active by other steroids, including estrogen, cortisone; while AR_{H874Y} can be activated by progesterone. Certain LBD mutations are also sufficient to convert AR antagonists to AR agonists. H874Y mutation was found in CWR22Rv1 cell lines, and shown to be abnormally activated by Cyproterone Acetate (CPA).
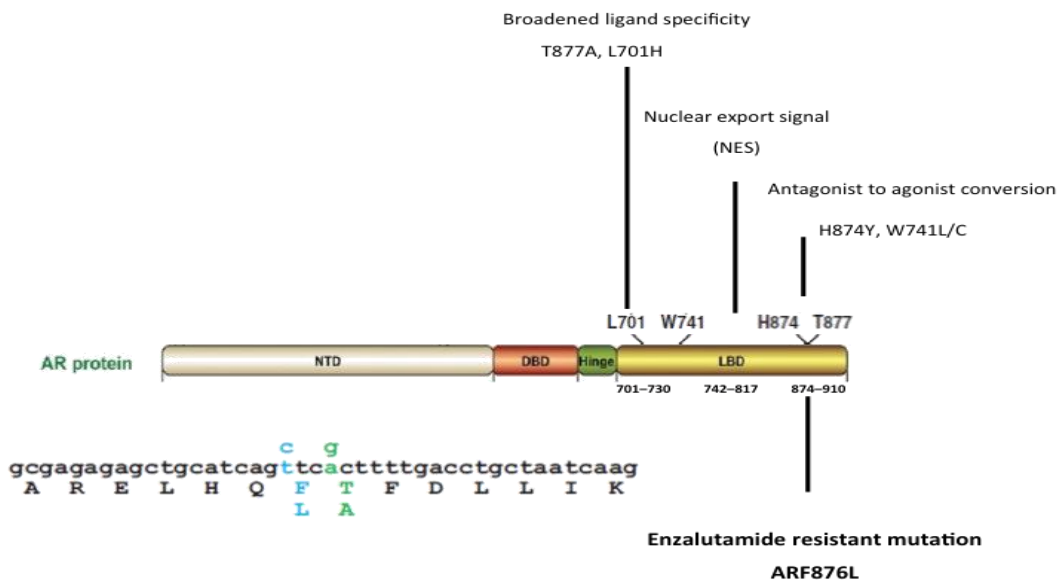
Figure 1.6 Schematic representation of the human AR with mutation encoding the LBD. Schematic representation of unique mutations in ligand banding domain of the human AR. Highlighting enzalutamide resistant mutation F876L in bold.

AR_{T877A} mutation, the amino acid substitution of threonine to alanine at codon 877 of the AR (Figure 1.6), was the first reported AR mutation and is expressed in the hormone-dependent LNCaP human prostate cancer cell line that is derived from a lymph node metastasis (Horoszewicz et al., 1980; Veldscholte et al., 1990). AR_{T877A} associated with AF-2 have been shown to produce a receptor capable of activation by AR antagonists Flutamide. In the clinic, Taplin *et al.* (1999) have shown that 31% of CRPC patients treated with Flutamide harbored the T877A mutation. This substitution enables the anti-androgen Flutamide to act as an agonist and hence patients who are refractory to Flutamide therapy regularly express AR_{T877A} mutation (Suzuki *et al.*, 1996; Monge *et al.*, 2006).

Recently, the crystal structure of AR_{T877A} upon binding of DHT has been solved (Figure 1.7 B) (Bohl *et al.*, 2007). Upon binding of DHT, the structure of wildtype AR (Figure 1.7 A) and AR_{T877A} (Figure 1.7 B) are essentially identical except at the point of the mutation. However, by substitution of alanine for threonine at residue 877, a polar interaction with DHT was lost. As a result, the size of the binding pocket is expected to increase compared with wildtype AR, and more space was

32

introduced allowing the accommodation of a larger functional group at this position, such as that found in Flutamide (Tan *et al.*, 2015a).
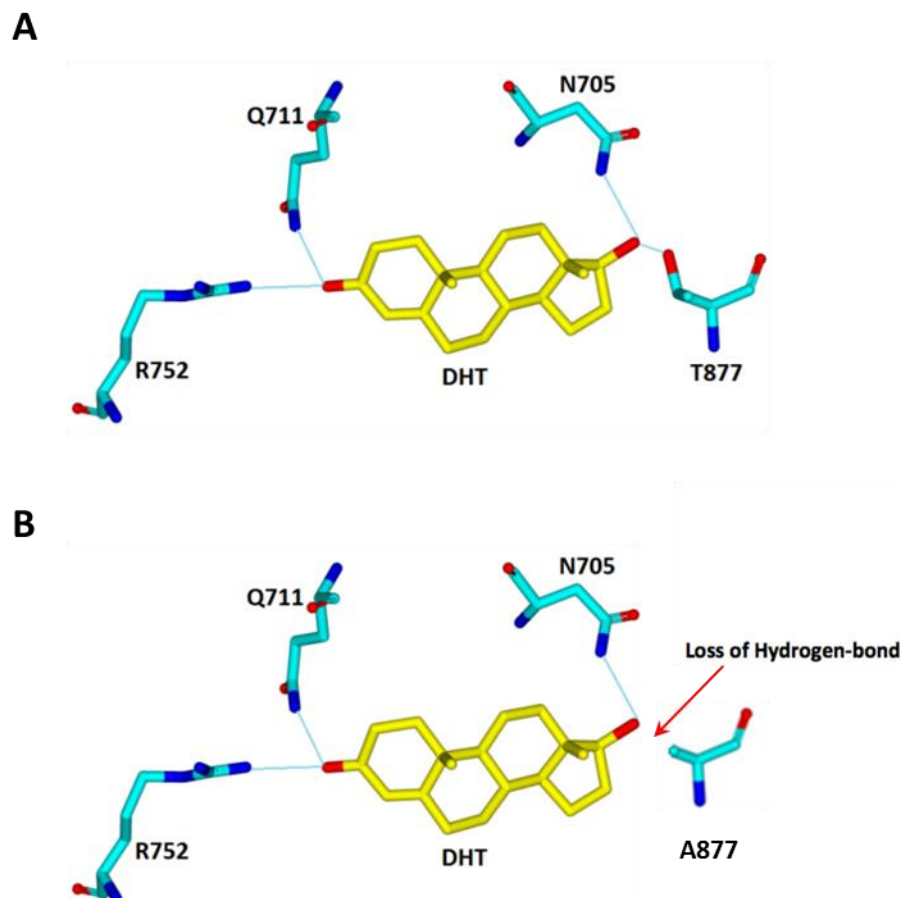
Figure 1.7 Structural representation of ligand binding to wildtype AR and AR$_{T877A}$. (A) Binding of DHT to wildtypeAR. (B) Binding of DHT to the AR$_{T877A}$ mutation. Important LBD residues are indicated in blue; the ligand is indicated in yellow. Hydrogen bonds are indicated with dotted lines. Figure taken from van de Wijngaart, Dubbink et al. (2012).

Another mutation, W741L was later found both in LNCaP and ADT-treated metastatic patient sample-derived xenograft tumours which exhibit increased tumour growth and PSA secretion in response to bicalutamide (Yoshida *et al.*, 2005). A stable cell model from Luke Gaughan's lab (O'Neill *et al.*, 2015) proved robust evidence of AR$_{W741L}$ being a bicalutamide-activated mutant.

Clinically, approximately 50% of patients after hormone therapy present with anti-androgen withdrawal syndrome (AAWS). This condition is characterised by cancers that grow in the presence of anti-androgens and whose growth is attenuated by stopping anti-androgen treatment (Paul and Breul, 2000; Sartor *et al.*, 2008). Acquiring somatic mutations in the *AR* gene is likely responsible for the 15–30% of patients that exhibit a withdrawal syndrome after cessation of first-generation therapies (Wyatt and Gleave, 2015). This evidence strongly suggested that mutation selection under pressure of anti-androgen treatment contributes, in part, to drug resistance. Long-term treatment with the AR antagonists could selectively enable outgrowth of tumour cells that are driven by AR mutants that turn anti-androgens from antagonists to agonists causing drug resistance.

1.7. AR$_{F876L}$

Similar to the bicalutamide-activated AR$_{W741L}$ mutation, a specific AR mutation, F876L within the LBD of AR, has been reported that is sufficient to confer partial resistance to enzalutamide and apalutamide *in vitro* and *in vivo* models of CRPC (Joseph *et al.*, 2013). Importantly, the mutation was later detected in plasma DNA of progressive CRPC patients after treatment with apalutamide.

It had been firstly reported that prolonged treatment with enzalutamide in prostate cancer cell lines led to the spontaneous emergence of AR$_{F876L}$ that converted enzalutamide into an AR agonist (Balbas *et al.*, 2013). Moreover, structural analysis of the mutated AR showed that F876L mutation affects the ligand- binding domain of the AR and is responsible for the switch of enzalutamide from antagonist to agonist. Joseph *et al.* (2013) showed that the F876L mutation was sufficient to convey acquired resistance not only to enzalutamide, but also to apalutamide in CRPC cell models. A published pre-clinical study (Korpal *et al.*, 2013b) latter confirmed that AR$_{F876L}$-bearing prostate cancer cells are not only resistant to enzalutamide but also dependent on the agonist effect of enzalutamide for cellular growth under androgen-deprivation conditions. Importantly, the same mutation has been detected in circulating tumour DNA from apalutamide-treated CRPC patients (Dellis and Papatsoris, 2018). Taken together, the evidence highlights the

selective outgrowth of AR_{F876L}-expressing cells is a clinically relevant mechanism of second-generation anti-androgen enzalutamide resistance.

1.8. Alternative AR targeting agents

It is well accepted that the AR signalling axis remains a suitable therapeutic target for advance PC treatment. However, from the latest studies on enzalutamide resistance and the much earlier reports of bicalutamide and flutamide resistance, it is possible that eventually every LBD-targeting agent will lead to the occurrence of a somatic mutation that causes a switch to agonistic activity. Therefore, it seems that the future of AR antagonists lies in the development of compounds with alternative targeting sites or impact on another point in the signaling cascade.
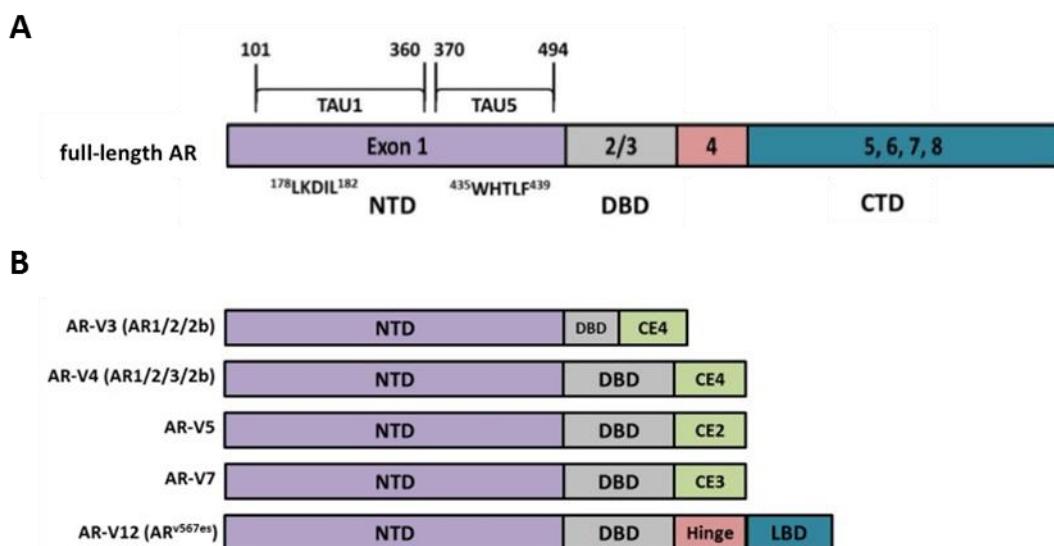
Figure 1.8 The graphic representation of Full-length AR (FL-AR) and AR splice variants (AR-Vs). (A) Graphic representation of Full-length AR (FL-AR). (B) Exon skipping or splicing of cryptic exons (CE) yield C-terminal truncated AR splice variants (AR-Vs). The splice variants lack the LBD and are constitutively active in the absence of ligand. Increased expression of AR-Vs has been identified in castration-resistant prostate cancer (CRPC).

In addition, several *AR* splice variants (AR-Vs) (Figure 1.8 B) have been recently found to be expressed in a high proportion of CRPCs; particularly metastatic disease. AR-Vs share an identical N-terminal structure to full length AR (FL-AR) with preservation of the NTD and DBD but are devoid of some of the hinge region and the entire LBD. Thus, they circumvent the need for ligand and are constitutively active transcription factors. AR-Vs were firstly found in the CWR22Rv1 cell line, a castrate-resistant PC cell line derived from the CWR-RD1 xenograft post-castration

(Sramkoski *et al.*, 1999; Tepper *et al.*, 2002), suggesting that androgen-ablation selected for these ligand-independent isoforms. (Watson *et al.*, 2010) initially reported that the proliferative effects of AR-V7 were mediated via full-length AR. Notably, however, convincing evidence from other groups (Kobayashi *et al.*, 2013) have recently shown that AR-Vs alone can drive expression of AR target genes. Although additional understanding is required in this area, clearly, constitutive, ligand-independent transcriptional activities of these isoforms accelerate the requirement for alternative AR targeting sites to inactivate these aberrantly functioning receptors.

The first question is that whether AR signaling inhibition can be achieved in an LBD-independent manner by targeting other critical steps of AR transcriptional pathway instead of hormone binding. For instance, compounds that do not act via the ligand-binding pocket but through other sites on the LBD, or other domains of the receptor will be of interest. Furthermore, the combination of compounds with a complementary action mechanism could lead to more efficient inhibition of AR and thus better control of disease.

1.9. Cross Talk between the AR and Glucocorticoid Receptor (GR)

At present, an increasing number of studies have focused on revealing the androgenic signalling-dependent mechanisms of tumor resistance to androgen deprivation and AR antiandrogen therapies which mainly includes: AR-mediated progression driven by *AR* amplification or somatic mutations that allow AR activation via nonandrogenic ligands binding (Tan *et al.*, 1997; Romanel *et al.*, 2015), as well as expression of constitutively active AR splice variants (Hu *et al.*, 2009). Importantly, AR-independent bypass mechanisms of CRPC progression have also been hypothesized to play a role, such as activated oncogenic pathways, including PI3K, c-MYC (Carver et al., 2011), and the increased expression and activity of another steroid receptor family member, the glucocorticoid receptor (GR) (Isikbay et al., 2014). By investigating GR function in CRPC, Arora et al. (2013) and (Isikbay *et al.*, 2014) uncovered that GR activity can indeed promote prostate cancer progression following AR blockade. GR antagonism has also been suggested as a therapeutic strategy for CRPC (Kach *et al.*, 2015).

More recently, the GR activation has been reported to contribute to CRPC resistance to various therapies including docetaxel (de Bono *et al.*, 2010) and enzalutamide (Crona and Whang, 2017). Clinically, significantly elevated GR levels were found in the bone metastases of PC patients after receiving enzalutamide treatment comparing to the treatment naïve group (Nadal and Bellmunt, 2016). Importantly, GR expression also correlated with poor prognosis of treatment outcome. *In vitro*, (Arora *et al.*, 2013) demonstrated that increasing GR expression is an alternative mechanism for enzalutamide resistance as up-regulated GR expression at both the mRNA and protein level in LNCaP cells resistant to the anti-androgens enzalutamide and apalutamide was detected. A dependency on GR activation for enzalutamide-driven growth was revealed by depleting GR in an enzalutamide-resistant cell line (named LREX) that was derived from an LNCaP xenograft refractory to chronic enzalutamide treatment. In addition, global gene expression profiling and GR/AR chromatin immunoprecipitation sequencing (ChIP-Seq) analyses in the LREX and parental cell lines demonstrated a significant overlap between the transcriptome and cistrome of the AR and those of the GR in the LREX' model. This observation is consistent with previous findings which demonstrated a positive role of the forkhead protein, FOXA1 in the redistribution of AR and GR in androgen deprived conditions (Yang and Yu, 2015).

GR-mediated resistance in CRPC does not seem to be limited to enzalutamide/ apalutamide. The involvement of GR in docetaxel-resistant PC has also been reported. A robust overexpression of GR was detected *in vitro* cultured PC cell line with an acquired docetaxel resistance as well as in docetaxel-treated patient's samples comparing to primary patients tissue (Kroon *et al.*, 2016). Additionally, by applying GR antagonists (mifepristone and CPA) in docetaxel-resistant PC cell lines, (Kroon *et al.*, 2016) demonstrated a restoration of sensitivity to docetaxel, supporting a role for the GR in docetaxel resistance which further supports the GR is a potential therapeutic target in advanced disease.

Given that the activating GR ligands glucocorticoids promote inhibitory effects on adrenocorticotropic hormone (ACTH) production, corticosteroids are routinely co-administered

with docetaxel and abiraterone in patients receiving chemotherapy (Han *et al.*, 2012). The administration of glucocorticoids has been shown to reduce PSA levels in patients due to further androgen blockage via interrupting feedback mechanisms in the pituitary gland. However, given the aforementioned role of GR in mediating resistance to PC therapies, it may seem counterintuitive to administer glucocorticoids for CRPC patients as corticosteroids might promote tumour progression in men whose tumours express GR. Recently, a phase I/II clinical trial (NCT 02012296) was initiated to test the treatment of patients with enzalutamide in combination either with or without mifepristone to further depict the role of the GR in CRPC (Arora *et al.*, 2013).

While improved AR-direct targeted agents have doubtlessly improved survival for prostate cancer patients, they are not curative in many cases and resistance eventually occurs in most patients who develop CRPC for which limited treatment options exist. Activation of the androgen receptor via alternative signalling cascades or activation of the AR target gene signature by a different nuclear hormone receptor, such as the GR, provide mechanisms to maintain a pro-survival phenotype in low androgenic conditions. More studies have demonstrated that GR can provide a mechanism of resistance to a number of current PC therapies and GR antagonists may provide clinical benefit in patients with CRPC.

1.10. The bromodomain and extra terminal domain (BET) family proteins involves in AR-mediated transcriptional programme.

Recently, by applying massive high-throughput analysis in parallel using hundreds of PC patients' tumour specimens, a comprehensive picture of the genetic alteration landscape that accompany cancer evolution in the prostate was revealed (Ruggero *et al.*, 2018). Of note, some crucial players in chromatin biology and epigenetic master regulators, mainly including: methyltransferases, demethylases, DNA methylation, histone acetylation (HAT), the bromodomain and extra terminal domain (BET) bromodomain epigenetic readers and pioneer transcription factors have been highlighted to be key alterations in metastatic CRPC and tumours that progress to CRPC upon

administration of next-generation anti-androgen therapy (Urbanucci *et al.*, 2017). Thus, identifying AR downstream signalling events and investigating the involvement of the epigenetic regulation of AR activity may become a new avenue for navigating potential prognostic markers and therapeutic targets for CRPC. To that end, in this study, we focus on investigating if two key epigenetic regulators, the BET family of bromodomain epigenetic readers proteins and the p300 histone acetyltransferase as potential therapeutic targets for AR-mediated anti-androgen resistance.

Bromodomains (BRDs) are approximately 110 amino acid-containing functional domains with conserved sequence, which recognises, principally, acetylated lysines of the N-terminal tails of histones (Sanchez and Zhou, 2009). BRDs motif are found in proteins with diverse functions, including histone acetyltransferases (HAT), histone methyltransferases (HMT), histone kinases, transcriptional modulators, ubiquitin ligases and chromatin re-modellers (Josling *et al.*, 2012). To initiate transcriptional regulation, recruitment of BRDs-containing proteins are generally required acting as chromatin readers to recognize mono-acetylated histones and trigger chromatin remodelling (Josling *et al.*, 2012). BRD-containing proteins have been identified in oncogenic rearrangements that lead to highly oncogenic fusion proteins, which have a key role in the development of several aggressive types of cancer. Mutations and deregulation of BRDs-containing proteins are commonly found involving in development of different type of cancer (Perez-Salvia and Esteller, 2017). Importantly, 42 known BRDs-containing proteins are found presenting genomic alterations in more than half of both local and advanced PC as well as over 70 percent of neuroendocrine PC (Ruggero *et al.*, 2018). Of particular note, the BRD and extra-terminal (BET) subgroup of bromodomain-containing proteins, including BRDT, BRD2, BRD3 and in particular BRD4, have been recently proposed to play a role in the progression to drug-resistant phenotypes in prostate cancer (Barbieri *et al.*, 2013).

A
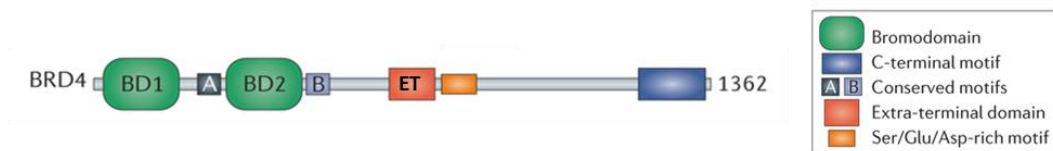
B
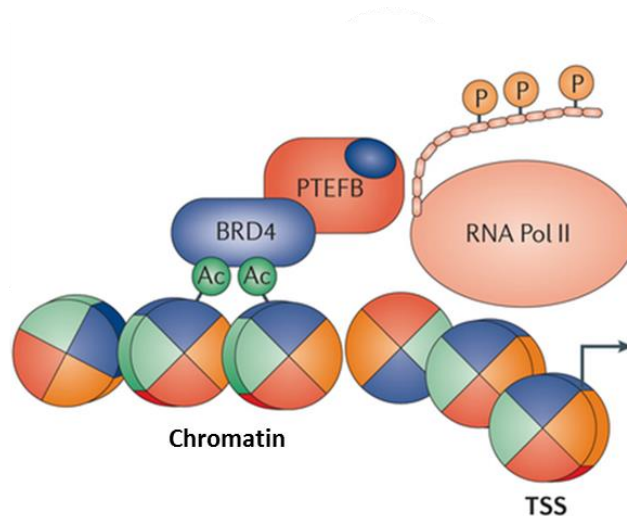
Figure 1.9 Domain Architecture of Human BET Proteins. (A) The functional domain of Brd4 as indicated. ET, extra-terminal domain. CTD, C-terminal domain. Isoform B of Brd4 has a unique C terminus, which interacts with condensin II complexes (Floyd et al., 2013). (B) The illustration of BRD4 at acetylated docking sites resulting mediator complex fusion which initiates a transcriptional programme with strong tumour-promoting properties. The arrows indicate the breakpoints where the gene transcription occur. The positive transcription elongation factor B, PTEFB; RNA polymerase II, RNA Pol II; TSS, transcription start site. Figure adapted form (Filippakopoulos and Knapp, 2014).

The BET subfamily is composed of two tandem BRDs in the N-terminus and a recruitment domain in the C-terminus (Figure 1.9 A). The conserved BET family includes BRD4, BRD2, BRD3, expressed ubiquitously, and BRDT, specifically expressed in the testis (Taniguchi, 2016). The BRD4 protein is one of the most characterised BRD-containing subfamily proteins. The dysfunction of BRD4 proteins was detected to associate with cancer and inflammation (Hongmao, 2016).

To exert its transcriptional modulation, BRD4 firstly recognises acetylated chromatin regions and recruits the positive transcription elongation factor B (P-TEFb) to subsequently stimulate RNA polymerase II-dependent transcription (Figure 1.9 B). BRD4 is found particularly enriched at

enhancer and super-enhancer regions, which strongly stimulates the expression of some oncogenes in cancer (Lamoureux *et al.*, 2014). Importantly, BRD4 have been shown to associate with transcription factors (TFs) including AR, ER and NFkB, and contribute to aggressive types of PC (Urbanucci *et al.*, 2017). Specifically, endogenous BRD4 is found physically interacting with the AR-NTD with a high-binding affinity which leads to transcriptional complex assembly at target loci, and promotes AR activity and expression of target genes in CRPC (Asangani *et al.*, 2014). In addition, a finding by (Zuber *et al.*, 2017) with implications in risk assessment shows that tissue-specific Single Nucleotide Polymorphism (SNPs) in super-enhancer sequence bound by BRD4 are significantly associated with increased prostate cancer incidence.

Moreover, BRD4 is found involved in resistance to anti-androgens. (Pawar *et al.*, 2018) and (Ruggero *et al.*, 2018) found that treatment with the BET inhibitor, JQ1, can effectively re-sensitise resistant tumours to enzalutamide. JQ-1 works downstream of AR and abrogates recruitment of the receptor to cis-regulatory elements resulting in removal of RNA polymerase II from AR target genes, to induce apoptosis and down-regulate AR-regulated gene transcription (Asangani *et al.*, 2014). An additional small molecule BET inhibitor ABBV-075 has been recently shown to inhibit AR-target gene expression by attenuating BRD4 loading at enhancer elements of AR target genes while leaving AR protein level unaffected (Faivre *et al.*, 2017). Taken together, the evidence suggests that BRD4 proteins could be beneficial targets in the development of new therapeutic strategies for antiandrogen resistant PC. In fact, several BET inhibitors (BETi) that interrupt BRD4 chromatin recruitment are being assessed in clinical trials for CRPC (https://clinicaltrials.gov). Furthermore, resistance mechanisms to these agents have been studied in models of PC; a BRD4-independent mechanism identified in a BETi-resistant PC cell line whereby reactivation of AR signalling via CDK9-mediated phosphorylation of AR was found to drive BETi-resistance (Pawar *et al.*, 2018). Furthermore, as a consequence of reduced expression of DNA repair genes in BETi-resistant cells, cells were more highly sensitive to PARP inhibitors indicating therapeutic potential of employing combination therapies for treating CRPC.

1.11. P300/CBP histone acetylation activity associates with progression of prostate cancer.

For the full activity of the AR to be elicited, and for it to be appropriately regulated once bound to target genes, the receptor actively recruits various co-regulator proteins of distinct function to target sites within the DNA. Two well characterised AR co-regulators are cAMP response element-binding protein (CREB)-binding protein (CBP) and p300 histone acetyltransferase (CBP/p300) (Takayama and Inoue, 2013) which function as transcriptional co-activators of the AR via inherent histone HAT activity (Legube and Trouche, 2003).

p300 and CBP, also referred to as CBP/ p300 proteins, share significant sequence homology (Kalkhoven, 2004) and contain several conserved regions that mediate most of the known functional activities of the protein (Figure **1.10** A): including a) three cysteine–histidine (CH)-rich regions (CH1, -2 and -3); b) the CREB binding site, and c) steroid receptor coactivator-1 interaction domain (SID). In addition, p300 and CBP each contain a HAT domain and a bromodomain that binds acetylated lysine. Each domain is connected by long stretches of unstructured linkers which are less conserved (Arany *et al.*, 1994). In fact, CBP/p300 are known as functional paralogs and their HAT domains show sequence identity of more than 90% (Santer *et al.*, 2011)

The functional involvement of the CBP/ p300 HAT activity has been demonstrated to be important in various pathologic processes (Kalkhoven, 2004). One important function of CBP/p300 involves chromatin remodelling, hence the two proteins are essential coactivators for a substantial number of transcription factors. Moreover, CBP/p300 can bind not only to target proteins and regulate DNA binding affinity, transcriptional activation, protein–protein interactions, and stability of transcription factors but also to other cellular proteins by acetylation (Legube and Trouche, 2003).

Recent evidence indicated that the expression of *CBP/p300* is commonly altered in different types of tumours (Kalkhoven, 2004; Culig, 2016). In cancer, the precise role of p300 and CBP is understudied and may depend on the physiological background of the cancers. In addition, although the two protein's functional domains share a high degree of homology similarity, the cellular roles of CBP and p300 were found not to be entirely redundant with unique roles *in vivo*. In fact, p300 was suggested to act as canonical tumour suppressor in breast, colorectal, and pancreatic cancers as p300 is targeted by viral oncoproteins and the mutated or truncated isoform is commonly detected (Santer *et al.*, 2011). In PC, however, the accumulating evidence clearly indicated the oncogenic function of p300 and CBP. Initially, overexpression of CBP/p300 was found associated with the agonistic effects of the anti-androgen hydroxyflutamide in PC cell line (Comuzzi *et al.*, 2003). In clinical specimens of PC, the expression of p300 correlates with the presence of the AR. CBP/p300 were also found may have induced transcription of androgen-dependent genes, even in the absence or very low level of AR. (Comuzzi *et al.*, 2004; Debes *et al.*, 2005; Heemers *et al.*, 2007). Moreover, increased p300 expression upon androgen starvation is crucial for cell survival and growth of prostate cancer cells (Heemers *et al.*, 2007). And in nude mice, CBP/p300 expression are found augmenting transcription of a subset of growth control target gene promoters (Fu *et al.*, 2003).

A
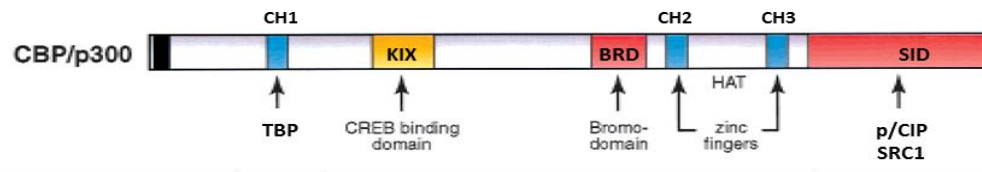
B
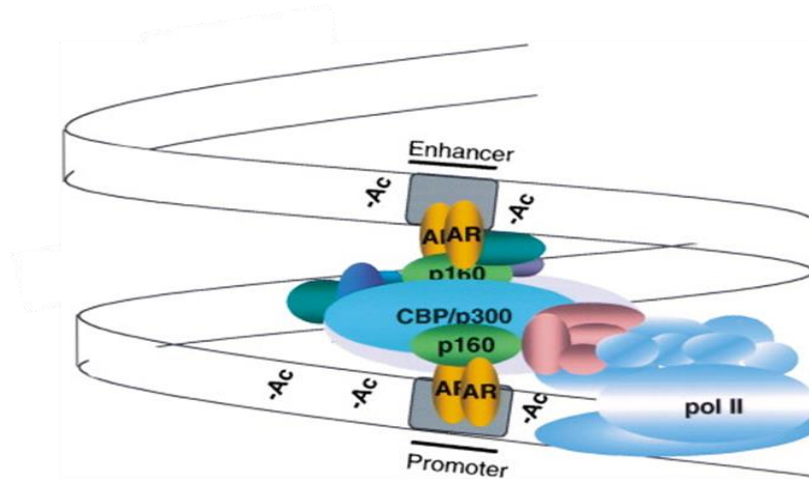
Figure 1.10 Schematic representation CBP/p300 protein Structure of the family and the model of the AR–CBP/P300 Transcription Complex. (A) Linear representation of the CBP/p300 proteins with regions and functional domains that are highly conserved between species indicated. CH1,CH2 and CH3 – three cysteine/histidine rich regions; KIX - the CREB and MYB interaction domain; BRD-the bromodomain, HAT-histone acetyltransferase domain and the p160 binding site (B). Agonist-bound ARs are recruited to both the enhancer and the promoter of the PSA gene. This is followed by a coordinated and ordered recruitment of p160 proteins, CBP, p300, and RNA polymerase II holoenzyme to form the AR transcription complex.

In PC cells, in the presence of agonist ligand, the AR translocates to the nucleus where it binds directly to promoter and enhancer elements of target genes, whereby the CBP/p300 is concurrently recruited alongside other co-regulators, including p160-family members and p300/CBP-associating factor (pCAF) which can interact with the basal transcriptional machinery forming an active transcription complex with RNA polymerase II on the transcription start site (TSS) (Figure **1.10** B, also see Figure **1.2**). The coactivator p300 augments AR activity, in part, via its intrinsic HAT activity (Fu *et al.*, 2003). Besides directly acetylating target lysines within histones H3 and H4, p300 also directly acetylates the AR at a conserved lysine-rich motif within the hinge region (Fu *et al.*, 2003). By inhibiting p300 HAT activity via a newly developed small molecule

p300 HAT inhibitor, C646, decreased cellular proliferation and migration of PC cells were observed (Santer *et al.*, 2011). In addition, by employing a novel CBP/p300 bromodomain inhibitor, a recent study reported the blockage of prostate cancer growth *in vitro* and *in vivo* (Jin *et al.*, 2017).

Taken together, these results suggest that BRD4 and CBP/p300 inhibition may be a promising approach for the development of new anticancer therapies. Importantly, the requirement of BRD4 or CBP/p300 for the activity of the AR_{F876L} mutant in enzalutamide resistance has not yet been studied. To exploit this vulnerability, the role of BRD4 and CBP/p300 activity for the transcriptional activity of the AR_{F876L} and its target gene expression will be studied in details in order to investigate the potential of targeting two co-regulators as a strategy for attenuating AR mutant-driven enzalutamide resistance.

1.12. The novel gene-editing technology is advancing current study tools.

In recent years, several advanced genome editing technologies have been developed. Of these the zinc finger nucleases (ZFNs), transcription activator-like effector nucleases (TALENs), and the Clustered Regulatory Interspaced Short Palindromic Repeats (CRISPR)/Cas9 RNA-guided endonuclease system are the most widely described (Mahfouz *et al.*, 2014). Each of these methodologies takes advantage of restriction enzymes to generate a DNA double stranded break (DBS) at a targeted genome location with the direction of homologous binding proteins or RNA (LaFountaine *et al.*, 2015). Such targeting is viewed as a significant advancement compared to current gene therapy methods that lack such specificity. The precise genome editing methods including the TALENs and CRISPR/Cas9 systems have proved to be effective and reliable tools for genome engineering in multiple disorders, including *in vivo* experiments, in mammals and even early phase human trials (Vassena *et al.*, 2016). Hence, those technologies were named as the methods of the year 'Method of the Year 2011' (2012) by Nature Methods In 2011.

1.13. ZINC finger and TALEN

Back in early 1996, a zinc finger protein domain, which predominantly recognizes nucleotide triplets, was demonstrated for the first time to couple with the FokI endonuclease domain and to act as a site-specific nuclease cutting DNA at strictly outlined sites *in vitro* (Kim *et al.*, 1996). The chimeric sequence-specific zinc finger nucleases (ZFNs) have later demonstrated to enable targeted mutagenesis and genome editing through directed chromosome cleavage (Figure 1.11 A) (Kim *et al.*, 1996). The ZFN-based technology since then has become the basis for editing cultured cells, including pluripotent stem cells, plant and animal models (Bibikova *et al.*, 2002; Townsend *et al.*, 2009; Nemudryi *et al.*, 2014). However, this method has a number of limitations which including the complexity and high cost of protein domains generation for each particular genome locus and lack of specificity of target DNA cleavage due to high tolerance of single nucleotide substitutions or inappropriate interaction between domains (Nemudryi *et al.*, 2014).

To overcome the disadvantages, a transcription activator-like effectors (TALE) protein that contains a modular DNA binding domain was adapted from plant pathogenic bacteria (Bogdanove and Voytas, 2011). TALE proteins code with a central DNA binding domain, a nuclear localization signal (NLS), and a domain that is responsible for activating target gene transcription (Schornack *et al.*, 2006). The DNA-binding domain consist of serval tandem repeats of monomers. The recognition specificity of TALE relies on the monomers within the DNA-binding domain as each of them binds to one nucleotide in the target nucleotide sequence (Lamb *et al.*, 2013). To exert its function *in vitro*, an artificial DNA-binding domain is required inserting into a construction of chimeric TALEN nucleases alongside a nuclear localization signal, half-repeat, N-terminal domain, and the FokI catalytic domain. Theoretically, by combining different monomers within the DNA-binding domain to construct artificial nucleases, the target of which can be any nucleotide sequence.
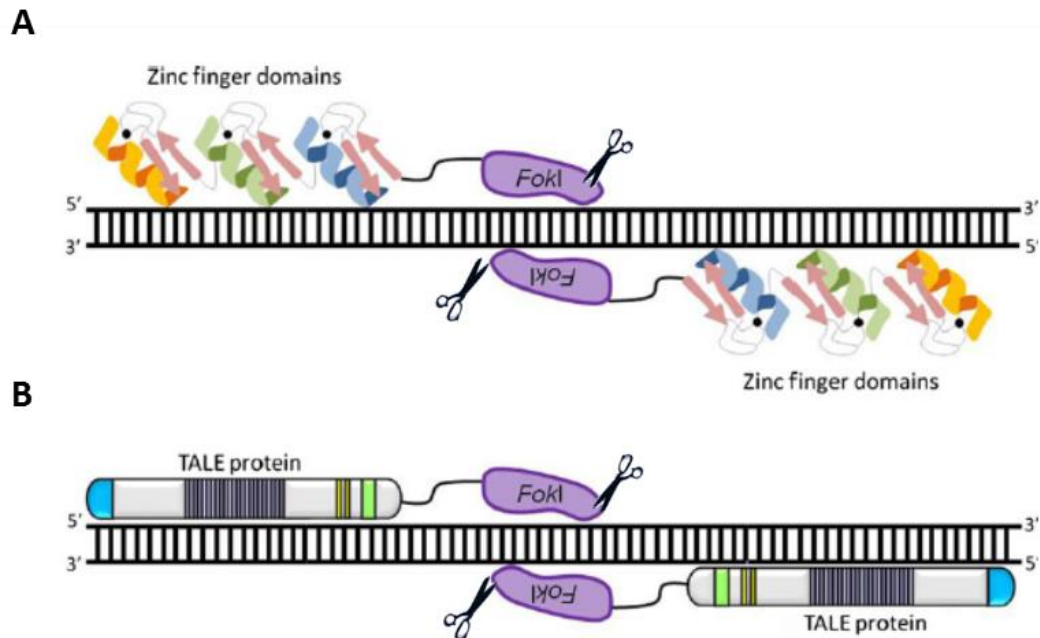
Figure 1.11 Schematic representation of various genome-editing platforms. (A) Zinc finger nucleases finger nucleases (ZFNs) are composed of DNA recognition domains and FokI nuclease catalytic domain fusions. Each zinc finger in the DNA recognition domains binds three nucleotides. On average three to four zinc fingers are fused to recognize 9–12 nucleotides. Two ZFNs are required to produce double-strand breaks (DSB) as the FokI domain requires dimerization to be catalytically active. (B) Transcription activator-like effector nucleases (TALENs) are composed of TAL central DNA-binding repeat domain and FokI catalytic domain fusions. DNA-binding specificity is determined by the 12th and 13th hypervariable residues of each repeat [repeat variable diresidue (RVD)]. Similarly, two TALENs heterodimer binding in a tail-to-tail orientation with proper spacer length to allow dimerization of the FokI domains are required for activity and DSB formation. Image was adapted form (Mahfouz et al., 2014).

Once in the nucleus (Figure 1.11 B), artificial TALEN nucleases bind to target sites: the TAL effector targeting domain direct the catalytic domain of the FokI nuclease function as a fusion protein, as a results, the FokI domains located at the C-termini of a chimeric protein dimerise to cause a DSB in a spacer sequence. A few drawbacks, however, have been realised with this technology, including the size of the actual constructed DNA-binding domains which usually consist of 20–30 selective monomers each with an approximate size 34 amino acid residues (Bogdanove and Voytas, 2011). These constructs are therefore large making delivery into cells challenging. In addition, as FokI functions as a dimer, both Zinc finger and TALENs are designed in pairs in order

to bind opposing DNA target sites separated by a spacer, allowing the FokI monomers to come together to create a DSB (Nemudryi *et al.*, 2014).

1.14. Mechanism and development of CRISPR

Soon after the discovery of the chimeric TALEN proteins, another genome editing technology, CRISPR, elements of which includes a non-coding RNA and a CRISPR associated (Cas) protein, were adapted from bacteria which provides acquired immunity against invading foreign DNA via RNA-guided DNA cleavage (Nemudryi *et al.*, 2014). In 2013, the CRISPR/Cas system was demonstrated for the first time to act as an advanced genetic editing tool in cultured mammalian cells (Cong *et al.*, 2013; Jinek *et al.*, 2013; Mali *et al.*, 2013b). Since then, it has rapidly emerged as a potentially fast and efficient alternative to ZFNs and TALENs for inducing targeted genetic alterations (Gaj *et al.*, 2013).

In general, CRISPR systems have been classified into 6 distinct types (I ~ VI) according to current categorisation of CRISPR–Cas loci (Makarova *et al.*, 2015; Shmakov *et al.*, 2015). Each group utilises a unique set of Cas proteins along with CRISPR RNAs (crRNAs) for CRISPR system activation (Wright *et al.*, 2016). Every group of CRISPR systems act distinctively: the type I and type III systems employ a large multi-Cas protein complex for crRNA binding and target sequence degradation (Wright *et al.*, 2016); in contrast, in the type II CRISPR systems, CRISPR/Cas9, relays a single DNA endonuclease, Cas9, to generate double-strand DNA (dsDNA) substrates. Due to its simplicity and flexibility, the CRISPR/Cas9 system has been wildly implemented as an exquisitely powerful tool for genome manipulation in a wide spectrum of organisms (Hsu *et al.*, 2014).

Two functional domains, the HNH nuclease domain and RuvC-like domain, are critical for Cas9 protein activation (Sapranauskas *et al.*, 2011). In addition, a small non-coding RNA, termed trans-activating crRNA (tracrRNA) is also important for Cas9 recruitment. In the nucleus, tracrRNA base-pairs with a 20 nucleotide (nt) spacer repeat sequence in the crRNA to form a unique dual-RNA hybrid structure (Figure 1.12 A) (Nemudryi et al., 2014). This dual-RNA guide directs Cas9 to cleave any DNA containing a complementary target sequence that upstream of protospacer adjacent motif (PAM) PAM (5'-NGG-3', N - any given nucleotides) (Deltcheva *et al.*, 2011; Jinek *et al.*, 2012). In the presence of Mg2+ ions (Makarova *et al.*, 2011; Jiang *et al.*, 2013), DNA cleavage occurs

with the HNH nuclease domain of the enzyme cutting the DNA strand complementary to crRNA, and the RuvC domain cutting the non-complementary one three nucleotides from the PAM site (Jinek *et al.*, 2012).

In contrast to the other two site-specific nucleases described above, DNA recognition by the CRISPR/Cas9 system is not specified by protein (Chandrasegaran and Carroll, 2016), but rather it relies upon complementarity between the target genome and crRNA sequence (Doudna and Charpentier, 2014). Currently, instead of two non-coding RNAs, a single chimeric sgRNA that combines the crRNA and tracrRNA into a single RNA transcript is often generated to simplify the system while retaining fully functional Cas9-mediated sequence-specific DNA cleavage (Nemudryi *et al.*, 2014). By replacing the guide RNA sequence (spacer) within the crRNA, the simplified two-component CRISPR/Cas9 system can be programmed to target virtually any DNA sequence of interest in the genome and further generate a site-specific blunt-ended DSB (Hsu *et al.*, 2014).

A

Cas9

Protospacer

PAM (Protospacer adjacent motif, NGG)

RuvC

PAM

HNH

crRNA

Linker loop

Spacer

tracrRNA

sgRNA

B

Double-strand break (DSB)

Endogenous DNA repairs at the DSB site

Donor DNA (ssODN or plasmid)

Nonhomologous end joining (NHEJ)

Homology directed repair (HDR)

Small insertion

Small deletion

Substitution

Knocked-in DNA sequence of interest
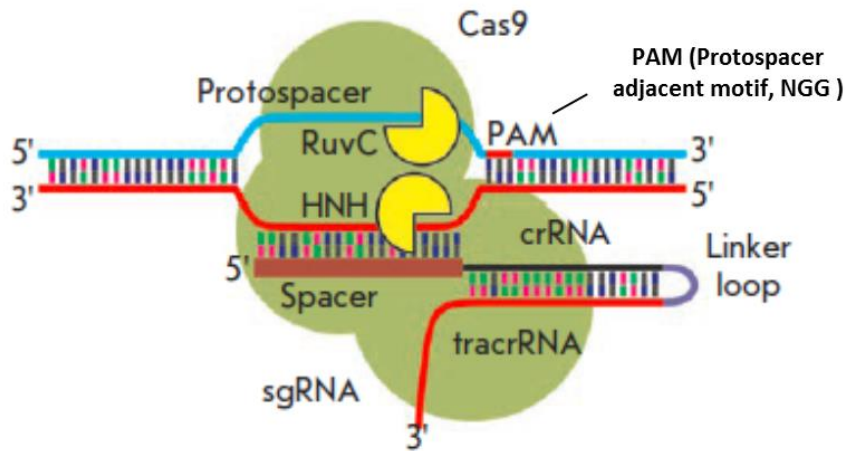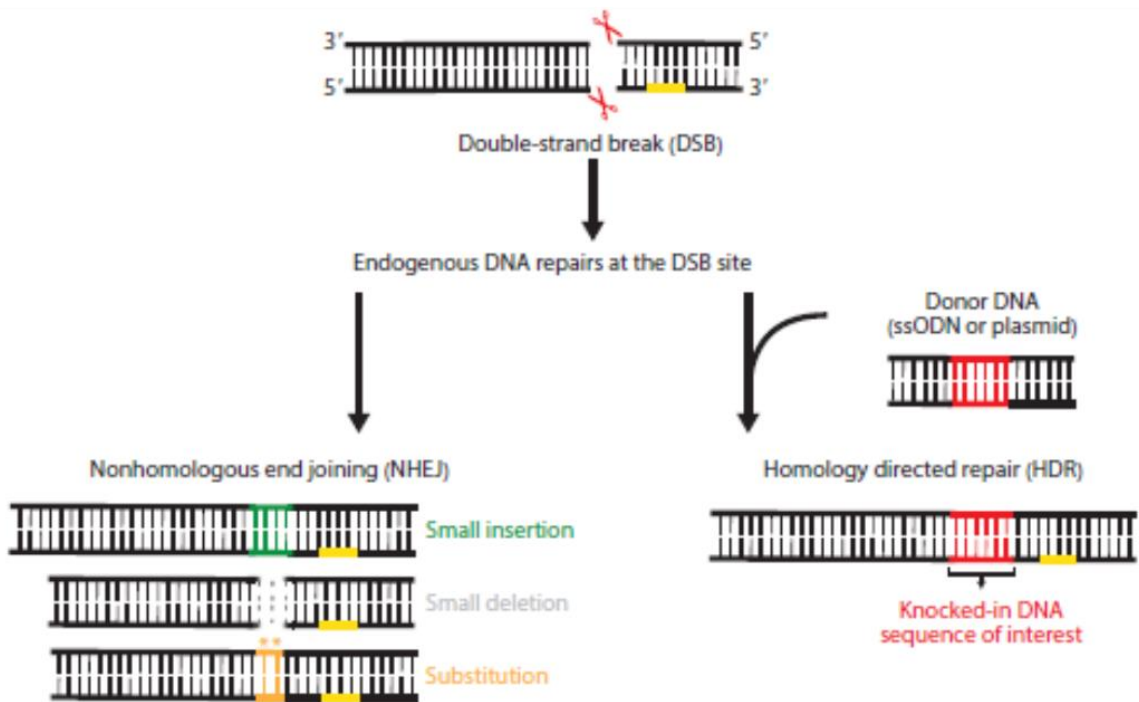
Figure 1.12 Schematic representation of single chimeric sgRNA to introduce double-stranded breaks into the target loci and the application of DNA repair pathway (A) The mechanism of CRIPR/Cas9-mediated genome engineering. A Cas9 endonuclease was guided through the synthetic sgRNA or crRNA–tracrRNA structure to almost arbitrary DNA sequence in the genome via a pre-defined 20-nt guide RNA sequence and subsequently guides Cas9 to introduce a double-strand break (DSB) in targeted genomic DNA. (B) The mechanism utilizing DNA repair pathway for genetic editing application. The Cas9 generated- DSB is repaired by host-mediated DNA repair mechanisms. Upon DSB, the error-prone nonhomologous end joining (NHEJ) pathway is prevalently activated and results random insertions and deletions (indels) or even substitutions at the DSB site, frequently resulting in the disruption of gene function. In the presence of a donor template containing a sequence of interest flanked by homology arms, the error-free homology directed repair (HDR) pathway can be initiated to

The DSB created by Cas9, in turn, activates the cellular DNA repair pathways, which can be harnessed to create specific DNA sequence modifications at or close to the break site (Kim and Kim, 2011). In nearly all cells, DSBs are repaired by one of two highly conserved processes, non-homologous end joining (NHEJ) and homologous recombination (HR) (Figure 1.12 B). For the NHEJ pathway, the broken genome site/chromosome is often rejoined imprecisely which commonly results in small insertions or deletions at the break site that can be exploited to interrupt gene function. Alternatively, HR occurs in the presence of DNA repair template, the DNA surrounding the cleavage site can be used for introducing foreign DNA. The sequence of the repair template can be designed or manipulated to replace with specific mutations or to insert additional sequences. Due to the flexibility of donor choice, a defined locus with desirable features (including restriction enzyme digestion sites, ectopic fusion tags, or selection markers) can be modified by incorporating these features with a piece of foreign homologous sequence. Either plasmid construct or synthesised DNA fragment can be employed as the donor template (Ran *et al.*, 2013). In general, the plasmid donor can be used when long insertions need to be incorporated (Beumer *et al.*, 2013; Beumer and Carroll, 2014). In comparison, for small insertions or deletions, single-stranded DNA (ssDNA) is preferred (Beumer and Carroll, 2014).

1.15. Application of CRISPR

Comparing to the ZFN and TALEN based methods, the CRISPR/Cas9 system is much easier to conduct as it can be directly portable to human cells by co-delivery of plasmids expressing the Cas9 endonuclease and the necessary crRNA components (Perez *et al.*, 2008; Chen *et al.*, 2011; Valetdinova *et al.*, 2015). CRISPR/Cas9 system is more efficient, as it is suitable for high-performance and multiplex genome editing by generation of CRISPR/Cas9 libraries (Nemudryi *et al.*, 2014) which allows one to perform functional screening of genomes. High-throughput

screens of CRISPR/Cas9 libraries may yield important information about the physiology and biochemistry in a variety of cell lines and in living organisms and could help uncover the molecular mechanisms of disease development and identify potential targets for drug and gene therapy (Lino *et al.*, 2018). CRISPR/Cas system is also more fixable as it the can be redefined to cleave virtually any DNA sequence by only replacing the 20-nt guide sequence of sgRNA. In fact, the programmable RNA-guided DNA endonucleases have demonstrated multiplexed gene disruption capabilities (Cho *et al.*, 2013) and targeted integration in induced pluripotent stem (iPS) cells (Cong *et al.*, 2013). In addition, CRISPR–Cas9 RNA-guided DNA targeting can also be uncoupled from cleavage activity by mutating the catalytic residues in the HNH and RuvC nuclease domains which converting DSB into nickases (Cho *et al.*, 2013), enabling an additional level of control over the mechanism of DNA repair. Making CRISPR/Cas9 system a more versatile platform for many other applications beyond genome editing.

CRISPR/Cas9 technology has been applied in numerous experimental settings to help: development of isogenic human stem cells (Horii *et al.*, 2013); methods to correct a mutant cell phenotype (Schwank *et al.*, 2013), studies of gene expression regulation (Bikard *et al.*, 2013; Farzadfard *et al.*, 2013; Gilbert *et al.*, 2013; Heintze *et al.*, 2013; Perez-Pinera *et al.*, 2013); functional relationships between large groups of genes (Shalem *et al.*, 2014; Wang *et al.*, 2014); and imaging regions of the active genome regions in living cells (Chen *et al.*, 2013). In addition to human cells, CRISPR/Cas-mediated genome editing has been successfully demonstrated in zebrafish (Hwang *et al.*, 2013) and bacterial cells (Jiang *et al.*, 2013).

Of particular note, the CRISPR/Cas9 system has opened new avenues for cancer research (Zhan *et al.*, 2018) as it has been employed as an effective technique for functional oncogene scanning in both *in vitro* and *in vivo* cancer models (Zhang *et al.*, 2017b). In particular, the use of genome-editing systems enables potential correction of cancer-causing point mutations in the cells obtained from patients by using both complex genetic constructs and single strand DNA oligonucleotides as donor molecules (Yang *et al.*, 2013b). Significantly, the very first clinical trial of applying CRISPR is now approved for therapeutic anti-cancer (Zhan *et al.*, 2018).

Chapter 2: Aims

The current commonly adopted method for studying AR mutant function is by transiently transfection of AR-encoding plasmids into AR null cells and therefore lacks physiological relevance. By incorporating the next-generation genomic editing strategies, we therefore aim to generate CRISPR-edited LNCaP and CWR22Rv1 cell lines expressing enzalutamide-activated AR_{F876L} mutant. In addition, this project will attempt to assess the function of enzalutamide-activated AR_{F876L} in cell line models and interrogate if BRD4 and CBP/p300 plays a part in controlling its activity. Overall, two main aims of this project are:

i. Generation and validation of an AR_{F876L} CRISPR model system, enabling a more physiological model of aberrant AR activity.

ii. Generation of an AR_{F876L} replacement model, using the LNCaP cell, enabling an enhanced understanding of the molecular mechanisms of enzalutamide resistance.

iii. Conduct global gene analysis, using an LNCaP_AR_{F876L} model, to define the AR_{F876L} global transcriptome and cistrome.

iv. Interrogate the involvement of BRD4 and CBP/p300 for AR_{F876L} transcriptional competence to offer new insights into discriminate functionality and opportunities for selective drug targeting of enzalutamide resistance-associated AR mutants.

Chapter 3: Methods and Materials

3.1 General expression plasmids and primers,

The following plasmids were used for mammalian cell transfection: wild-type pVP16-AR-TD, wild-type pM-Gal4DBD-AR-DBD/LBD, pCMV-FLAG-AR (full length), pCMV-FLAG-ARF23A/F27A (full length), pGAL4AR- Luciferase reporter, (TATA) Luciferase-ARE reporter plasmid and pCMV-β-gal and have been reported previously (Gaughan et al., 2005). All primers and siRNA were pushed form Sigma-Aldrich unless stated otherwise.

3.2 Bacterial transformations and plasmid preparation

For each transformation, 1 µg of sample plasmid was added to 25 µl of E.coli Top 10 competent cells (Invitrogen) incubated on ice for 30 minutes, then heat-shocked at 42°C for 30 seconds and immediately placed on ice for 2 minutes. 500 µl of Luria bertani (LB) medium was then added and incubated at 37°C with rotary shaking at 220 rpm for 1 hour. After incubation, 100 µl of the cell sample and competent cells only (as transformation control) was plated onto LB-agar plates containing ampicillin (50 µg/ml) and incubated at 37°C overnight. Resultant clones were transferred into 10 ml LB containing ampicillin (50 µg/ml) and incubated for approximately 8 hours or overnight with rotary shaking. A 2 ml aliquot cell suspension was then transferred to 200 ml LB ampicillin medium and incubated at 37°C overnight with rotary shaking. Cells were then harvested the following day by centrifugation at 4500 rpm at 4oC for 15 minutes and pellets were subject to prep or stored at -20°C.

Plasmid Maxi Prep kits (QIAGEN and Life Sciences) were used for plasmid prep, according to the manufacturer's protocol. Prepped plasmids were eluted with molecular grade H_2O and concentration/purity measured using a Nanodrop ND-1000 spectrophotometer (Thermo Scientific) prior to storage at -20°C.

3.3 Site- directed mutagenesis

All site-directed mutagenesis was conducted using the QuikChange II Site-Directed Mutagenesis

Kit (Stratagene), according to the manufacturer's protocol. Mutagenesis primers were designed manually (sequences listed in Table 3.2) and mutations verified by Sanger sequencing (Beckman Coulter Genomics, UK). Mutated AR coding sequences were cloned into the pLVx vector (Clontech). PCR reaction for Site-Directed Mutagenesis was set up as below:

Denaturation step: 95°C, 30 seconds;

Annealing step: 55°C, 1 minute;

Extension/elongation step: 68°C 1minute/kb for 18 cycles.

Mutant plasmids were then transformed into XL1-Blue supercompetent cells (Stratagene) according to the manufacturer's protocol.

3.4 Primers

Table 3.1 The list of all the general primers used in this thesis.

AR mutation	Forward Primer	Reverse Primer
FLAG AR_F876L	5' - AGAGAGCTGCATCAGTTCGCTTTTGACCTGCTAATC	5' - GATTAGCAGGTCAAAAGCGAACTGATGCAGCTCTCT

3.5 Mammalian cell culture and passage

All tissue culture media and supplements used were supplied by Sigma-Aldrich and plasticware and plates were purchased from Corning (Corning Ltd, UK).

Full medium or 10%FCS medium — Gibco® RPMI 1640 (R5886) medium (containing 25mM HEPES buffer and 1% 20mM L-Glutamine) supplemented with 10% heat-inactivated fatal calf serum (FCS).

DCC media — Gibco® RPMI-1640 +1% L-glutamine + 10% dextran-coated charcoal treated FCS

that contains reduced levels of androgens and is used for AR inactivation/reactivation studies.

Basal media — Gibco® RPMI 1640 (R5886) supplemented with 25mM HEPES buffer and 1% L-Glutamine (20mM).

Cells were grown at 37°C in the presence of 5% CO_2 and passaged every 3-4 days (upon reaching 80% cell confluence). For each cell passage, 5 ml phosphate-buffered saline (PBS) was used to wash adherent cells twice prior to addition of 1x Trypsin-EDTA solution (10% volume of cell medium) and incubation at 37°C for 5 minutes. Cells were then mixed with full medium to neutralise trypsin and collected by centrifugation at 2000 rpm for 5 minutes. A 10 ml volume of fresh full medium was used to resuspend the cell pellet and 1ml of resultant cell suspension was transferred to a fresh flask continuing culture with an appropriate volume of full media.

3.6 Transient plasmid DNA transfection

In general, an appropriate number of cells were plated in DCC medium, unless otherwise stated, and transfection performed on the following day. For transfection reaction preparation, DNA was diluted in basal medium and TransIT-LT1 (Mirus) transfection reagent was added, according to the manufacturer's guidelines, and mixed completely by gently pipetting up and down. After incubation at room temperature for 30 minutes, transfection mixes were added drop-wise to different areas of the wells and gently rocked back-and-forth and side-to-side to evenly distribute the DNA-LT-1 complexes. Cells were incubated for an additional 48 hours at 37oC in the presence of 5% CO2 before harvesting and analysis as required.

3.7 Construction of lentiviral expression vectors

A lentiviral-based transduction strategy was chosen to generate an LNCaP cell line derivative that stably expresses AR_{F876L}. This requires initially generating a recombinant mammalian lentiviral construct containing AR_{F876L} cDNA which will be used to transduce LNCaP cells. To this

end, the F876L point mutation was induced into the pCMV-Flag-AR plasmid, containing FLAG-tagged ARwt (O'Neill et al., 2015), by mutagenesis (QuikChange II Site-Directed Mutagenesis Kit, Thermo Scientific) according to manufacturer's recommendations. Once verified, AR_{F876L} cDNA was amplified by PCR using the primers list in Table **3.1** and then ligated into pENTR-V/TOPO vector (Life Sciences). Recombinant vectors were selected and incorporated into an LR recombination reaction (Life Sciences) with pLenti6.3 plasmid to generate the pLenti-6.3-Flag-AR_{F876L} construct. Successful recombinant constructs were subject to maxiprep (PureLink™ HiPure Plasmid Filter Purification Kits, life Technologies) and stored at -20°C as stock.

3.8 Virus production and titre determination

pLenti6.3-Flag-AR_{F876L} or Cas9/sgRNA196- containing virus was produced using ViraPower™ Lentiviral Expression System (Life Technologies) according to the manufacturer's recommendation. HEK293FT cells (life Technologies, UK) were cultured with complete medium containing 500 µg/ml Geneticin for 3 passages pre-virus transductions. The lentiviral expression plasmids were produced as described in (O'Neill *et al.*, 2015).

3.9 SDS-polyacrylamide gel electrophoresis (SDS-PAGE) and Western blotting

Protein expression in mammalian cell culture was assessed using Western blotting. Prior to analysis, cells were seeded in 6 well-plates containing 2 ml 10% DCC medium. After 48 hours of 500 ng vector per well transfection, cells lysates were collected from culture wells by directly adding 100 µl SDS sample buffer (100 mM dithiothreitol, 125 mMTris-HCl (pH 6.8), 2% SDS, 20% glycerol and 0.005% bromophenol blue) post PBS wash to lyse cells.

Lysates was denatured at 100°C for 10 minutes before loading onto a 10% polyacrylamide gel according to manufacturer's recommendations (Mini-PROTEAN III system, Bio-Rad, UK). Fermentas Spectra™ Multicolor Broad Range Protein Ladder (ThermoScientific Pierce, UK) was used to determine protein size.

Table 3.2 The list of all the general antibodies used in this thesis.

Antibody	Species	Supplier	Applications	WB Exposure time
AR (N-20) (sc-816)	Rabbit	Santa Cruz	WB, IP, ChIP	< 1 min
AR (C-19) (sc-815)	Rabbit	Santa Cruz	WB, IP, ChIP	< 1 min
AR-V7 (ab198394)	Rabbit	Abcam	WB, IP	< 20 min
PSA (2E9)	Mouse	Kind gift from Kim Pettersson	WB	<10 min
α-tubulin (T9026)	Mouse	Sigma Aldrich	WB	< 10 secs
FLAG-tag	Mouse	Sigma Aldrich	WB, IP, ChIP	< 1 min
P300	Mouse	abcam	WB, IP, ChIP	< 1 min
GR (G-5)	Mouse	Santa Cruz	WB	< 10 min
Rabbit IgG	Rabbit	Diagenode	IP, ChIP	N/A

3.10 Cytoplasmic and nuclear extract preparation

Cells were seeded in DCC medium at a density of 1.5x105 per well in 6-well plates for 24 hours. 500 ng of pLenti6.3-AR constructs per well were transfected for 48 hours and subsequently treated with 10 nM DHT or 1 μM enzalutamide. Cells were then trypsinised, washed in PBS and pelleted. Cytoplasmic and nuclear fractionation was carried out on cell pellets using the NE-PER Nuclear and Cytoplasmic Extraction Reagents Kit (Catalog #40010 & 40410, Thermo Scientific) according to manufacturer's protocol.

Briefly, cells were pelleted by centrifugation, resuspended in 500 µl Hypotonic Buffer, and incubated for 15 minutes on ice. 25 µl of CER II buffer was added and the sample was vortexed for 10 seconds at the highest setting. The cell lysate was subject to centrifugation for 30 seconds at 14,000×g at 4°C and the supernatant (cytoplasmic fraction) was transferred into a microcentrifuge tube and stored at -80°C until needed. The nuclear pellet was resuspended in 50 µl NER buffer and subjected to vortexing for 10 s, incubated for 30 minutes on ice, and centrifuged for 10 minutes at 14,000×g at 4°C. The supernatant (nuclear fraction) was transferred into a microcentrifuge tube and stored at −80°C. Subcellular fractions were analysed by western blotting.

3.11 Immunofluorescence

An appropriate number of HEK293T cells were seeded on glass coverslips in 6-well tissue culture vessels and allowed to adhere for 48 hours. Following drug treatments, cells were fixed with 2 ml paraformaldehyde (2% v/v) per well overnight at 4oC. Cells were then washed twice in PBS and permeablised with 0.1% Triton-X-100 in PBS for 15 minutes. Cells were blocked in 2 ml, 0.1% Triton-X-100/ 4% BSA per well for 1 hour at room temperature before being incubated with an anti-AR antibody (N20; 1:50 dilution) in 1 ml blocking solution overnight at 4oC. Cells were then washed 3x with PBS before being incubated with secondary Alexa Fluor 594 antibodies (1:200 dilution) (Life Technologies) for 1 hour at RT. Excess antibody was removed by washing twice with PBS and coverslips were mounted to glass slides with DAPI (vectorshield) and visualised using a Leica DMR fluorescent microscope.

3.12 Co-immunoprecipitation sample preparation

Pre-prepared cultured cells were trypsinised and collected following 3 ice-cold PBS washes. Cell samples were spun down at 13,000g for 5 minutes. Pellets were subject to IP sample preparation (or snap freezing at -80 ℃). Each cell sample was lysed with 1ml of fresh made IP lysis buffer: 50 nM Tris, 150 mM NaCl, 0.2mM of Na3VO4, 0.5% NP-40, 1mM of PMSF, 1mM DTT and a protease inhibitor tablet (Roche Applied Science) adding dH2O to a final volume of

10ml. Samples were then incubated on ice for 1 hour (or overnight until lysis was complete). 50µl aliquot of each sample was transfer into a fresh tube to act as inputs and stored at -20°C.

To prepare Protein G-sepharose (PGS) beads, 700 µl of PGS (GE Healthcare) was spun at 1,400g for 3 minutes and supernatant discarded. Then, 500µl IP lysis buffer was added and thoroughly mixed using a vortex-mixer. Beads were then spun at 1,400g for 3 minutes. The wash step was repeated a further 2-3 times. After final supernatant removal, fresh IP lysis buffer was added to reach an overall volume of 700µl. The pre-prepared beads were then stored on ice.

Each completely lysed IP samples were centrifuged at 4°C 1,400g for 3 minutes. Supernatants were transferred into a fresh tube and added with 20 µl of fresh prepared PGS and rotated at 4°C for 1 hour to remove any proteins that interacted non-specifically with PGS. After spinning down at 13,000g for 3 minutes, per-cleared supernatants were split into two fresh tube and incubated with antibody and appropriate isotype IgG control at 4°C overnight. Additional 20 µl of PGS was added into each tube the following day, and incubated at 4°C for 1 hour. PGS-protein complexes were collected by centrifugation at 13,000g for 3 minutes and then washed in 1 ml buffer A (PBS, 350 mM NaCl, 0.1% NP-40) and 1 ml buffer B (PBS, 350 mM NaCl). The final PGS (including corresponding inputs) were diluted with an appropriate volume of SDS sample buffer and subjected to western blotting as described above to analyse the protein-**protein interaction of interest.**

3.13 Cell proliferation assays

To investigate the effect of each anti-androgen on cell proliferation, an appropriate density of cells (~3000 cells / well) were seeded into each well of a 96-well plate at a volume of 90 µl growth medium using an Eppendorf Repeater Stream pipette. Cells were allowed to adhere for 24 hours before being treated with 10 µl of a pre-diluted 10 nM DHT or anti-androgens stock, bringing the final volume to 100 µl/well with desired drug concentration. Cells were incubated with compound for 7 days. Each well surface coverage is measured in real-time (every 6 hours) using the Inucyte Zoom (Essen Bioscience) and later analysed using the Basic Analyzer Software (Essen

Bioscience). Analysis parameters were implemented to eliminate the detection of dead cells when quantifying the confluence.

3.14 RNA extraction, reverse transcription and real-time quantitative PCR

3.14.1 RNA extraction

TRIzol (Life Technologies) was used for extracting RNA from prepared cells according to the manufacturers' instruction. In short, culture medium were removed from each well (typically 6-well plates), before washed twice with 2 ml PBS/per well. To harvest cell samples, 1 ml TRIzol was directly added on top of each well and shaken gently for 10 minutes at room temperature. The homogenised samples were transferred into 1.5 ml Eppendorf tubes and 200 μl of chloroform (Sigma Aldrich) was added into each tube before shaking vigorously. Samples were incubated at RT for 3 minutes allowing phase separation, before centrifugation at 12,000g for 15 minutes at 4°C. The aqueous phase (clear upper layer) were transferred to a fresh tube and mixed with 500 μl of isopropanol (Fisher Chemicals) and incubated at RT for 10 minutes before centrifugate at 12,000g for another 10 minutes at 4°C. The supernatant was removed and the visible RNA pellet was washed with 75% ethanol in nuclease-free water (Life Sciences, Invitrogen) and centrifugate at 7,500 g for 5 minutes at 4°C. The ethanol wash was then discarded and the RNA pellet was air-dried for approximately 10 minutes. RNA was resuspended in 30 μl of DEPC-treated H_2O before incubation at 55°C for 10 minutes. Quantification of RNA samples was determined using a Nanodrop spectrophotometer (Thermo Scientific). RNA samples was subject to reverse transcription (see below) or kept at -80°C for long-term storage.

3.14.2 RNA reverse transcription

To reverse transcribe mRNA to cDNA, moloney murine leukaemia virus reverse transcriptase (M-MLV RT) (Promega) was used according to the manufacturer's protocol. Briefly, 1 μg RNA of each sample was diluted with DEPC H2O to a final volume of 12.7 μl. For each sample, a RT cocktail

mastermix was prepared as list in Table 3.1. Diluted RNA was briefly incubated at 65°C for 5 minutes to reduce RNA secondary structure. The RNA sample and pre-pared cocktails were mixed and incubated at 37°C for 2 minutes before combining into one tube.

Table 3.3 A table outlining the reagent mix for 1µgRNA reverse transcription reaction

Component	Volume
5x M-MLV reaction buffer	4µl
Free dNTPs	2µl
Oligo-dT	1µl
M-MLV enzyme	0.3µl
Total volume	7.3µl

Combined sample were incubated at 37°C for 1 hour after which the samples were transferred to 95°c for 2 minutes to inactivate the M-MLV enzyme. Addition of 80 µl DEPC treated H_2O was added into each complete cDNA samples. cDNA samples were further analysed by RT-PCR or stored at -20°C until used.

3.14.3 PCR Quantitative real-time polymerase chain reaction (qPCR)

The gene expression was quantified by subjecting cDNA samples to qPCR using SYBR Green I Dye (Life Technologies) in 7900HT Fast Quantitative real-time PCR (qPCR) system (Applied Biosystems). PCR reaction was carried out using the 384-well plate ABI 7900HT thermocycler (Applied Biosystems). For each well, 8 µl of reaction cocktail (Table 3.4) with appropriate primers were added first, and 2 µl of pre-prepared cDNA sample were added manually into each well. In

addition, a standard curve was employed using a serial dilution of a sample known to express the gene of interest and included 5 dilution data points: 10%, 5%, 2%, 1%, 0.5% and H2O only was included as negative control. A list of PCR primers used can be found in section Table 2.5 Table 2.6 Table 6.1 and Table 6.2.

Table 3.4 A table outlining the reagent mix per RT-PCR reaction

Component	Volume/well
SYBR Green I Dye	5µl
dH$_2$O	2.2µl
Forward primer	0.4µl
Reverse primer	0.4µl
Total volume	8µl

The following PCR conditions was used for sample analysis: 95oC for 10mins, 95oC 15 seconds, 60oC 1 min for 40 repeats or stored at -20oC. The data was analysed using Sequence Detection System software (SDS) version 2.3 (Applied Biosystems).

Table 3.5 primers used for gene expression validation in q-PCR.

Gene	Forward primer sequence (5'-3')	Reverse primer sequence (5'-3')
PSA	GCAGCATTGAACCAGAGGAG	AGAACTGGGGAGGCTTGAG
TMPRSS2	CTGCTGGATTTCCGGGTG	TTCTGAGGTCTTCCCTTTCTCCT
KLK2	AGCATCGAACCAGAGGAGTTCT	TGGAGGCTCACACACCTGAAGA

AR-FL	AAGAGAAGTACCTGTGCGCC	TTCAGATTACCAAGTTTCTTCAG
HPRT1	TTGCTTTCCTTGGTCAGGCA	AGCTTGCGACCTTGACCATCT

Data acquired was analysed using Sequence Detection System (SDS) software version 2.3 (Applied Biosystems). Relative quantities for each gene of interest was calculated from the standard curve generated, these values were subsequently normalised using the relative quantity HPRT1 gene expression values for each sample.

3.14.4 Chromatin Immunoprecipitation

The protocol for chromatin immunoprecipitation (ChIP) assays was optimised from (Schmidt *et al.*, 2009) and typically consists of six steps: cell fixation via formaldehyde cross-linking, chromatin preparation and sonication, dynabeads preparation and immunoprecipitation, elution/cross-link reversal and protein digestion, DNA purification and DNA quantification. To prepare each ChIP assays, $3x10^6$ cells were seeded using 150 mm tissue culture dishes with the appropriate media and the treatment were conducted as indicated.

3.14.5 Cross-linking fixation

The cross-linking buffer was prepared as below: 50mM HEPES-KOH (pH7.5), 100 mM NaCl, 1 mM EDTA, 0.5 mM EGTA and 11% formaldehyde. Prepared cells were fixed by directly adding 10% volume of cross-linking buffer on top of culture media and incubated at room temperature for 10 minutes. 10% volume of 1.25 M glycine was added to quench additional cross-linking reaction by incubated at RT for 7 minutes before discarding all medium. To harvest cells, ice-cold PBS was used to wash cells twice prior to cell collection by scraping into 2 ml ice-cold PBS containing protease inhibitor cocktail (Roche) and transferred into a pre-chilled 15 ml falcon tube. The cell suspension was centrifuged at 2000g for 5 minutes at 4°C. The supernatant was discarded and the cell pellets was collected for chromatin preparation or were snap frozen with liquid nitrogen and placed at -80 °C for long-term storage.

3.14.6 Chromatin preparation and sonication

Fresh cell pellets (or snap frozen pellets thawed on ice first) were suspended using 10 ml pre-prepared LB1 buffer: 50 mM HEPES-KOH (pH 7.5), 140 mM NaCl, 1 mM EDTA, 10% glycerol, 0.5% NP-40, 0.25% Triton-X-100. Cell suspensions were rocked gently on ice for 5 minutes before centrifugation at 4°C for 5 minutes at 2,000 x g. The supernatant was discarded before adding 10 ml of LB2 buffer: 10 mM Tris-HCl (pH 8.0), 200 mM NaCl, 1 mM EDTA, 0.5 mM EGTA. Cell samples were gently rocked on ice for second 5 minutes then centrifuged at 2,000g for 5 minutes at 4°C to pellet cell nuclei. These were then resuspended in 400 μl of LB3 buffer: 10 mM Tris-HCl (pH 8.0), 100 mM NaCl, 1 mM EDTA, 0.5 mM EGTA, 0.1% Na-deoxycholate, 0.5% N-lauroylsarcosine. Each sample was split equally into 2 Eppendorf tubes prior to sonication.

A Bioruptor with regulated cooling system (Diagenode) was used to sonicate nuclear fractions on the 'high' setting for 30 minutes using cycles of 30 seconds on, 30 seconds off at 4°C. The sonicated samples were centrifuged at 11,000g for 10 minutes at 4°C in order to remove nuclear debris. The supernatant was transferred to new tubes before using a Nanodrop (Thermo Scientific) to quantify DNA concentration.

3.14.7 Dynabead preparation and Immunoprecipitation

40 μl magnetic dynabeads (Life Technologies) was used for each immunoprecipitation sample. To prepare dynabeads, 700 μl of syringe filtered 0.5% BSA in PBS was used to wash 3 times. For each sample, 2 μg of appropriate primary antibody was added into beads preparation buffer and were incubated for at least 6 hours on a rotating wheel at 4°C.

For each sample, 100 μg aliquot of chromatin was diluted in LB3 buffer containing 1% Triton X-100 a final volume of 700 μl. Samples were mixed and a 10% volume of LB3 buffer-containing chromatin sample was isolated as 'inputs' samples and stored at -20°C. The primary antibody incubated dynabeads were collected by discarding bead preparation buffer and the remaining 630 μl of chromatin/LB3 samples were added and incubated for 16 hours at 4°C with rotation.

3.14.8 Cross-link reversal

Following immunoprecipitation, the beads were collected magnetically and chromatin/LB3 solution was removed. RIPA buffer (50 mM HEPES-KOH, pH7.5, 500 mM LiCl, 1 mM EDTA, 1% NP40, 0.7% Na-deoxycholate) was used to wash beads 5 times and 1xTBS was used for the last wash. Dynabead/DNA complexes were incubated with 200 µl elution buffer (50 mM Tris-HCl, pH 8.0; 10 mM EDTA; 1% SDS) to elute DNA. The inputs samples were also processed in elution buffer in parallel. All samples were incubated at 65°C with gentle mixing every 5 minutes for the first 15 minutes. Following this, the samples were left to incubate for 8 hours.

3.14.9 Protein digestion and DNA purification

Following the cross-link reversal, 200 µl TE buffer (pH8) and 4 µl of proteinase K (Qiagen) was added into all samples and incubated at 55 °C for 1 hour to degrade proteins. Finally, the GenElute™ Mammalian Genomic DNA Miniprep Kit (Sigma Aldrich) was employed to elute DNA according to the manufacturer instruction.

3.14.10 Quantification of protein enrichment by QPCR.

Resultant DNA was measured by quantitative PCR (see section 3.14.3) using appropriate primers in Table **3.5** and Table **6.1**. The data was analysed using the percentage input method, as this includes normalisation for background recruitment and the amount of chromatin added.Data was calculated as % Input using Ct (cycle threshold) values attained from the qPCR in the following equation: % Input=$100 \times 2^{((\text{Input Ct-3.2})-\text{IP Ct})}$. Data was subsequently presented as fold change of % Input between different experimental arms.

Table 3.6 Primer sequences of specific androgen response elements of target genes

DNA element	Forward primer sequence (5'-3')	Reverse primer sequence (5'-3')
PSA ARE I promoter	CCTAGATGAAGTCTCCATGAGCTACA	GGGAGGGAGAGCTAGCACTTG

PSA ARE III enhancer	TGGGACAACTTGCAAACCTG	CCAGAGTAGGTCTGTTTTCAATCCA
TMPRSS2 ARE enhancer	TGGTCCTGGATGATAAAAAAAGTT	GACATACGCCCCACAACAGA
Control AR exon I	GTGCTGTACAGGAGCCGAAG	AACTTCACCGAAGAGGAAAGG

Chapter 4: Generation of CRISPR-edited PC model.

4.1 Introduction

In the past 5 years, a novel 'gene-editing' technique, the prokaryotic type II CRISPR/Cas9 (clustered regularly interspaced short palindromic repeats/CRISPR-associated) system of viral defense in bacteria, has emerged that enables scientists to manipulate and interrogate genes of interest in a wide range of model systems. The general CRISPR system contains two modules: a CRISPR RNA (crRNA) module that specifies the target DNA sequence, and a CRISPR associated (Cas) endonuclease module that cleaves double-stranded DNA. The *S. pyrogenes* type II CRISPR system is the most studied and wildly used genetic editing tool of all CRISPR types. Functional analysis revealed the constitute CRISPR type II activity requires three components: the Cas9 endonuclease, a target specific crRNA, and a structural trans-activating CRISPR RNA (tracrRNA) (Jinek *et al.*, 2012). This system was further simplified by fusing the crRNA and tracrRNA to form a single guide RNA (sgRNA).

The CRISPR/Cas9 system has recently been adapted for genome engineering in many organisms including zebrafish (Hwang *et al.*, 2013; Xiao *et al.*, 2013), mouse (Wang *et al.*, 2013; Yang *et al.*, 2013a) and Drosophila (Bassett *et al.*, 2013; Gratz *et al.*, 2013; Kondo and Ueda, 2013; Ren *et al.*, 2013; Yu *et al.*, 2013; Sebo *et al.*, 2014). This core methodology of CRISPR/Cas9 relies upon an engineered sgRNA to direct and enable Cas9-mediated endonuclease double-strand DNA cleavage at a specific genomic locus. The resultant DNA break is recognized by the host cell's surveillance machinery and triggers the process of DNA repair via two cellular mechanisms: non-homologous end-joining (NHEJ) and homologous recombination/homology-directed repair (HDR); both of which can be exploited for genome editing. NHEJ is an imprecise/ error-prone process that, through the activity of Ku70/ 80 heterodimer and DNA-dependent protein kinase catalytic subunit (DNA-PKcs) (Tomkinson *et al.*, 2013), results in small insertions and deletions (Indels) of DNA at the site of cleavage. In the context of genome editing, CRISPR utilizes this mechanism of DNA repair to irreversibly compromise the integrity of the targeted locus and effectively introduce gene knockouts in mammalian cells. By designing sgRNA targets at open

reading frames, CRISPR/Cas9 is recruited to the desired gene region where cleavage occurs and subsequent repair by NHEJ results in indels that often cause frame-shifts in the target gene. This leads to either the production of a non-functional, truncated protein or the degradation of mutant mRNA through non-sense mediated mRNA decay. Whereas RNA interference (RNAi) rarely achieves complete silencing, CRISPR/Cas9 can generate genuine gene knock-out models.

Additionally, CRISPR/Cas9 is utilized for precision genome engineering through enrollment of the HDR pathway to facilitate mutations, precise deletions and insertions. By supplying the cell with a donor DNA sequence homologous to the Cas9-targeted locus, but containing a desired mutation or Indel, CRISPR/Cas9-mediated DNA breaks repaired by HDR will enable accurate generation of knock-in mutations/indels at precise regions of the target gene. Furthermore, it can also be used for tagging protein-coding genes or the generation of duplicate genes. In the context of cancer biology, this approach is particularly useful for the generation of cell line and animal models with complex genetic alterations that mimic the mutational landscape of human tumors.

CRISPR-Cas9 provides a robust technology for studying genomic rearrangements and the development and progression of cancers and other diseases. In fact, the flexibility and programmable capability of the CRISPR-Cas9 system has already led to the development of numerous genome engineering applications, most of which have been conducted successfully in the field of cancer genetics, such as lung cancer (Choi and Meyerson, 2014), acute myeloid leukemia (Chen *et al.*, 2014a), and Ewing's sarcoma (Torres *et al.*, 2014). Moreover, , Heckl *et al.* (2014) and Xue *et al.* (2014) have recently reported the application of an improved CRISPR-Cas9 method for liver cancer and myeloid malignancy mouse model generation. Furthermore, by designing and using an efficient CRISPR system, Shtraizent *et al.* (2015) successfully corrected the oncogenic driver, Y163C hotspot mutation of *TP53* in breast cancer cell lines. Significantly, in 2016, the first clinical trial of applying CRISPR for cancer therapy has enrolled the first patient at Sichuan University's West China Hospital in Chengdu (Cyranoski, 2016). Another human trial has

been approved in the US (Jubair and McMillan, 2017) for application of CRISPR-Cas9 to enable T cells to recognize and target several types of cancers.

Although new treatments for castrate-resistant prostate cancer (CRPC), such as enzalutamide and abiraterone, have shown promise, moderate response rates and development of resistance to these agents has limited their clinical effectiveness. It is therefore vital we improve our understanding of the androgen receptor (AR) re-activation in advanced disease, focusing particularly on regulatory processes governing activity of AR mutants and splice variants (AR-Vs), to enable the development of patient orientated treatments in CRPC. By incorporating CRISPR-based technology, we wanted to enable more physiological modelling of disease- particularly ADT-resistant tumours in which the AR was mutated. Hence, the expected outcomes for this chapter was to comprehensively profile aberrant AR signalling that is vital for therapeutic exploitation by incorporating the next-generation genomic editing strategies to ultimately benefit advanced PC patients. Given the existence of the F876L mutation in enz-resistant patients, it is important to improve our understanding of the mutant receptor for the development of new treatments. To this end, we designed a CRISPR workflow with the intention of generating CRPC cells lines containing this endogenous mutation.

4.2 Specific material and methods

4.2.1 Expression plasmids and constructs

Lentiviral-CRISPR vectors (pLV-U6g-EPCG) sgRNA/CRISPR_186 (sgRNA: CATGTGTGACTTGATTAGC AGG) and sgRNA/CRISPR_196 (sgRNA: AAGTCACACATGGTGAGCGTGG) that express CAS9 and the specific guide RNA, were purchased from Sigma-Aldrich, order number 8019135988. Maxiprep kit (Sigma-Aldrich) was used to prepare the sgRNA/CRISPR_186 and sgRNA/CRISPR_196 plasmids.

4.2.2 Primers and repair DNA template

Table 4.1 Primers for AR exon 8 amplification and Sanger sequencing

Primers	Sequences (5' to 3')	Ref
ARex_8 s'	GAGGCCACCTCCTTGTCAACC	*Used for AR exon 8 PCR amplification*
ARex_8as'	CAGGCAGAAGACATCTGAAAG	
CRISPR_LNCaP_e8 F	CAGTGGATGGGCTGAAAAAT	For Sanger sequencing
CRISPR_LNCaP_e8 Re	AATTCCCCAAGGCACTCAG	

4.2.3 Repair oligo sequences (5' to 3'):

ssODN_wt:

ggctagcagaggccacctccttgtcaaccctgttttctccctcttattgttccctacagattgcgagagagctg**Cat**cagttc**Act**ttttgacctgctaatcaag tcacacatggtgagcg**tCg**actttccggaaatgatggcagagatcatctctgtgcaagtgcccaagatcctttctgggaaagtcaagcccatcta

ssODN_F876L:

ggctagcagaggccacctccttgtcaaccctgttttctccctcttattgttccctacagattgcgagagagctg**Cat**cag**CtcAct**ttttgacctgctaatcaagtcac acatggtgagcg**tCg**actttccggaaatgatggcagagatcatctctgtgcaagtgcccaagatcctttctgggaaagtcaagcccatcta

The designed single stranded donor oligonucleotides (ssODN) was chosen as a repair donor to 'knock-in' F876L via homology direct repair (HDR) post Cas9 induced-double strand break (DSB). **'Cat'**

and '**Act**' in each ssODN was used to substitute endogenous mutation H874Y and T877A in CWR22Rv1 and LNCaP cell lines, respectively. **Ctc** was used to knock in F876L mutation. **tCg** was used to silence PAM code as well as introduce a *Sal* I restriction site for downstream RFLP analysis.

All the primers used to detect single-stranded oligodeoxynucleotides (ssODN) incorporation are list below:

Table 4.2 primers for detecting ssONDF876L in LNCaP and 22Rv1 cells.

Primers	Sequences (5' to 3')	Ref
LNCaP_T877A F	CAGTTCGCTTTTGACCTGCT	Used to verify ssOND$_{F876L}$ incorporation in LNCaP cells
LNCaP_F876L F	CATCAGCTCACTTTTGACCT	
LNCaP Re	GGGGTGGGGAAATAGGGTTT	
22Rv1_H874Y F	CTGTATCAGTTCACTTTTGACCT	Used to verify ssOND$_{F876L}$ incorporation in CWR22Rv1 cells
22Rv1_F876L F	CATCAGCTCACTTTTGACCT	
22Rv1 Re	GGGGTGGGGAAATAGGGTTT	

4.2.4 Nucleofection

Nucleofection transfection protocol for PC cells was optimized using Amaxa® Nucleofector® Kit (Lonza Cologne AG, USA /Canada). For each transfection reaction, 5 µg sgRNA/CRISPRs plasmids and 40 µl of 50 mM ssDNA (1 µl of a 10 µM ssODN template stock) were add into 100 µl room temperature Nucleofector® Solution R (including 18 µl supplement). $2*10^6$ cells were trypsinised and cell pellet was collected by centrifugation at 100g for 10 minutes. The cell pellet and prepared DNA/ Nucleofector Solution and all components were transferred into a certified cuvette and subject to the Nucleofector® Program T-009 (T-09 for Nucleofector® I Device) for transfection. ~400 µl of the pre-equilibrated culture medium was immediately added to the cuvette once the program completed before transferring into the prepared polyLysine-coated 6-well plate (final volume 1.5 ml per well) and incubated at 37°C for 8-20 hours before examining GFP expression. Images were acquired using a Leica DMR fluorescent microscope with appropriate filters.

4.2.5 Fluorescence-activated cell sorting (FACS).

The efficiency of CRISPR/CAS9 genomic editing in nucleofected LNCaP and CWR22Rv1 cells was assessed by the Surveyor (CEL-1) assay. This required cells to be initially sorted based on expression of GFP as a marker of uptake of the pLV-U6g-EPCG vector. Two days after transient transfection, cells were sorted using FACS (Aria III, BD Biosciences) and GFP-positive cells were identified and sorted by comparing to a non-transfected population of cells. GFP-positive cells were collected and plated accordingly. For the Surveyor assay, 1×10^4 cells were plated on 6-well plates and maintained until confluent; whereas for isolation of individual clones, cells were plated on 10-cm dish at 500-2,500 cells per dish with puromycin containing medium (10μg/ml) until individual colonies were visible.

4.2.6 Surveyor assay

The Surveyor assay (optimized from Surveyor Mutation Detection Kit protocol, Integrated DNA Technologies) was used to assess sgRNAs/CRISPR targeting efficiency. HEK293, CW22Rv1 and LNCaP cells were nucleofected for 48 hours before being subject to fluorescence-activated cell sorting (FACS) to sort GFP-positive, pLV-U6g-EPCG-containing cells. FACS enriched cells were seeded back into 6- well plates and cultured with puromycin-containing media for 7 days. 1 week post transfection, genomic DNA was extracted (GeneElute Genomic DNA extraction kit, Sigma) from each control and CRISPR transfected cell pool and subject to PCR (Platinum™ Taq Green Hot Start DNA Polymerase, Invitrogen) to amplify the regions spanning CRISPR/Cas9 cut sites using specific primers pairs (Table 4.1). Plasmids C and G fragments (Transgenomics, Inc.) were also amplified and run in parallel as a positive control.

 The optimized PCR reaction as bellow:

Composition	Volume
10* reaction buffer	5 µl
50 µM MgCl$_2$	1 µl
10 mM dNTP mix	1.5µl
10 nM AR exon8 primer forward	1µl
10 nM AR exon8 primer reverse	1 µl
Genomic DNA sample	≤ 100 ng
DNA polymerase	0.2 µl
Nuclease-free H$_2$O	Up to 50 µl

Thermocycler reaction was set up as bellow:

Initial denaturation	94°C 2 minutes
Denature	94°C 30 seconds
Anneal	~55°C 30 seconds
Elongation	72°C 2 minute
PCR cycles	30

To facilitate the formation of mismatched fragments, 400 ng control or hybridised DNA was denatured at 95°C for 10 minutes and re-annealed by gradually ramping from 95 °C to 85 °C at 2 °C/s, 85 °C for 1 minute, ramping from 85 °C to 75 °C at 0.3 °C/s, 75 °C for 1 minute, ramping from 75 °C to 65 °C at 0.3 °C/s, 65 °C for 1 minute, ramping from 65 °C to 55 °C at 0.3 °C/s, 55 °C for 1 minute, ramping from 55 °C to 45 °C at 0.3 °C/s, 45 °C for 1 minute, ramping from 45 °C to 35 °C at 0.3 °C/s, 35 °C for 1 minute, ramping from 35 °C to 25 °C at 0.3 °C/s, and 25 °C for 1 minute to 25°C before digesting with 1 unit of Surveyor endonuclease enzyme for mismatching detection.

Each digestion reaction component including:

Composition	Volume
Control/ hybridized DNA	400 ng
	(within ≤ 10 µl 1*PCR reaction buffer)
0.15 M MgCl$_2$ Solution	1 µl
Surveyor Enhancer S	1 µl
Surveyor Nuclease S	1 µl

After incubation at 42°C for 60 minutes, 1.3 µl stop solution was added. The digestion products were resolved on a 2% Agarose TBE gel and the fragments were visualized using Bio-Rad Chemi XRS Gel Documentation system and Bio-Rad Quantity One® software (Bio-Rad Laboratories, Inc.). The fragments quantified using Image J.

Indels were calculated using the following formula,

$$indel(\%) = 100 \times \left(1 - \sqrt{\frac{b + c}{a + b + c}} \right)$$

where *a* is the intensity of the undigested fragment, and *b* and *c* are the intensities of the cleavage products.

4.2.7 DNA polyacrylamide gel electrophoresis (DNA-PAGE)

PCR products that consisted of amplicons shorter than 300 bp were run using a PAGE gel in order to provide appropriate separation of the bands. The electrophoresis was performed on 8% PAGE in 1 x TBE buffer as denoted below.

Table 4.3 8% PAGE composition

Composition	Volume	Final concentration
1 x TBE	8 ml	~1 x
30% acrylamide/bis-acrylamide	2.5 ml	8%
10% ammonium persulfate	120 µl	0.1%
TEMED	10 µl	0.1%

The gel was run on vertical electrophoresis apparatus using 1 x TBE buffer as running buffer. Each sample was mixed with 6 x loading dye and subject to PAGE at 50 V for approximately 1 hour. Afterwards, the gel was stained with GelRed (Biotum) and visualised using a Geldoc camera and software (BioRad).

4.3 Results

4.3.1 Design and testing of Cas9/sgRNA complexes targeting exon 8 of the AR gene to facilitate generation of the enzalutamide-activated AR_{F876L} mutant.

Firstly, LNCaP and CWR22Rv1 were chosen for CRISPR model generation. Both PC cell lines are commonly used in *in vitro* cell culture assays as well as in xenograft mouse experiments. LNCaP is an androgen-sensitive and full-length AR (AR-FL)-expressing cell line that was derived from a lymph node metastasis (Zhau *et al.*, 1996); whilst CWR22Rv1, a cell line derived from a xenograft tumour grown in castrate conditions, co-express AR-FL and AR-Vs species (Dehm and Tindall, 2011). Of particular note, as shown in Figure **4.1**, LNCaP and CWR22Rv1 cell lines endogenously express one LBD-mutation, T877A (ACT-GCT) and H874Y (TTC-CTC), respectively.
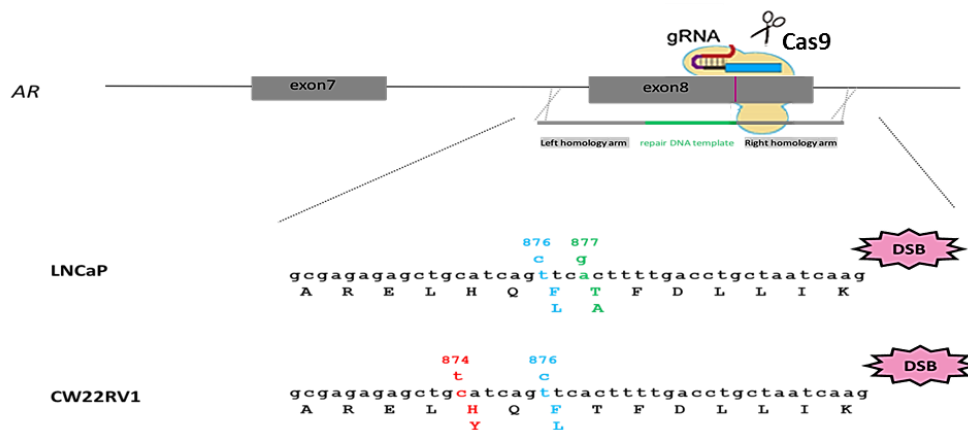
Figure 4.1 Schematic representation of desired CRISPR-induced editing in LNCaP and CWR22Rv1 cells. The AR exon8 and exon7 coding region are indicated by grey color. F876 mutation site is highlighted in blue and endogenous mutations H874Y and T877A within CWR22Rv1 and LNCaP shown in red and green, respectively.

Two all-in-one lentiviral CRISPR vectors (pLV-U6g-EPCG, purchased from Sigma), that express both *S. Pyogenese*-derived Cas9 and bespoke gRNAs, were used to target *AR* exon 8. Each plasmid (Figure **4.2** A) encodes one Cas9 enzyme and one gRNA, and were named sgRNA186 and sgRNA196. Both gRNAs targeted *AR* exon 8 at distinct sites based on the position of the protospacer adjacent motif (PAM, highlighted in pink in Figure **4.2**.B). In addition to the custom designed CRISPR reagents, a single-strand oligodeoxynucleotide (ssODN) complementary to exon

8 was designed as a repair donor template to facilitate 'knock-in' of the AR$_{F876L}$ mutation via HDR post Cas9-induced DNA break.
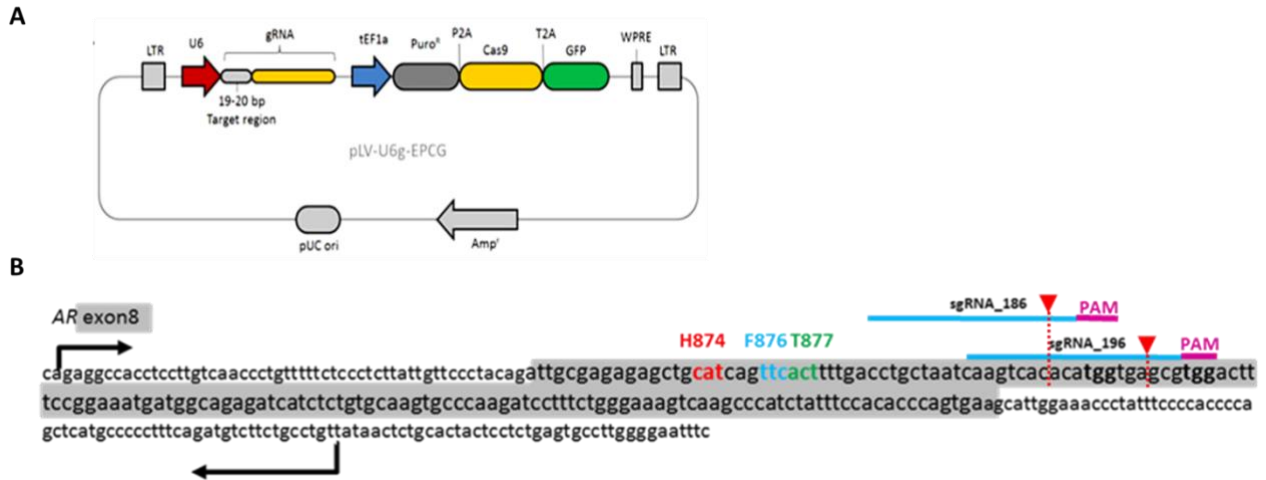
Figure 4.2 Design of the Cas9/sgRNA targeting AR exon 8. (A) Vector map of the all-in-one CRISPR vector pLV-U6g-EPCG. Cas9 open reading frame (ORF) flanked by puromycin and GFP elements allows for selection, and enrichment of desired positive cells. (B) Schematic of custom designed sgRNA186 and sgRNA196 target site in AR exon 8 coding sequence. Each target sequence (protospacer) and 'PAM code' for sgRNA186 and sgRNA196 are given in bold. Red arrows and vertical dotted line indicate the expected cleavage site of each sgRNA. Black arrows represent PCR primers using to amplify targeted regions.

To validate 'on-target activity' of the two CRISPRs, HEK293T cells were firstly transfected with Cas9/sgRNA expression plasmids using LT-1 (Mirus Bio) for 72 hours. GFP expression derived from the plasmids was subsequently analysed using a fluorescent microscope as an indication of transfection efficiency. As shown in Figure 4.3 A, in HEK293T cells, both plasmids demonstrate high GFP expression post Cas9/sgRNA186 and Cas9/sgRNA196 transfection.

Next, CRISPR target efficiency was assessed. Genomic DNA was extracted from transfected and non-transfected cell pools and subject to *AR* gene exon 8 amplification by PCR using pre-designed primers (list in Table 4.1) before incorporation in to the Surveyor assay (Figure 4.3 B). This experiment relies upon a mismatch-specific DNA endonuclease, Surveyor Nuclease, which cuts both strands of a DNA heteroduplex on the 3'-side of the mismatch site with high specificity. This initial optimisation experiment relies upon NHEJ-based DNA repair to ligate the CRISPR-induced

cleavage event. Due to the error-prone nature of this mechanism, CRISPR efficiency can be assessed using the Surveyor Nuclease to quantify the rate of indels within the targeted DNA region as a measure of CRISPR efficiency.
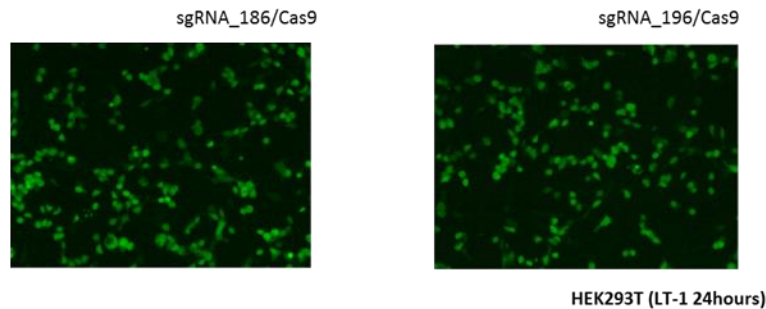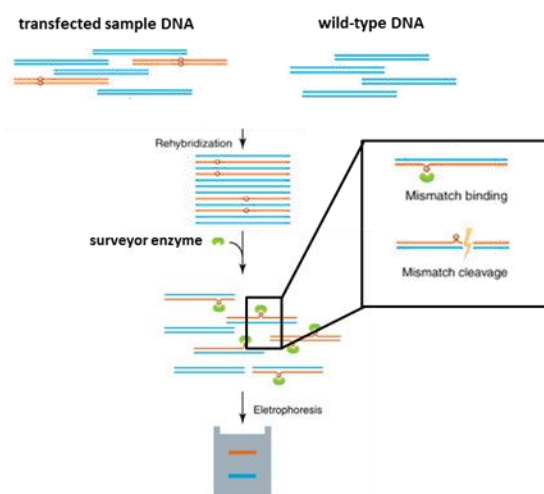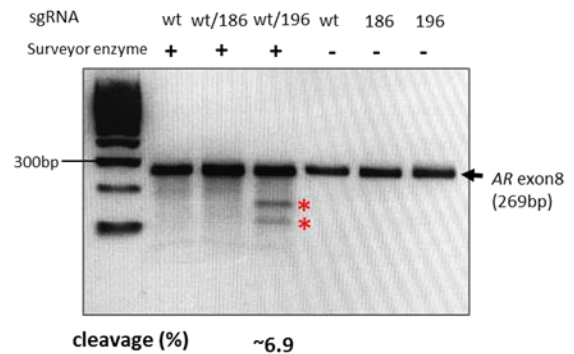
Figure 4.3 Assessing designed- Cas9/sgRNA targeting efficiency using Surveyor mutation detection assay. (A) Equal amounts of two designed Cas9/sgRNA plasmids were transfected into HEK293T cells. The florescence image is taken 24 hours post-transfection. (B) The flow chart of Surveyor assay. Genomic DNA is harvested from the transfected pool of cells and amplified at the locus of interest. The PCR product is denatured and re-annealed creating heteroduplexes between wild-type and modified amplicons. The Surveyor mismatch endonuclease assay results in cleavage of heteroduplex molecules. The Surveyor enzyme digests are resolved by PAGE. The observed ratio of cleavage product to parental band indicates the fraction cut, and hence, efficiency of DSB. (C) Surveyor Nuclease digestion products of amplicons derived post transfection and the control/ wildtype sequence in HEK293T cells. Lane heading indicates non-transfected wildtype cells (wt) and sgRNAs index names. "-" denotes PCR amplicon products of control or Cas9/sgRNA transfected cells prior to Surveyor treatment. "+" indicates Surveyor enzyme digestion products. Red arrows highlight Surveyor enzyme detected heteroduplexes in the plasmid-transfected/wild-type samples. Cleavage frequency was analyzed using Image J.

As illustrated in Figure 4.3 B, equal quantities of PCR amplicons containing potential Cas9-induced Indels are denatured and reannealed with the wild-type amplicon and then digested with Surveyor nuclease to discriminately cleave on the 3'-side of the heteroduplexes formed between mismatched Indel- and wild-type-containing duplexes. The resultant DNA is resolved using 2% agarose gel electrophoresis and successful Cas9-mediated cleavage was identified by shifts in fragment size with respect to the wild-type fragment.

As shown in Figure 4.3 C, the total size of AR exon 8 is 269 bp based on pre-design primers. Upon CAS9-induced cleavage and NHEJ-mediated DNA repair at the desired site, a 116 bp, and 153 bp size was observed as a consequence of digestion by the Surveyor enzyme. The indels were identified at a frequency of ~6.9% in cells transfected with sgRNA196, which contrasted with cells expressing sgRNA186 which demonstrated negligible heteroduplex formation, suggesting that the sgRNA196 plasmid performs more efficiently to cleave exon 8 of the *AR* gene.

4.3.2 Cas9/sgRNA196 is 'on-target' in CWR22Rv1 and LNCaP cells.

Having confirmed that the Cas9/sgRNA196 had more efficient 'on-target' capability *in vitro*, we next moved to assess its editing ability in both LNCaP and CWR22Rv1 cells. As both cell lines are challenging to transfect, particularly with large plasmids such as pLV-U6g-EPCG, several delivery approaches were performed to elevate transfection efficiency sufficiently to facilitate generation of edited cells lines downstream.

Table 4.4 Optimising Cas9/sgRNA delivery methods for different cell lines. To achieve sufficient transfection efficiency, several exogenous nucleotide delivery approaches were used in HEK393T, LNCaP and 22Rv1 cell line.

	LT-1/Lip200	Nucleofection	Nucleotransfection + FACS	Lentivirus transduction
HEK293T	Yes	N/A	N/A	N/A
CW22RV1	No *	Yes	N/A	N/A
LNCaP	No	No	No	Yes

* GFP+/ SURVEYOR−

As listed in Table 4.4, lipophilic reagents, such as LT-1, are sufficient to transfect HEK293T cell, but not for LNCaP cells. Surprisingly, post LT-1 transfection, GFP was expressed in CWR22Rv1

cells to modest levels, but resultant Indels were not detected within *AR* exon 8 (data not shown) (Appendix 4B A), suggesting a more improved means of plasmid delivery is required for both prostate cancer cells lines.

Given that CWR22Rv1 cells demonstrated modest lipophilic-based transfection, it was next sought to address if electroporation-based methods may elevate uptake of the Cas9/sgRNA196-expressing plasmid. To this end, we applied Nucleofection to introduce the CRISPR plasmid into CWR22Rv1 cells, and after 48 hours GFP-positive cells were sorted and cells harvested for Surveyor assay. As results show in Figure **4.4** A, post 48 hours Nucleofection, GFP expression was detected in approximately 75% of CWR22Rv1 cells indicating that transfection efficiency is markedly improved using this technique. Importantly, the Surveyor assay confirmed Cas9/sgRNA196's 'on-target activity' as evidence by approximately 16% heteroduplex formation in transfected cells compared to untransfected cells (Figure **4.4** B). Importantly, cleavage products were dependent on the presence of the Surveyor enzyme and are not artefacts of the PCR reaction. As shown Figure **4.4** B, comparing lane 1, additional two small size of DNA fragments can be seen in lane 2 in the presence of Surveyor enzyme, suggests that the Cas9/sgRNA196 plasmid presenting 'on-target' activity in 22Rv1 cells. The lanes 3 and 4 were severed as negative control for wild-type amplicon and Surveyor enzyme, respectively. Given successful Indel detection, the Surveyor assay was applied to all subsequent CWR22Rv1 cell experiments.
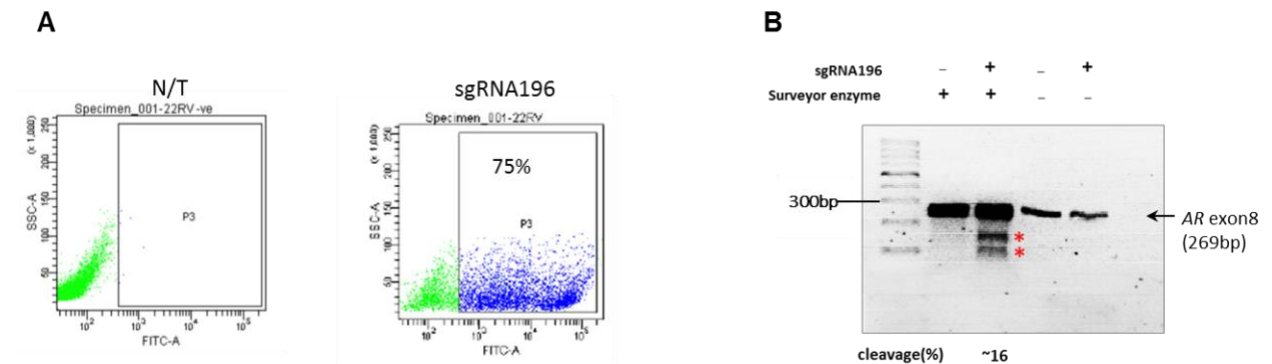
Figure 4.4 Nucleofection of CWR22Rv1 results in a successful Cas9/sgRNA196 mediated-cleavage at AR exon 8. (A) 48 hours post-Nucleofection, GFP positive cells in CWR22Rv1 cells were sorted using a FACS

Although Nucleofection increased GFP expression in LNCaP cells in comparison to LT-1 reagent, the subsequent Surveyor assay failed to detect any heteroduplexes (Appendix 6A) indicating transfection efficiency remains too low to effectively edit the LNCaP genome. Therefore, we decided to package Cas9/sgRNA196 plasmids into lentivirus to transduce LNCaP cells, which in theory will increase efficiency significantly.

Lentiviral particles containing the Cas9/sgRNA196 plasmid was generated using HEK293T cells as described in section 3.8. 7 days post viral infection, GFP expression was assessed using fluorescent microscopy. As shown in Figure **4.5** A, compared to the bright field image, most LNCaP cells transduced with the Cas9 plasmid express GFP, albeit heterogeneously. Importantly, the Cas9/sgRNA196 plasmid presenting 'on-target' activity in LNCaP cells as evidenced by detection of approximately 15% cleavage events within the target locus using the Surveyor assay (Figure **4.5** B).
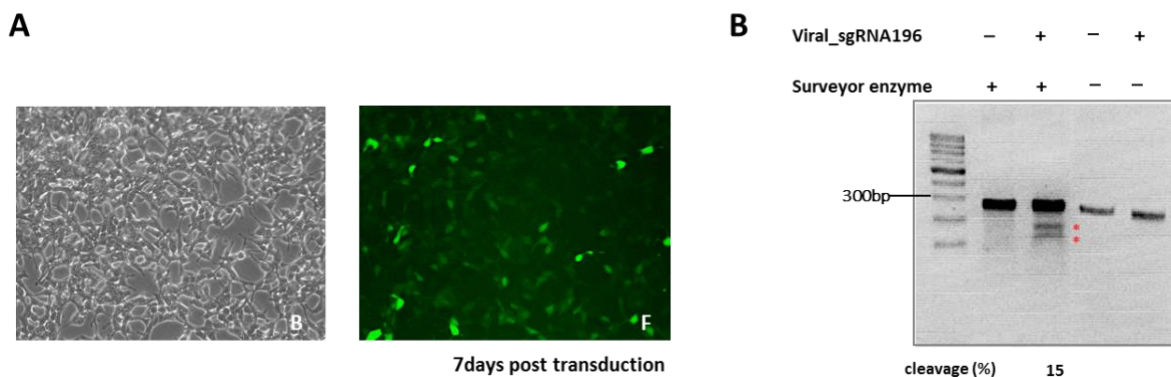
Figure 4.5 Targeting *AR* gene exon 8 in LNCaP cells. (A) Representative images of LNCaP cells infected with the Cas9/sgRNA196-containing lentivirus. Fluorescence images were taken 7 days post-transduction of LNCaP cells with virus particles containing pLV-U6g-EPCG_ Cas9/sgRNA196. Transduced group, (B) bright field, (F) fluorescent field. (B) Surveyor assay confirmed genomic editing in transduced LNCaP cells within the target locus.

4.3.3 Confirming Cas9/sgRNA196-mediated genome editing of *AR* exon 8 using a Sanger sequencing-based approach.

As a consequence of imperfect DNA repair after Cas9-mediated cleavage, DNA in the transfected cell pool consists of a mixture of wild-type and Indel-containing sequences as demonstrated above using the Surveyor assay. To confirm the effect of Cas9/sgRNA196 editing of exon 8 of the *AR* gene, the PCR amplicons from both control (untransfected) and Cas9/sgRNA-transfected cells were subject to Sanger sequencing. The resultant sequencing chromatogram was subject to analysis using an online tool, named TIDE (Tracing Indel by DEcomposetion), to validate and quantify Indel type in each sample (Brinkman *et al.*, 2014). TIDE software quantifies sequence trace data from two standard capillary (Sanger) sequencing reactions. By decomposing target sequence traces, and based on identification of the predominant types of insertions and deletions (indels) in the DNA of a targeted cell pool, TIDE can ultimately quantify editing efficacy of specific CRISPRs.

As shown in Figure **4.6** A, compared to non-transfected CWR22Rv1 cells, cells transfected with the Cas9/sgRNA196 clearly revealed a heterogeneous sequencing pattern 3 bp upstream of the PAM sequence, which is consistent with NEHJ-mediated repair (Wu *et al.*, 2014)). The sequence trace after cleavages site (vertical dotted line in Figure **4.6** B) consists of a mixture of signals derived from both intact DNA and cleaved DNA. A different number of nucleotides therefore are shifted due to insertions and deletion following Cas9-induced DNA cleavage. The overall Cas9/sgRNA196-induced Indel frequency in CWR22Rv1 cells was approximately 34% that is consistent with previous reported Surveyor assay results. However, quantification of CRISPR efficiency using TIDE demonstrates a 2-fold increase compared to that calculated using the Surveyor assay (Figure **4.4**) which may be due to the less accurate Image J-based method being not fully quantitative.
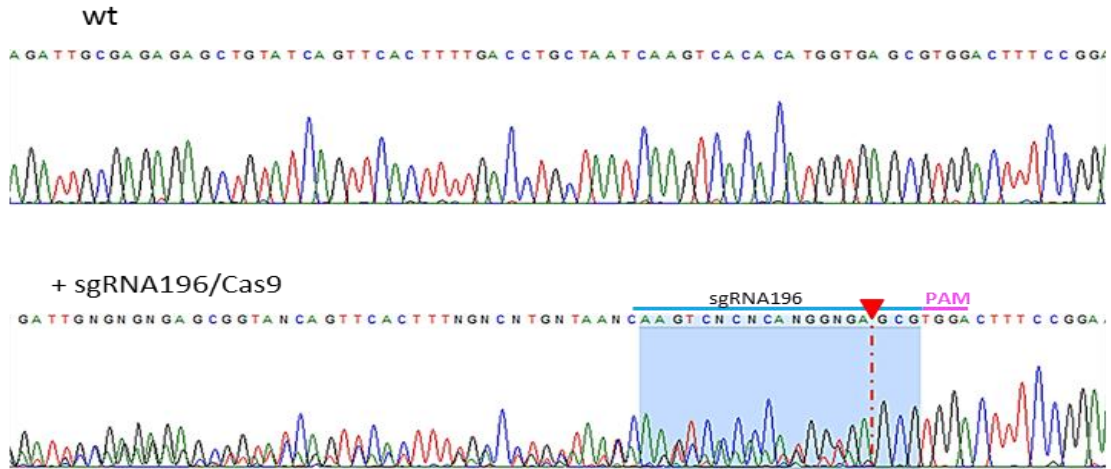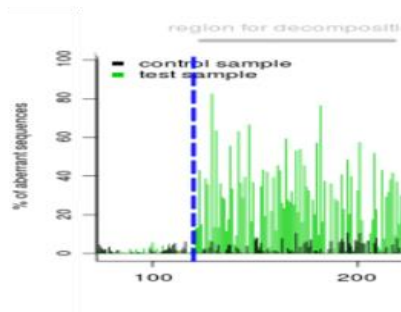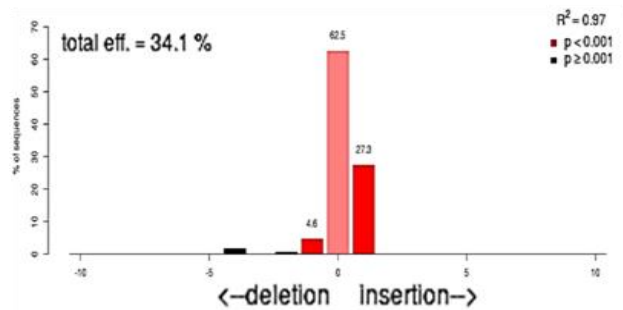
Figure 4.6 DNA sequencing chromatograms of Cas9-targeted region in *AR* exon 8 and TIDE analysis. (A) Chromatograms of *AR* exon 8 amplicon sequencing from a control and Nucleofected cell pool. The positioning of the gRNA196 and PAM site were indicated in relation to the sequencing plot. The predicated cutting site was indicated with red-arrow. (B) Assessment of genome editing efficiency by TIDE to quantify the overall Indel frequency and major Indel type in the sample. Visualization of aberrant sequence signal in wild-type (black) and sgRNA196 sample (green), the expected break site (vertical dotted line) and the region used for decomposition (grey bar). See main text and http://tide.nki.nl for explanation (C). Decomposition yielding the spectrum of indels and their frequencies; the TIDE software decomposes the composite sequence trace into its individual components by means of multivariate non-negative linear modeling, with the control sequence trace serving as a template to model the individual indel components. This decomposition results in an estimate of the relative abundance of every possible indel within a chosen size range.

4.3.4 Enrichment of positive cell populations for increased gene editing events in LNCaP cells.

We next sought to determine whether enrichment of successfully-transduced LNCaP cells would enhance Cas9/sgRNA196 efficiency in order to increase knock-in efficiency when the repair template was incorporated in future experiments. Therefore, 7 days after lentivirus infection, LNCaP cells were cultured with/without puromycin-containing medium for an additional week to enrich Cas9/sgRNA196-transfected cells before conducting PCR and CRISPR efficiency analysis.

As can be seen from the sequencing chromatogram in Figure **4.7** B, puromycin-selected cells show higher 'on-target' effects when compared to control and cells not under puromycin selection pressure. The total efficiency of Cas9/sgRNA196 is approximately 30% in LNCaP cells without selection and is increased to 46.6% post-puromycin selection. These results are consistent with the Surveyor assay data (shown in Figure **4.7** C) that demonstrates Indel frequency of AR exon 8 is increased from 15% to over 21% post-antibiotic selection, indicating that selection increases editing events in LNCaP cells by enriching transfected cells from a mixed-cell pool.
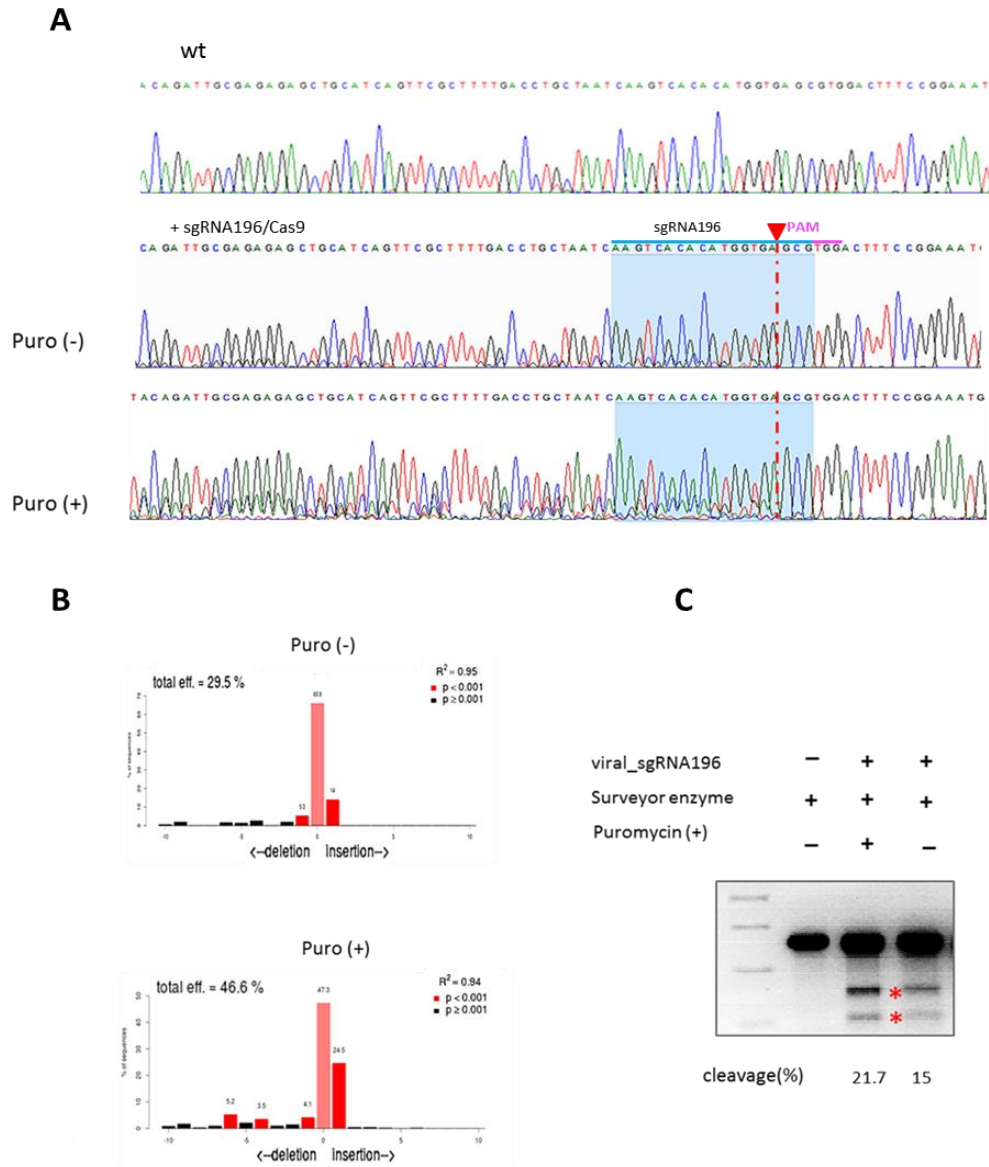
Figure 4.7 Enrichment of cell populations for increased gene editing events in LNCaP. (A) DNA sequencing chromatograms of AR exon 8 amplicons from control and Cas9/sgRNA196-transfected cells with and without puromycin selection post viral infection. (B) The enhanced Indel frequency in the LNCaP post puromycin selection culture as calculated by TIDE analysis. (C) Surveyor assay was conducted using same gDNA from (A). Surveyor-generated small fragment were indicated with red dots. Compared to puromycin-lacking samples, the puromycin-selected cell samples contains higher level of DNA indels within *AR* exon 8.

4.3.5 Design of donor template and knock-in of the F876L mutation.

Given that the Cas9/sgRNA196-expressing plasmid was shown to effectively induce Indels within *AR* exon 8, it was important to next design and utilize a 200 bp single-strand oligodeoxynucleotide (ssODN) (Figure **4.8** A) containing the AR_{F876L} mutation that would enable the creation of knock-in clones via HDR that express the enzalutamide-activated AR_{F876L} mutant in LNCaP and CWR22Rv1 cells. The ssODN contains a 200 bp sequence homologous to exon 8 of the *AR* gene, encompassing the F876 codon, as well as two homology arms on both sides (see 4.2.3, full sequence see Appendix 4C). In addition, we also designed an ssODN with wild-type sequence in order to reverse endogenous mutations T877A and H874Y back to wild-type in LNCaP and CWR22Rv1 cells, respectively. In addition to removing the PAM (T**G**G-T**C**G) site to avoid Cas9-mediated cutting once the knock in mutation was achieved, we purposefully introduce a novel restriction digest site (*Sal* l, G^TCGAC) into each ssODN. Thus, post HDR, the successful knock-in mutation within the genome of LNCaP and CWR22Rv1 cells can be identified using a restriction fragment length polymorphism (RFLP) assay.

Interestingly, co-delivery of the Cas9/sgRNA196 plasmid and ssODN by nucleofection into CWR22Rv1 resulted in cells forming colonies; with GFP expression lasting up to 7 days. As heterogeneous GFP expression was detected in the (Figure **4.8** C), 10 colonies were selected for potential successful insertion/ or gene replacement detection.
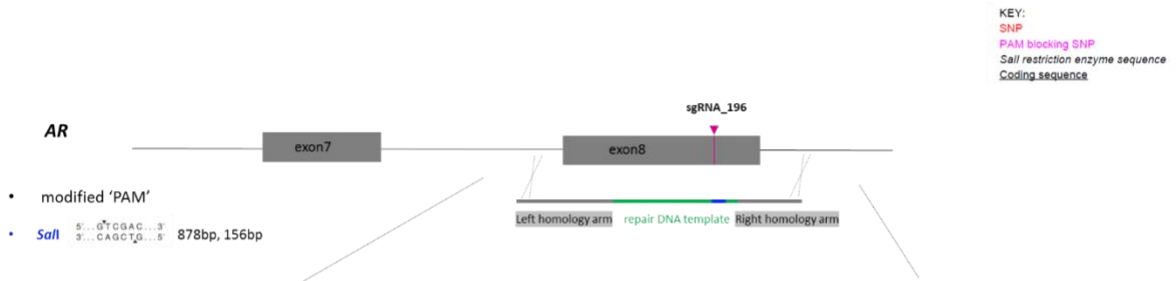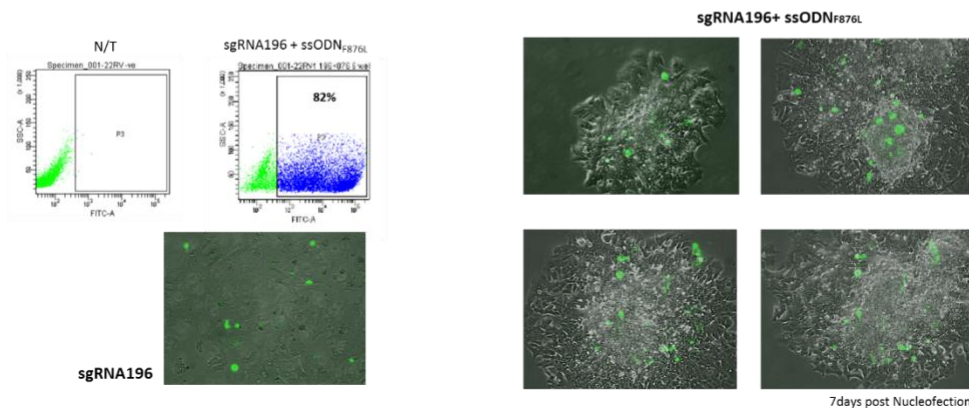
Figure 4.8 Co-transfection of CWR22Rv1 cells with Cas9/sgRNA196 plasmid and ssODN. (A and B) A schematic of designed ssODN donor template. F876L coding sequencing is introduced via two homology arms (gray regions). The additional inserted restriction enzyme sequence is indicated in blue. (C) CWR22Rv1 cells formed colonies post nucleofection with Cas9/sgRNA196 and the ssODN. Fluorescence image taken 7 days post co-transduction.

The CRISPR-targeted sequence of *AR* exon 8 was amplified from selected colonies by PCR and the resultant product was purified and digested with the *Sal* I restricted enzyme which represented our bespoke RFLP assay to detect knock-in mutations. All colonies screens harbored Cas9-induced Indels at the targeted locus, but unfortunately, none of them showing successful ssODN insertion following RFLP analysis (Appendix 4A). The same results were observed in LNCaP cells (Appendix 4B). It may be due to HDR events being generally less frequent than the repair of DNA by non-homologous end-joining. Additionally, the sensitivity of RFLP may not be sufficient to detect low level of ssODN 'incorporation' that occurred in a small cell population.

4.3.6 Screening successful gene editing events in heterogeneous samples.

In order to validate whether desired knock-in events were present in the heterogeneous LNCaP cell pool, we designed two pairs of specific primers in an attempt to enhance our sensitivity of knock-in mutation detection by quantitative PCR. Both primer sets (Figure **4.9** A) share the same reverse primer that anneals downstream of the target region. The first forward primer amplifies outside of the target region to be used as a reference, whilst the second forward primer, termed the detection primer, is complementary to the knock-in mutant sequence.
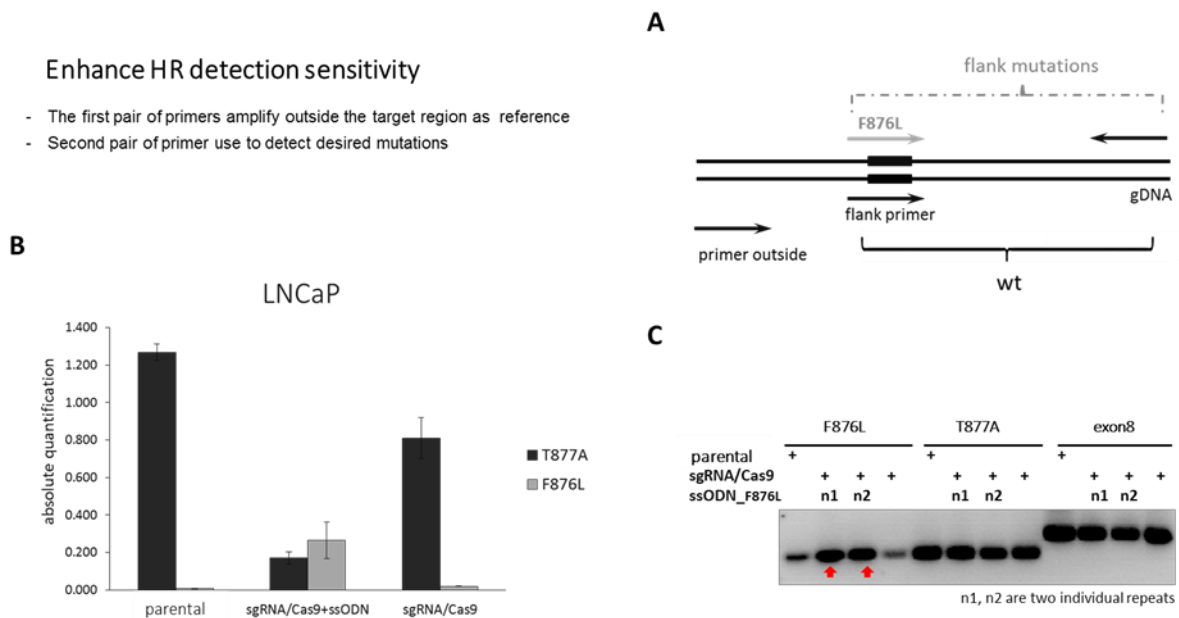
Figure 4.9 Screening successful gene editing events in heterogenetic sample. (A) Two pairs of primers were designed to detect ssODN 'knock-in' level from whole CRISPR-edited heterogenetic cell pool. Both primer set share the same reverse primer while the first forward primer amplifies outside of target region and is used as a reference; whilst the second forward primer (indicated as grey dotted line) flanks the desired mutation sequence. Samples were analysed using both quantitative PCR (B) and conventional PCR (C).

Using quantitative PCR analysis incorporating genomic DNA derived from LNCaP cells 7 days post transfection with either control, Cas9/sgRNA196 or Cas9/sgRNA196 + ssODN, it is shown in Figure **4.9** B that by using the F876L primer, which should only detect the F876L mutants, the F876L mutation was specifically detected in the Cas9/sgRNA196 + ssODN co-transfected sample but not in parental or cells that were only transfected with the Cas9/sgRNA196 plasmid. Similar results

were obtained using conventional PCR (Figure **4.9** C). Co-transfected LNCaP (n1, n2 are two individual repeats) shows higher F876L amplify products than that in parental or cells post single Cas9/sgRNA transfection. Of particular note is that although repeated readouts were consistent between experimental repeats, there is only one nucleotide difference between the wild-type and mutant detection forward primers, hence it would be more robust to verify the efficiency of each primer pair by performing a QPCR on plasmids encoding wild-type vs F876L.

Pure clonal isolation from a single progenitor cell is a critical step in the genetic and functional characterisation of mutations achieved by the CRISPR/Cas9 system. Hence, having confirmed a low level of desired editing events in mixed cell populations, we next sought to generate 'knock-in' clones that were derived from single cells. LNCaP and CWR22Rv1 cells were transfected with Cas9/sgRNA196 and ssODN according to their optimized conditions (indicated in black and red, respectively, Figure **4.10** A). To enrich for GFP-positive cell populations, FACS sorting was carried out in each cell pool before plating in 48-well plates to obtain transfection-positive cells. Although it is desirable to establish clonogenic cultures from single cells, it was difficult to propagate cells post-selection when seeded individually in culture vessels which may due to the impact of FACS sorting or compromised growth as a consequence of diminished cell to cell contact.
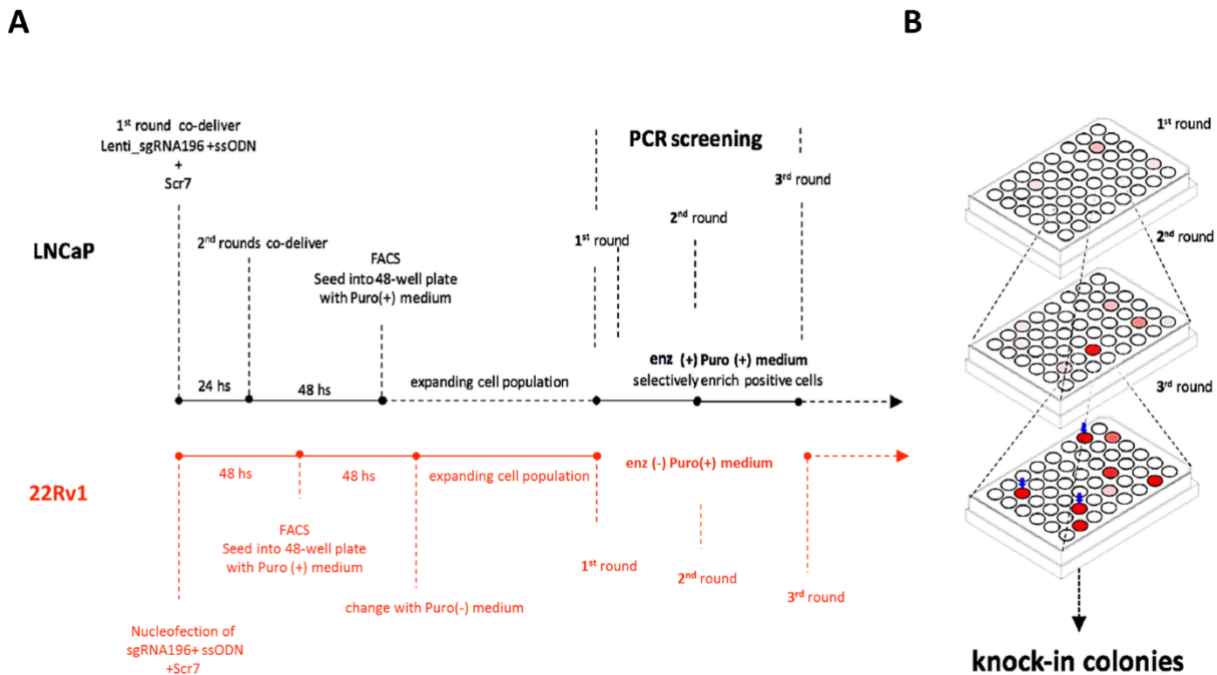
Figure 4.10 Overview of the approach to isolate rare 'knock-in' mutants from mixed populations. (A) The optimised CRISPR approach applied in LNCaP and CWR22Rv1 cells. The two PC cell line are transduced/Nucleofected with both Cas9/sgRNA and ssODN accordingly. (B) Sequential PCR screening of 'knock-in' colonies. Through first (top), second (middle) and third (bottom) round screening, the F876L coding sequence frequency in each well will be measured as described in Figure 4.9. Red dots indicate wells that contain mutated cells; blue arrow highlights the best well.

Therefore, further consideration was made by increasing cell number in each well after FACS sorting and additional selection condition was included to enrich the desired 'knock-in' cells. Firstly, given that repair of Cas9-induced DSBs can be mediated by either NHEJ or HR pathways, it was sought to facilitate detection of knock-in mutants by utilizing the QPCR-based mutation reporter assay as described above. In addition, the enzalutamide containing medium was used for selective growth in the heterogeneous cell populations of LNCaP cells. Of note, it wasn't used for CWR22Rv1 due to the presence of AR variants expression. As illustrated in Figure **4.10** B, in order to sequentially select and enrich AR_{F876L} 'knock-in' colonies, half of the cells from each 48-well plates post-FACS sorting were analyzed for 'knock-in' frequency. More specifically, the primers used in Figure **4.9** was used to identify the wells containing F876L coding sequence. Cells from the corresponding replica plate well was subdivided into another 48-well plate. In addition,

as the intended 'knock-in' F876L mutation enables enzalutamide resistance, theoretically, upon Cas9-mediated 'knock-in', the F876L mutation may further support selection of genome edited cells by long-term growth in enzalutamide. To that end, puromycin- and enzalutamide-containing medium was used as additional selection pressure to facilitate outgrowth of successfully edited LNCaP and CWR22Rv1 cells. Therefore, after sequential PCR screening, we should enrich the progeny of mutant cells with each round of selection. Ultimately it should allow us to isolate AR_{F876L} knock-in clones.
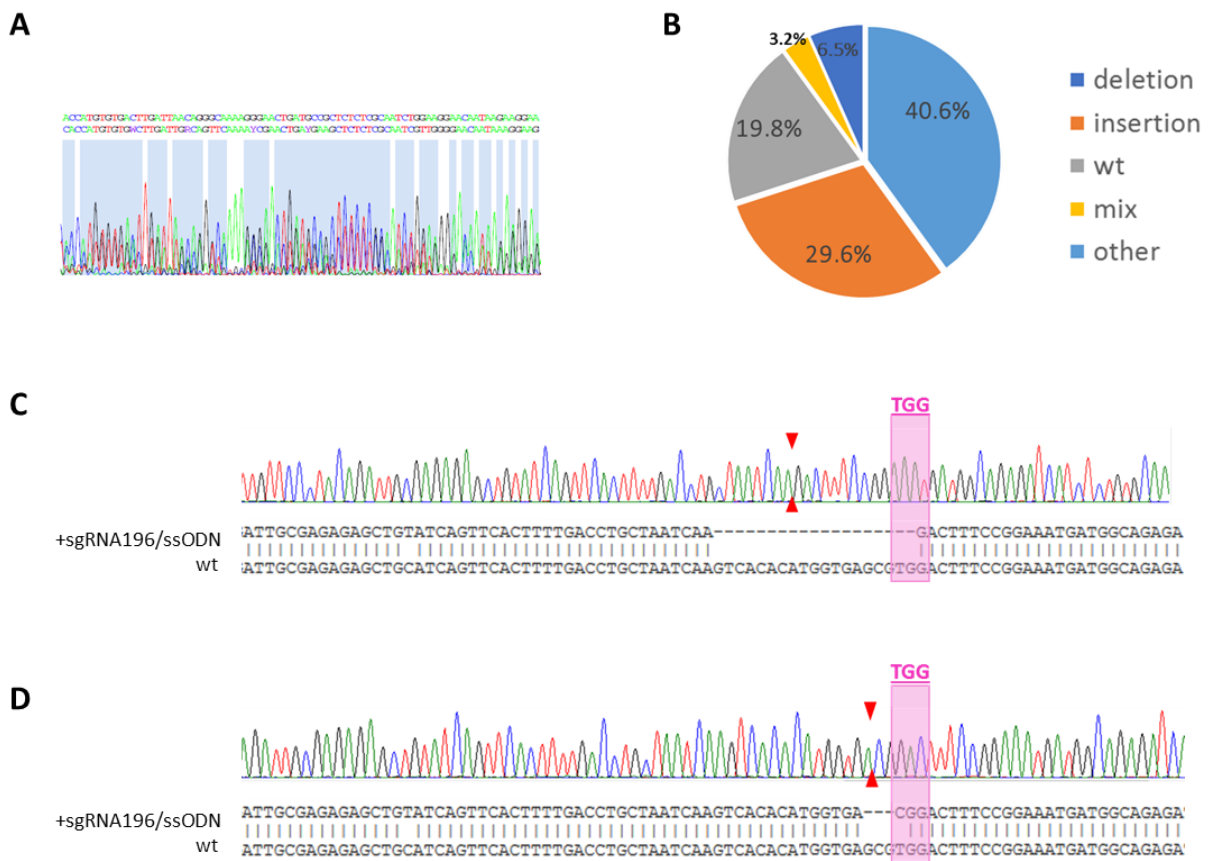
Figure 4.11 Summary of the sequencing screening of mixed LNCaP and CWR22Rv1 cell population. (A). Characterisation of indels induced by CRISPR-Cas9 as determined by Sanger sequencing of selected colonies. Deletion/inversion frequency and characterisation of outcomes when using *AR* exon 8 primers. (B). Mutation patterns in single-cell colonies were determined by Sanger sequencing. (C & D). Sanger sequencing chromatogram reveals large fragment insertion and deletion upon Cas9/sgRNA196 cleavage.

Both LNCaP and CW22RvI cells were transfected/transduced with both Cas9/sgRNA196 and ssODN components as described in Figure **4.10** . PCR amplicons containing *AR* exon 8 from

enriched cell colonies were subsequently processed by Sanger sequencing analysis. Compared to the unenriched heterogeneous population (Figure **4.11** A) that, as expected, displays considerable sequence variation within the targeted locus, near clonal populations of cells demonstrated a significantly reduced signal noise (Figure **4.11** C &D). Genomic features of *AR* exon 8, including deletion, insertion, scar, and complex alleles or no editing frequency, for all 91 clones were calculated across both LNCaP and CWR22Rv1 examined in detail and summarized in Figure **4.8** B. A large number of colonies were found to undergo Cas9/sgRNA-mediated NHEJ: 37 colonies (40.6%) displayed small or larger DNA fragments deletion and 27 (29.6%) had small nucleotides insertion (one example of each are presented in Figure **4.11** C &D). 18 sub-clones (19.8%) were 'uncut' or wild-type while the remaining 9 clones reveals genomic scar-based sequencing failure (9.7%).

Disappointingly, no intended AR_{F876L} mutation was detected in all selected colonies; this was confirmed in 2 randomly selected cell populations by cloning the genomic DNA PCR product and sequencing. One potential reason for this observation is that not all cells were edited as intended due to NHEJ predominating as the DNA repair pathway in these growth conditions. Additionally, given that the cell populations were not truly clonal, outgrowth of wild-type or NHEJ-repaired cells may have occurred at the expense of precise knock-in mutations. Clonogenic isolation and assessment of genomic editing type is time-consuming and labour-intensive. To design the most effective screening strategy, a crucial step is to realistically estimate the chance of obtaining the desired mutant cells in the pool undergoing CRISPR-mediated genome engineering. Although a number of successful 'knock-in' events have been reported (Richardson *et al.*, 2016; Wang *et al.*, 2016; Yoshimi *et al.*, 2016), a considerable number of unstudied factors may have also impacted the ultimate efficiency of Cas9-mediated knock-in via HDR. This will be discussed in more detail in the next section.

4.4 Discussion

4.4.1 Design and generation of sgRNA/Cas9-editied enzalutamide-resistant PC cell model by knock-in of the AR_{F867L} mutation.

CRISPR/Cas9 contains two key components, a small guide RNA and a Cas9 protein. Upon delivery into cells, the Cas9 protein is readily targeted to DNA sequences of interest based on designed sgRNAs. For the *Streptococcus pyogenes* Cas9 particularly, the enzymatic activity is driven by a 20 nucleotide DNA sequence that is complementary to the crRNA and upstream of a 'NGG' protospacer adjacent motif (5'-PAM-3'). Binding between Cas9 and PAM is vital for the initiation of target activity. Cas9 unwinds the DNA duplex upstream of the PAM to allow cleavage of both the target and nontarget strands of substrate DNA (Fuguo and Jennifer, 2017). Upon cleavage, Cas9-mediated DSB site undergo DNA repair which most frequently leads to genetic aberration as a consequence of error-prone NHEJ repair and the generation of indels. This approach is now often used for gene knockout studies (Li *et al.*, 2014). Alternatively, in the presence of a repair template, the Cas9-targeted double-strands break site undergoes HDR, which can be used to insert a gene (Yoshimi *et al.*, 2016) or in our case, used for precise gene editing of desired knock-in mutations.

In our CRISPR system, we initially designed two small guide RNA that targets *AR* exon 8 that are adjacent to the F876 codon (Figure 4.1). By co-delivery of our Cas9/sgRNA with a repair DNA template containing the F876L mutation into LNCaP cells, our primary objective was to introduce the F876L mutation within *AR* exon 8 gene of the PC cell line. An additional aim using a wild-type DNA template, was to reverse the endogenous T877A mutation in LNCaP cells back to wild-type (wt-AR). From this wt-AR LNCaP cell line, CRISPR would then subsequently enable the generation of an LNCaP_AR_{F876L} mutant cell line by incorporating a distinct donor template containing the F876L mutation.

In addition, in this Chapter, we have also employed the CW22Rv1 cell line that expression both AR-FL and several splice variant isoforms of the receptor (AR-Vs) that lack the ligand-binding domain. This truncated version of the receptor has been recently discovered and has been found to play an important role in disease progress (Dehm and Tindall, 2011). Importantly, AR-Vs has been found overexpressed in over 60% of CRPC patients (Zhang *et al.*, 2011). Therefore, CWR22Rv1 cells provide an additional cell line to establish the CRISPR pipeline and represent a further clinically-relevant background to study the impact of AR mutations; critically since they express an endogenous AR_{H874Y} mutant (Figure **4.1**) that is abnormally activated by the antagonist Cyproterone Acetate (CPA). Importantly, a clinical correlation between estrogenic stimulation and H874Y mutation has recently been reported (Vasudevamurthy *et al.*, 2017). One PC patient was found to harbor the H874Y mutation following ADT therapy and who later had a poor response to enzalutamide. Therefore, by reversing the endogenous mutation back to wild-type or performing knock-in of the F876L, we will provide an extensive repertoire of models to study enzalutamide resistance in the presence of AR-Vs and pre-existing AR mutants. Critically however, these exciting aims were never realized due to the challenge of generating specific knock-in mutations within both cell lines as discussed below.

4.4.2 Targeting of *AR* gene exon 8 in LNCaP and CWR22Rv1 cells.

Two individual sgRNA with different PAM sites encompassing the F876 codon in exon 8 (Figure **4.2**) were designed and cloned into a single vector system encoding Cas9 and a GFP transfection marker (Figure **4.2**). We next assessed the most efficient of the CRISPRs by delivering the two Cas9/sgRNA plasmids into HEK293T cells. The delivery approaches of CRISPR are flexible: for *in vivo* experiments, CRISPRs are often introduced into whole organisms, such as mouse, zebrafish (Hwang *et al.*, 2013; Xiao *et al.*, 2013) and Drosophila (Ren *et al.*, 2013; Yu *et al.*, 2013; Sebo *et al.*, 2014) by microinjection; whilst for *in vitro* assays, typical transfection/transduction approaches are utilised. By using lipid-based transfect reagents, we firstly observed, via analysis of GFP expression, that both CRISPR plasmids can be easily delivered into HEK293T cells (Figure **4.3**), which may not be surprising as HEK293T cells are a well-accepted vehicle line for the expression of ectopic proteins (Thomas and Smart, 2005). In fact, the HEK293T/HEK293FT cell lines are commonly used for validating the efficiency of the TALEN and CRISPR/ Cas systems in a

human *in vitro* model, because they can be transfected easily by plasmids and are relatively simple to maintain (Sanjana *et al.*, 2012; Cho *et al.*, 2013; Cong *et al.*, 2013; Hu *et al.*, 2013; Mali *et al.*, 2013a).

Validation of transfection efficiency of Cas9/sgRNA is a vital step for generating genetically-edited models. For our CRISPR system, detecting GFP expression is the most efficient and convenient approach, as it can be simply visualized by florescence microscopy (Figure **4.3**). Moreover, by FACS sorting florescence in cells, GFP expression can also be quantified as an indicator for transfection efficiency (Figure **4.4**). The successful transfection of Cas9/sgRNA plasmids were confirmed via detecting of GFP expression in tested cell line.

Once transfection has been validated, it is important to subsequently assess CRISPR efficiency. To date, several methodologies are commonly undertaken to screen NHEJ-induced Indels (Local Point Mutation, Insertion, and Deletion) produced by the CRISPR/Cas9 system, including the Surveyor nuclease and T7 Endonuclease I (T7E1) assays; High Resolution Melting Analysis (HRMA) and PAGE electrophoresis (Miller *et al.*, 2007; Gravina *et al.*, 2010; Guschin *et al.*, 2010; Niu *et al.*, 2014; Sung *et al.*, 2014; Zhu *et al.*, 2014). Additionally, several modified methods have also been developed for detecting CRISPR/Cas9-induced mutants that utilise microfluidic capillary electrophoresis or fluorescent PCR (Ramlee *et al.*, 2015; Chenouard *et al.*, 2016; Kc *et al.*, 2016) however, these methods are expensive, as pre-designed probes and expensive equipment are required.

Surveyor nuclease and T7 endonuclease I (T7EI) assays are wildly used among all validation approaches as both are relatively easy to perform and can be carried out using standard equipment. Importantly, these endonuclease-based assays are suitable for any target sequence and can recognise and digest mismatched heteroduplexed DNA. By conducting Surveyor assays in HEK293T cells transfected with our two CAS9/sgRNA-expressing plasmids, Cas9/sgRNA196-

mediated indels were observed at exon 8 of the *AR* gene (Figure **4.1** C), but not in cells containing Cas9/sgRNA186. Hence, Cas9/sgRNA196 was considerably more efficient at targeting the desired locus than the sgRNA186-containing CRISPR vector and hence was subsequently selected for the AR$_{F876L}$ knock-in pipeline.

Although using cationic lipid-based reagents is the conventional and most popular methods for plasmid DNA (and siRNA) transfection, it can be toxic and restricted to certain cell types and both LT-1 or lipofectamine 2000 was not sufficiently efficient for delivery of Cas9/sgRNA196 into LNCaP and CW22Rv1 cell lines (Table **4.4**). Recently, Nucleofection (Lonza Cologne AG, USA /Canada) has been reported as an attractive electroporation approach for delivering CRISPR into transfection-resistant cell types. Indeed, we observed positive transfection of Cas9/sgRNA196 in CW22Rv1 48 hours post nucleofection (Figure **4.4**) using the Surveyor assay.

However, this method does not appear to be compatible with LNCaP cells. Although GFP expression was visualized (data now shown), there was no detectable cleavage within the target region in LNCaP cells. (Holkers *et al.*, 2013) and (Owens *et al.*, 2012) previously investigated transfection capability of CRISPR's counterparts TALEN and ZFN into primary cells or cells refractory to plasmid transfection. They found that viral vectors were among the most effective gene transfer vehicles. (Li *et al.*, 2011) showed that using viral vectors can enhance the efficiency of TALEN-mediated HDR and drive ZFN-mediated gene editing *in vivo*. Moreover, (Gwiazda *et al.*, 2016) have successful achieved CRISPR-mediated gene-editing in multiple mammalian cells using adenovirus vectors. Hence, as an alternative to non-viral gene delivery systems, we packaged the Cas9/sgRNA196 plasmid into lentivirus in an attempt to increase efficiency of plasmid delivery into LNCaP cells. After infection, comparing to control cells, we were able to detect the custom designed Cas9/sgRNA196-mediated endogenous AR gene disruption in LNCaP cells (Figure **4.5**). Ultimately, Cas9/sgRNA-delivered CWR22Rv1 and LNCaP cell pools were sorted based on GFP expression and 75% and 31% transfection-positive cells were detected, respectively (Figure **4.4**). In all, our results suggest a specific cell-type dependency for effectively delivering CRISPR

plasmids into CWR22Rv1 and LNCaP cells (Table 4.4). **Importantly, the desired Cas9/sgRNA196-mediated 'on-target' effects were achieved among all studied cell lines.**

Although Cas9/sgRNA196-medicated indels were detected in both LNCaP and CWR22Rv1 cell lines using the Surveyor assay (Figure **4.3**, Figure **4.4** and Figure **4.5**), the endonuclease-associated methodologies have limitations involving DNA extraction, PCR, amplicon purification and gel electrophoresis which are time-consuming and labour-intensive. Moreover, the Surveyor assay lacks a robust means of quantifying CRISPR efficiency as it utilizes densitometry to compare intensity of wild-type and mutant heteroduplexes post electrophoresis. To enable a more quantitative means of assessing CRISPR-mediated indels within *AR* exon 8, we sequenced PCR amplicons encompassing the targeted region and analysed the sequencing data using TIDE (Tracking of Indels by Decomposition, https://tide.deskgen.com/) which is a web tool designed to facilitate analysis of CRISPR-Cas9 efficiency. By uploading control and sample chromatogram alongside the sequence of the gRNA, TIDE will predict the cutting site of the CRISPR and subsequently analyses differences between control and CRISPR-modified sequences both up- and downstream of the cleavage site (typically 3 bp from the PAM site). As shown in Figure **4.6** A and Figure **4.7**, the Cas9/sgRNA196 combination induced random insertions and deletions at proximately 3 bp upstream of the PAM code in both CW22Rv1 and LNCaP cell lines. Furthermore, by decomposing the chromatogram sequences around the target site, details of deletion and insertion was also quantified in both cell line (Figure **4.6** and Figure **4.7**). We therefore utilized this method for confirming CRISPR efficiency in all of the subsequent experiments.

4.4.3 ssODN design and knock-in F867L mutation via Cas9-mediated HDR

Having confirmed the successful delivery and selective enhanced 'on target' efficiency of Cas9/sgRNA196 in both CWR22Rv1 and LNCaP cells (Figure **4.7**), we next sought to co-deliver the pre-designed repair template in order to achieve the desired 'knock-in' AR_{F876L} mutation. Firstly, to enhance indel frequency and increase the chance of cells uptaking the repair template, LNCaP cells were transduced with CRISPR expression virus. By selectively culturing cells with puromycin containing medium, higher efficiency on-target effects and indels was observed in selected cells.

Cas9 contains two nuclease domains, HNH and RuvC. Upon binding of chromatin, Cas9 makes a double-strand break in the target locus in the presence of Magnesium ions; with the HNH nuclease domain of the enzyme cutting the DNA strand complementary to crRNA, and the RuvC domain cutting the non-complementary strand (Chen *et al.*, 2014b). By labelling substrate DNA on each side of the nuclease cut site with a distinct fluorophore and monitoring the dissociation of cut fragments. (Richardson *et al.*, 2016) demonstrated that before complete dissociation, Cas9 preferentially releases HNH nuclease domain from the 3' end of the cleaved DNA strand while RuvC domain remains bound with complementary to the sgRNA (nontarget strand). This observation suggests that donor DNA complementary to the nontarget strand may be more effective than donor complementary to the target strand. In support of this theory, by using symmetric single stranded donor oligonucleotides (ssODNs) that are complementary to the nontarget strand, (Lin *et al.*, 2014) and (Yang *et al.*, 2013b) successfully introduced mutation in to *EMX1* and *AAVS1/PPP1R12C* loci in human cell lines, respectively. Hence, the single-stranded DNA (ssDNA) donors of the optimal length complementary to the strand that is released first was considered for incorporation into the AR CRISPR/sgRNA196 knock-in pipeline.

Using repair templates for insertion of specific mutations by CRISPR, homology arms complementary to the ends of the planned DNA break is required for the flanking regions of the donor template. The length of the homology arm is also proposed to play an essential role in increasing HDR rate. Several gene-editing studies focusing on homology arm length have recently been conducted and overall, they suggested that increasing the homology arm size may increase modification frequency. Although (Yoshimi *et al.*, 2016) observed robust HDR with homology arms of 30–60 bases when creating small insertions, by increasing homolog arm length from 50 bp to 200 bp in the same Cas9+ssODN system, (Li *et al.*, 2014) increased the frequency of inserting a 720 bp fragment by 8-fold at the *Oct4* locus.

Considering the large size of an ssODN may result in low transfection efficiency and may be difficult for synthesis, a 200bp sequence complementary to the target sequence in exon 8 was chosen as the ssODN (Figure 4.8 A) that contains the F876L mutant codon with 75bp homology arms flanking both sides. Within the donor template, the PAM 'TGG' site was substituted with 'TCG' to prevent re-cutting of the site by Cas9 which may subsequently remove the knock-in mutation by NHEJ-mediated repair. Additionally, for further assessing the successful insertion of the donor template within the genome, *Sal* 1 restrict digest site (G^TCGAC) was also artificially insert into the ssODN. Hence, upon CRISPR-mediated knock-in of the donor template, RFLP assays will specifically identify successful genome editing events using *Sal* I digestion as an initial diagnostic tool.

Upon co-transfection of the CWR22Rv1 cell line with the repair donor and the Cas9/sgRNA196 plasmid, it was observed that the phenotype of the cells appeared distinct from the group that were transfected with the plasmid only (Figure 4.8). Typically, cells co-transfected with two components demonstrated altered growth characteristics to the extent that grew as colonies as opposed to a more evenly distributed layer as seen in the control arm. GFP expression was observed 7 days post nucleofection. Hence, 10 colonies was picked for potential successful ssODN insertion/knock-in mutation detection. Unfortunately, no successful desired knock-in mutation was detected by the polymerase chain reaction (PCR)/restriction enzyme (RE) assay (Appendix 4B). This was disappointing, but not a surprising result as this is a decidedly difficult process due to the process of HDR, which is required for the insertion of the donor template into the genome, occurring at a low frequency in the cell population; most repair in interphase is conducted by NHEJ. (Cong *et al.*, 2013) demonstrated that in the absence of a repair template, the Cas9-mediated Indel frequency was 7-27% in human cells which is consistent with the efficiencies observed in both CWR22Rv1 and LNCaP cells in this study. In contrast, however, the same study indicated that co-transfection of cells with a ssODN template and measurement of HR activity was merely 0.46% indicating that considerably more colonies will need to be assessed

before potentially detecting a precise knock-in clone. Similar results were also reported in other studies (Lin *et al.*, 2014; Schumann *et al.*, 2015).

Although CRISPR/Cas9 has a broad range of applications in science and human therapeutics, the results presented in this chapter indicate that several factors affect efficiency and specificity of utilizing CRISPR for precise genome editing, including delivery approaches, short guide RNA design, target gene loci selection, off-target effects and the incidence of homology-directed repair. In the rest of the discussion, I will summarize the potential factors that affect the application of CRISPR/Cas9 for precise gene editing, as well as possible strategies for resolving these problems.

As noted previously, Cas9 nuclease mediated DSBs at desired target sites can stimulate two distinct endogenous DNA repair mechanisms, NHEJ and HDR. Evidently, the choice of DNA-repair pathways is largely beyond experimental control. In general, NHEJ is error-prone but highly efficient, hence, even in the presence of donor templates, NHEJ is the more frequently repair pathway when using CRISPR/Cas9 systems. NHEJ is initiated by the recruitment of Ku70/ 80 heterodimer and DNA-PKcs (Tomkinson *et al.*, 2013). This complex stabilizes the two DNA ends and a series of proteins was subsequently recruited, including DNA ligase IV, to ligate the DNA breaks (Robert *et al.*, 2015). Whilst for HDR, the DNA strands break are cleaved to generate 3'-ssDNA overhangs that can recruit a set of repair proteins and invade with a homologous donor template (Robert *et al.*, 2015). Critically, impairing NHEJ components in cell lines increases the level of HDR suggesting that two repair processes are in direct competition (Srivastava et al., 2012; Tomkinson et al., 2013; Chu et al., 2015; Vartak and Raghavan, 2015; Yu et al., 2015). Knockdown of KU70/80 or DNA ligase IV by short hairpin RNA sequences, (Chu et al., 2015) were able to promote HDR efficiency in both human and mouse cells. In addition, (Robert *et al.*, 2015) also confirmed that by using two small molecule inhibitors of DNA-PKcs (NU7441 and KU-0060648) NHEJ was reduced and conversely, the frequency of HDR was enhanced. Hence, by

silencing key component that are required for NHEJ in our cell line model, this may increase the incidence of F876L knock-in via Cas9-mediated HDR pathway.

The cell-cycle phase upon which HR occurs in repair mechanism may be another considering factor to improve the efficiency of knock-in rate. NHEJ is generally the predominant repair mechanism in the growth 1 (G1) and the mitotic (M) phases of cell cycle whilst HR takes place in the synthesis (S) and the premitotic (G2) phases when there are sister chromatids available (Mao *et al.*, 2008). Therefore, by incorporating small molecule cell-cycle inhibitors of the S and G2 phases to elevate the cell populations in these HR-proficient phases may also enhance desired knock-in incidence.

Another possible issue surrounding the protocol employed here is achieving the appropriate level of Cas9/sgRNA196-mediated DNA damage to occur simultaneously with a repair template proximal to the site of damage. Successful transfection and subsequent transcription/translation of the Cas9 enzyme and interaction with the sgRNA196 activity requires upwards of 8 hours; while once bound to DNA, the dissociation of the Cas9/sgRNA from the target locus is as slow as 6 hours (Richardson *et al.*, 2016) suggesting that it may be challenging to maintain optimal chromatin environments for Cas9-ssODN interactions and precise HDR-mediated editing. Moreover, transfected plasmids and the ssODN remain episomal and hence are lost over successive cell cycles which further reduces the window for successful genome engineering. Hence, one of the potential solutions to these issues is to ectopically express the ssODN sequence, containing the AR_{F876L} mutation, from the Cas9/sgRNA196 plasmid to achieve optimal expression of the three components required for generating knock-in mutations. In addition, using phosphorothioate bonds at both 5'- and 3'- ends of ssDNA donor oligonucleotides, (Prykhozhij *et al.*, 2017) demonstrated more efficient HDR comparing to control donor template. Thus, stabilizing donor template by phosphorothioation of the ssODN may also be another partially strategy to improve knock-in events.

The distance between the predicted cutting site and the desired editing site (e.g. mutation) has recently also been suggested to be a major consideration for improving uptake and incorporation of the ssODN into the process of HDR (Paquet *et al.*, 2016). The less nucleotides between the desired editing site and the site of Cas9 cleavage has been found to robustly enhance knock-in mutation frequencies by HDR. Although we have chosen the more robust 'on-target' and efficient Cas9/sgRNA196 for the purpose of knock-in generation, the F876 target codon sits over 30 nt distal to the Cas9/sgRNA196-mediated cutting site which, according to previous studies, will have a detrimental effect to precise editing efficiency.

For future studies, a more robust approach may be to switch to another type of CRISPR class type that relies on different PAM codes for directed DNA cleavage. For instance, SmCms1 and AsCpf1 (both from CRISPR Type V) utilizes respective 'TTN' and 'TTTN' as the PAM code for their activity. Similar to Cas9, both CRISPR Type Vs result in a DSB site adjacent to PAM code (Begemann *et al.*, 2017). Hence, by employing other CRISPR types that utilize distinct PAM sites, it may be possible to mediate DSB cleavage adjacent to the F876 codon and hence improve knock-in efficiency.

In this chapter, we have firstly verified our designed sgRNA/Cas9 'on-target activity' at *AR* exon 8 in the two PC cell lines. Moreover, we optimized a systemic high throughput screening approach to enable detection of knock-in mutants that did provide some evidence of precise editing in pooled cell populations, but these were never clonally expanded due to technical difficulties. However, with low level of transfection/transduction efficiency and HDR frequency in both cell lines, it is likely that a larger number of colonies will need to be screened in order to create a clonal AR_{F876L}–expressing cell line derivative. Considering the time-scale of the work conducted in this chapter and the lack of a genuine CRISPR edited cell line for study, a contingency plan was carried out in parallel which was based on a recently published AR rescue system developed by the Gaughan lab (O'Neill *et al.*, 2015). Instead of persisting with the CRISPR model system for the full duration of study, LNCaP cells were transduced with lentiviral mammalian expression vector encoding a FLAG-tagged-AR_{F876L} construct to generate a stable AR_{F876L}-expressing LNCaP derivative to enable analysis of this mutant in a physiological background upon depletion of the

endogenous AR_{T877A}. Moreover, this new cell model can also be an excellent platform for testing of next generation targeted therapies. Our previous research utilizing an AR-replacement model in LNCaP cells demonstrated that the bicalutamide-activated AR_{W741L} mutant selectively regulates a gene-set distinct from endogenous AR_{T877A}. My current results shown in the next two chapters suggests that the AR_{F876L} mutant retains activity in the presence of enzalutamide in LNCaP cells and offers insights into discriminate functionality of the mutant receptor and opportunities for selective drug targeting of AR mutants. The details of cell line model will be focus on discuss in next two chapters.

Chapter 5: Generation and characterise of stable LNCaP-AR$_{F876L}$ cell line

5.1 Introduction

With increasing understanding of the physiology and molecular mechanism of AR function in advanced disease in the past two decades, the development of direct or indirect AR targeting agents has seen marked improvements to PC treatments in the UK and beyond. Many AR-targeting drugs have been developed and are most frequently used in the clinic for intermediate- and high-risk patients, principally in combination with ADT, such as LHRH agonists.

Although initially sensitive to anti-androgen and ADT therapies, unfortunately, most PC patients will relapse, with disease progressing to refractory, untreatable CRPC. At this stage, tumours either become endocrine-therapy resistant during the course of treatment or possesses a small population of pre-existing hormone-refractory cells that remain viable in spite of castration levels of androgen (Heck *et al.*, 2012). By selective outgrowth of resistant cells with acquired genetic alterations that could contribute to disease progression, tumors aggressively progress, are refractory to current therapies and eventually claim the life of patients.

Clinically, approximately 50% of patients after hormone therapy present with anti-androgen withdrawal syndrome (AAWS). This condition is characterized by cancers that grow in the presence of anti-androgens and whose growth is attenuated by stopping anti-androgen treatment (Gottlieb *et al.*, 2012). Acquiring somatic mutations in the *AR* gene is likely responsible for the 15–30% of patients that exhibit a withdrawal syndrome after cessation of first-generation therapies (Paul and Breul, 2000).

DNA sequencing of tissue biopsied from CRPC patients identified 159 *AR* gene coding mutations (last update 2012). Importantly, almost 50% of them were found to reside within the LBD cofactor binding regions (Schweizer and Antonarakis, 2012). This evidence strongly suggested that mutation selection under pressure of anti-androgen treatment contributes, in part, to drug resistance. Long-term treatment with the AR antagonists could selectively enable outgrowth of tumor cells that are driven by AR mutants causing drug resistance by turning anti-androgens from antagonists to agonists. These included L701H, H874Y and

T877A, noticeably, all of which were identified from patients that had been treated with anti-androgens (Steketee *et al.*, 2002). Further studies (van de Wijngaart *et al.*, 2012) found that most mutations resulted in reduced ligand specificity and hence permitted inappropriate receptor activation by binding to adrenal androgens or other steroid metabolites. AR_{L701H} is activated by other steroids, including estrogen, cortisone; while AR_{H874Y} is activated by progesterone. Certain LBD mutations identified are also sufficient to convert AR antagonists to AR agonists *in vitro*. T877A and H874Y mutations were found in LNCaP and CWR22Rv1 cell lines, respectively, and were shown to be abnormally activated by the antagonists Flutamide and Cyproterone Acetate (CPA). Another mutation, W741L was later found both in LNCaP and ADT-treated metastatic patient sample-derived xenograft tumors which exhibit increase tumor growth and PSA secretion in response to bicalutamide (Yoshida *et al.*, 2005b). This was confirmed in an LNCaP derivative cell line stably expressing the AR_{W741L} mutant (O'Neill *et al.*, 2015) which demonstrated endogenous AR-target gene expression upon bicalutamide-activation of the ectopic mutant.

A next-generation anti-androgen enzalutamide (Xtandi™) has recently been FDA-approved for use in advanced prostate cancer and has had a positive clinical impact in prolonging longevity and quality of life of advanced prostate cancer patients (Silberstein *et al.*, 2013). Consistent with other AR-targeted agents however, the efficacy of enzalutamide therapy is reasonably short-lived, extending median survival by only 2-8 months and upwards of 50% of patients are refractory to treatment. Most forms of CRPC are still dependent on the AR-axis for survival (Dhingra *et al.*, 2013). Recently, a specific AR mutation, F876L has been reported that is sufficient to confer partial resistance to enzalutamide and the related AR antagonist apalutamide (Joseph et al., 2013). The mutation was discovered by the Sawyers's Group, using a reporter based mutation screen approach, and was found to confer resistance to enzalutamide (Balbas et al., 2013). This observation was then supported by *in vivo* and *in vitro* experiments that demonstrated specific AR_{F876L} mutations can confer partial agonist activity to enzalutamide in models of CRPC (Rodriguez-Vida et al., 2015). Importantly, the mutant was later detected in CRPC patients after treatment with apalutamide (Nelson and Yegnasubramanian, 2013).

In view of this antagonist to agonist switch phenomenon in response to chronic enzalutamide treatment, it is hypothesised that patients harbouring the F876L-mutated AR might clinically benefit from withdrawal of enzalutamide. Importantly, the same mutation has been detected in circulating tumor DNA from apalutamide-treated CRPC patients (Dellis and Papatsoris, 2018). Taken together, the evidence highlights the selective outgrowth of AR_{F876L}-expressing cells is a clinically relevant mechanism of second-generation anti-androgen resistance.

The current commonly adopted method for studying AR mutant function is by transient transfection of AR-encoding plasmids into AR null cells and assessment of receptor function principally by luciferase-based read-outs. Although useful, this approach lacks physiological relevance. To understand the molecular mechanisms of AR_{F876L} function, and to model more physiologically the mutant in order to assess sensitivity to other clinically-relevant targeted agents, we sought to generate an AR rescue/replacement system to permit a more effective platform to determine the endogenous activity of AR_{F876L}. This is consistent with the model developed by the Gaughan group (O'Neill *et al.*, 2015) to study the bicalutamide-activated AR_{W741L} mutant.

This chapter will commence by firstly using an androgen-responsive luciferase reporter as a surrogate for assessing the agonistic activity of enzalutamide towards AR_{F876L} and to confirm previous reports (Balbas et al., 2013). It will be then be followed by generation and thorough validation of an AR_{F876L} rescue model system in the androgen-responsive LNCaP cell line which will enable more robust modelling of the AR mutant and assessment of response to next-generation AR antagonists and other therapeutics, including bromodomain inhibitors.

5.2 Specific method and materials

5.2.1 siRNA oligo design (and transfection)

LNCaP or LNCaP-AR$_{F876L}$ (~3 x 10^6) were seeded in 20 ml 10% FCS medium in a 150 mm dish for 48 hours until cell confluence reached over 80% per dish before replacing medium with steroid-depleted media. siRNAs (25 nM final concentration) were transfected with 2 ml basal medium (free of phenol-red) per dish for 48 hours. A second round of siRNA transfection was repeated following 48 hours of culture. 96 hours post-transfection, the indicated treatments (DHT-10 nM; bicalutamide-10 µM, enzalutamide-10 µM) were applied to cells for the last four hours of the experiment. Post-2x ice cold PBS washes, the cells were trypsinised and spun down, collecting pellets to be used for the subsequent mRNA extraction (as descripted in 3.14) or Western blotting. Alternatively, cells were scraped prior to ChIP assay as described in 3.14.4.

5.2.2 Luciferase-activity assay

AR-negative PC3 and HEK293T cells were seeded at a density of 2x10^4/well in 24-well plates (Corning) in steroid-depleted media for 24 hours. 50 ng pCMV-FLAG-AR wild-type or pCMV-FLAG-AR$_{F876L}$ and the AR-dependent ARE Luciferase reporter (containing a three repeats of a consensus ARE)(O'Neill *et al*., 2015) or PSA Luciferase reporter (containing ~600 bp of the *PSA* promoter region) were transiently transfected into the cell lines using LT-1 transfect reagent. 100 ng/well of transfection control vector pCMV-β-galactosidase was also co-transfected. 24 hours after transfection, indicated treatments were applied for an additional 24 hours. Cell lysates were harvested using Luciferase reporter lysis buffer (Promega, UK). Luciferase activity was determined using a FLUOstar plate reader, Omega, and normalized to β-galactosidase activity (see below). Luciferase activity was presented as relative hormone-induced luciferase activity (Figure 5.1). Each bar represents the mean of three independent experiments performed in triplicate. Transcriptional activation of wild-type AR by DHT was set to 100%. All statistical analysis was performed using GraphPad Prism software (GraphPad, San Diego, CA, USA) by one-way analysis of variance (ANOVA).

5.2.3 β-galactosidase normalization assay

β-gal assays, which utilises the β-galactosidase (β-gal) substrate o-nitrophenyl- β-D-galactopyranoside (ONPG), was used to measure β-gal activity in each transfection. 10 μl of cell lysate were added to in a clear bottomed 96-well plate and mixed with 10 μl β-gal assay substrate prior to incubation at 37°C for approximately 5-10 minutes until samples yielded a yellow colour. Reactions were then neutralized by addition of 50 μl 1M Na_2CO_3 and absorbance measured at 415 nm using a 96-well model 680 plate reader (BioRad). β-galactosidase readings were used to normalise corresponding luciferase assay data as described above and presented using GraphPad Prism software (GraphPad, San Diego, CA, USA) by one-way analysis of variance (ANOV activity in each transfection).

5.2.4 Cell proliferation assays using the Incucyte Zoom platform

To investigate the effect of each anti-androgen on cell proliferation, an appropriate density of cells (~3000 cells / well) were seeded into each well of a 96-well plate in a volume of 90 μl steroid-depleted growth medium using an Eppendorf Repeater Stream pipette. Cells were allowed to adhere for 24 hours before being treated with 10 nM DHT or 10 μM bicalutamide/enzalutamide to bring the final volume to 100 μl/well. Cells were subsequently incubated for 7 days. Cell confluency, as a measure of well surface coverage, is measured in real-time (every 6 hours) using the Inucyte Zoom (Essen Bioscience) and later analysed using the Basic Analyzer Software (Essen Bioscience).

5.2.5 Proliferation assays using Sulforhodamine B assay

Sulforhodamine B (SRB) assays were performed according to Skehan *et al.,* (1990). Briefly, cells were seeded out as described above (3,000 cells per well in 90 μl steroid-depleted medium in 96-well plates). Cells were incubated with compounds (DHT, bicalutamide and enzalutamide) at appropriate concentrations for 5 days before being fixed with 25 μl ice cold 50% trichloroacetic acid for 1 hour at 4°C.

Fixative was removed by washing with tap water and cells were stained with 0.4% (wt/vol) SRB dissolved in 1% acetic acid. Excess was removed by washing five times with 1% acetic acid. Plates were then air-dried at RT, after which bound SRB was dissolved with 10 mM Tris-HCl, pH 10.8. Absorbance was measured at 570 nm using a 96-well plate reader (BioRad).

5.3 Results

5.3.1 Enzalutamide Increases transcriptional activity of AR$_{F876L}$ in luciferase assays.

Investigating the regulatory mechanisms of the AR$_{F876L}$ mutant may potentially provide new therapeutic targets to enable inactivation of AR$_{F876L}$-driven enzalutamide resistance in CRPC. To interrogate the roles of AR mutant function, model optimization was required prior to assessing the transcriptional potential of AR$_{F876.}$ A luciferase reporter method therefore was first selected to determine whether the next-generation anti-androgen enzalutamide is indeed an agonist for the AR$_{F876L}$ mutant.

For the luciferase-based reporter assay, AR mutant expression plasmids and an AR-dependent luciferase reporter were transiently transfected into the AR negative PC cell line. A pGAL4-β-galactosidase plasmid was co-transfected to act as a transfection efficiency control. As illustrated in Figure 5.1 A, the luciferase reporter expression is driven by a promoter region which contains three repeats of a consensus 15-mer ARE sequence. In the presence of an activating ligand, the ectopically expressed AR can actively bind to the ARE region and promote activation of luciferase, therefore providing a direct readout of AR transcriptional activity.
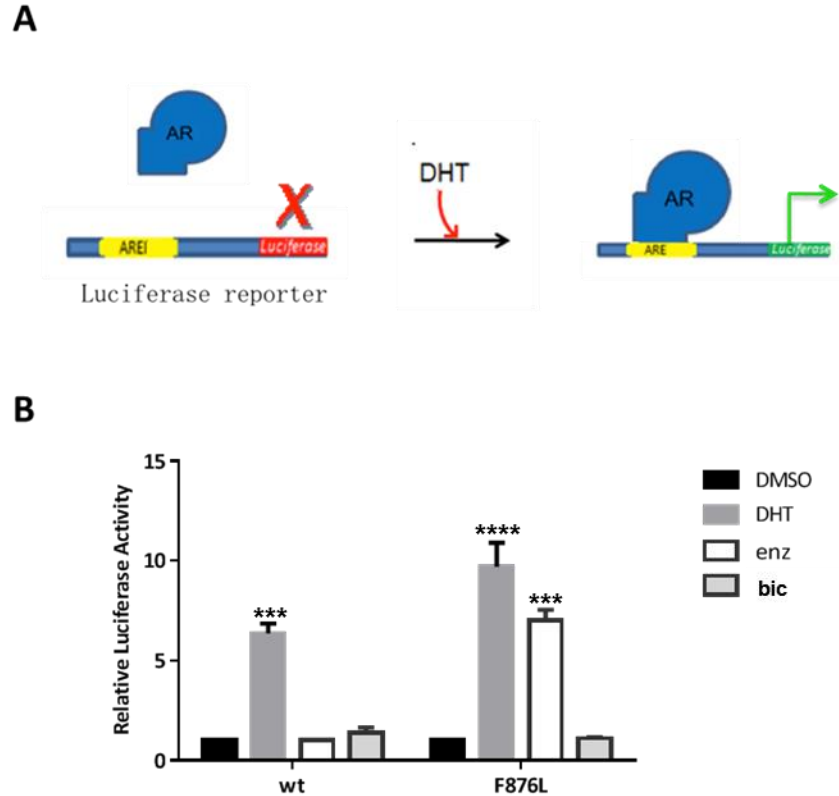
Figure 5.1 Enzalutamide increases ectopic AR$_{F876L}$ activity in AR negative PC3 cells. (A) A. Diagrammatic representation of the luciferase reporter assay to assess AR activity; showing activated AR binding to an androgen response element (ARE) and driving expression of the downstream luciferase gene. (B) Bar graphs showing normalized luciferase activity following transfection of HEK293T cells with wild-type AR (WT) or AR$_{F876L}$ (F876L) expression constructs and a PSA reporter in steroid-depleted medium. The indicated treatment of vehicle (DMSO), 10 nM DHT, 10 µM enzalutamide (enz) or 10 µM bicalutamide (bic) were conducted for 24hours. All data are normalized to DMSO control. Each AR derivative and data represents the mean of triplicate experiments performed in quadruplicate (+/- SEM;). All statistical analysis was performed using GraphPad Prism software (GraphPad, San Diego, CA, USA) by one-way analysis of variance (ANOVA). Values are presented as mean±SEM, ***p-value <0.001**** <0.0001 as calculated using a student's T-test.

As shown in Figure 5.1 B, in the presence of 10 nM DHT, wild-type AR (ARwt) transcriptional activity as expected increased over 6-fold, whilst no increased activity was observed following enzalutamide and bicalutamide treatment. It suggests that both anti-androgens do not present agonistic activity on wild-type receptor. Consistent with ARwt, 24 hours DHT treatment increased AR$_{F876L}$ activity by over eight-fold indicating the mutant remains responsive to natural agonists. In contrast, however, enzalutamide treatment alone significantly induced AR$_{F876L}$ activity over 7-fold compared to control whilst no increase to activity was observed following bicalutamide

treatment. This result is consistent with previously published data (Korpal *et al.*, 2013a) that reported enzalutamide functions as an agonist for the AR$_{F876L}$ mutant. Furthermore, our data also suggested that AR$_{F876L}$ does not presents agnostic activity to bicalutamide. The luciferase data overall suggests that in the presence of enzalutamide, the F876L mutant possesses a similar active response as wild-type AR response to DHT. In addition, my results also indicate that no agonistic activity of bicalutamide was observed on AR$_{F876L}$.

5.3.2 Generation of pLenti6.3 AR$_{F876L}$ constructs.

Although the data from the luciferase reporter-based assay supported our theory of the F876L mutant exhibiting agonistic response to enzalutamide, most current models are based on transient overexpression of mutant receptors in AR negative cells, which is suitable for assessing transcriptional activity on candidate reporters but provides very little information regarding their role in global transcriptomics. In order to have a more physiologically-relevant background study model, we next adapted a lentiviral-based strategy to establish a stable prostate cancer cell model which can facilitate more global analyses of the AR$_{F876L}$ mechanism of action.
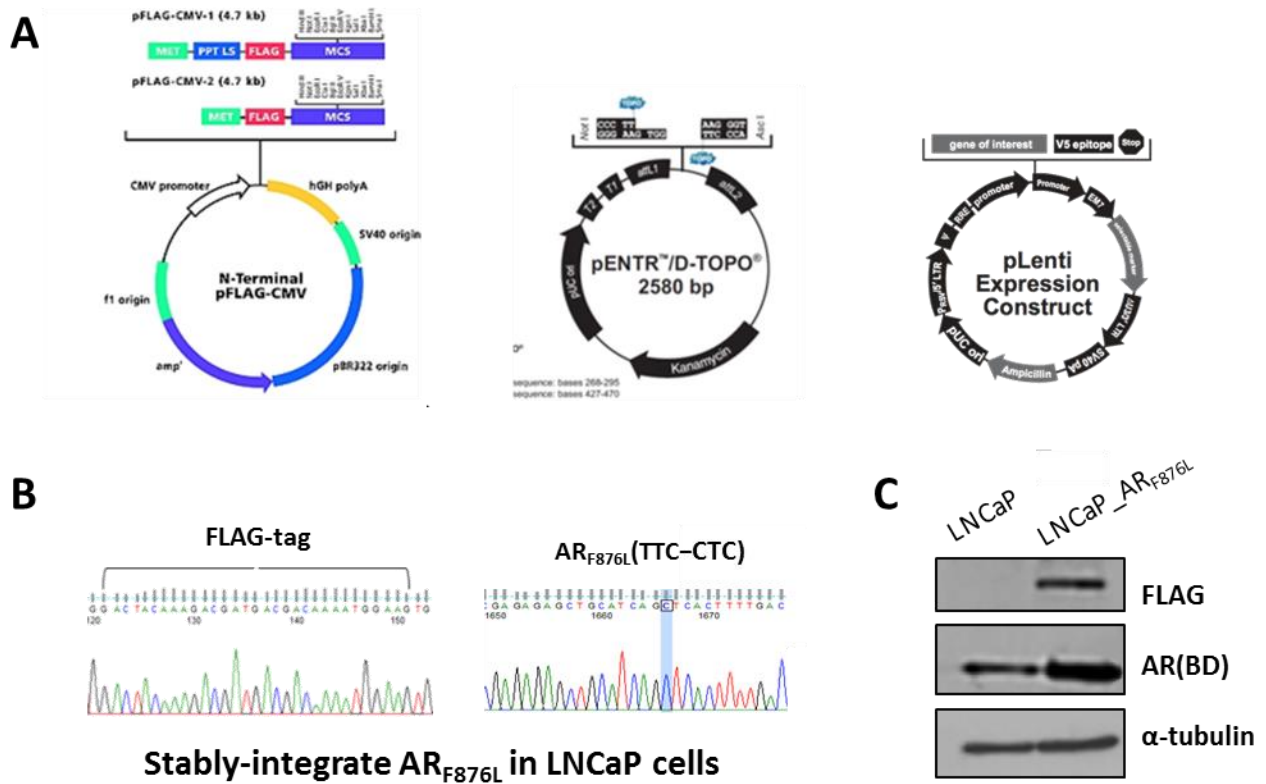
Figure 5.2 The workflow for generating the pLenti6.3-AR$_{F876L}$ construct. (A) The illustrated workflow of generating the pLenti6.3 AR$_{F876L}$ construct. (B) Sanger sequencing chromatogram and protein expression of pLenti6.3-FLAG-AR$_{F876L}$. Sanger sequencing chromatogram outlining relevant elements of the vector backbone shows successful ligation of pLenti6.3 FLAG-AR$_{F876L}$. (C) Western blotting verifying transient expression of pLenti6.3ARwt and pLenti6.3AR$_{F876L}$ in HEK293T cells.

A lentiviral-based expression construct was generated using a previously established system (O'Neill et al., 2015) in order to create an LNCaP cell derivative that expressed AR$_{F876L}$. The desired pLenti6.3-AR$_{F876L}$ construct was generated as illustrated in Figure 5.2 using a two-step approach (Gateway; Life Sciences). Firstly, FLAG-tagged AR$_{F876L}$ cDNA was PCR amplified from the original pCMV-AR$_{F876L}$ plasmid using pre-designed primers (Table **3.1**); the forward primer incorporating a 5'-'CTCC sequence to facilitate subsequent recombination. The overhang can facilitate PCR product cloning into the pENTR/ D-TOPO vector (Life Sciences) to further enhance ligation into an entry clone. Lastly, the destination vector pLenti-AR$_{F876L}$ was generated by conducting an LR

recombination reaction between the recombinant entry clone and the pLenti-6.3 plasmid backbone.

To determine the orientation of insert, the pLenti6.3-AR$_{F876L}$ construct was subject to Sanger sequencing (Beckman, UK) using a CMV forward primer. The sequencing chromatogram (Figure 5.2 B) confirmed the successful recombination of FLAG-AR$_{F876L}$ cDNA into the pLenti6.3 V5/DEST vector, including annotated elements of the backbone, the 5' CACC sequence to ensure directional cloning carried forward from pENTR/ D-TOPO cloning and the 5' sequence of the FLAG tag upstream of the AR coding sequence. The M13 reverse primer was used to confirm that the AR$_{F876L}$ sequence was maintained throughout pLenti6.3 V5/DEST vector cloning.

Next, to establish a stable AR$_{F876L}$-expressing LNCaP cell line, viral particles containing pLenti6.3 AR$_{F876L}$ were produced using the ViraPower™ Lentiviral Expression System (Life Sciences) according to manufacturer's recommendations. HEK293FT cell line (life Technologies, UK) were cultured with complete culture medium containing Geneticin for 3 passages before co-transfecting with pLenti-AR$_{F876L}$ and ViraPower™ Packaging Mix. 48 hours after co-transfection, viral particles were harvested form culture medium by ultracentrifugation.

Before transducing into LNCaP cells, AR$_{F876L}$-expressing lentivirus stock was transiently transduced into HEK293T and LNCaP for 48 hours and 7 days, respectively, to assess expression of ectopic protein. Whole cell lysates were collected and subsequently subject to western blotting (Figure 5.3) using the AR N-20 polyclonal antibody (Santa Cruz Biotechnology). As LNCaP endogenously express AR, anti-FLAG (Sigma-Aldrich, USA) monoclonal antibody was used to exclusively detect ectopic FLAG–tagged AR$_{F876L}$ expression in LNCaP cells.
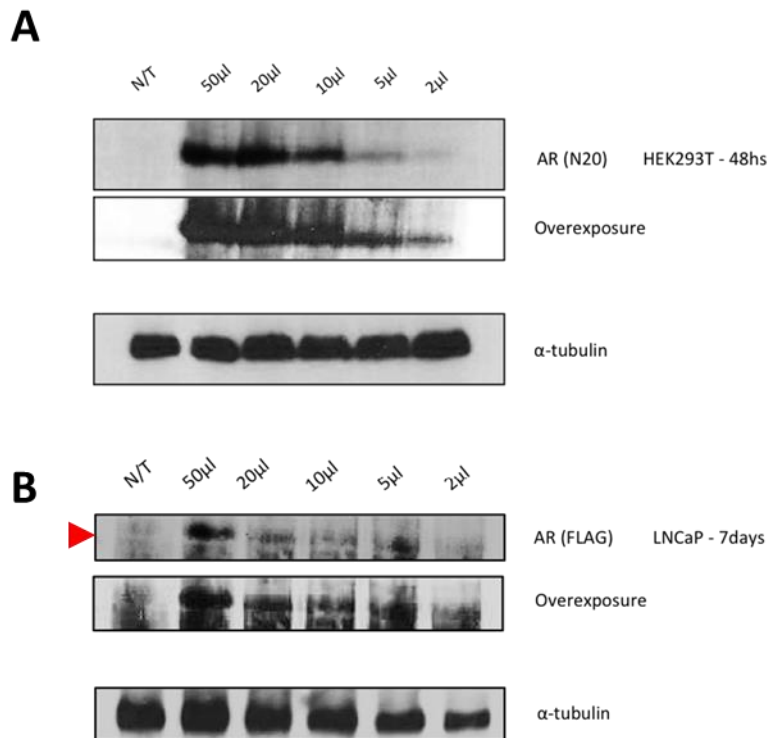
Figure 5.3 Successful transduction of pLenti6.3-AR_F876L in HEK237T and LNCaP cells. Increasing amounts of virus stock was transiently transduced into both HEK293T (A) and LNCaP (B) for 48 hours and 7 days, respectively. Antibodies used for each blots are indicated above. α-tubulin was probed as loading control. N/T represents as non-transduction negative control.

As shown in Figure 5.3, by using specific antibodies, ectopically expressed AR (as arrow indicated in red) can be detected in both HEK293T and LNCaP cells, but not in non-transduced control samples. Moreover, the expression level of AR gradually elevated with increasing amounts of transduced virus. After successfully confirming expression of AR_F876L, LNCaP cells were transduced for 24 hours and subsequently cultured in blasticidin-containing medium to clonally select pLenti-6.3-FLAG-AR_F876L stable integrants for further study.

To generate a stable homogenous population of cells culture, the transduced LNCaP cell population were seeded into 96 well-pates at 1 cell/well and cultured with selection medium.

Antibiotic-resistant colonies were picked 2 weeks post selection and FLAG expression and endogenous AR targets expression in the clonal populations was firstly assessed. A total of 10 individual clones were picked and 7 of them were able expanding growth for ectopic FLAG-tag expression. The subsequent AR-regulated gene expression were carried out for each clones (Appendix 5A). By comparing to LNCaP cells, clones c3 were subsequently selected and named as LNCaP-AR$_{F876L}$ for the subsequent studies.

Expression of the endogenous AR-target genes *PSA* and *KLK2* in the newly developed LNCaP-AR$_{F876L}$ cells in response to DHT and enzalutamide was compared to parental LNCaP cells by Q-PCR (Figure 5.4). As expected in LNCaP parental cells, *PSA* and *KLK2* expression was increased in the presence of DHT, but not enzalutamide. This indicates that the endogenous AR$_{T877A}$ mutant expressed in LNCaP cells is not activated by enzalutamide. Consistent with parental LNCaP cells, DHT induced *PSA* and *KLK2* expression in the LNCaP-AR$_{F876L}$ cell line. Importantly, in contrast to LNCaP cells, expression of the two AR-target genes *PSA* and *KLK2* was markedly up-regulated by enzalutamide in the LNCaP-AR$_{F876L}$ derivative, suggesting that enzalutamide induces expression of endogenous AR-target genes via the ectopic AR$_{F876L}$ mutant.
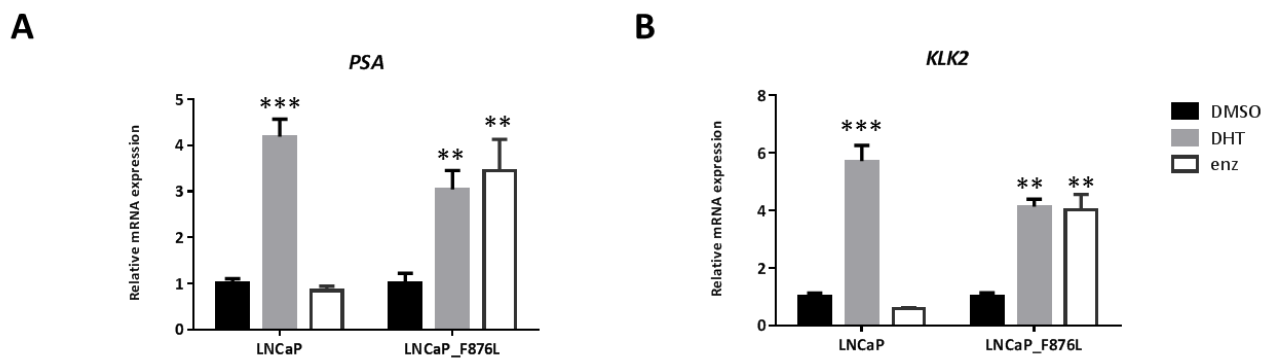
Figure 5.4 Enzalutamide actively induces AR target gene expression in the LNCaP-AR$_{F876L}$ derivative. Expression of the endogenous *PSA* and *KLK2* genes in the LNCaP cell line derivative that stably expresses AR$_{F876L}$ cells was assessed using QRT-PCR and compared to LNCaP parental cells. 10 nM DHT

and 10 µM enzalutamide were applied to both cell lines grown in steroid-depleted media for 24 hours. All statistical analysis was performed using GraphPad Prism software (GraphPad, San Diego, CA, USA) by one-way analysis of variance (ANOVA). Values are presented as mean±SEM, ***p-value <0.001**** <0.0001 as calculated using a student's T-test.

5.3.3 Up-regulated AR target gene in LNCaP-AR$_{F876L}$ is driven through ectopically expressed AR$_{F876L}$ in response to enzalutamide.

Given the fact that LNCaP parental cells endogenously express AR, to further discriminate AR$_{F876L}$ function from endogenous receptor, two siRNA oligos were manually designed according to Tuschl's rules of siRNA design (Elbashir et al., 2001) to deplete either endogenous AR$_{T877A}$, via a 3'-UTR sequence not present in the ectopic AR$_{F876L}$ cDNA (referred to as siAR$_{T877A}$), or ectopic AR$_{F876L}$ via a sequence within the linker region encompassing the FLAG sequence upstream from the AR$_{F876L}$ cDNA (referred to as siAR$_{F876L}$)(Figure 5.5 A).

To validate the effects of the endogenous- and ectopic-AR-targeting siRNAs, knockdown of AR levels was firstly assessed using western blot analysis in LNCaP parental cells and the LNCaP-AR$_{F876}$ derivative (Figure 5.5 B). An N-terminal AR antibody was used to detect endogenous AR$_{T877A}$ and ectopically-expressed AR$_{F876L}$ (total AR level), whilst the FLAG antibody was used to specifically determine ectopic AR expression in LNCaP- AR$_{F876L}$ cells.
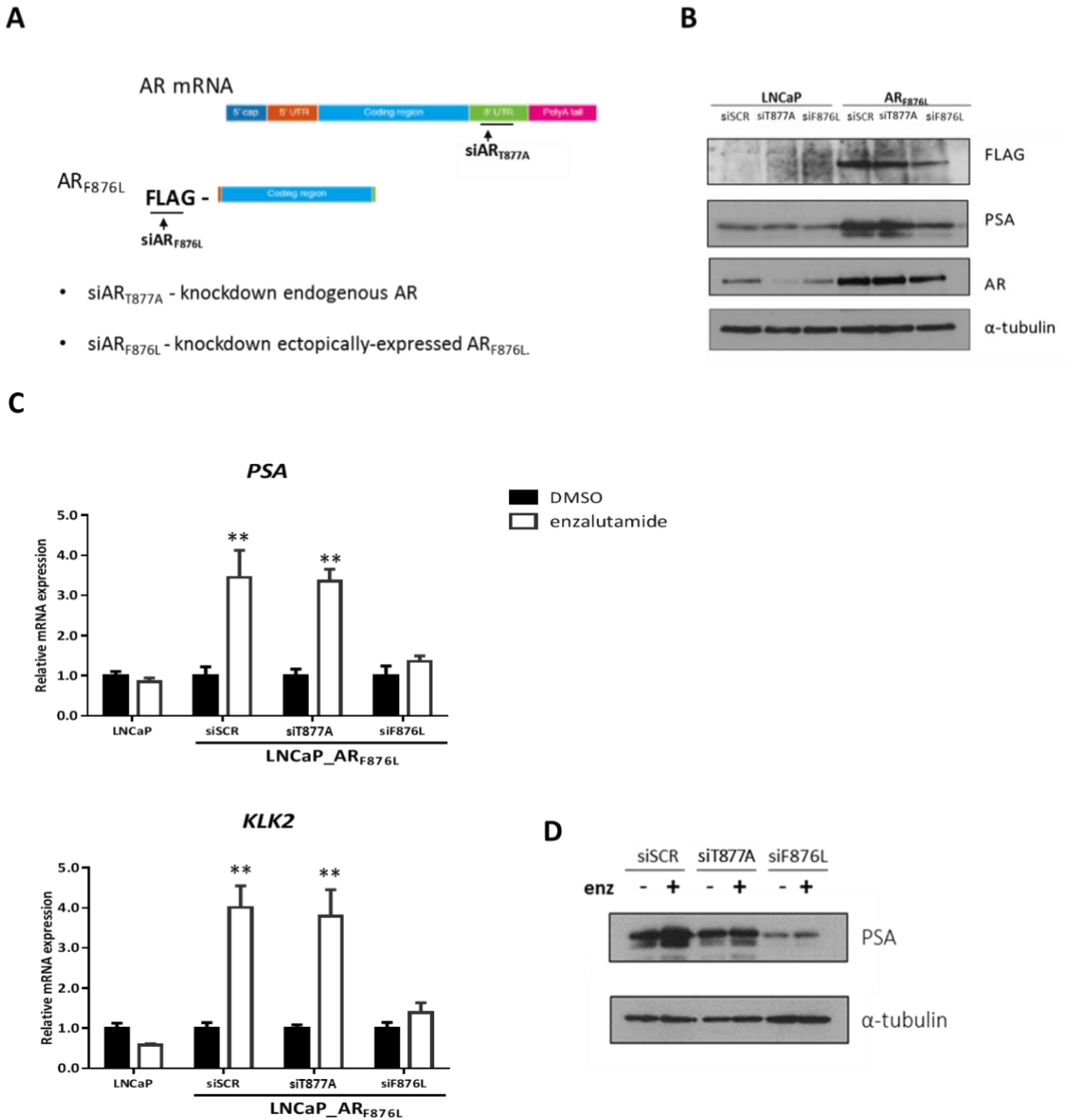
Figure 5.5 Up-regulated AR target gene expression in LNCaP-AR$_{F876L}$ is driven through ectopically expressed AR$_{F876L}$ in response to enzalutamide. (A) The illustration of target site for custom designed oligonucleotides siAR$_{T877A}$ and siAR$_{F876L}$. (B) AR western analysis to assess efficacy of endogenous and ectopic AR-targeting oligonucleotides in LNCaP and LNCaP-AR$_{F876L}$ cells. LNCaP and LNCaP-AR$_{F876L}$ cells were grown in full media and transfected with 25nM of scrambled (siSCR), siAR$_{T877A}$ or siAR$_{F876L}$ siRNA for 48 hours prior to western analysis using AR and FLAG antibodies. (C and D) Validation AR target gene expression in LNCaP AR$_{F876L}$ cells upon enzalutamide treatment. Data represents N=3 ± SEM. Cells were seeded in steroid-depleted media for 48 hours and transfected as above prior to 24-hour enzalutamide treatment and Q-PCR and western blot analysis.

As shown in Figure 5.5 B, transfection of pre-designed oligonucleotides confirmed the ability of $siAR_{T877A}$ to specifically target endogenous AR_{T877A}; whereas $siAR_{F876L}$ had no effect on endogenous receptor expression levels in LNCaP parental cells. The level of total AR was expectedly elevated in LNCaP-AR_{F876L} cells compared to the parental cells due to ectopic expression of AR_{F876L} in addition to endogenous receptor isoforms. Transfection of LNCaP cells with the AR_{T877A}-targeting siRNAs demonstrated effective reduction in AR expression not in the presence of $siAR_{F876L}$. Conversely in LNCaP-AR_{F876L} cells, transfecting $siAR_{F876L}$, which specifically targets ectopic AR_{F876L}, had no effect on endogenous AR_{T877A} whilst it effectively knocked down expression of FLAG AR_{F876L}. This result suggests that our designed siRNA can specifically target the 3'UTR of endogenous AR mRNA whilst permitting the ectopic expression of an AR mutant in the stable derivative cell clone.

Having developed and validated a system enabling the modulation of endogenous and ectopic AR protein levels, we next sought to assess the function and activity of AR_{F876L} by starting with investigating AR-regulated gene expression. In contrast to parental LNCaP cells, enzalutamide elevated expression of both endogenous *PSA* and *KLK2* genes (Figure 5.5 C) in the presence of both scrambled and AR_{T877A}-targeting oligonucleotides. In contrast, enzalutamide-activated *KLK2* and *PSA* gene expression was largely abrogated/ reduced when AR_{F876L} expression was down-regulated using $siAR_{F876L}$, which suggests that ectopically expressed AR_{F876L} promotes endogenous *PSA* and *KLK2* expression in the presence of enzalutamide. The downregulation effects of $siAR_{F876L}$ on AR targets was further confirmed using western blots. As Figure 5.5 D shows, in the presence of enzalutamide, the increasing PSA protein level is driven through AR_{F876L} not endogenous receptor.

5.3.4 Enzalutamide increases co-enrichment of AR$_{F876L}$ and RNA polymerase ll at *cis*-regulatory elements of target genes.

Having confirmed up-regulated endogenous *PSA* and *KLK2* mRNA expression in response to enzalutamide in the LNCaP-AR$_{F876L}$ derivative, we next sought to examine in greater detail transcriptional activation of endogenous genes by the AR$_{F876L}$ mutant in response to enzalutamide.

In order for AR to exert its transcriptional effect upon target genes, it is first recruited to androgen response elements (AREs) of *cis*-regulatory regions whereby recruitment of transcriptional machinery and additional transcription factors are required for target gene expression. Chromatin immunoprecipitation (ChIP) assays therefore were performed to investigate FLAG-AR$_{F876L}$ recruitment to AR target genes in response to agonistic ligands in LNCaP AR$_{F876L}$ cells. AR (N-20) has been previously used in ChIP to assess the recruitment of endogenous AR to the distal enhancer regions of the *PSA* promoter in parental LNCaP cells (O'Neill *et al.*, 2015). By having demonstrated AR recruitment to canonical *AREs* in the presence of DHT in parental cells, FLAG and phospho-Serine 5 RNA polymerase II antibodies were used in ChIP to investigate the effect of DHT and enzalutamide on AR chromatin binding.
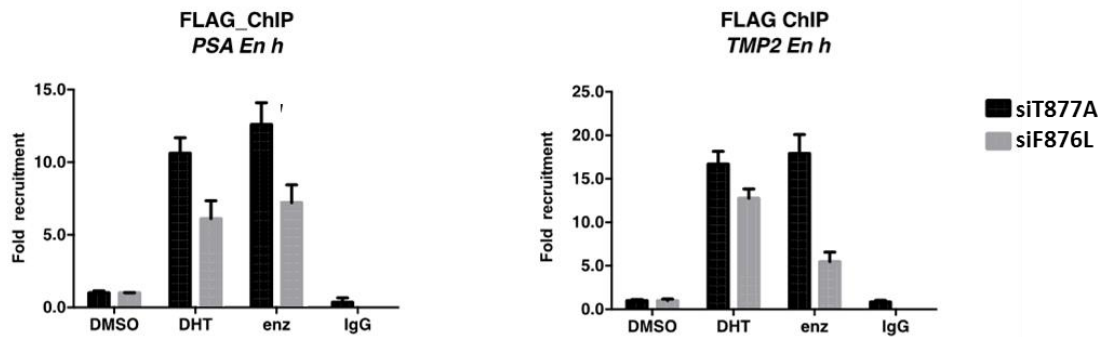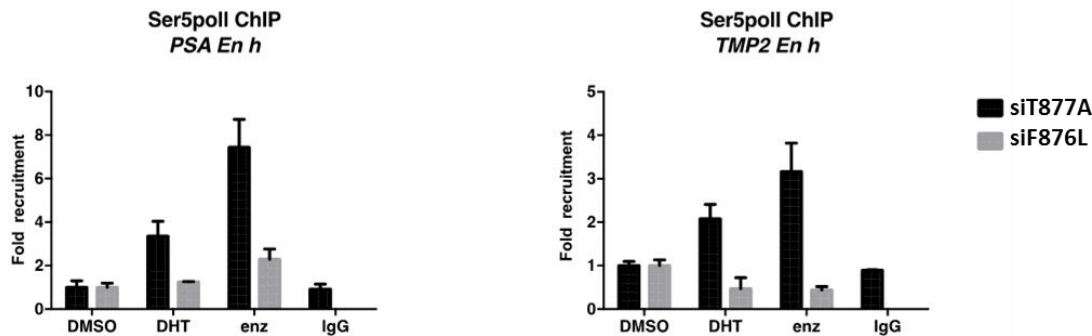
Figure 5.6 Increasing co-recruitment of AR$_{F876L}$ and RNA polymerase II at *cis*-regulatory elements of target genes in response to DHT and enzalutamide. LNCaP-AR$_{F876L}$ cells grown in steroid-depleted media were transfected twice with 25 nM of indicated siRNA before being treated with DHT (10 nM) or enzalutamide (10 µM) for 4 hours. Cells were subject to ChIP analysis using (A) anti-FLAG and (B) anti-phosphorylated serine 5 RNA polymerase (pSer5 RNA pol II) antibodies. Recruitment was determined by qPCR using primers specific to the enhancer regions of the *PSA* and *TMPRSS2* genes. Data represents N=3 ± SEM.

As shown in Figure 5.6 A, in the presence of DHT, AR$_{F876L}$ was found to be recruited to both *cis*-regulatory elements of *PSA* and *TMPRSS2*, with respective 12-fold and 17-fold increase in enrichment compared to vehicle control. Importantly, FLAG-AR$_{F876L}$ recruitment was robustly elevated upon enzalutamide treatment to levels equivalent to DHT. AR$_{F876L}$-targeting siRNAs were subsequently used to confirm AR enrichment in response to enzalutamide was ectopic AR$_{F876L}$; in the presence of DHT and enzalutamide AR$_{F876L}$ recruitment to both *PSA and TMPRSS2* enhancer regions was markedly diminished following transfection of the FLAG-

targeting oligo, which demonstrates competency for chromatin binding of the AR_{F876L} mutant in this model.

To determine whether the recruitment of FLAG- AR_{F876L} to *cis*-regulatory elements could promote the assembly of an active transcription complex, the recruitment of phosphorylated RNA polymerase II at serine 5 was next examined as a marker of transcriptional initiation. pSer5 RNA polymerase II antibody was used in ChIP assays to indicate transcriptional competency of AR-target genes in response to both DHT and enzalutamide in cells depleted of either endogenous or ectopic AR isoforms. At the *PSA* enhancer, DHT and enzalutamide increased pSer5 RNA pol II recruitment by approximately 2- and 4-fold, respectively (Figure 5.6 B). Similarly, at the promoter regions of *TMPRSS2,* DHT and enzalutamide treatment increased pSer5 RNA pol II co-recruitment by approximately 2- and 4-fold, respectively. Consistent with Figure 5.6 A, knockdown of AR_{F876L} before treatment with DHT and enzalutamide results in robust reduction in enrichment of pSer5 RNA polymerase II at the enhancer of both genes.

In all, the ChIP data indicates that in the presence of enzalutamide, AR_{F876L} mutant is recruited to *cis*-regulatory regions of AR target genes, *PSA* and *TMPRSS2*, facilitates recruitment of an active transcriptional complex and subsequently drives transcription of these genes.

5.3.5 Enzalutamide promotes AR_{F876L} cells growth in androgen-depleted conditions.

Having confirmed AR target gene activation in response to enzalutamide in the LNCaP-AR_{F876L} cell line derivative, we next sought to determine whether this agonistic effect of the anti-androgen is sufficient to impact cell phenotype.

To this end, proliferation assays were conducted to investigate if enzalutamide was pro-proliferative in the presence of ectopic AR_{F876L}. This was assessed using SRB assays which relies on sulforhodamine B stoichiometric binding to proteins under mild acidic conditions; with the amount of bound dye used as a proxy for cell mass and hence as a surrogate for cell number/proliferation. LNCaP parental and LNCaP-AR_{F876L} cells were seeded in androgen-depleted media supplemented with or without enzalutamide for 5 days before assessing cell number by SRB analysis. As shown in Figure 5.7 A, LNCaP parental cells cultured in the presence of enzalutamide for 5 days demonstrated reduced cell growth, while in contrast, enzalutamide did not down-regulate growth of the LNCaP-AR_{F876L} cell derivative, and instead caused a modest increase in proliferation compared to untreated cells.

A
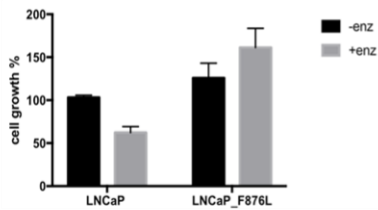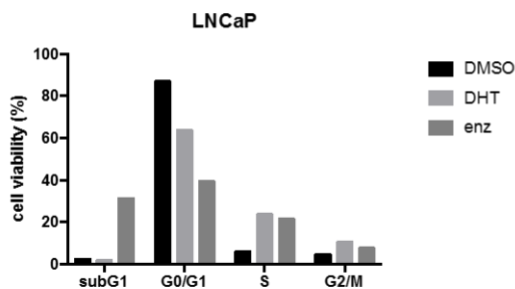
B   **C**
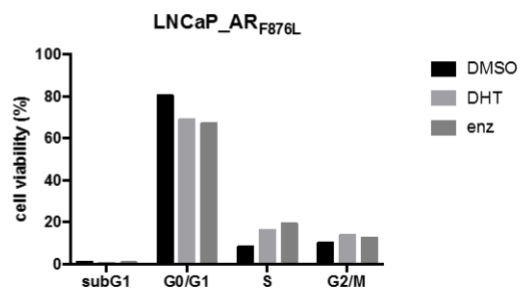
Figure 5.7 Enz-induced AR_{F876L} signalling promotes the growth of LNCaP-AR_{F876L} cells. (A) Sulforhodamine B (SRB) growth assays performed in LNCaP parental cells and LNCaP-AR_{F876L} derivatives after being grown in steroid-depleted media +/- enzalutamide for 5 days. (B) Cell cycle analysis of LNCaP and LNCaP-AR_{F876L}(C) using propidium iodide staining.

We next assessed overall cellular phenotype of the LNCaP-AR$_{F876L}$ cell line derivative, using light microscopy, upon depletion of AR$_{T877A}$ or AR$_{F876L}$ and grown for 48 hours in steroid-depleted media supplemented with either DHT or enzalutamide. Given these indications, propidium iodide (PI)-based flow cytometry was utilised to analyse the impact of AR$_{F876L}$ expression on LNCaP cell cycle status in greater detail. The percentage of cellular DNA content in each cell cycle stage was quantified using PI staining which allows the percentage of cells in each of the distinct phases of the cell cycle to be calculated. LNCaP parental and LNCaP-AR$_{F876L}$ derivative cells grown in full media were treated with DHT or enzalutamide for 48 hours. In response to DHT (Figure 5.7 B), an increase in the percentage of LNCaP parental cells undergoing DNA replication (S-phase) and transition to mitosis (G2/M) were observed; whilst enzalutamide significantly enhanced the proportion of cells in the apoptotic sub-G1 phase of the cell cycle. In contrast, treatment of DHT and enzalutamide significantly promoted the proportion of LNCaP-AR$_{F876L}$ cells (Figure 5.7 C) in S- and G2/M-phases of the cell cycle without any cytotoxic effects which is consistent with data in Figure 5.7 A indicating that the AR$_{F876L}$ mutant can drive proliferation of LNCaP cells in the presence of enzalutamide. Overall, our data has successfully demonstrated that the F876L mutant can drive AR target gene expression and importantly maintain a tumor phenotype in the presence of enzalutamide.

5.4 Discussion

It is well-accepted that acquiring gain of function mutations within the ligand-binding domain of the AR contributes to resistance to AR-targeted therapies, including enzalutamide. By conducting a reporter-based mutagenesis screen, Balbas and colleagues (Korpal *et al.*, 2013a) recently identified the F876L mutation as the only amino acid substitution within the ligand-binding pocket of the AR that is capable of inducing an antagonist to agonist switch for enzalutamide. Molecular structure simulations of the F876L amino acid residue revealed a repositioning of the LBD which results in a favorable conformation of helix 12 to enable transcriptional activation

when bound to enzalutamide (Joseph *et al.*, 2013). Consistent with these early indications, our initial luciferase-based transactivation experiments indicated that the F876L mutation enables an agonistic response to enzalutamide (Figure 5.1).

Despite the development of improved PC therapies over the past decade, including enzalutamide and abiraterone, resistance to these treatments invariably occurs, but cells remain largely dependent on the AR signalling cascade suggesting new AR targeted agents could be efficacious in this setting. Given that acquisition of AR mutations has been identified as a driver of therapy resistance, it is important that the activation profile of these aberrant AR species is analyzed in response to a cohort of antagonists to assess clinically-relevant sensitivities. Importantly, how one particularly AR mutant identified in disease that is resistant to second-generation anti-androgens, e.g. enzalutamide, responds to hormonal therapies utilized at an earlier stage of the treatment pipeline, such as bicalutamide, may suggest alternate application of agents to improve patient outcome. This notion is supported by our luciferases results investigating sensitivity of the AR_{F876L} mutant to anti-androgens (Figure 5.1). In response to 24 hour bicalutamide treatment, we found that no increasing luciferase reads were observed suggesting that unlike the previously characterised AR_{W741L}, transactivation of AR_{F876L} retains sensitivity to bicalutamide. However, we did not determine if bicalutamide would out-compete enzalutamide to inactivate the F876L mutant, which would be a useful experiment to perform. It is interesting to speculate that because of enzalutamide-mediated activation of receptor signaling, combination therapy with structurally distinct anti-androgens either in combination or in series together with ADT may provide an appealing therapeutic strategy for combating AR-mediated enzalutamide resistance mechanisms.

In vitro and *in vivo* experimental models of PC are vital tools for discovery of mechanisms of drug resistance, and for the evaluation of new and alternate therapies. However, the most commonly adopted methods for studying AR mutant function are conducted by transient expression of AR isoforms into receptor negative cells and assessment of activity using reporter-based methods

(as shown in Figure 5.1) which lacks physiological relevance. Hence, having confirmed the agonistic activity enzalutamide towards the AR_{F876L} mutant, an LNCaP cell line that stably expresses AR_{F876L} mutant was generated to enable more robust modelling of the mutant and provide a better understanding of the driver mechanisms behind resistance.

Our lab has previously created a rescue cell line model and applied it successfully to study the molecular function of the bicalutamide-activated AR_{W741L} mutant (O'Neill *et al.*, 2015). This system relies upon the ability to deplete endogenous AR via 3'UTR siRNA oligonucleotides which enables analysis of the ectopic mutant in the physiologically-relevant LNCaP cell line. Here, the same strategy was employed to generate an LNCaP cell line derivative that stably expressed FLAG-tagged AR_{F876L}, named LNCaP-AR_{F876L} (Figure 5.3). In support of the luciferase transactivation data, by analysis of mRNA expression of AR target genes *PSA* and *KLK2* in LNCaP-AR_{F876L} cells, we observed similar agonism by DHT and enzalutamide on stably expressed AR_{F876L} (Figure 5.4). Importantly, compared to previous luciferase transactivation data, this model offers the capability to assess mutant AR activity in a CRPC cell line upon endogenous target genes and to enable assessment of sensitivity of the mutant to other agents and provide potential biomarkers of AR_{F876L} expression. These findings indicate that not only can the ectopically-expressed AR_{F876L} respond to ligands and activate endogenous target genes *PSA* and *KLK2* consistent with its endogenous AR_{T877A} counterpart, it confirms the antagonist-agonistic switch of enzalutamide in a more physiologically-relevant model that can be further explored to improve our understanding of how the AR_{F876L} mutation functions in CRPC.

LNCaP cells endogenously express AR_{T877A} that is activated by DHT and the first-generation antagonist flutamide which may interfere with bespoke analysis of the ectopic AR_{F876L} mutant in the LNCaP-AR_{F876L} cell line. To enable discriminate analysis of either AR_{T877A} or AR_{F876L} isoforms, a custom siRNA oligonucleotide, named $siAR_{T877A}$, was designed to specifically target the 3'UTR of endogenous AR mRNA as the target sequence is not present on the ectopic AR_{F876L} transcript

(Figure 5.5 A). Using this approach, endogenous AR_{T877A} can be depleted; leaving ectopic AR_{F876L} to be studied without hindrance from the potentially competing isoform (Figure 5.5 B). We firstly confirmed that $siAR_{T877A}$ is able to effectively knockdown endogenous AR protein levels for up to 96 hours (Figure 5.5 C) which was deemed to be sufficient for subsequent experiments that focussed on gene expression and cell phenotype analyses. Importantly, the $siAR_{T877A}$ oligo was not able to target transiently expressed FLAG-wtAR in PC-3 cells (data not shown) or FLAG tagged AR_{F876L} in LNCaP-AR_{F876L} cells due to the absence of the 3'UTR siRNA target sequence (Figure 5.5 D).

By confirming the efficiency of specific endogenous AR knockdown in LNCaP and LNCaP-AR_{F876L} cells, another oligonucleotide was designed to target the FLAG tag/ linker sequence upstream of the AR_{F876L} start codon, termed $siAR_{F876L}$. By optimising transfection conditions, it was shown that $siAR_{F876L}$ had no effect on endogenous AR expression while it is able to specifically target the FLAG-AR_{F876L} mutant resulting in substantial knockdown (Figure 5.5 B). The $siAR_{F876L}$ and $siAR_{T877A}$ siRNAs therefore served to increase the flexibility of the model by being able to regulate both endogenous ($siAR_{T877A}$) and ectopic ($siAR_{F876L}$) AR isoforms in the LNCaP-AR_{F876L} derivative. Importantly, both the $siAR_{T877A}$ and $siAR_{F876L}$ oligo consistently achieved substantial levels of specific AR isoform knockdown.

Of note, comparing to parental LNCaP cells, western blot analysis in the LNCaP derived AR_{F876L} subclone cells displayed a substantial higher level of total AR. The same enhanced level of total AR was previously reported in LNCaP-developed subclones which stably express wtAR (Chen *et al.*, 2004), as well as in the LNCaP-AR_{W741L} derivative (O'Neill *et al.*, 2015). It is important for us to modulate enhanced AR expression levels by using siRNA oligonucleotides as the similar elevated AR is rather commonly observed in PC patients with advance disease (Waltering *et al.*, 2009). Of note, in the control experimental arm from work described in O'Neill *et al.*, 2015, using an AR wild-type expressing LNCaP derivative, we did not detect any major changes to AR target gene

expression- hence even though total AR abundance was higher in the W741L cell line, it was the activation of the mutant that caused most of the distinct changes to the AR transcriptome. Also, given that in this report, we are using enzalutamide to activate the ectopic AR, the endogenous AR will be inactive and hence active forms of the AR will be equivalent to normal LNCaP cells.

Loading of the AR at androgen response elements (AREs) adjacent to target genes in response to activating ligands is an essential step in the receptor signalling cascade that is required to facilitate downstream transcription. In the typical pathway, ligand-activated AR translocates to the nucleus and binds to AR-targeted *cis*-regulatory elements in chromatin and recruits co-regulators to form a pre-initiation complex and together with the basal transcriptional machinery initiates transcription of specific AR target genes. By using ChIP experiments in LNCaP cells, the DHT-bound AR was found to be recruited to both enhancer and promoter regions containing AREs of genes, such as *PSA*, but not to sequences in-between that lacked these specific target sequences. Several studies, e.g. (Louie *et al.*, 2003) have latterly reported that compared to promoter regions, more robust hormone-induced recruitment of the AR was observed at enhancer regions of AR targets, such as *PSA*. By using FLAG-specific antibody in ChIP assays, we observed higher recruitment of FLAG-AR at enhancer regions (Figure 5.6) than to the promoter of *PSA* in the LNCaP-AR$_{F876L}$ cell line derivative–which is consistent with endogenous AR$_{T877A}$ in parental LNCaP cells (Appendix 5B). Moreover, enrichment of AR$_{F876L}$ occupancy was also detected at *PSA*, and *KLK2* in response to enzalutamide supporting the concept that AR$_{F876L}$ utilises enzalutamide as an agonist to promote AR-target gene expression. Of note, comparing DHT versus enzalutamide ChIP data, there was still AR$_{F876L}$ present on chromatin when siAR$_{F876L}$ was utilised, which may be due to enhanced stability of a population of ectopic receptor when bound to chromatin and hence is resistant to knockdown.

For AR to exert transcriptomic regulation, RNA polymerase and other co-regulators are required to be recruited to regions proximal to the target gene (Louie *et al.*, 2003; Wiench *et al.*, 2011).

Hence, we used ChIP assays as surrogate for analysis of the activation status of the AR-bound gene. We next sought to assess if the ectopic AR can not only bind target sequences, it can also recruit RNA pol II to commence transcription. By employing phosphorylated serine 5 RNA polymerase II antibody which is a marker of transcriptional initiation, we have successfully detected occupancy of RNA polymerase II within same regulatory elements of analysed AR target genes. Importantly, enzalutamide-induced transcriptional regulation of AR_{F876L} was further confirmed by silencing of FLAG-AR_{F876L} which resulted in reduced enrichment of RNA polymerase II at *PSA* and *KLK2* genes (Figure 5.6).

Having shown that the AR_{F876L} mutant drives gene expression in the presence of enzalutamide, including *PSA* and *KLK2*, and hence mimics the effects of DHT-activating endogenous AR_{T877A} (Wang, 2006), it was important to address if AR_{F876L} activation by enzalutamide could impact cell phenotype. To this end, cell cycle analysis was carried out using propidium iodide (PI)-based flow cytometry to analyse the percentage of cells in a particular cell cycle phase based on DNA content. Cells were grown in full medium and supplemented with either DHT or enzalutamide. The cell cycle analysis indicated that enzalutamide promotes AR_{F876L}-driven cell cycle progression that was, as expected, not observed in parental LNCaP cells (Figure 5.7). Enzalutamide treatment caused LNCaP parental cells to undergo apoptosis, as indicated by elevated numbers of cells in sub-G1, while in contrast, the anti-androgen increases the proportion of AR_{F876L} cells in S-phase at the expense of G1- and G2/M-phases of the cell cycle. Importantly, these observations of enzalutamide acting as a driver of cell proliferation in the LNCaP-AR_{F876L} derivative were confirmed by SRB assay, as increasing cell numbers was detected under prolonged treatment with enzalutamide.

By showing that the AR_{F876L} mutation in our stable model induces an antagonist to agonist switch for enzalutamide that can promote AR signalling and growth of cells, we next asked whether AR_{F876L}-bearing cells become dependent on this switch for cellular growth under androgen-

deprivation conditions, a dependence that has been observed in the clinic for other anti-androgens such as flutamide (Korpal *et al.*, 2013a). By growing cells in the presence of DHT and enzalutamide post knockdown AR_{T877A} and FLAG-AR_{F876L}, we firstly found that consistent with the resistance phenotype observed before, the absence of endogenous AR has no effects on enzalutamide-induced proliferation of LNCaP-AR_{F876L} cells whilst knockdown of AR_{F876L} restores cell sensitivity to enzalutamide (Figure 5.7 B). This result is consistent with previous reports that ectopic expression of AR_{F876L} rescued the growth inhibition of enzalutamide treatment (Balbas *et al.*, 2013).

To further explore the molecular mechanisms that drive resistance, we next conducted global transcriptomics analysis of LNCaP-AR_{F876L} cells in the presence and absence of endogenous AR and AR_{F876L} following treatment with enzalutamide for 24 hours. The next chapter will therefore focus on global transcriptomic regulation by AR_{F876L} upon treatment with enzalutamide.

Chapter 6: Global analysis of AR$_{F876L}$-driven gene expression that depict transcriptomic mechanisms of enzalutamide resistance.

6.1 Introduction

Despite the recent successes in application of newly-approved therapies in prostate cancer treatment, including abiraterone and the second-generation anti-androgen enzalutamide, durable responses are limited, presumably owing to acquired resistance via deregulated AR signalling. Over the past decade, our understanding of the role of androgen signalling as a molecular driver of CRPC has significantly improved, but there are also mechanisms that possibly govern resistance to ADT that do not directly involve androgen signalling. In the previous chapter, by using Luciferase reporter as a surrogate, we have initially demonstrated elevated AR_{F876L} activity in response to enzalutamide compared to AR_{wt}. Furthermore, we have established a stable AR_{F876L} expressing LNCaP cell line that enables analysis of the clinically-relevant antagonist to agonist switch of enzalutamide in a physiologically-relevant setting. Although the previous chapter indicated that the enzalutamide-activated AR mutant facilitated expression of the endogenous *PSA* and *KLK2* genes, it is critical that a study of global transcriptomics in response to activation of the AR_{F876L} mutant is undertaken as it has the potential to highlight biomarkers for enzalutamide resistance and other therapeutically-exploitable pathways for improved patient care. Therefore, in this chapter, global gene expression will be assessed in the LNCaP-AR_{F876L} cell line in response to enzalutamide. From this data, other pathways that drive enzalutamide-resistance, including activation of the glucocorticoid receptor (GR) pathway, will be assessed. Finally, as a means of utilising this rescue model to assess efficacy of novel AR signalling targeting agents, this chapter will also interrogate the therapeutic potential of impairing activity of the bromodomain and extraterminal (BET)-family of bromodomain-containing proteins, including BRD4, in the background of AR_{F876L}-driven enzalutamide resistance to establish clinically-relevant sensitivities.

By analysing the global transcriptome of the enzalutamide-activated AR_{F876L} mutant in the LNCaP-AR_{F876L} derivative, we aim to understand if this receptor isoform displays altered gene regulation distinct from the endogenous AR which may provide clues to how AR_{F876L} drives

disease progression. Importantly, we observed that enzalutamide-activated AR_{F876L} drives a gene profile that strongly overlaps with a reported GR-regulated gene signature. Hence, we here focus on further exploring the interplay mechanism between AR_{F876L}-driven agnostic signalling programme and GR-regulated transcriptomic profiling in CRPC.

The primary sequence of the DNA-binding domain of AR and GR share 80% homology and share an extensive overlap of chromatin-binding and transcriptional activities. One recently proposed mechanism of enzalutamide-resistance in PC is by selective activation of the GR signalling pathway that acts to mimic AR function to facilitate disease progression (Kach *et al.*, 2017). A significant increase in the number of GR positive cells was detected in patients who were tolerant of enzalutamide compared to both baseline and enzalutamide-responsive patients (Wadosky and Koochekpour, 2016). By administering dexamethasone (an alternative glucocorticoid) in LNCaP cells that stably express GR, and applying ChIP-seq, Arora *et al.* (2013) found that over half of the occupation of AR DNA binding sites was bound by the GR. Additionally, by conducting ChIP-Seq in the VCaP cell line that expresses endogenous GR and AR, it was revealed that a 58% overlap existed between AR and GR cistromes, which indicates the contribution of GR transcriptional regulation to disease progression (Isikbay *et al.*, 2014); Moreover, using an enzalutamide-resistant LNCaP-derived xenograft model, Arora *et al.* (2013) detected increased mRNA and protein levels of GR compared to enzalutamide-sensitive LNCaP cells and observed enhanced GR activity in this enzalutamide insensitive population which suggests a selective outgrowth of cells with elevated GR function to override the effects of the anti-androgen. Altogether, the evidence presented above indicates that increased GR expression and function is a potential mechanism governing continued survival of CRPC during second-line ADT with enzalutamide.

Currently, over 50% of CRPC patients who have failed conventional hormonal treatments have at least one aberration of the AR pathway (Asangani and Chinnaiyan, 2014). Hence,

targeting 'downstream' of AR has been considered as alternative therapeutic strategies for treating CRPC. A number of current studies have recently reported the promising progression of targeting BET-family protein in CRPC treatment (Raina *et al.*, 2016). Unlike enzalutamide, which directly targets the LBD of the AR, BET domain inhibitors function downstream of the receptor. By competitively binding to the acetyl lysine recognition pocket within the bromodomain of the BET family of proteins, BET inhibitors, such as JQ-1 and I-BET762, diminish AR recruitment to *cis*-regulatory elements of target genes and subsequent AR-mediated gene transcription (Filippakopoulos *et al.*, 2010). However, these experiments were performed in non-AR_{F876L}–expressing backgrounds hence it is important to address the efficacy of these compounds in mutant backgrounds. To that end, this chapter will focus on two bromodomain inhibitors that selectively target the bromodomains contained within the BET family of transcriptional regulators and p300. The purpose of these experiments is to address the potential of bromodomain suppression on reducing activity of the clinically-relevant AR_{F876L} that could provide important pre-clinical indications that BET/p300/CBP inhibitors may be efficacious in models of enzalutamide resistance.

BRD4 is a conserved member of the BET family of proteins. Similar to other family members, BRD4 has a critical role in transcription regulation by facilitating the recruitment of RNA polymerase II (RNA Pol II) and positive transcription elongation factor P-TEFb (Yang *et al.*, 2005). BRD4 has been recently found to play a role in several malignancies, including breast cancer (Crawford *et al.*, 2008), non-small cell lung cancer (Shimamura *et al.*, 2013) and melanoma (Segura *et al.*, 2013). It is a co-regulator for the AR; facilitating transcription of AR-target genes by associating with acetylated chromatin and enabling recruitment of the basal transcription machinery (Coutinho *et al.*, 2016). Moreover, several BET inhibitors (BETi) that interrupt BRD4 chromatin recruitment are being assessed in clinical trials for CRPC (https://clinicaltrials.gov).

p300 is a histone acetyltransferase (HAT) enzyme which has been long known to be an AR co-activator which is largely dependent upon the HAT activity of the enzyme to facilitate receptor function via both histone and AR acetylation (Fu *et al.*, 2000 ; Gaughan et al., 2002). In PC cells, p300 is found play a role for androgen-dependent and independent transactivation of the AR (Debes *et al.*, 2002). In clinical samples, expression of p300 positively correlates with AR protein levels in human PC specimens (Zhong *et al.*, 2014). Here this chapter we will take BRD4 and P300 as example for investigating sensitivity to bromodomain inhibition in the background of our AR_{F876L}-signalling-competent human CRPC model.

6.2 Specific methods and materials

6.2.1 Sample preparation for HT-12v4.0 Illumina Bead chip gene expression.

To prepare RNA for micro-array analysis, LNCaP-AR_{F876L} cells were reverse transfected with siAR $_{T877A}$ and siAR$_{F876L}$ siRNAs (25μM) in 6-well plates (Corning) and cultured in 2 ml 10% steroid-depleted medium for 48 hours before performing a second siRNA transfection. 96 hours post-transfection, 10 nM DHT and 10μM enzalutamide were added for 24 hours prior to harvesting and RNA extracted using TRIzol (Life Technologies) according to the manufacturer's manual.

The RNA samples were quality checked and normalised by HTG. All RNA samples were processed using the Illumina TotalPrep-96 RNA Amplification Kit followed by the Illumina Whole-Genome Gene Expression Direct Hybridisation Assay. The labelled RNA was then hybridised to Human HT- 12_V4_BeadChip for gene expression. All samples achieved the minimum number of ≥8000 detected genes (whereby P=0.01). The number of detected genes ranges from 9526 to 10724. We thank the High-Throughput Genomics Group at the Wellcome Trust Centre for Human Genetics (funded by Wellcome Trust grant reference 090532/Z/09/Z) for the generation of gene expression data.

6.2.2 Sample analysis

Illumina HT-12v4 BeadChip array analysis was performed using GenomeStudio software (Illumina). Basic differential expression analysis was accomplished using Illumina's in-built normalisation and error model to include multiple testing correction using the Benjamini and Hochberg false discovery rate (p < 0.05). Genes were filtered further using custom equations to exclude genes with an insignificant detection p-value as recommended by Illumina (p< 0.05). Compound treated samples were expressed as fold-change by dividing the average sample signal by vehicle treated controls. Data is represented as the mean of three independent experiments. Genes without a gene symbol/ID and those with locus specific entries were removed from the overall analysis. Genes that were analysed in greater detail were validated by qPCR according to section 3.14.3.

6.2.3 Specific primers and compounds

Table 6.1 primers used for gene expression validation in q-PCR.

gene	Forward Primer	Reverse Primer
ORM1	5' –AGCATTTCGCTCACTTGCTG -3'	5'-GACAGCCCCCAGTTCTTCTC-3'
ACSL3	5' -TGACACAAGGGCGCATATCT-3'	5'- CCAGTCCTTCCCAACAACGA -3'
LRIG1	5'-CCTTCTCCTTCTCTGGCTGC -3'	5'- AACTCAGGTTTAGGCTCCGC - 3'
VCL	5'- CGCTGAGGTGGGTATAGGTG-3'	5'- GTAGCTTCCCGATGCAAGGA - 3'
NFIB	5'- CGAACTCCACCTCCACCTTC-3'	5'- TGGTTTGTGGACTGGATGGG-3'
LIFR	5'- CCTAACCCTCTCTCCCAGAAC-3'	5'- GATGAATGAGTCGCAGAGGC-3'
PDIA5	5'- GAAAGTTGACCTGAGCCCGA-3'	5'- GGGCCCTTTTGGATCCTTCA-3'
ATP1A1	5'- GTCACCTCCTTCTCCTTCCTTTTC-3'	5'- GGAGCGCGCCTTTCCTCA-3'
LONRF1	5'-CAGGAGGGAGTCGGGAGATG -3'	5'-CTTCCCAGAACCGGCCTC -3'
FBXO31	5'- GTGTGTGCTCGCCTTTGC-3'	5'- TCCTCCTCGGGGTCTGTG-3'
ELF1	5'-GCTGAAGCACAGACACCACT -3'	5'- AGCTTCTTGGCCTTCAAGTATT-3'

RAB3B	5'-CACAGGAAGCACCCTCAGTC -3'	5'-TGATAAGACTGCCCTGCCCT -3'
NR3C1	5'-TCTGAACTTCCCTGGTCGAA-3'	5'-GTGGTCCTGTTGTTGCTGTT-3'
KLK3	5'-TCATCCTGTCTCGGATTGTG-3'	5'-ATATC AGAGCGGGTGTGG-3'
MKP1	5'-CCTGACAGCGCGGAATCT-3'	5'-GATTTCCACCGG GCCAC-3'
SGK1	5'-AGGCCCATCCTTCTCTGTTT-3'	5'-TTCACTGCTCCCCTCAGTCT-3'
GAPDH	5'-GAGTCAACGGATTTGGTCGT-3'	5'-TTGATTTTGGAGGGATCTCG-3'

Table 6.2 ChIP primers used for gene expression validation in q-PCR.

gene	Forward Primer	Reverse Primer
ORM1_ChIP	5'-GGGTCATTTCCACCACCTCAAACA-3'	5'-GGAGAAAGGCCTTACAGTAGTCTC-3'
SGK1_ChIP	5'-ACCTCCTCACGTGTTCTTGG -3'	5'- AAC ATTTGTCCGTTCCGCA -3'
NRC31_ChIP	5'-AGTTAACCTTCTCTGGGCTGG -3'	5'- CGCCTGAGAACAATGTGTG -3'
MKP1 ChIP	5'-AAACATTTCTCCACGGCCCA -3'	5'-TGTGCCAGGTACTGCTAAGG -3'

Table 6.3 siRNA sequences used to inhibit specific gene expression by RNAi

siRNA target	siRNA sense sequence
siAR	GCCAGCCACACAAACGUUUdTdT
siGR	CCGAGAUGUUAGCUGAAAUdTdT

Compound treatments

Cells were typically treated with indicated doses of enzalutamide (10 µM), DHT (10 nM), JQ1 (500 nM) p300 bromodomain inhibitor (Compound G) and the p300/CBP HAT domain inhibitor C646 (1 uM) for 24 hours unless otherwise stated.

6.3 Results

6.3.1 Enz-AR$_{F876L}$ driven gene profile shows overlap with a GR-regulated gene signature.

Having confirmed the mutant can drive proliferation in response to enzalutamide in the established LNCaP-AR$_{F876L}$ cell line (Figure 5.7; previous chapter), it was important to determine if the genes driven by endogenous vs. ectopic AR are different. Hence, to provide a global view of gene expression in our LNCaP-AR$_{F876L}$ cell line that is driven by AR$_{F876L}$, we performed microarray analysis to examine expression changes upon ectopic AR$_{F876L}$ knockdown and compared to depletion of endogenous AR$_{T877A}$. The experimental setup and sample preparation were conducted as described above and resultant data was processed using x GenomeStudio software (Illumina). A cut-off of >1.5-fold change for studying differential gene expression was applied which is consistent with numerous publications (Nelson *et al.*, 2002; Chen *et al.*, 2004; Nyquist *et al.*, 2013; Polkinghorn *et al.*, 2013; O'Neill *et al.*, 2015). Akin to studies described in Chapter 5, endogenous AR knockdown was applied to enable a more robust read-out of the enzalutamide-activated AR$_{F876L}$ transcriptome prior to micro-array analysis. By comparing enzalutamide treatment to vehicle treated controls in the endogenous AR knockdown arm, a total of 615 genes were identified as being upregulated > 1.5-fold in the presence of enzalutamide (shown as siAR$_{T877A}$ in Figure 6.1 A). Additionally, as ligand-induced genes were the primary end-point, hence only genes that exhibited increased expression were focussed on in this report.

A

Micro-array
gene expression profiling in LNCaP_AR$_{F876L}$

siAR$_{T877A}$+ enz
vs.
siAR$_{T877A}$+ DMSO
(1.5 folds, n=615)

siAR$_{F876L}$ + enz
vs.
siAR$_{F876L}$ + DMSO
(1.5 folds, n=151)

484   131   17
27   59

Laz + DHT
vs.
Laz + DMSO
(1.5 folds, n=86)
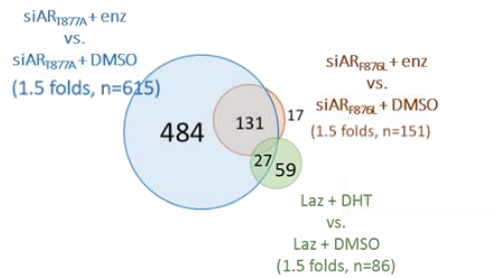
B

	enz-F876L (1.5 fold FDR<.05)	DHT-laz_ARwt (1.5 fold FDR<.05)
match to GR-seq(122)=	73	36
match to AR-seq(73)=	63	39
match to GR-selective gene(67)=	43	15
match to AR-selective gene(39)=	29	17

C

≥1.5 folds (12)	+ enz	Description
ACSL3	8.908421843	acyl-CoA synthetase long-chain family member 3
LRIG1	4.649793033	leucine-rich repeats and immunoglobulin-like domains 1
VCL	3.840420439	vinculin
NFIB	2.937618509	leukemia inhibitory factor receptor alpha
LIFR	2.932838635	nuclear factor I/B
PDIA5	2.277916326	protein disulfide isomerase family A, member 5
ATP1A1	2.239320929	ATPase, Na+/K+ transporting, alpha 1 polypeptide
LONRF1	2.113700547	LON peptidase N-terminal domain and ring finger 1
FBXO31	2.009444435	E74-like factor 1 (ets domain transcription factor)
ELF1	1.677543961	F-box protein 31
MBOAT2	1.508600708	membrane bound O-acyltransferase domain containing 2 (RAB4A, member RAS oncogene
RAB3B	1.506417088	RAB3B, member RAS oncogene family

Figure 6.1 Generating an enzalutamide-activated AR$_{F876L}$ transcriptome in LNCaP-AR$_{F876L}$. A. diagram of enzalutamide-AR$_{F876L}$-driven signature gene lists overlapping with DHT-driven gene list in LNCaP_Laz cells. AR$_{F876L}$ signatures were defined as all genes showing ≥1.5 fold change (FDR <. 05) after 24 hours enzalutamide treatment in cells depleted of either AR$_{T877A}$ or AR$_{F876L}$ knockdown, respectively. (B) Enzalutamide-activated AR$_{F876L}$-driven gene profiling shows high overlap with GR-regulated subset of AR targets (Arora *et al.*, 2013). (C) Top 12 most upregulated gene from our list that matches GR-regulated genes were chosen for further analysis.

To verify the core list of enzalutamide-upregulated gene in our LNCaP-AR$_{F876L}$ cell line, we next compared gene expression profiling in the presence of enzalutamide upon AR$_{F876L}$ knockdown relative to both the siAR$_{F876L}$ vehicle and siAR$_{T877A}$ vehicle control arms (shown as siAR$_{F876L}$ in Figure 6.1 A). Firstly, post AR$_{F876L}$ knockdown, genes that exhibited a >2fold increase in expression following enzalutamide treatment were considered as enzalutamide-independent genes and were eliminated from the core list of AR$_{F876L}$-driven enzalutamide-upregulated genes. Comparison of the siAR$_{F876L}$ transfected arm in the presence of enzalutamide relative to the

siAR$_{F876L}$ vehicle control identified 154 differentially expressed genes, with only 17 out of 154 genes not matching to the 615 core data set (Appendix 6A) (Figure 6.1 A), suggesting activation independent of the ectopic AR$_{F876L}$ isoform. Of note, most of the up-regulated genes upon AR$_{F876L}$ knockdown had expression fold changes on the verge of the cut-off threshold. It is possible that incomplete knockdown of AR$_{F876L}$ may account for the persistence in expression of these identified genes in response to enzalutamide. Importantly, further annotation analysis of the 17 genes revealed no significant functional clustering and the majority of the genes had expression fold-changes on the verge of the cut-off threshold. Analysis of the siAR$_{F876L}$ arm in the presence of enzalutamide relative to the siAR$_{T877A}$ control arm outlined only 4 genes, *FKBP5 SLC45A3 and TIPARP* to have increased expression, with only *MIR1974* not matching to the 615 up-regulated gene signature. Intriguingly, *MIR1974* has been identified as co-regulated by DHT in PC cells (Li et al., 2016). The increasing gene expression may be the consequence of basal AR function. Hence, *MIR1974* was considered as enz-independent gene and was removed from following analysis.

A direct compassion was also conducted with a list of androgen-dependent AR-target genes from LNCaP-LacZ cells following 10 nM DHT treatment (O'Neill *et al.*, 2015). These cells are a control derivative of the LNCaP cell line that has the pLenti6.3-LacZ backbone stably integrated into the genome and were used previously to compare AR$_{T877A}$ and AR$_{W741L}$ activity in LNCaP cells. We observed a 30% (26 of 86 genes, Figure 6.1 A and Appendix 6B) overlap between the DHT-activated LNCaP-LacZ and enzalutamide-activated AR$_{F876L}$ expression signatures lists, including *KLK2, KLK3 TMPRSS2 and EAF2*, which are all well characterised AR-target genes. Moreover, nearly all of these genes decrease in response to AR$_{F876L}$ knockdown (Appendix 6B). This similarity outlines that enzalutamide is able to drive a similar androgenic signature via the AR$_{F876L}$ isoform. Some of most up-regulated genes driven by enzalutamide, such as *ORM1, TIPARP* and *NDRG1* were not up-regulated in the DHT-induced LNCaP-LacZ gene signature. This observation potentially suggests the ability of activated AR$_{F876L}$ to preferentially upregulate a distinct subset of target genes. In addition, we have shown in Chapter 5: that no activating effects of

enzalutamide on selected AR target genes was observed in LNCaP parental cells and is consistent with published transcriptomics data (Guerrero *et al.*, 2013), which reported that enzalutamide lacked AR agonistic activity LNCaP cells. Critically, it attenuates agonist-induced expression of genes involved in processes such as cell adhesion, angiogenesis, and apoptosis.

The 615 enzalutamide-activated genes from the LNCaP-AR$_{F876L}$ cell line derivative are listed in (Appendix 6A); with the top 20 overexpressed genes including several well-known androgen-regulated genes such as *TIPARP, FKBP5, NDRG1* and *EAF2*. Interestingly, the most highly up-regulated genes in response to enzalutamide in LNCaP-AR$_{F876L}$ were *ACSL3, ERRFI1, ORM1* and *SGK/SGK1* which are also GR-target genes. Furthermore, as GR activation has recently been shown to play an important role in models of enzalutamide-resistant CRPC, the ability for this AR mutant to drive genes associated with GR activity is intriguing and may suggest mimicry of the GR by this ectopically-expressed receptor isoform.

To investigate this question in more detail, we compared the core 484 gene list of enzalutamide-activated AR$_{F876L}$ genes with AR- and GR-ChIP seq data derived from enzalutamide-sensitive and -resistant LNCaP xenograft tumors (Arora *et al.*, 2013). Direct comparison of our list with the enzalutamide-induced gene sets revealed that 73 (highlighted green in Appendix 6C) of the 122 enzalutamide-induced genes (Isikbay *et al.*, 2014) , 60% matched directly to GR-bound AR targets in the enzalutamide-insensitive tumors. Moreover, 43 genes from our AR$_{F876L}$-driven signature matched to the 67 GR target gene signature derived from the xenograft samples (64%, Appendix 6D). Additionally, nearly all of these genes are diminished upon depletion of the AR$_{F876L}$, which suggests these genes are controlled by the mutant receptor. This GR-specific signature was defined as the gene-set that demonstrated elevated expression in response to the GR agonist dexamethasone compared to DHT treated samples.

In contrast, in the DHT up-regulated gene-set derived from the LNCaP-LacZ derivative (O'Neill *et al.*, 2015), only 36/122 (29%) and 15/67 (22%) matches were observed with the GR-bound AR gene expression and GR-selective gene signatures respectively (see Appendix 6C and Appendix

6D). These findings raised the possibility that the AR_{F876L} may drive a GR gene expression signature in our model system. Hence, the top 12 most upregulated genes from our list that matches GR-target genes were chosen for further analysis (Figure **6.1** C).
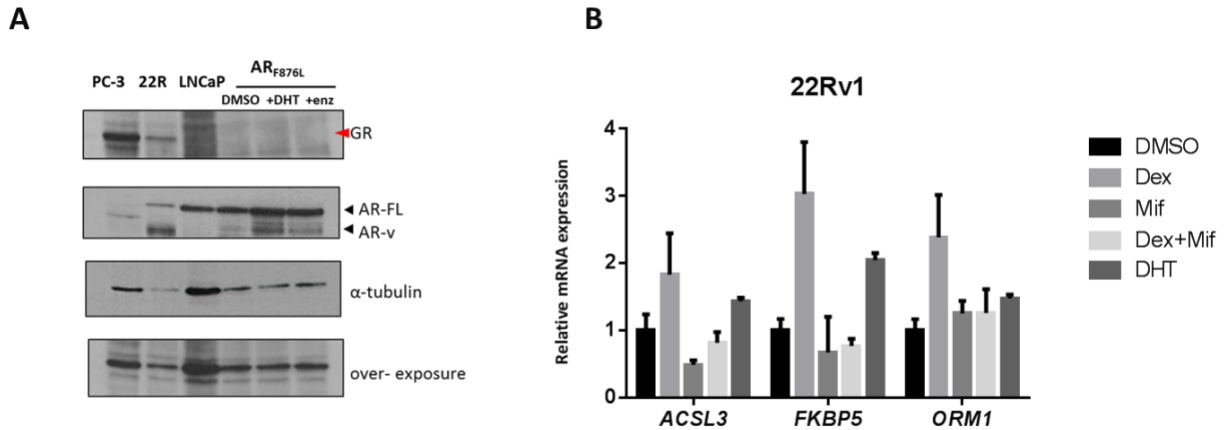
Figure 6.2 Assessing AR-/GR-regulated gene expression in CW22Rv1 cells. A. Protein lysates were collected from PC-3, CWR22Rv1, LNCaP and LNCaP-AR_{F876L} cell lines. LNCaP-derived AR_{F876L} cell were maintained in androgen-depleted media and then treated with DMSO, 10 nM DHT and 10 µM enzalutamide for 48 hours prior to harvesting. Immunoblotting was performed with antibodies specific for AR, GR, PSA and α-tubulin. B. CWR22Rv1 cells were maintained in androgen-depleted medium for 48 hours before applying the indicated treatments for 24 hours and then RNA extraction. Relative mRNA levels of selected genes were measured by RT-qPCR. Data represents N=3 ± SEM.

To investigate the possible role for increased GR signalling in enzalutamide resistance, GR expression in AR-negative cell lines PC3 and commonly studied AR-positive PC cell lines CW22Rv1 and LNCaP cell derivatives was firstly assessed. For protein expression analysis, all selected cell lines were cultured in steroid-depleted media prior western blot analysis. As shown in Figure **6.2**A, the strong baseline of GR expression was observed in the AR-negative cell lines PC3, while the CWR22Rv1 shows similar high expression of both GR and AR. In contrast, no GR protein expression was detected in LNCaP parental cells.

Although elevated expression of the *NR3C1 (GR)* gene was not detected in our microarray data, we further assessed whether the LNCaP-AR$_{F876L}$ cell line has elevated GR expression in the absence of serum and/or in the presence of DHT and enzalutamide. Cells were seeded in the presence of 10 % charcoal stripped medium of 48 hours before treatment with 10 nM DHT or 10 µM enzalutamide for 48 hours and GR protein expression in cells was examined. In androgen-depleted conditions, GR protein was undetectable in LNCaP AR$_{F876L}$ cells and remained so in the presence of DHT and enzalutamide (highlight with red in Figure **6.2**A). This data represents an important piece of evidence that supports the theory that in the LNCaP-AR$_{F876L}$ cell line, GR activation is unlikely to be involved in driving the enzalutamide-activated GR gene signature.

We next sought to examine AR$_{F876L}$-upregulated genes in CW22Rv1 given that they express the GR. Cells were grown in steroid-depleted media in the presence and absence of 10 m DHT, 10 µM enzalutamide, 100 nM of the GR agonist dexamethasone (Dex) and 100 nM of the GR antagonist mifepristone (Mif) for 24 hours before QRT-PCR. Consistent with CW22Rv1 cells demonstrating GR expression (Figure **6.2** A), dexamethasone shows significant induction of GR-target genes ACSL3, FKBP5 and *ORM1* relative to DMSO (Figure **6.2** B). Of note, CW22Rv1 cells express both AR variants and full-length AR, which harbours the H874Y mutation within LBD, that is able to be activated by other non-androgen hormones, including dexamethasone (Steketee *et al.*, 2002). Moreover, AR-Vs are constitutively active which makes the CW22Rv1 cell line a poor comparator model for our LNCaP-AR$_{F876L}$ cell line to address parity between AR$_{F876L}$- and GR-driven gene signatures.

We therefore employed the LAPC4 cell line, which is an AR/GR-expressing PC cell line, to further examine AR$_{F876L}$-upregulated genes in the background of a GR-expressing cell line in the presence and absence of defined ligands. We firstly confirmed that GR was expressed in LAPC4 cells and compared *NR3C1* (GR) expression in LAPC4 cells to the LNCaP-AR$_{F876L}$ cell line (Figure **6.3** A).
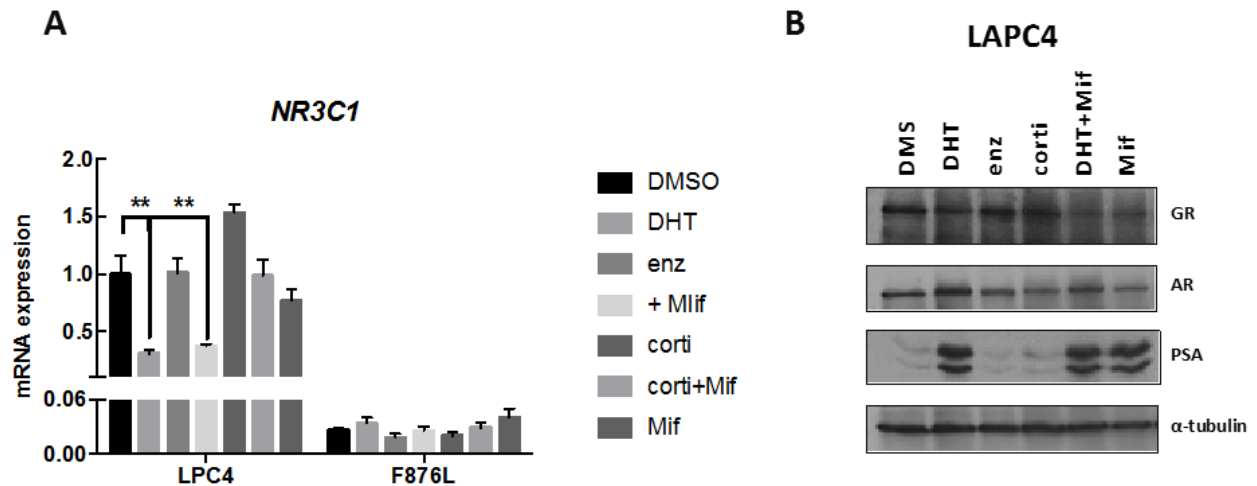
Figure 6.3 Analysis of *NR3C1 (GR)* expression in LAPC4 cells in the presence and absence of defined ligands. Effect of various ligands on changes of GR mRNA expression in LAPC4 and LNCaP-AR$_{F876L}$ cell lines. Cells were seeded in steroid-depleted media for 48 hours before treating with indicated ligands. After 24 hours treatment, cells were harvested, and samples analysed by (A) gene expression profiling and (B) immunoblotting. 10 nM DHT, 100 nM Dex, 100nM Mif and 10 µM enzalutamide were used for both experiments. Data represents N=3 ± SEM.

As shown in Figure **6.3** A, markedly higher GR mRNA levels were observed in LAPC4 cells compared to the LNCaP-AR$_{F876L}$ derivative. As expected, dexamethasone subtly induced GR mRNA expression in LAPC4 cells which was revered by co-treating with the GR antagonist mifepristone. Consistent with the AR negatively regulating GR expression (Xie *et al.*, 2015), DHT treatment down-regulated GR mRNA levels while enzalutamide had no effect, presumably because the cells were already grown in steroid-depleted conditions. These results were replicated at the protein level in LAPC4 (Figure **6.3**B). These results suggest that ligand-induced AR activation down-regulates GR expression at both mRNA and protein levels. To confirm this theory, we next sought to compare PSA expression in the same conditions to assess whether GR activation was inversely correlated with PSA production, a marker reflecting AR activation.

A

NR3C1 in LAPC4

B

NR3C1 in F876L

C

PSA in LAPC4

D

PSA in F876L
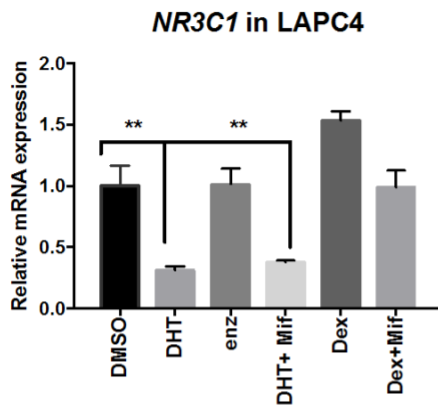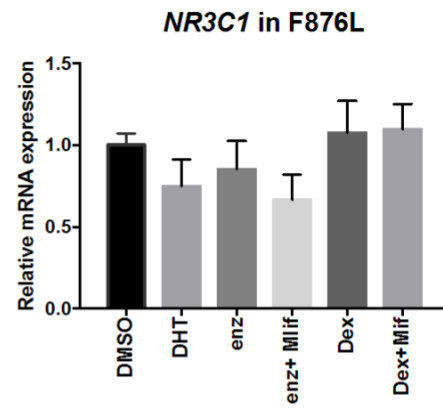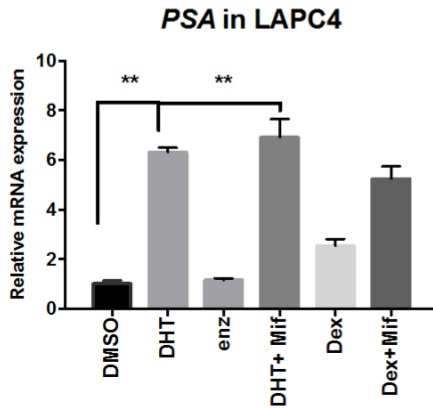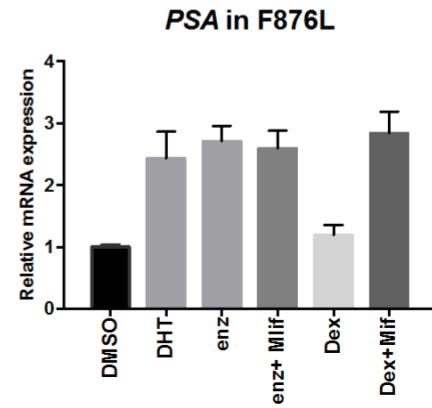
Figure 6.4 Activated-AR mediated feedback repression of GR expression in LAPC4. GR expression levels following AR inhibitor therapy was analyzed using LAPC4 and LNCaP-AR$_{F876L}$ cell lines. 24 hours of 10 nM DHT, 10 μM enzalutamide, 100 nM dexamethasone and 100nM mifepristone were used as indicated before mRNA expression analysis by qRT-PCR. GR and PSA expression level was normalized to GAPDH and depicted as fold change relative to vehicle. Data represents N=3 ± SEM.

As expected, in LAPC4 cells (Figure **6.4** A and C), DHT increased PSA mRNA expression while down-regulating GR expression. Enzalutamide, in contrast, suppressed AR function as indicated by diminished *PSA* expression, and did not stimulate GR mRNA downregulation. In LNCaP-AR$_{F876L}$ cells (Figure **6.4** B and D), although increased PSA levels correlated with activated AR$_{F876L}$ by DHT and enzalutamide, RT-PCR did not reveal an effect of the various ligands on GR expression in this cell line. Of note, mifepristone did not down-regulate enzalutamide-driven PSA expression, while

dexamethasone failed to increase PSA mRNA levels, which together supports the theory that genes upregulated in the LNCaP-AR$_{F876L}$ cell line is driven through AR$_{F876L}$ rather than GR activation.

By conducting global DNA sequencing using ChIP sample, Asangani *et al.* (2014) found that ligand-activated AR signalling can negatively regulate GR expression by directly binding to *cis*-regulatory elements of the *GR* gene. In addition, Xie *et al.* (2015) also found that GR expression in prostate cancer is diminished via AR occupancy at the upstream enhancer and subsequent polycomb-mediated gene silencing. To that end, the occupancy of AR at promoter regions of the *GR* gene in LNCaP parental cells and LNCaP-AR$_{F876L}$ stable cell line was next assessed to assess if endogenous and ectopic AR isoforms bind the *GR* locus to repress GR expression.
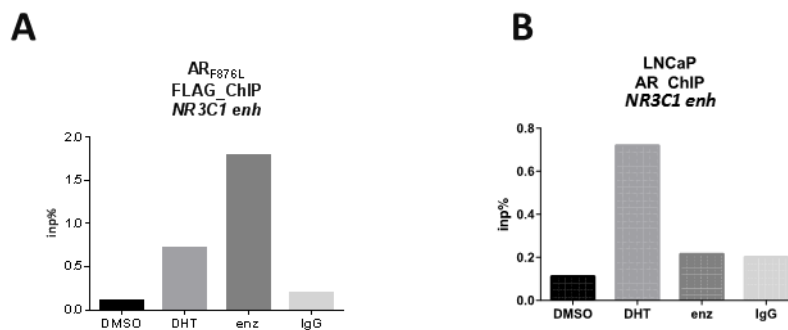
Figure 6.5 AR negatively regulate GR transcription by stimulating loading of AR on the promoter. (A & B) Cells were maintained in androgen-depleted medium for 48 hr. ChIP assays following by real-time qPCR were performed using LNCaP parental and -AR$_{F876L}$ cells treated with DMSO, DHT, and/or enzalutamide for 24 hours. Data represents N=2 ± SEM.

We conduced ChIP-qPCR using both LNCaP parental and LNCaP-AR$_{F876L}$ cells to further assess potential AR regulation of *GR* expression in LNCaP cells. Consistent with published results, as shown in Figure 6.5 A, LNCaP AR$_{F876L}$ cells demonstrated increased AR occupancy at the promoter regions of *GR* relative to DMSO treatment and control IgG ChIP in response to both DHT and enzalutamide. Moreover, enzalutamide triggered a higher recruitment at the *GR* enhancer compared to DHT. In contrast, in LNCaP parental cells, although DHT induced chromatin

occupancy of the endogenous AR, recruitment of the receptor was not observed at the *GR* enhancer upon enzalutamide stimulation. This suggests that the AR_{F876L} mutant may maintain repression of the *GR* in the presence of enzalutamide and hence expression of GR-target genes in the LNCaP-AR_{F876L} derivative is likely as a result of AR_{F876L} activity.

Together, the results presented above demonstrate that in the LNCaP-AR_{F876L} cell line, AR is a negative regulator for *GR* transcription and can be maintained by enzalutamide. Furthermore, it also provided evidence that GR signalling was not contributing to the effects of enzalutamide treatment in the LNCaP-AR_{F876L} cell line.

To help support this notion, we next examined AR_{F876L} upregulated genes in the presence and absence of defined ligands. LNCaP parental and LAPC4 cell lines were used as the comparison.
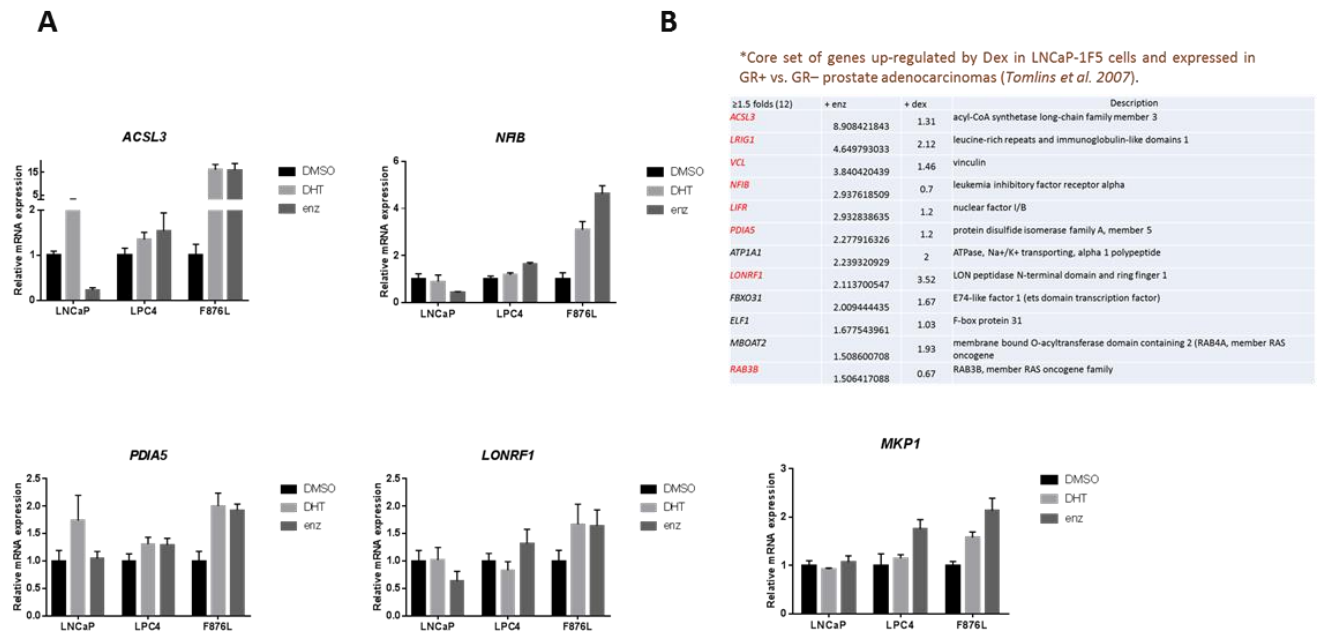
Figure 6.6 Profiling AR/GR-regulated gene in LNCaP parental, LAPC4 and LNCaP-AR_{F876L}. (A and B). mRNA was collected from each of the three cell lines grown in steroid-depleted conditions and treatment for 24 h with 10 nM DHT and 10 µM enzalutamide. Gene expression was assessed by qRT-PCR using specific primer as list in 6.2.3 Data represents N=2 ± SEM.

By comparing the three cell lines, we found that both DHT and enzalutamide-induced gene expression in AR_{F876L} stable cell line is more similar to LAPC4 cells rather than to the LNCaP parental cells. As results show in Figure 6.6 A, expression of GR-target genes *ACSL3, NFIB, PDIAD5, LONPR1* and *MKP1* increases modestly in LAPC4 and LNCaP-AR_{F876L} cells. Importantly, in the presence of enzalutamide, 8 (highlighted in red) out of 12 tested geneincreased in both LAPC4 and LNCaP-AR_{F876L} cells, but not in LNCaP parental cells.

As LAPC4 cells express both AR and GR, we suspected that upregulated GR-target gene expression in LAPC4 cells may be driven through GR activation in the presence of enzalutamide. Therefore, as a prove-of-concept, we next went to interrogate whether enzalutamide activated GR or AR function in LAPC4 cells by knockdown of either AR or GR.
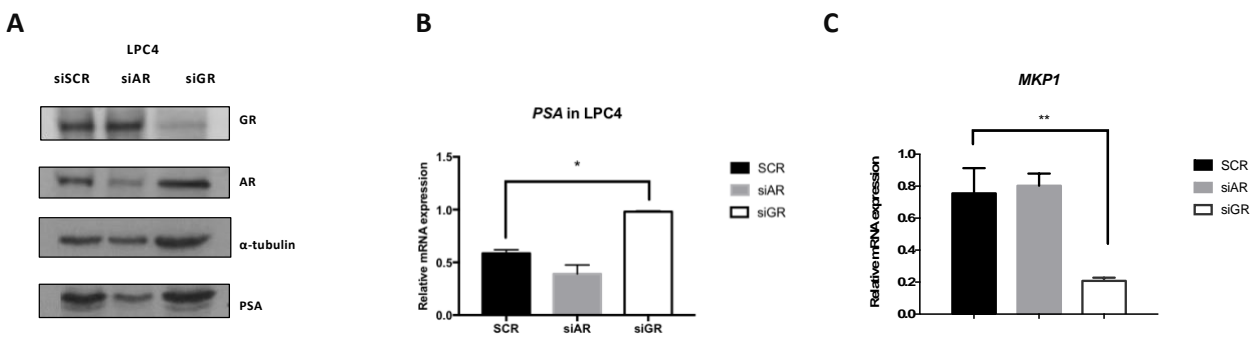
Figure 6.7 Profiling AR-/GR-regulated genes in LAPC4. (A) Knockdown efficiency of siAR and siGR in LAPC4 cells. Cell lysates were harvest post siRNA-mediated AR and GR depletion and nuclear receptor levels and PSA expression was assessed by western blots. (B) PSA mRNA expression level in LAPC4 cells upon AR or GR knockdown. (C) GR-target gene *MPK1* expression was analyzed in the presence of 10 μM enzalutamide using specific primers in LAPC4 cells post AR or GR knockdown. Data represents N=3 ± SEM.

AR and GR knockdown was firstly confirmed via western blots as shown in Figure 6.7 A. Comparing to siSCR control, knockdown of AR was effective and reduced PSA levels in in LAPC4 cells. In contrast, in response to GR knockdown, PSA expression was not affected. Of note, loss of GR expression in LAPC4 results in a modest increase in the level of AR and is consistent with RT-qPCR results demonstrating an increase in PSA mRNA in response to GR knockdown (Figure

6.7 B). Importantly, in the presence of enzalutamide, *MKP1* expression was diminished only upon GR knockdown (Figure 6.7 C) supporting our previous data suggesting that GR is a driver of GR-target genes in LAPC4 while it is in LNCaP-AR$_{F876L}$ which drives these genes in the LNCaP-AR$_{F876L}$ derivative.
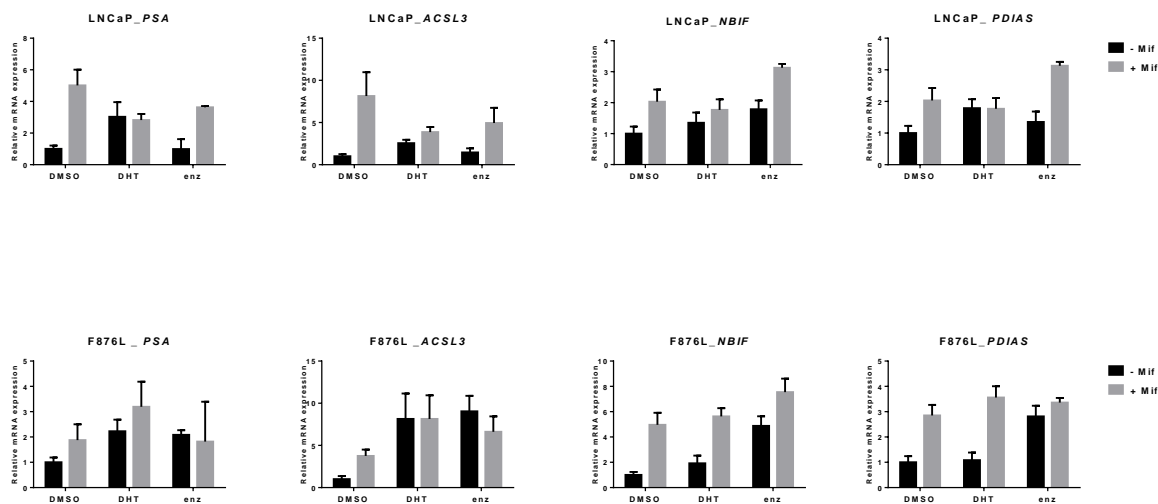
Figure 6.8 Mifepristone demonstrates an agonistic effect for AR. Mifepristone exhibits agonist activity in both parental and AR$_{F876L}$ –expressing LNCaP cells. qPCR analysis of expression of AR target genes in LNCaP and LNCaP-AR$_{F876L}$ cells treated with DMSO or DHT, enzalutamide - /+ Mifepristone for 24 hours. Data are presented as percentage of expression in enz-treated sample relative to DMSO. Data represents N=2 ± SEM.

During the gene profiling validation, we noticed that Mifepristone demonstrated agonistic activity for receptor-target gene expression in both LNCaP parental and LNCaP-AR$_{F876L}$ cell lines. We therefore investigated this effect further. As results demonstrate in Figure **6.8**, AR target genes *PSA, ACSL3, NFIB* and *PDIAS* were significantly increased upon mifepristone treatment alone. Consistent results were also observed in parental LNCaP cells; a phenomenon previously reported demonstrating the compound has a high binding affinity for AR and can function as an AR agonist (Song *et al.*, 2004). Kang *et al.* (2004) also found that Mifepristone exhibited agonist activity in LNCaP cells, by stimulating loading of AR and recruitment of Pol II and p300 on the

promoter. As mifepristone is currently used in clinical trials in combination with ADTs for CRPC patients (https://clinicaltrials.gov/ct2/show/NCT02012296), the potential of mifepristone as an AR modulator in clinical prostate cancer has yet to be explored, here, our results for the first time provide evidence of transactivation by mifepristone of wild-type and F876L mutant receptors in models of CRPC.

In all, our results presented above demonstrate that the AR_{F876L} mutant drives a GR-target gene signature in the LNCaP-AR_{F876L} derivative that lacks GR expression suggesting potential nuclear receptor mimicry to promote GR-target gene expression.

6.3.2 Investigate sensitivities of AR_{F876L} to BET inhibitors

The identification and therapeutic targeting of co-activators or mediators of AR transcriptional signalling is being actively pursued as an alternative strategy to treat CRPC, including newly developed BET family bromodomain inhibitors. Hence, in the second part of this chapter, experiments in which a panel of BET inhibitors were applied to the LNCaP-AR_{F876L} cell line are described to discover new treatment options for AR_{F876L}-driven enzalutamide resistance in CRPC. JQ1 is a small-molecule compound that been designed to target bromodomains 1 and 2 of the BET family, including BRD4. Given that BET inhibitors are being applied in the clinic as part of early phase clinical trials after patients have failed ADT (including enzalutamide), the requirement to study their efficacy in distinct AR mutational backgrounds as a result of ADT resistance is important. Pawar et al. (2018) and Ruggero et al. (2018) found that treatment with the BET inhibitor, JQ1, can effectively re-sensitise resistant tumours to enzalutamide. JQ-1 works downstream of AR and abrogates recruitment of the receptor to cis-regulatory elements resulting in removal of RNA polymerase II from AR target genes, to induce apoptosis and down-regulate AR-regulated gene transcription (Asangani et al., 2014). Hence, JQ-1 was firstly used in the newly-derived LNCaP-AR_{F876L} cell line model to investigate the potential of BET-inhibition as a tractable treatment for diminishing AR_{F876L}-regulated signalling.
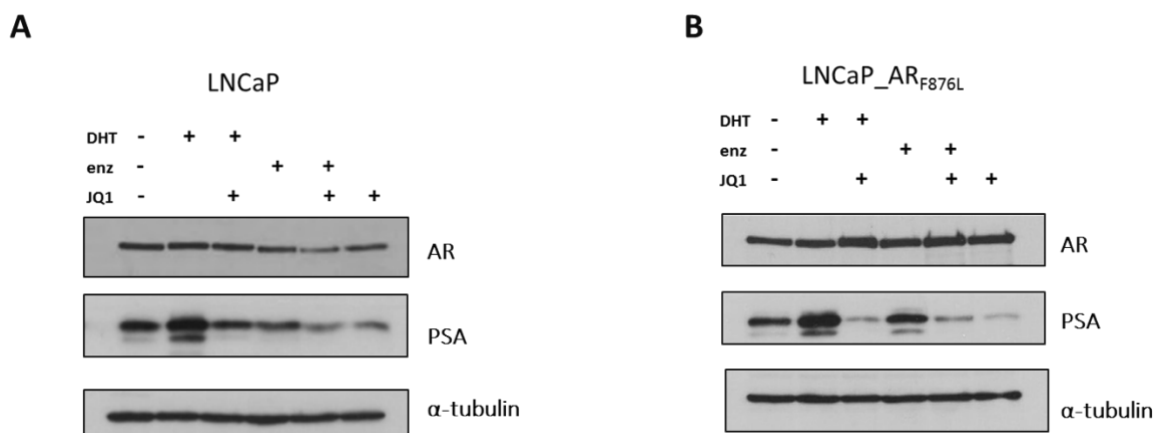
Figure 6.9 JQ1 down-regulation of PSA level in LNCaP parental cells and AR$_{F876L}$. (A) JQ1 reduced DHT-resulted PSA level in LNCaP. (B) JQ1 shows inhibitory effects on AR$_{F876}$. JQ1 reduced enzalutamide-driven PSA level in LNCaP-AR$_{F876L}$ cells. AR-441 (abcam) and PSA antibodies were used for detection of total AR protein levels in both cell lines.

LNCaP and LNCaP-AR$_{F876L}$ cells were cultured in steroid-depleted media for 24 hours before application of 10 nM DHT, 10 μM enzalutamide and/or 0.5 μM JQ-1 for an additional 24 hours. Whole cell lysates were then collected before AR and PSA analysis by western blotting. α-tubulin was used in each sample as loading control. As results show in Figure **6.9** A, AR protein levels were not markedly affected by JQ1 treatment in both cell lines. Importantly, a marked down-regulation of DHT-induced PSA level was observed in LNCaP parental cells; and a similar inhibitory effect of JQ1 was observed on DHT- and enzalutamide-activated AR$_{F876L}$-driven PSA expression in the LNCaP-AR$_{F876L}$ cell line (Figure **6.9** B).

We next determined the consequences of JQ1 treatment on cellular phenotype by measuring cell proliferation and viability using the IncuCyte® ZOOM system.
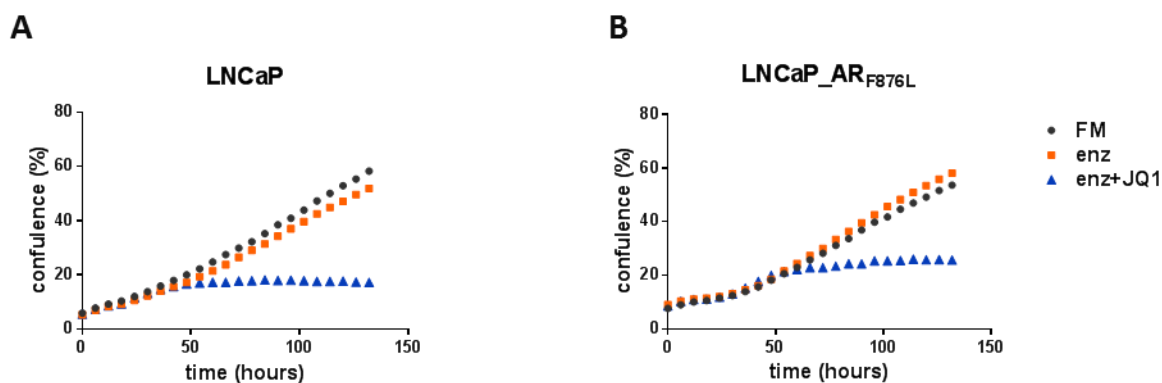
Figure 6.10 JQ-1 treatment attenuates enzalutamide-driven cell growth of LNCaP-AR$_{F876L}$. (A & B) Parental and AR$_{F876L}$ LNCaP cells were seeded in steroid-containing media in 96-well plates containing 10 μM enzalutamide or enzalutamide plus 0.5 μM JQ1. Cell confluency of each well was measured in real-time for 7 days using the IncuCyte® ZOOM as described in section 5.2.4.

In contrast to LNCaP-AR$_{F876L}$ cells, the presence of enzalutamide in LNCaP cells resulted in a modest reduction of cell growth. Inhibiting the bromodomain function of the BET family with JQ1 resulted in markedly decreased cell proliferation (Figure **6.10** A). Importantly, LNCaP-AR$_{F876L}$ also demonstrated a significant decrease in cell growth after around 48 hours of BET inhibition, suggesting that enzalutamide-driven cell proliferation can be attenuated by JQ-1.

Given that AR-positive cell growth was preferentially sensitive to JQ1, we next explored expression levels of selected AR-target genes in the LNCaP-AR$_{F876L}$ cell line in the presence and absence of enzalutamide. LNCaP-AR$_{F876L}$ cells were seeded in the absence of androgen for 48 hours then treated with DHT (10nM), enzalutamide (10 μM) and JQ1 (500 nM) for 24 hours before AR gene expression profiling.

A

B
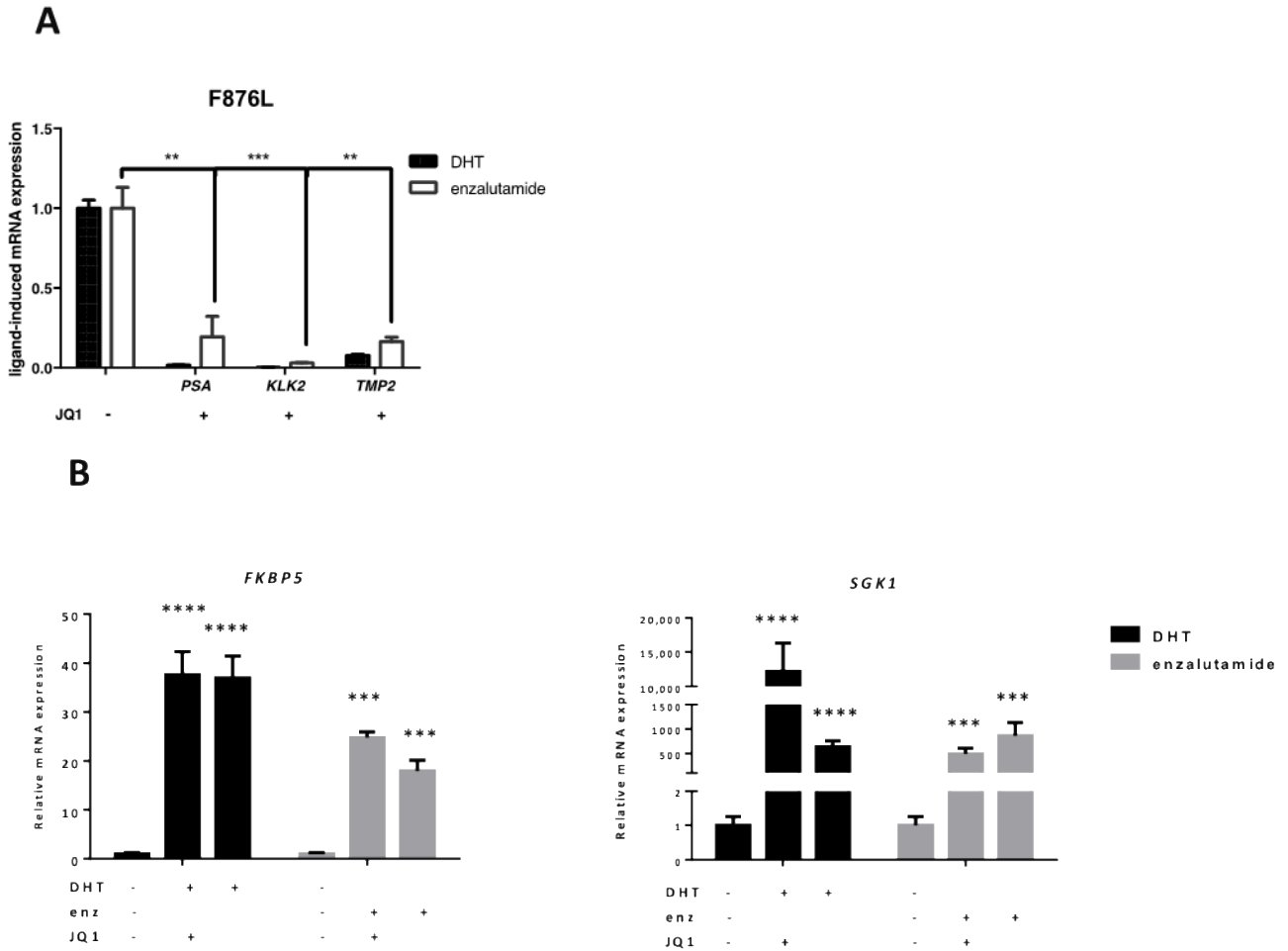
Figure 6.11 Co-treatment with the BRD4 inhibitor JQ-1 attenuates expression of DHT-/ enzalutamide-AR_{F876L}-induced *PSA KLK2 TMPRSS2, SGK1* expression, but not *FKBP5* expression. (A & B) Quantitative RT-PCR analysis of *PSA, KLK2, TMPRSS2, FKBP5* and *SGK1* gene expression in LNCaP AR_{F876L} cells treated with combinations of vehicle (DMSO and ethanol), 0.5 μM JQ1, 10 nM DHT or 10 μM enzalutamide as indicated for 24 h. Data represent mean $+/-$ standard error of the mean (s.e.m.) (n =3)

To aid comparison, DHT and enzalutamide-induced gene expression in the absence of JQ-1 were normalized to 1 and the effect of JQ-1 on *PSA*, *KLK2* and *TMPRSS2* expression was shown as a fold change compared to this arbitrary value (Figure **6.11** A). As expected, both DHT and enzalutamide-activated *PSA* expression was effectively downregulated upon JQ1 treatment. This result is consistent with our early data showing that JQ1 reduced enzalutamide-elevated PSA protein levels (Figure **6.9** B). In addition, another two AR-regulated gene, *KLK2* and *TMPRSS2* also

showed similar negative effects of JQ1. Interestingly, we observed that not all selected genes demonstrated diminished expression in response to the BET inhibitor; in the presence of DHT and enzalutamide, *FKBP5* expression was not affected by JQ-1, while only DHT-activated SGK1 mRNA expression was diminished by JQ-1 (Figure **6.11**B). To sum up, JQ-1 presents selective down-regulated effects on the AR_{F876L} mutant in LNCaP-AR_{F876L} cell line.

6.3.3 Compound G inhibits AR_{F876L} transcriptional function by disrupting with co-recruitment of p300 at androgen-responsive elements.

Although we have shown that several canonical AR-target genes are sensitive to JQ1, it is not clear why only a subset of genes responds to BRD4-BET inhibitors. Recently, a number of BET-family proteins were shown to interact with sequence-specific DNA-binding transcription factors in a gene-specific manner in CRPC. As the genetic and epigenetic landscape differs between PC model types, it is possible that distinct transcriptional regulators that associate with AR might influence the action of BET inhibitors. Hence, we next tested inhibitory capacity of targeting another bromodomain-containing family protein candidate, p300, by applying a newly-developed p300 bromodomain inhibitor called Compound G in our cell line model.

p300 has been shown to regulate AR signalling in CRPC, in part, via direct acetylation of the receptor and modulating histone acetylation (Cucchiara *et al.*, 2017). Given that p300 is known to engage with sequence-specific DNA-binding proteins and other coregulatory proteins, resulting in modulation of transcription through altered protein-protein interactions, thus this compound was assessed in our model system is to examine if compound G is effective against the AR_{F876L} isoform; and hence represents another tractable target in enzalutamide-resistant disease.
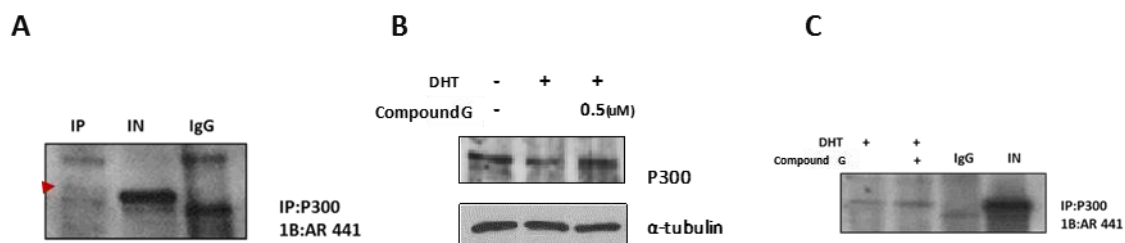
Figure 6.12 Bromodomain of p300 is not required for AR-p300 interaction. (A) LNCaP cells were cultured in normal growth condition and immunoprecipitation was performed using whole cell lysates using a p300 antibody before probing immunoprecipitates with an anti-AR antibody. (B) Endogenous p300 expression in LNCaP cells was assessed in the presence and absence of 0.5 µM Compound G and DHT. (C) IP assay akin to (A) with inclusion of Compound G to assess impact on AR-p300 interaction.

Using immunoprecipitation assays, we were firstly able to detect endogenous AR-p300 interaction in LNCaP cells which confirms previous reports (Heemers *et al.*, 2008). Next, cells were treated with DHT or DHT plus Compound G for 24 hours. As results indicated in Figure **6.12**B, Compound G treatment did not affect endogenous p300 protein levels in LNCaP cells. Importantly, as shown by immunoprecipitating p300 from cells treated with and without Compound G, the p300-AR interaction was not affected (Figure **6.12** C) and supports the concept that the bromodomain of p300 is not required for AR interaction.

Binding of enzalutamide to AR_{F876L} leads to its translocation from the cytoplasm to the nucleus, where it binds to regions of DNA harboring androgen-responsive elements (AREs) and results in subsequent recruitment of proteins involved in transcriptional activation or suppression in a gene-specific manner (Figure **6.11**). p300 modulates gene expression via interaction and modification of chromatin, via histone acetylation, as well as DNA-binding transcription factors, leading to context-dependent transcriptional regulation of target genes. The p300 bromodomain has also been suggested to be important for specific chromatin substrate recognition and for chromatin remodeling (Chen *et al.*, 2010). Having earlier observed that the AR–p300 interaction is not disrupted by Compound G, we next explored whether inhibition of the p300 bromodomain

affects transcriptional activation of AR function by interrupting chromatin occupancy. To that end, we performed ChIP-qPCR with antibodies against FLAG-AR and p300 in LNCaP-AR$_{F876L}$ cells that were either starved of steroids, treated with either enzalutamide or +/- Compound G.
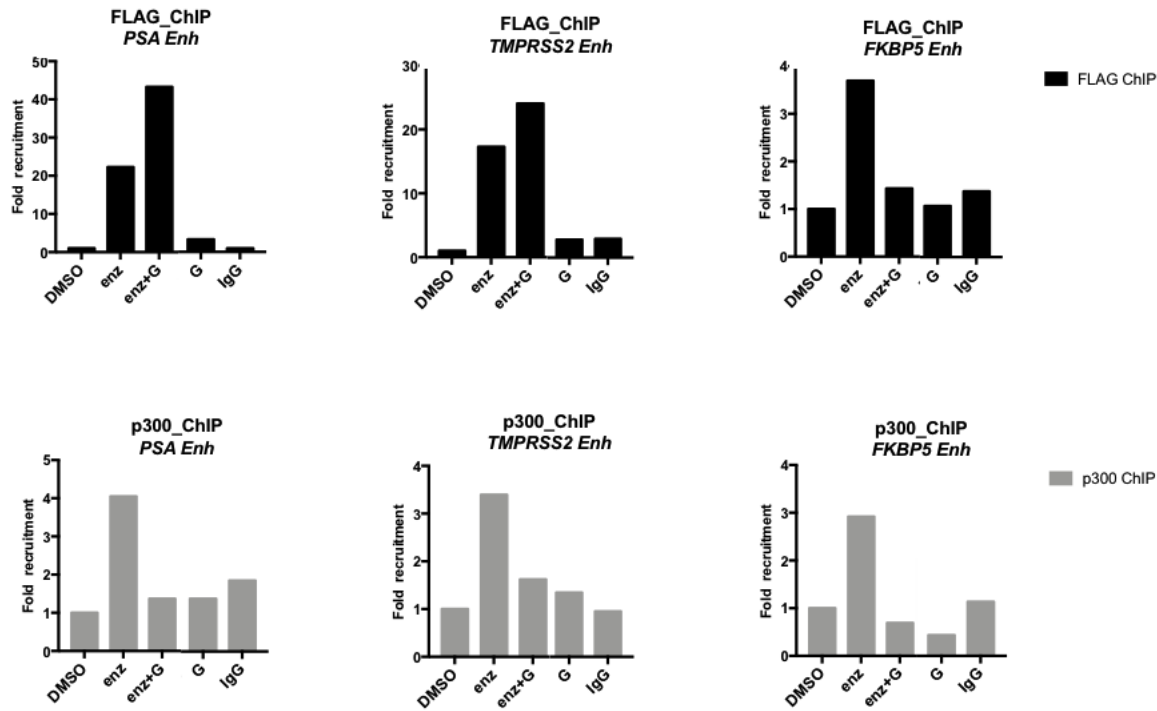
Figure 6.13 p300 loading at *cis*-regulatory regions of AR-target genes is lost upon Compound G treatment in LNCaP-AR$_{F876L}$ cells. Indicated treatments were conducted in LNCaP-AR$_{F876L}$ for 24 hours. Enzalutamide-mediated recruitment of AR$_{F876L}$ and p300 to enhancer regions of *PSA, TMPRSS2* and *FKBP5* was assessed by ChIP-qPCR. DMSO-dimethylsulphoxide, enz-enzalutamide, G-Compound G. Data represents N=2.

As expected, comparing to DMSO and IgG control arm, FLAG-AR was highly enriched at *PSA* enhancer in enzalutamide-treated cells (Figure **6.13**). Robust co-association of p300 recruitment was also observed within the same promoters of AR-regulated genes. Although enzalutamide-driven AR$_{F876L}$ enrichment remains at similar level upon Compound G treatment, interestingly, recruitment of p300 to target loci was attenuated. Furthermore, Compound G blocked p300 recruitment consistently at enhancer regulatory regions of *TMPRSS2*. In contrast, enrichment of both AR$_{F876L}$ and p300 were largely removed from enhancer regions of *FKBP5* upon enzalutamide and Compound G dual treatment. It suggests that bromodomain inhibition has profound effects

on p300 chromatin binding while loss of p300-BET function may also impact on AR chromatin occupancy in a gene-specific manner.

Based our observation of AR and p300 co-association at specific regulatory elements of AR-target genes, we next sought to determine the functional consequences of Compound G treatment by measuring the expression levels of selected AR-target genes.
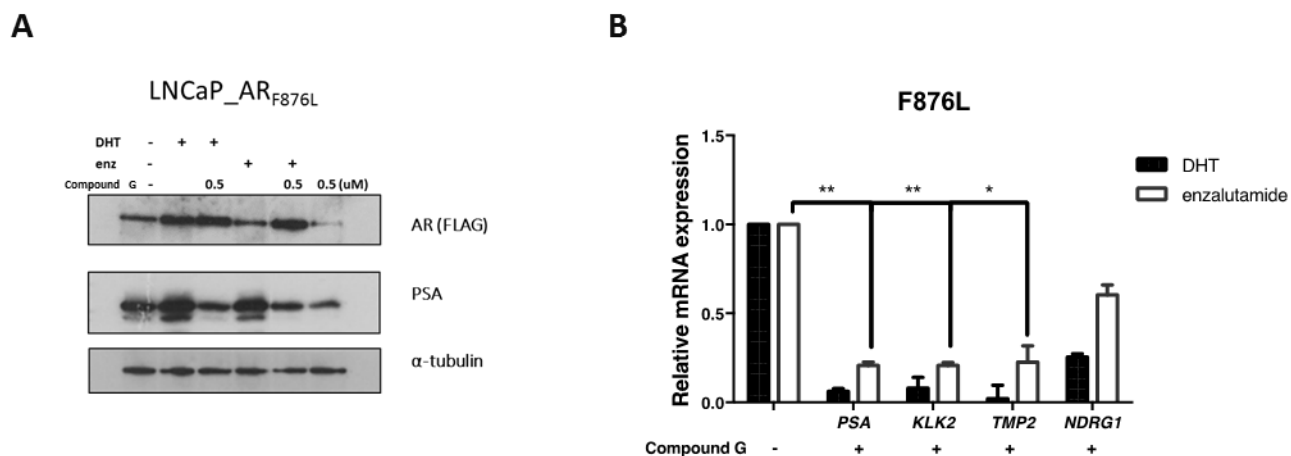
Figure 6.14 Compound G down-regulates DHT- and enzalutamide-activated AR$_{F876L}$-target gene expression in LNCaP-AR$_{F876L}$. (A) Western blots were performed with lysates from LNCaP-AR$_{F876L}$ cells treated with DHT, enzalutamide or Compound G as indicated. Blots were probed with antibodies specific to the FLAG-tag, PSA and α-tubulin. (B) Quantitative RT-PCR analysis of AR target gene mRNA levels in LNCaP-AR$_{F876L}$ cell lines treated as indicated. For comparison purposes, DHT and enzalutamide-induced gene expression level were set to 1. Data represents N=3 ± SEM.

In LNCaP-AR$_{F876L}$ cells, PSA protein levels are elevated in response to DHT and enzalutamide which can be reversed with p300 bromodomain inhibition (Figure **6.14** A), Consistent with the PSA western data, the selected AR-target genes *PSA*, *KLK2*, *TMPRSS2* and *NDRG1* were up-regulated by both DHT and enzalutamide. Importantly, co-treating LNCaP-AR$_{F876L}$ cells with Compound G efficiently down-regulated both DHT- and enzalutamide-induced AR target gene regulated gene expression (Figure **6.14** B).

Next, to evaluate p300 bromodomain inhibitor repression of AR activity in an androgen-dependent setting, both LNCaP parental cells and LAPC4 were treated with either DHT alone or DHT together with escalating concentrations of Compound G for 24 hours. As results show in Figure **6.15**, both cell lines demonstrate a dose-dependent decrease in DHT-induced PSA protein levels upon Compound G treatment.

A

B
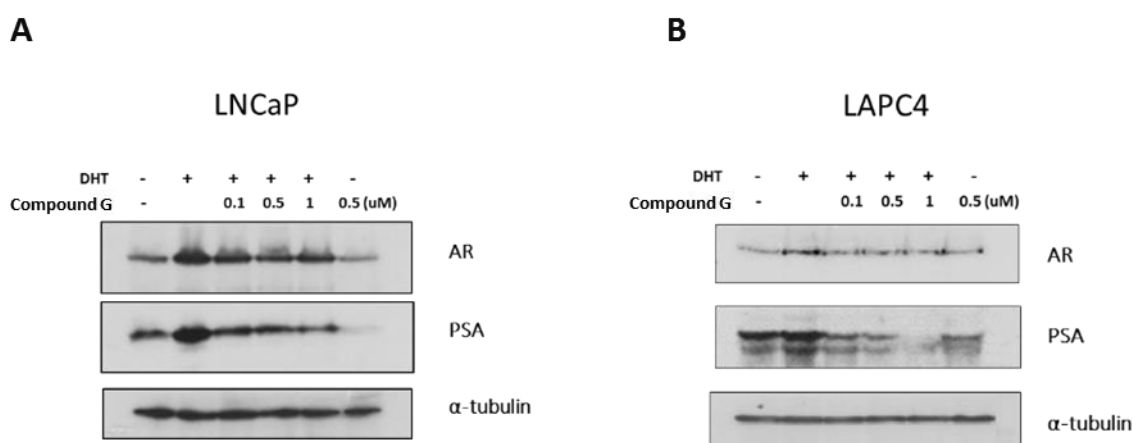
Figure 6.15 Inhibition of the p300 bromodomain by Compound G reduces PSA protein levels in LNCaP and LAPC4 cell lines. (A & B) Immunoblot analyses of AR and PSA levels in LNCaP and LPC4 cells treated with 10 nM DHT and/or the indicated doses of Compound G for 24 hours. α-tubulin served as a loading control. Data represents N=3.

Together, these data indicate that Compound G-mediated inhibition of the p300 bromodomain results in down-regulated AR transcription function across numerous AR backgrounds by potentially interrupting chromatin loading of the enzyme which could perturb histone acetylation levels required for AR activity.

The HAT domain of p300 for histone and AR acetylation is a requisite for receptor activity (Gaughan *et al.*, 2002). Moreover, the recent evidence that the Bromodomain and HAT domain are intrinsically linked indicates that compound G may also be inactivating the HAT activity. Hence, in this study, we next sought to assess the effect of an additional, but related reagent that

targets p300 HAT activity, C646, on receptor function in different backgrounds of AR signalling in models of CRPC.
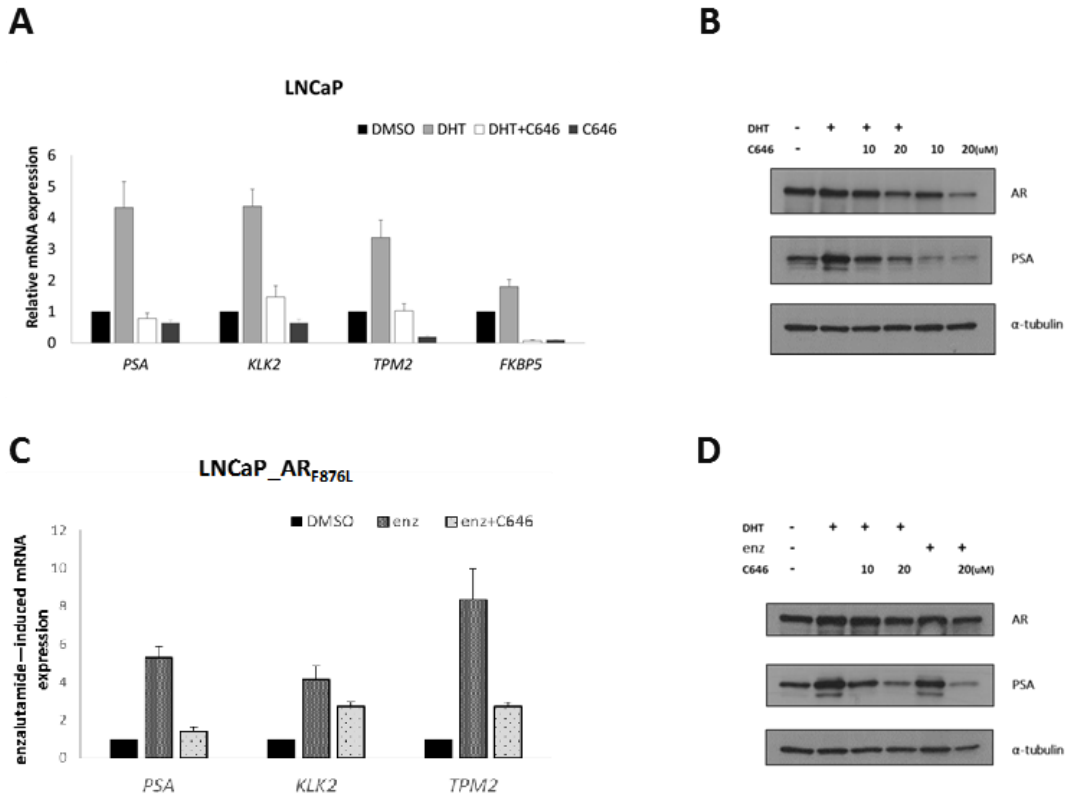
Figure 6.16 p300 HAT inhibitor C646 suppresses DHT- and enzalutamide-induced AR-target gene expression in parental and AR$_{F876L}$ LNCaP cell line derivatives, respectively. (A and C). QRT-PCR analysis of selected AR-target genes upon 24 hours of either 10 nM DHT or 10 µM enzalutamide -/+ 10 µM C464 treatment. Data represents N=2 ± SEM. B and D. Western blot analysis of protein lysates from LNCaP and LNCaP-AR$_{F876L}$ cells treated as in (A) and (C) using antibodies specific for AR, PSA and α-tubulin.

Inhibition of the p300 HAT domain was carried out by conducting 24 hours C464 treatment in both LNCaP and LNCaP-AR$_{F876L}$ cells. As shown in Figure **6.16** A and C, attenuating p300-HAT activity via C646 treatment decreased expression of AR-regulated genes *PSA, KLK2, TMPRSS2* and *FKBP5* in the context of DHT- and enzalutamide-activation in LNCaP and LNCaP-AR$_{F876L}$, respectively. Consistently, down-regulation of AR function was also observed at the protein level as demonstrated by reduced PSA levels in response to C464 treatment (Figure **6.16** B and D). Together these results demonstrate that diminished p300 HAT activity using c646 reduced DHT-

/enzalutamide-stimulated AR activity in both LNCaP and LNCaP-AR$_{F876L}$, respectively. Of note, during these experiments, we noticed that 24 hours C646 treatment resulted in marked elevation of cell death in both cell lines which suggests inhibiting p300 activity is cytotoxic and is consistent with reports indicating the histone acetyltransferase activity of p300 promotes PC cell survival and growth (Gao *et al.*, 2013). To examine this further, we next assessed whether suppression of p300 HAT function impacts on the cell cycle of PC cells using flow cytometry.
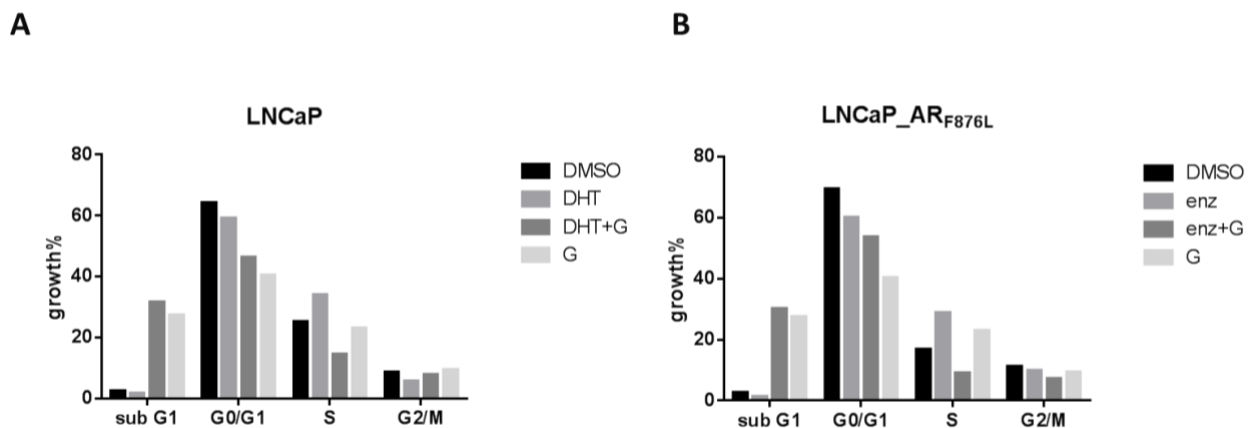
Figure 6.17 The p300/CBP HAT inhibitor C646 induces apoptosis in LNCaP and LNCaP-AR$_{F876L}$ cells. (A & B) LNCaP and LNCaPAR$_{F876L}$ cells were treated with and without 10 µM enzalutamide and 1 µM C646 as indicated. Cell cycle distribution was measured after staining the cells with propidium iodide (PI), and percentage of positive cells was determined by flow cytometry. Data represents N=2 ± SEM.

To test whether inhibition of p300 HAT activity has anti-proliferative effects in LNCaP and LNCaP-AR$_{F876L}$, we measured cell cycle distribution after staining cells with propidium iodide (PI) to analyse the percentage of cells in particular cell cycle phases based on DNA content (Figure **6.17**). Compared to DMSO, DHT and enzalutamide treatment, as expected, increased abundance of cells in the S- and G2/M- phases of the cell cycle at the expense of G0/G1 phase in the LNCaP and LNCaP-AR$_{F876L}$ cell lines, respectively. Quantification of the sub-G1 peak in both cell lines post treatment with C646 revealed that downregulation of p300-HAT by C646 leads to an increase of apoptosis in both cell lines. Hence, we concluded that the histone acetyltransferase activity of

p300 is essential for the survival of LNCaP parental and are also important for AR_{F876L}-driven cell growth (Figure **6.17** B) in the presence of enzalutamide.

6.4 Discussion

The selective outgrowth of AR mutations in advance androgen-insensitive PC has been demonstrated as a mechanism whereby the AR mutants are capable of remaining active following anti-androgen treatment (Brooke and Bevan 2009, Steinkamp et al., 2009). The regulatory mechanisms by which AR mutations provide a growth advantage, includes the mediation of co-regulator protein recruitment and enhanced ligand promiscuity which results in AR transactivation by non-conventional ligands. In the previous chapter, we established and have validated an AR replacement PC model in the LNCaP cell line to study the enzalutamide-activated AR_{F876L} mutant. Following endogenous AR_{T877A} knockdown via a pre-designed siRNA targeted to the 3'- UTR of AR mRNA, the role and function of AR_{F876L} could be assessed. Overall, it was found that treatment with enzalutamide resulted in enrichment of AR_{F876L} to AR-target genes, leading to increased expression of the AR target genes *PSA* and *KLK2,* as well as increasing cell proliferation. Therefore, given the capability of the model to recapitulate the antagonist to agonist switch observed in clinical samples, we sought to understand the enzalutamide-induced transcriptional program mediated via AR_{F876L} that could indicate potential distinctions between the transcriptomes of CRPC-relevant AR isoforms and hence provide important information on subsequent patient-tailored treatments and biomarker identification. Hence, in this chapter, we conducted global gene analysis in our validated AR_{F876L}- driven LNCaP cell line using an Illumina Bead CHIP-based micro-array. In all, we found that enzalutamide-activated AR_{F876L} is able to drive a similar androgenic signature to that of endogenous receptor, while possessing the ability to preferentially upregulate a distinct subset of target genes outside of those controlled DHT-activated ARwt, including a GR-like gene signature.

Preclinical and clinical studies have conclusively demonstrated that in most cases, acquired resistance to traditional ADT is the consequence of reactivation of the AR pathway. Critically,

increased selection pressure conferred by second-generation anti-androgens, such as enzalutamide, can also result in alternative resistant mechanisms, including GR-mediated AR mimicry (Balbas *et al.*, 2013; Joseph *et al.*, 2013; Korpal *et al.*, 2013a). The functional involvement of the GR in resistance to enzalutamide was firstly documented by Arora *et al.* (2013) and Isikbay *et al.* (2014). Enhanced GR expression was observed in enzalutamide-resistant tumours *in vivo* and in tumour biopsies from enzalutamide-treated PC patients (Arora *et al.*, 2013). By exploring AR and GR-signalling regulation in an LNCaP cell lines model derived from enzalutamide-resistant xenografts *in vitro* using ChIP-seq and gene expression profiling for both steroid receptors, it was reported that AR and GR have a distinct but significantly overlapping cistrome and transcriptome. In this chapter, by conducing global gene expression analysis in our validated AR_{F876L}- driven LNCaP cell line, which is a model of the common mutation identified in enzalutamide-resistance, we discovered a 60% overlap between the AR_{F876L} gene-set and the GR-regulated gene-set identified from the enzalutamide xenografts (Aurora et al., 2013). Specifically, we found 73 AR_{F876L}-upregulated genes overlapped with a 122 gene-containing GR signature (representing GR-bound AR-target genes) and 43 matches to a GR-activated gene-set totalling 67 genes. In contrast, a DHT-upregulated gene-set in the LNCaP-Laz cell line derivative (O'Neill et al., 2015) was found to have considerably less overlap with the GR-bound and GR-activated signatures; with 36/122 and 15/67, respectively. Transcriptomic analysis of enzalutamide-activated AR_{F876L} in LNCaP-AR_{F876L} cells demonstrates considerable overlap with GR-targeted subset of AR targets, including *STK39, MPK1*, which has been previously found up-regulated via GR activation in glucocorticoid-dependent breast epithelial cells growth (Isikbay *et al.*, 2014).

Hence, we here propose two theories accounting for our observations in LNCaP-AR_{F876L}:

a. Up-regulation of endogenous GR enhances GR-target gene expression (due to compensation or selective pressure from acute enzalutamide exposure).
b. Upon enzalutamide binding, AR_{F876L} actively binds to GR-target gene response elements and mimics GR-signalling activation.

To investigate these proposed theories, LNCaP parental and LAPC4 cell lines were chosen to provide comparisons against the LNCaP-AR$_{F876L}$ derivative. By firstly examining GR expression in LNCaP-AR$_{F876L}$, we found there was no increase in endogenous GR mRNA and protein expression (Figure **6.3**) in response to enzalutamide. Furthermore, expression of the GR was undetectable by western analysis in both LNCaP and LNCaP-AR$_{F876L}$ derivatives suggesting that up-regulation of GR in the LNCaP-AR$_{F876L}$ cell line is an unlikely explanation for GR-target gene expression in response to the anti-androgen.

As GR activation can be negatively regulated by direct AR binding to a *cis*-regulatory element upstream of the *GR* gene (Xie *et al.*, 2015), we next went on to interrogate GR and AR function in LAPC4 cells. Indeed, we found that AR activation reduces GR expression in LAPC4 cells, while GR depletion up-regulates AR protein levels (Figure **6.4**). This phenomenon was further supported by detecting occupancy of AR at GR *cis*-regulatory elements upon DHT stimulation. Importantly, we showed that in the LNCaP-AR$_{F876L}$ cell line, ectopic AR$_{F876L}$ is also recruited to the *GR* gene enhancer in the presences of enzalutamide which may help to maintain low GR levels in this cell line (Figure 6.5).

Moreover, it was found that enzalutamide- and DHT-induced GR-target gene expression in the LNCaP-AR$_{F876L}$ cell line was largely distinct to parental LNCaP and LAPC4 cells supporting the concept that AR$_{F876L}$ has an altered target gene-set to that of endogenous AR T877A in LNCaP cells and wild-type AR in LAPC4 cells (Figure **6.6**). In the presence of enzalutamide, over half of the tested genes increased in LNCaP-AR$_{F876L}$ cells whilst not in LNCaP. A smaller number of genes were elevated in LAPC4 in response to enzalutamide, including *MPK1*. We suspected that enzalutamide-induced elevation of genes in LAPC4 may be driven through activation of endogenous GR as a consequence of derepression of GR expression in response to AR inactivation. This notion was confirmed by knockdown of GR in LAPC4 which blocked enzalutamide-induction of *MPK1* expression (Figure 6.7). It therefore seems that the second of the two predicted models may provide a more valid description of the observed elevated GR signature in the LNCaP-AR$_{F876L}$ cell line.

To further strengthen our comparative observations, functional clustering was performed using the Database for Annotation, Visualization and Integrated Discovery (DAVID) on enzalutamide-induced core gene list. By applying Functional clustering using Kyoto Encyclopaedia of Genes and Genomes (KEGG) pathway analysis (Appendix 6E), genes induced by enzalutamide in LNCaP-AR_{F876L} were mostly associated with metabolic pathways, protein trafficking, pathways in cancer, steroid and protein biosynthesis, focal adhesion, fatty acid metabolism and cell division. Furthermore, cluster comment function type analysis of AR_{F876L} up-regulated genes (Appendix 6F) revealed only 4.9% of genes are kinase-related signalling molecules; with only one kinase, *SGK1* which is directly related to serum glucocorticoid regulation. More importantly, cells were not chronically treated with enzalutamide long-term, in fact no longer than 24 hours, prior to microarray analysis, hence generation of GR ligands by glucocorticoid synthesis-related enzymes and SGK1 would be an unlikely reason why GR-target genes are elevated in our LNCaP-AR_{F876L} derivative. Moreover, expression of GR is undetectable in the LNCaP parental and AR_{F876L}-expressing derivative, even upon enzalutamide treatment indicating that although ligands may be generated, no GR will be available to drive gene expression in our model.

The controversial roles of GR had been reported in several studies and no consensus had been drawn on whether GR acts as a driver or a facilitator for development of CRPC. By showing a substantial overlap in transcriptome, (Arora *et al.*, 2013) proposed that GR is able to take over AR function. As a consequence, stimulation of GR activity can rescue cells from enzalutamide-induced cell death. However, this is not in agreement with a later study by (Xie *et al.*, 2015), which proposes that GR function is not positively correlated with aggressive phenotypes of prostate tumours. They also suggest that GR signalling is unable to replace AR in driving tumour progression in all prostate cancers, even though two steroid receptors share the ability to upregulate overlapping transcriptional targets. This is of interest, particularly given that not all enzalutamide-resistant LNCaP xenografts are GR positive or have GR overexpressed. Due to the complexity of GR function in PC and heterogeneity of CRPC progression, selective growth of cell

subpopulations that have elevated expression of AR mutants (such AR_{F876L}) may be just one of many contributors for ultimate ADT resistance.

For these reasons, we here propose an interesting observation that both AR_{F876L} mutant activity and GR activation upon enzalutamide therapy are more likely driving a similar transcriptional gene-set which enables cellular survival and pro-proliferation rather than a genuinely distinct set of 'AR_{F876L} only 'or 'GR only' target genes. It will be of interest to explore whether just one or a small number of downstream targets are responsible for resistance and also whether enzalutamide-driven AR_{F876L} would activate transcription at the vast majority of the "GR unique" binding sites. We postulate that variables such as chromatin context, co-factors and other signalling events may be important.

Recently, several studies described the BET-subfamily of bromodomain proteins, including BRD4, as a promising epigenetic target for the blockade of oncogenic drivers in pre-clinical models of CRPC. JQ1, a newly developed selective small molecule inhibitor that is designed to interfere with the function of bromodomain 1 of the BET family by preventing interaction with acetylated-lysine residues; principally on target histones H3 and H4 (Filippakopoulos *et al.*, 2010). By competitively binding of the acetyl lysine recognition pocket of BRD4, JQ1 has demonstrated the down-regulation effects of AR-driven oncogenic effects *in vitro* and *in vivo* models of advanced prostate cancer (Lochrin *et al.*, 2014), although how efficacious it is against distinct mutational backgrounds of the AR remains ill-defined. Hence, JQ1 was applied in the LNCaP-AR_{F876L} model to test whether inhibiting the BET protein family is a potentially efficacious method for attenuating the function of AR_{F876L} in a model of enzalutamide resistance.

JQ1 inhibits BRD4-AR interaction in DHT-stimulated LNCaP cells and removes RNA polymerase II from AR-target genes leading to down-regulation of gene transcription and subsequent

diminished AR signalling (Asangani *et al.*, 2014). Similar to endogenous AR in LNCaP cells, analysis of AR$_{F876L}$ activity in response to varying concentrations of JQ1 showed down-regulation of DHT- and enzalutamide-induced expression of AR target genes *PSA, KLK2 and TMPRSS2* (Figure **6.11**). This corresponds with immunoblot analyses of PSA protein in LNCaP-AR$_{F876L}$ cells upon enzalutamide exposure which displays a dose-dependent decrease in PSA expression in response to JQ1 treatment (Figure **6.9**). Phenotypically, interfering with the function of BET family members using JQ-1 in androgen-responsive PC cell lines (VCaP, LNCaP, and CWR22Rv1) induced dose-dependent cell cycle arrest (Lochrin *et al.*, 2014). Consistent with these reports, in response to 48 hour treatment of JQ1, LNCaP-AR$_{F876L}$ cells exhibited anti-proliferative effects on enzalutamide-driven cell growth (Figure **6.10**).

Although the function of BRD4 has been widely implicated in the regulation of gene expression in various malignancies (Filippakopoulos *et al.*, 2010), BRD4 inhibition displays selective regulation of gene expression in prostate cells. Consistent with this, in LNCaP-AR$_{F876L}$ cells, enzalutamide activated AR target gene expression in response to JQ-1 was varied with *PSA* and *KLK2* being downregulated, while expression of *FKBP5* and *SGK1* were unchanged (Figure **6.11**), suggesting regulation at these latter loci may be BET family-independent. This finding may be due to the involvement of other protein factors or *cis*-regulatory elements targeted by AR, but not bound by BET family members. Critically, there are other bromodomain proteins expressed in CRPC, including the HAT protein p300, which has been suggested to play a part in aberrant AR-signalling in CRPC. Therefore, to extend and further explore applicability of our PC model, another bromodomain-targeting agent selective for p300 was applied to the LNCaP-AR$_{F876L}$ cell line to compare sensitivity to other PC cell lines. In addition to Compound G, a characterized HAT domain inhibitor of p300 was applied to the same cell line models to address if the enzalutamide-activated AR$_{F876L}$-driven cell line was sensitive to this other therapeutic agent.

By applying the two agents designed to individually target the bromodomain and HAT domain of p300, both Compound G and C646 down-regulated AR activity in LNCaP parental cells as indicated by reduced AR-target gene expression (Figure **6.14**). In LNCaP-AR$_{F876L}$ derivative cells, DHT- and enzalutamide-activated gene expression was reduced in response to both compounds (Figure **6.16**), including *FKBP5* and *SGK1*.

p300/CBP proteins are versatile transcriptional co-activators that can participate in gene regulation to control different physiological processes, including cell growth, proliferation and differentiation; all of which are important for cancer development. In fact, p300/CBP is an important cell cycle regulator (Moran, 1993) and is involved in controlling survival and invasion of prostate cancer cells (Santer *et al.*, 2011). The induction of apoptosis in our prostate cancer cells model was confirmed by the use of C646 in our cell line (Figure **6.17**). How effective these compounds and clinically-relevant derivatives will be in patients remains to be addressed, but our model has at least indicated that CRPC patients expressing AR$_{F876L}$ may be sensitive to agents within these drug classes.

Interestingly, in our early stages of validating the role of AR$_{F876L}$ as a GR mimic, we noticed that the GR antagonist, mifepristone, possesses agonistic properties for AR stimulation. Compared to DMSO, 24 hours mifepristone treatment significantly induced AR-regulated gene expression (Figure **6.8**). This is consistent with observations reported previously (Song *et al.*, 2004) that mifepristone has a high binding affinity for AR and can function as an AR agonist. Mifepristone has also been shown to facilitate recruitment of p300 to *cis*-regulation of AR-target genes (Kang *et al.*, 2004). Consistent with this, in our stable LNCaP-AR$_{F876L}$ cell line, we demonstrated that enzalutamide can drive AR$_{F876L}$ and p300/CBP co-enriching at GR/AR regulatory elements (Figure **6.13**). Mifepristone is currently used for CRPC patients in combination with ATD in a Phase II clinical trial (Phase II, NCT01867710, https://clinicaltrials.gov/). The mechanism of this antagonist in the background of AR$_{F876L}$-driven enzalutamide-resistance, however, has not been established. Thus, it is vital to have clinically-relevant model depicting the mechanism of mifepristone combined with enzalutamide in the background of CRPC expressing the F876L mutant. We here

for the first time shown that mifepristone can drive AR_{F876L} transcriptional activity and co-recruitment with p300 to cis-regulatory elements in AR-target genes. Importantly, the inhibitor of the p300 bromodomain can attenuate the co-association of both factors from binding regions (Figure 6.13).

Chapter 7: Summary of key points and final conclusions

In the clinic, the majority of patients that will receive next-generation anti-androgens are those with advanced PC. The development of these agents has been a positive step to towards improving patient healthcare, but their effectiveness is limited to approximately 50% of individuals and resistance to these agents remains a major issue. Critically, given that specific AR mutations are selected for during the first round of anti-androgen therapy, such as bicalutamide, it is of major clinical relevance to determine whether next-generation anti-androgens, such as enzalutamide, have efficacy in the background of pre-existing AR mutations.

We are keen to implement next-generation precise genome editing using the CRISPR/Cas9 method to to generate a PC model that endogenously expressed the clinically-relevant enzalutamide-activated AR_{F876L} mutant which is urgently required for improving our understanding of the function of this aberrant receptor and to provide better models for drug development purposes. Hence, in Chapter 4, we firstly designed and verified sgRNA/Cas9 'on-target activity' of a specific CRISPR reagent at *AR* exon 8 in the LNCaP and CWR22Rv1 PC cell lines. Importantly, we optimized a systemic high throughput screening approach to enable detection of 'knock-in' mutants that did provide some evidence of precise editing in pooled cell populations, but these were never clonally expanded due to technical difficulties. Clearly, compared to the considerable ease of applying Cas9 for gene knock-out studies, relatively little is known about how to design a gRNA to make the desired precise gene-editing event more efficient. Multiple factors determine the success of any given CRISPR experiment, including the quantity of Cas9 proteins and guide RNA, chromatin accessibility of the targeting *loci*, and cellular response to CRISPR-induced DNA lesions. Most of these issues are beyond experimental controls. Of note, most of those factors remains little known when our project started. Although some of the developments enabling more efficient knock-in editing while project were progressing, such as using a double cut HDR donor (Zhang *et al.*, 2017a), phosphorothioate linkages at oligo ends (Prykhozhij *et al.*, 2018), additional studies with will be required to better understand locus-

dependent differences in the efficiencies of HDR and Indel mutation induction in our experiment setting.

With low level of CRISPR delivery efficiency and HDR frequency in both cell lines, it is likely that a larger number of colonies will need to be screened in order to create a clonal AR_{F876L}–expressing cell line derivative. Given the time-schedule for this was outside of the parameters of the studentship, particularly with respect to fully validating the cell line once generated, an alternative strategy was utilised to generate a lesser, but still reasonably-physiological model system in the background of LNCaP cells that would also permit the interrogation of AR_{F876L} function. To determine the impact of first- and second-generation antiandrogens enzalutamide on AR mutant transcriptional activity, we firstly employed a Luciferase reporter-based assay in AR negative PC3 cells to assess the anti-androgens ability to inhibit the ligand-induced transactivity of AR_{F876L}, which is essential for the receptor function. Initially, we found that neither bicalutamide nor enzalutamide induced the AR-wildtype transactivity when administered alone and both inhibited the DHT-induced AR activity. Importantly, enzalutamide exhibited agonist-like properties on AR_{F876L} when administered alone. In addition, we have demonstrated that bicalutamide effectively blocked AR_{F876L} transcriptional activity, suggesting the applicability and potential use in patients harbouring this mutation.

Given the previous finding, we next developed an AR rescue/replacement LNCaP PC model that allows the stable expression of a lentiviral delivered FLAG-tagged AR mutant, whilst concurrently depleting endogenous AR using a custom 3'UTR targeting siRNA. We confirmed that the 3'UTR targeted siRNA did not affect the expression of integrated AR_{F876L}. Furthermore, we demonstrated that in response to enzalutamide, AR_{F876L} was recruited to the promoters of AR-target genes and initiated active transcription, which resulted in increased cell proliferation. Overall, in Chapter 5, it was demonstrated that the cell line was a suitable model for defining the function of AR F876L and the resultant phenotype of the cells in response to enzalutamide.

To explore the effect of AR_{F876L} further, a microarray was performed in Chapter 6 to investigate the enzalutamide-induced transcriptional program. Overall, it was determined that the enzalutamide/ AR_{F876L} program was similar to that of the endogenous AR-induced program, although a select number of previously identified androgen-regulated genes were expressed at high levels in response to enzalutamide, including: *TIPARP, FKBP5, NDRG1* and *EAF2*. Expression analysis of these genes across a panel of reported PC models identified a high overlap between the AR_{F876L} gene-set and the GR-regulated gene-set identified from enzalutamide-resistant xenografts. Whilst it is understood that further target validation is required, given the initial remarkable parity between our generated LNCaP model and the patient derived xenograft, our work has shown that the AR_{F876L} mutant drives a distinct transcriptional programme to the endogenous AR in LNCaP cells and may mimic GR activity. In addition, based on the findings presented here, screening of patients CTCs for AR mutation may help to provide relevant data elevating the issue of dosing patients with mifepristone.

Simply replacing a single direct AR-targeted inhibitor with another may provide temporary benefit for CRPC patients. It is, however, inevitable that resistance will ensue via reactivation of AR function in most cases; AR mutation(s) being a likely candidate for anti-AR drug resistance. Importantly, consistent with other mechanisms related to anti-androgen resistance, development of enzalutamide resistance seems to be very heterogeneous. Hence, identification of novel targets will likely lead to therapies which are not solely limited to AR inhibition. To that end, in chapter 6, we focused on targeting co-regulators of AR, and here provides evidence for considering BET-protein family inhibition as a rational therapeutic approach inactivating AR_{F876L}-mediated transcriptional signalling in enzalutamide-resistant disease.

In summary, our well-defined LNCaP_AR_{F876L} cell line model has provided a comprehensive transcriptomics data-set to provide an insight into how an enzalutamide-activated AR mutant can drive a distinct gene-set in advanced prostate cancer. Certainly, employing ChIP-seq in the LNCaP-

AR$_{F876L}$ cell line would help increase the understanding of the ectopic AR in this model. Moreover, by more thoroughly investigating AR mutant regulated-transcriptomic alterations, we may potentially identify AR$_{F876L}$-specific biomarkers and additional targets for therapy that are driven by this AR isoform.

Chapter 8: Appendix

8.1 Appendix 4A

A

B

C

pEXPR (*sal* 946, 3331bp)
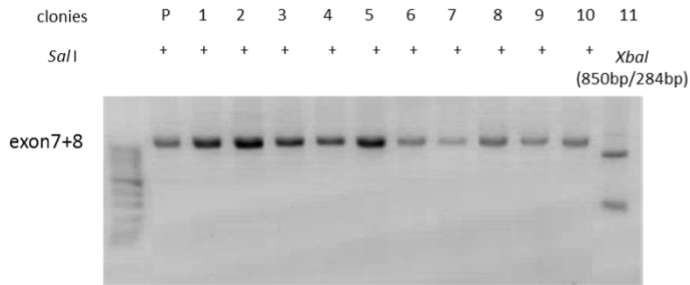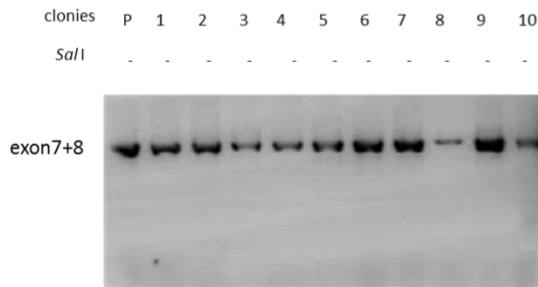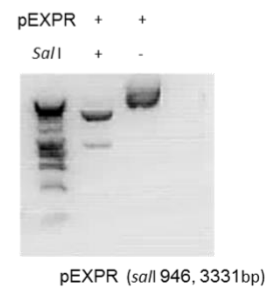
Appendix 4A- RFLP analysis HDR-mediated designed ssODN insertion within desired regions. RFLP results from selected 10 clones derived from 22Rv1 cell following co-delivery Cas9/sgRNA196. Primers used to amplify the genomic DNA were indicated in 4.2.2. (A) Lane 1: marker; P-parental cell line (non-editing cell line), lane 2–10: PCR amplicon digestion with Sall. Lane11: parental cell line digested with Xbal using as positive control for PCR amplification. (B) Indigestion PCR amplicon for parental cells and all selected cell colonies. (C) Positive control for Sall enzyme. Appendix data. Donor oligo sequence.

8.2 Appendix 4B

A
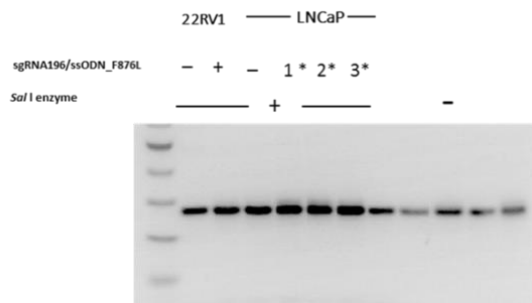
B
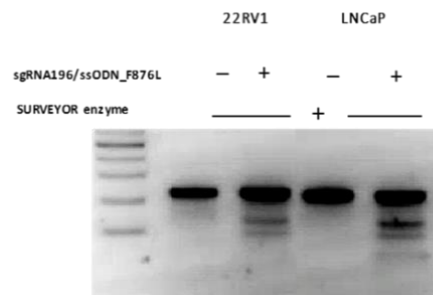
Appendix 4B- (A) the subsequent Surveyor assay failed to detect any heteroduplexes in 22Rv1 and LNCaP upon delivery sgRNA196 and repair templates. (B) The successful detection of Cas9-medicated DSB at AR exon 8 upon co-delivery Cas9/sgRNA196 and repair template prior subject for Sanger sequencing.

8.3 Appendix 4C

1.AR ex8 wt (5' to 3'):

> ggctagcagaggccacctccttgtcaaccctgtttttctccctcttattgttccctacagattgcgagagagctg**Cat**cagttc**Act**tttgacctgctaatcaagtcacacatggtgagcg**tCg**actttccggaaatgatggcagagatcatctctgtgcaagtgcccaagatcctttctgggaaagtcaagcccatcta

2.AR ex8 F876L:

> ggctagcagaggccacctccttgtcaaccctgtttttctccctcttattgttccctacagattgcgagagagctg**C**atcag**CtcAct**ttttgacctgctaatcaagtcacacatggtgagcg**tCg**actttccggaaatgatggcagagatcatctctgtgcaagtgcccaagatcctttctgggaaagtcaagcccatcta

8.4 Appendix 5A
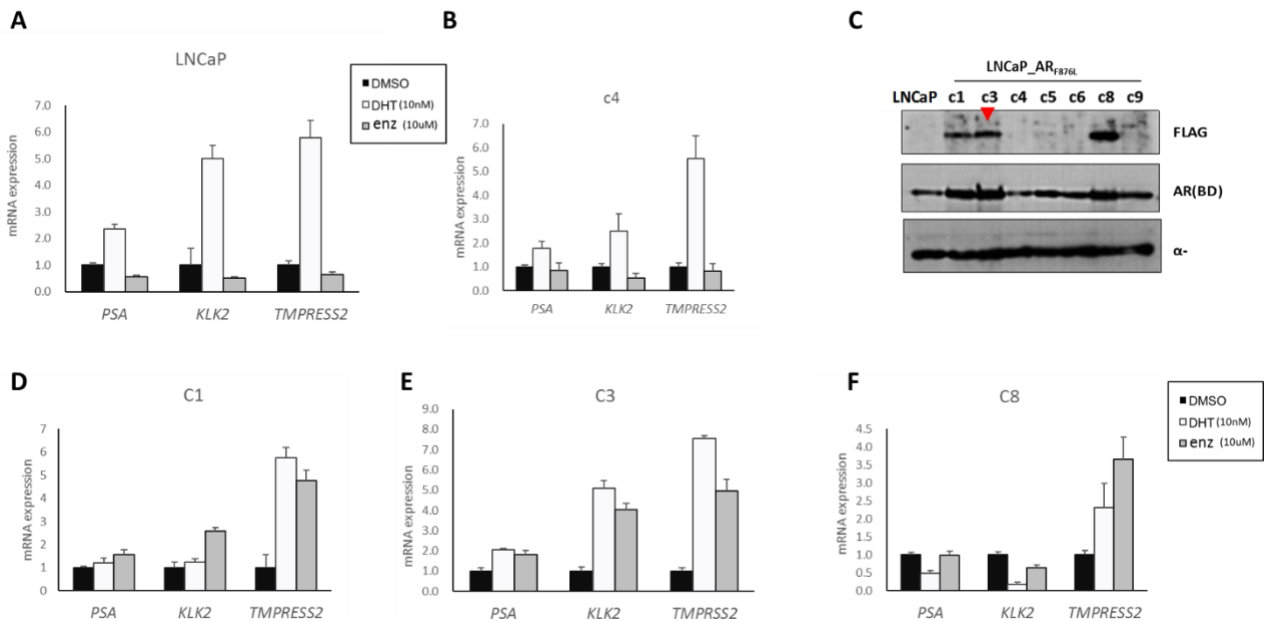
Appendix 5A - The gene expression of AR targets in LNCaP parental cells (A) and selected colonies (B,D,E and F). (C) FLAG_tag expression in LNCaP and all initially selected viral transduced colonies. Clone 3 (c3) were closed for all rest study in this report.

8.5 Appendix 5B

A
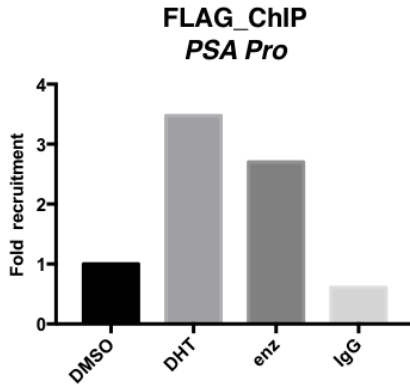
B
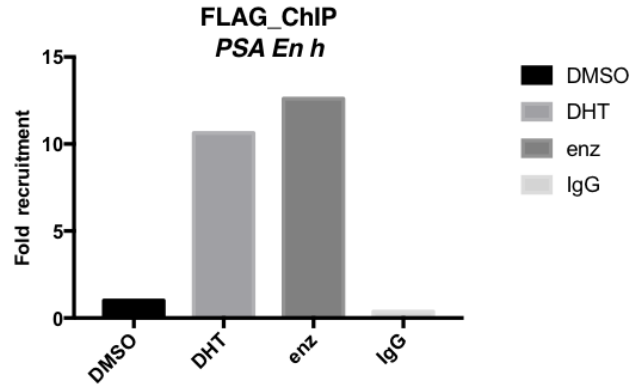
Appendix 5B – Chromatin loading of AR$_{F876L}$ at enhancer (A) and promoter (B) region of *PSA cis-regulatory* regions upon DHT and enzalutamide treatment.

8.6 Appendix 6A

SYMBOL	fold change (≥ 1.5folds)
RASD1	32.46582806
ORM1	31.65248495
TIPARP	25.59354801
SPRYD5	20.65925549
FKBP5	20.10147541
ORM2	17.03976723
LOC399939	13.86534555
SLC2A3	13.38139968
NDRG1	12.28636673
LOC729384	11.30273904
SLC16A6	10.82408116
TRIM48	10.49241718
SLC45A3	9.880929334
NCAPD3	9.385527129
RHOU	9.374939536
LOC340970	9.10688876
LOC100134006	9.096026021
FAM105A	8.983921488

ACSL3	8.908421843
EAF2	7.681759891
TMPRSS2	7.44336537
ERRFI1	7.217316686
TARP	6.984953005
SGK	6.972653696
WIPI1	6.962302447
LPAR3	6.893218905
UGT2B28	6.730692167
PAK1IP1	6.613388834
KLK3	6.099503364
VPS33B	5.955763303
CENPN	5.947516105
HPGD	5.936439549
NKX3-1	5.587800399
ANKRD37	5.528673935
SGK1	5.505949329
TUBA3D	5.059784869
SRD5A1	4.983396745
TSKU	4.886237079
EDG7	4.823899124
LOC440040	4.767708218
FADS1	4.731175911
LOC729768	4.725744329
LRIG1	4.649793033
RDH10	4.508463937
ELL2	4.463940043
DNAJB9	4.399720477
ANKRD22	4.309204184
LOC100131392	4.223836585
RHOB	4.213336184
F2RL1	4.211141187
SIPA1L2	4.192121174
FOXD4	4.108924893
SORD	4.050709572
ELOVL5	4.033916579
SMS	3.98329017
LOC642590	3.969213448
AMACR	3.867712519
RALY	3.863060745
HMOX1	3.862319555
VCL	3.840420439
PYGB	3.826745543

STK39	3.782399211
LOC646347	3.764439984
STEAP4	3.718466125
ACAD8	3.686247301
PDLIM1	3.671298689
ALDH1A3	3.594320959
DBI	3.525431262
TBC1D8	3.516385962
PHACTR2	3.5066654
PTPRM	3.50325931
FRAG1	3.501796213
LIMS1	3.440357419
CAP2	3.404908107
KCTD3	3.398465006
ERN1	3.395797715
LGMN	3.386133462
UGT2B11	3.351075752
KLK4	3.284496196
SHRM	3.277356388
SCAP	3.260152064
ST3GAL4	3.247992893
PACSIN2	3.196350167
HIPK2	3.190454522
FOXD4L1	3.184907688
MYL12A	3.182856348
TPM1	3.164654049
LOC642362	3.155550679
PMEPA1	3.146617665
CNN2	3.142556971
TSC22D1	3.137491887
FKSG30	3.133345354
THYN1	3.106696823
PIAS1	3.096587627
TUBA3E	3.088542112
TRIM53	3.084855509
SLC35F2	3.060698575
HIF1A	3.060081611
ZNF812	3.045436356
KRT8	3.040270899
HOMER2	3.038311293
MYADM	2.966163837
ATAD2	2.963673145
MTMR9	2.958865361

GLUD1	2.943545165
NSDHL	2.940164372
NFIB	2.937618509
LIFR	2.932838635
CBWD5	2.925040559
MOCOS	2.921729127
H2AFZ	2.910795265
LOC647954	2.898392741
C1orf116	2.886012837
LOC644743	2.852031693
KIAA0194	2.83507588
KCNMA1	2.832942493
SLC41A1	2.827354599
PGM3	2.825839889
NAMPT	2.810599778
ABHD2	2.795477366
LOC440459	2.777761391
SERP1	2.769681073
POTEF	2.758219279
CBWD3	2.751112122
GFM1	2.73877868
KLF6	2.733690491
LAMC1	2.725328194
ZNF189	2.722072029
TNFRSF10B	2.717939597
LOC402221	2.702347777
CREB3L2	2.699229607
GADD45G	2.685094198
LOC653111	2.658926379
PARVA	2.651284924
HMGCS1	2.649659721
UGDH	2.645803126
NAT1	2.644594813
ANG	2.638283615
KRT19	2.6283823
VIL2	2.616765401
BBX	2.607356779
LOC728969	2.605812658
FASN	2.599757089
LRRFIP2	2.587589528
PRAGMIN	2.581434548
HK2	2.577106952
CCDC15	2.569746418

SC4MOL	2.559341356
LOC646567	2.547481705
SSR1	2.53727477
LOC647349	2.535491691
NPPC	2.519697685
LRRC16	2.496981275
MAP7D1	2.489500299
ZBTB16	2.488926793
IDI1	2.487718815
FADS2	2.478673091
C17orf79	2.475135214
NFKBIA	2.473432776
EDEM1	2.471113211
LDLR	2.462980576
ACTB	2.462160188
AZGP1	2.452833383
HERPUD1	2.446288161
MCCC2	2.434240278
MERTK	2.429433064
NAGK	2.42906471
SELS	2.426632446
DHCR7	2.424469326
ENDOD1	2.413780913
ZDHHC9	2.397573962
PRC1	2.396918242
WWC1	2.395785063
SNAI2	2.393726355
C1orf149	2.389370615
RAB4A	2.384175367
LOC100129882	2.383720194
EZR	2.375416022
BCL6	2.375047452
PGC	2.345985212
COL6A1	2.333083099
SRP19	2.330254897
LOC646723	2.328153725
LOC493869	2.325143903
FAM105B	2.324747111
MPHOSPH9	2.320839267
ABCC4	2.319165832
C1orf122	2.318250788
UCK2	2.316726538
AGR2	2.316017525

KDELR2	2.31374666
LOC653381	2.300296829
RPRC1	2.292216013
PWP1	2.289978299
YTHDF1	2.289022625
PDIA5	2.277916326
CRISPLD2	2.277819733
AP3S1	2.270819614
LOC113386	2.270237948
MRFAP1	2.266724877
MLPH	2.263374898
PPP2CB	2.258021588
LOC654244	2.255940772
CAPZB	2.25501421
ANXA2	2.252064241
GMPPA	2.24937978
ARMET	2.245590027
GPT2	2.241922264
ATP1A1	2.239320929
GADD45B	2.238913666
MPZL1	2.237002043
SEC11C	2.23650265
GARS	2.233264817
LCOR	2.232379181
KRT18P13	2.223474353
GBE1	2.220273376
FNDC3B	2.219833092
MAFB	2.218027905
MFSD6	2.217549273
C2orf30	2.217269796
LOC728877	2.215770224
PRDX6	2.203510986
C12orf44	2.201428886
LPIN1	2.191742494
CPEB4	2.183868374
HIST1H4H	2.173751814
SLC38A2	2.172315556
CBLL1	2.167006146
TMED9	2.16403229
ATF3	2.154943341
HBEGF	2.144639177
SHROOM3	2.141437032
CEBPD	2.138652089

CDR2	2.135769054
GTF3C6	2.134688606
OSTC	2.134573361
UBE2G1	2.133032672
PEX10	2.131248453
PECI	2.126402285
CYR61	2.125761003
GFPT1	2.125489348
IMPDH1	2.124971069
RGPD8	2.124694565
SEC24D	2.116674573
AXUD1	2.115678381
LONRF1	2.113700547
LOC93622	2.113490465
UCHL3	2.111974321
LOC644563	2.106435322
CLPTM1L	2.102722768
PNMA1	2.102087265
C9orf119	2.101977837
TXNDC17	2.094314639
MAP7	2.092166145
DHCR24	2.092156247
KLHL36	2.086965685
C19orf10	2.078191767
FOXO3	2.077987398
FLJ40504	2.063774215
TMEM87A	2.06294443
CUL4B	2.061298262
LONP2	2.059472874
RER1	2.059208853
PRKAB2	2.058514338
AKAP13	2.057913607
STT3A	2.057697273
LOC401074	2.05013027
ACSL1	2.049681932
F5	2.048284245
C19orf48	2.048023204
LOC149501	2.047177726
CLDN12	2.046184358
VPS37B	2.039366383
HIBCH	2.037141009
AHNAK	2.032773459
SURF4	2.032674602

UAP1	2.03018191
ITPR3	2.027270159
GUCY1A3	2.027115186
NANS	2.026225135
CITED2	2.024619742
FRAP1	2.024273503
KLF15	2.021629996
SEC23B	2.019249598
PACS1	2.017537057
PTRH2	2.017431843
PSMA6	2.015545159
TUFT1	2.013911581
VLDLR	2.012818997
LOC643431	2.01144139
LIN7B	2.011227865
NEDD4L	2.010775392
TMED7	2.010098485
FBXO31	2.009444435
WDR1	2.002637359
UOX	2.002078449
EGLN2	2.001417872
MALT1	1.996578616
MEAF6	1.995188154
ITGAV	1.995143635
KRT73	1.994452798
FICD	1.994303247
ZFP36	1.994174443
SLC1A5	1.993989837
C2orf76	1.992724862
TSPAN13	1.988576411
ABCD3	1.987898446
SASH1	1.986529952
C16orf61	1.986144148
LRRC8A	1.985833192
PSMD8	1.98183067
TARS	1.980271423
GMPPB	1.980227601
CLIC4	1.978663068
SLC38A1	1.977550646
GDPD5	1.976578329
STAU2	1.97446557
LOC100130308	1.971868198
SAT1	1.96982955

CALU	1.967480183
BRP44	1.965840056
ZNF259	1.965638428
LOC100129781	1.962124822
TCEAL3	1.961302834
EVL	1.960045559
ODC1	1.959320993
PNLIP	1.95786479
ZNF350	1.955910648
CRELD2	1.955676421
ZNF613	1.953920497
BNIP3	1.952429917
TNFRSF12A	1.949645566
EFNA1	1.94945211
C17orf48	1.948420243
C3orf58	1.947821281
MIPEP	1.946838936
SPCS3	1.946826592
EEF2K	1.945355418
CMAS	1.943654946
TRIB3	1.941624474
INSIG1	1.939747764
H1F0	1.939666031
MED31	1.939292705
MGC18216	1.938386122
ZFHX3	1.936312733
ADM2	1.936306876
HERC3	1.933047784
B4GALT1	1.932575764
NDFIP2	1.932050538
TMED5	1.926640238
SLC33A1	1.925967957
KIF22	1.923782033
SRPRB	1.920763647
MTP18	1.9200851
TXNDC11	1.918727961
KCNG1	1.917912852
TNFAIP8	1.917236341
SPDEF	1.917216021
SNX25	1.910905603
THOC5	1.908845615
SHC1	1.906267323
TUBA3C	1.904317611

NUDT18	1.904285966
SCNN1G	1.901936023
C5orf13	1.898286003
RBM24	1.895587096
ZNF419	1.893210049
SLC29A2	1.888803155
MPHOSPH10	1.88420219
ACADM	1.883365714
SSR2	1.875810377
RAB32	1.873272813
DAPK3	1.872048515
SEC61B	1.869508162
STARD3NL	1.869488741
MINPP1	1.867694694
C12orf65	1.863441701
FKBP11	1.860155172
S100P	1.85826271
TBX15	1.854798983
DNM2	1.853059692
NDEL1	1.852933994
LOC648682	1.850174384
STAMBPL1	1.847746345
ALDH3A2	1.845468816
KRT8P9	1.84180985
HMGCR	1.840503978
CDC25A	1.838125138
PQLC1	1.833604787
C1orf21	1.83300722
ITGB1	1.832863837
TMEM49	1.83178751
CYTSA	1.830262493
GSTT2	1.828247686
DNAJC10	1.827231485
SPINK5L3	1.827204611
C9orf152	1.826754859
CA12	1.82518767
WDR41	1.824150069
ARRDC1	1.820228892
PDLIM5	1.819930368
PPP1CB	1.819579925
C9orf91	1.818783343
CHKA	1.818236657
SC5DL	1.81796958

GRPEL2	1.817939624
SSR3	1.817749482
DYNLL2	1.817301754
MICAL1	1.814785778
DNASE2B	1.81328698
PCTP	1.811752531
ATOH8	1.811527603
SND1	1.811363346
MCFD2	1.808806404
ELOVL1	1.807137831
CROT	1.806421965
PPFIBP2	1.804856662
FBXW2	1.804034067
B2M	1.801820063
FAM103A1	1.800593916
ACAT2	1.800539097
MORF4L2	1.800394318
WDYHV1	1.799659362
GALNTL4	1.798674738
GOT1	1.797768825
SLC6A3	1.79715782
ARF4	1.79272829
GNMT	1.791935906
RRBP1	1.791540703
ZC3H12A	1.791360065
CEBPG	1.790910785
GOT2	1.789644048
AMY1C	1.78881432
LOC652864	1.787719505
SOCS2	1.783642948
RBM45	1.781839916
CHAC1	1.780514704
CAMSAP1L1	1.779136516
RBM47	1.778855147
LYPLAL1	1.777539759
GHR	1.77750969
C17orf58	1.775565626
CBX4	1.772016782
RHBDF1	1.769723229
SLC2A1	1.762661335
FLJ20254	1.760912622
DEFB32	1.760371239
ZCCHC9	1.76032898

189

RNASE4	1.760217731
MORC4	1.758047982
CCDC53	1.757877617
PTGER4	1.753047878
PPAPDC1B	1.752889895
LOC642282	1.745974336
GSTT2B	1.745591717
TMEM2	1.745433203
P704P	1.745374105
MGAT1	1.745039611
MAP1LC3B	1.745005969
IMPA2	1.744267344
FAM129B	1.74415981
LOC641825	1.743536329
NSUN2	1.743152214
LOX	1.742734775
LOC653566	1.74068496
FERMT2	1.737133381
MAP2K1IP1	1.736874478
KIAA1191	1.733863893
USO1	1.733063958
LOC652481	1.732868441
ENTPD6	1.73129225
LOC650518	1.731003563
HADH	1.730117378
GOLGA5	1.729105387
SH3GLB1	1.72835671
UBE2E1	1.727734696
RIT1	1.723576572
RPN1	1.719510638
ASIP	1.718949524
C7orf68	1.717541775
SLC25A13	1.716542132
SLC7A1	1.716219743
LOC151579	1.716201468
IFRD1	1.714768402
FDFT1	1.714418052
TACC2	1.714281842
EML1	1.713849427
RRAS	1.713305419
ZYX	1.712680231
RALBP1	1.712064976
PPAPDC2	1.711774474

TRAPPC2P1	1.711607243
DNM1L	1.709437061
CAP1	1.709013405
PASK	1.707112358
ARCN1	1.707086205
CSK	1.705875083
PDXDC1	1.704406795
TSC22D3	1.704138229
LOC641785	1.702549473
PFKFB4	1.70115465
GALK2	1.699664029
RNF14	1.698860411
SYVN1	1.698692976
C15orf23	1.698202466
DUSP14	1.697525625
CTBS	1.696306591
LOC644936	1.696252323
NRAS	1.695686655
CDK2AP2	1.694717506
DERL2	1.69446009
P4HA1	1.692654054
SEC13	1.691064627
PDIA6	1.6874959
ITPRIP	1.684278069
CKAP2	1.68363619
FAM107B	1.682128525
MED8	1.680310352
ANXA5	1.679094155
CEBPB	1.678703091
ELF1	1.677543961
TIMM23	1.677347139
EPDR1	1.675502562
TMED10	1.675152366
CLDN7	1.6717393
KIAA2010	1.670196366
CYP2U1	1.668438996
C4orf34	1.66813073
EPHX2	1.66810156
DDIT3	1.666646198
RHOG	1.665390052
GCAT	1.665030841
LOC399965	1.664463011
TSPYL2	1.663112455

LOC344595	1.661003988
DKFZp761P0423	1.660679588
FBXO38	1.660254307
NT5DC3	1.660138353
FLJ43663	1.659609039
ZNF518B	1.658681766
SPSB1	1.657164332
TMEM214	1.656350093
COPB1	1.656289555
M160	1.654035255
SAR1B	1.652821941
LRRC16A	1.652652245
ANKFY1	1.650094396
AK3L1	1.649947211
CCDC6	1.649760978
KRT10	1.649270913
SH3TC1	1.648932291
RAB11FIP1	1.647926802
PEA15	1.647803514
GPR89C	1.647774224
PMM2	1.647553243
SQLE	1.646826768
NAPA	1.646027099
EFNA5	1.645151328
JUN	1.643178555
STK40	1.642871051
ATP6V1G1	1.642636484
LSS	1.641935513
ERO1L	1.637729899
TMED2	1.637449771
ALDH6A1	1.636193685
EBP	1.635518744
FAM18B	1.634086698
OCRL	1.633231979
PRSS27	1.632473059
SEPP1	1.632154086
MGAT2	1.631030873
SLC30A7	1.630890803
SF3B5	1.630760194
EDEM2	1.630669878
PPA1	1.626648901
HEG1	1.62653223
COPG	1.625853671

TCEB1	1.625230196
LOC730820	1.624635878
TBC1D16	1.624447529
FAM174B	1.622968741
PXMP3	1.622881252
FBXO8	1.621077946
GNG5	1.619707447
PIK3C2A	1.618344839
DISP1	1.617945546
DNAJB14	1.617046866
SLC35F5	1.616170794
PDE9A	1.615053761
SLC5A6	1.614689245
UBFD1	1.614458221
PAWR	1.614337077
LDHA	1.611843578
PPP1R13B	1.611374352
RAB5A	1.611314744
C6orf81	1.610162733
PAPSS1	1.609386522
WDFY2	1.608674247
LOC643031	1.607580066
WDR13	1.606466103
ZFAND3	1.605295356
C6orf85	1.604560521
ABCC1	1.603872768
RAB2A	1.603433961
NRIP1	1.603273478
KLK2	1.603228123
LOC100132418	1.601875501
SLC10A7	1.601823364
CTNNAL1	1.601797919
TRPM4	1.599758006
ARID5B	1.599544108
PACSIN1	1.599027883
PICALM	1.598961989
NBPF20	1.598829417
NOSTRIN	1.598431404
COPS3	1.597763177
IFNGR1	1.597664221
ATP6V0E1	1.595372012
USP10	1.593116428
SLC30A5	1.592197961

ABHD3	1.592068237
BCL7C	1.589118772
SLC10A3	1.589015553
CLGN	1.587773932
RHOBTB2	1.586121854
BMPR1A	1.585242799
MTHFD2	1.584793603
SELK	1.584395762
SEC24C	1.584125134
PTPN21	1.583989127
SEC16A	1.583124385
PRDX4	1.582175492
PRRC1	1.580955208
LOC100130886	1.579374115
NUDT9	1.578761622
EHF	1.578555204
LOC649260	1.578474227
NBPF10	1.57843718
FZD5	1.577607093
TRIM24	1.577101273
TMEM41B	1.574451181
TMEFF2	1.574415085
CHPT1	1.573571396
DNAL1	1.572387866
ELOF1	1.57161304
LOC399748	1.569253232
LPP	1.568606018
ERGIC2	1.56767875
SPCS2	1.567606167
ZDHHC6	1.567294922
YARS	1.566481739
BIRC2	1.56613927
ARL1	1.565580191
HK1	1.565222408
SBDSP	1.564288048
PREB	1.56404063
IQUB	1.563310881
MIR635	1.561752828
BET1	1.561586532
ZBTB10	1.561318763
PRKCA	1.560915989
PDHX	1.560567837
UFM1	1.559763902

FAM69A	1.559141841
LOC652773	1.558823242
FGFRL1	1.558390342
LOC728037	1.5577326
FAM119B	1.554433688
CHFR	1.553518295
STC2	1.553380573
PDIA4	1.552778312
GPR89A	1.552396241
LOC100128163	1.549165449
LOC730432	1.548603905
GK5	1.547987288
TUBB2A	1.547041775
ANAPC13	1.5459588
FAM104A	1.544880601
ZFAND2A	1.543453039
RRAS2	1.542078519
CBWD7	1.541368374
RASSF1	1.540939862
LOC145853	1.540644126
VPS26B	1.540527493
COMMD1	1.538524443
GDF15	1.538052962
PTPLB	1.537970875
P4HB	1.537563908
SDF2L1	1.537041606
MARS	1.535462522
SLC20A1	1.535440619
EXOSC3	1.535333927
C7orf54	1.534877331
BAG3	1.533405685
GOLGA2	1.531500077
GBF1	1.531106428
TMEM8	1.530708829
KLF9	1.530696607
MRPS23	1.53020676
INTS6	1.529586994
DUSP1	1.529084383
ORMDL1	1.529054747
ACBD3	1.529008587
GLB1L2	1.528438466
SEC61G	1.527930007
POP1	1.526942959

195

DIAPH1	1.526939965
MON2	1.526785008
NCKAP1	1.526624096
COPB2	1.523830595
C17orf91	1.523817858
DIS3L2	1.522464454
FGD4	1.52242998
ADAM9	1.522163507
TMEM14C	1.521658008
LOC730167	1.52092052
MYH9	1.520508508
CHN2	1.519163426
ACAA1	1.519109858
SLC31A2	1.518781327
STX5	1.518386245
SLC35A2	1.517892321
ATF4	1.517788136
FLJ31568	1.516933936
IMPAD1	1.51511742
IGF2R	1.51502983
USP38	1.51455947
SEC31A	1.514052344
TAX1BP3	1.513716385
MYCBP2	1.513581963
KCTD9	1.512432401
NBL1	1.510922402
OSBPL5	1.510737336
MSX1	1.509650815
PLOD1	1.509484916
AFF4	1.509232759
XPNPEP1	1.509187996
MBOAT2	1.508600708
TRIM5	1.508364126
GADD45A	1.50754233
WBP5	1.506682955
RAB3B	1.506417088
SSX2IP	1.50616148
LOC644935	1.506084664
HSP90B1	1.505929466
C20orf24	1.505409903
NPC1	1.503981294
WNT7B	1.503969785
GPR89B	1.503488974

C13orf1	1.501725579	
SRP54	1.500995482	
LOC731486	1.500101981	

Appendix 6A - The core list of 615 genes () found to upregulated following treatment with 10uM enzalutamide for 24 hours in LNCaP AR$_{F876L}$ cells.

8.7 Appendix 6B

	siT877A+enz (fold changes)	siF876L+enz (fold changes)
ALDH1A3	3.594320959	2.376500018
C1orf116	2.886012837	2.150905059
FAM174B	1.622968741	1.56364679
HOMER2	3.038311293	2.649381728
KLK3	6.099503364	3.834462507
ABCC4	2.319165832	2.381164319
C19orf48	2.048023204	2.028027081
CENPN	5.947516105	5.121067906
CROT	1.806421965	1.480716744
EAF2	7.681759891	3.029340986
KLK2	1.603228123	1.651087138
PASK	1.707112358	1.61097063
TMEFF2	1.574415085	1.527812302
TMPRSS2	7.44336537	3.282562937
TUBA3D	5.059784869	2.652713618
NKX3-1	5.587800399	3.692878564
PDIA5	2.277916326	1.666417604
PMEPA1	3.146617665	3.907311686
SLC45A3	9.880929334	6.903293974
TUBB2A	1.547041775	0.947094024
CLGN	1.587773932	1.315333876
DHCR24	2.092156247	1.725000581
ELOVL5	4.033916579	4.394735082
KLK4	3.284496196	2.285950381
MCCC2	2.434240278	1.944002581
ZBTB16	2.488926793	1.751295224

Appendix 6B- a gene list of overlap between the enzalutamide-activated AR$_{F876L}$ expression signatures lists and DHT-activated LNCaP-LacZ. And the comparison of enzalutamide-induced gene fold changes of siT877A and siF876L arm.

8.8 Appendix 6C

GR signature probe sets (Dex 1.6 fold FDR<.05)	match to enz-F876L(1.5 fold FDR<.05)	no match to DHT-laz_ARwt (1.5 fold FDR<.05)	siT877A+enz (fold changes)	siF876L+enz (fold changes)
ABCC4				
ABHD2		No match	2.795477366	1.612163415
ACTA2	No match	No match		
ALDH1A3			3.594320959	2.376500018
ATAD2			2.963673145	2.175572197
AZGP1			2.452833383	1.97820866
BAMBI	No match	No match		
BCL6		No match	2.375047452	1.643139556
BRDT	No match	No match		
C11ORF92	No match	No match		
C17ORF48			1.948420243	1.269424632
C19ORF48			2.048023204	2.028027081
C1ORF116			2.886012837	2.150905059
C1ORF149		No match	2.389370615	1.71292531
C6ORF85		No match	1.604560521	1.090379649
C7ORF63	No match	No match		
C9ORF152			1.826754859	2.156986874
CEBPD		No match	2.138652089	1.493144838
CGNL1	No match	No match		
CHKA		No match	1.818236657	1.404357595
CRY2	No match	No match		
DBC1	No match	No match		
DDIT4	No match	No match		
EDG7				

Gene				
EEF2K		No match	1.945355418	1.344368441
ELL2				
EMP1	No match	No match		
ERRFI1			7.217316686	3.254157864
F2RL1		No match	4.211141187	3.079385851
FAM105A			8.983921488	6.036153385
FAM49A	No match	No match		
FKBP5			20.10147541	11.39907853
FLJ22795	No match	No match		
FOXO3		No match	2.077987398	1.343095774
GADD45B		No match	2.238913666	1.019830169
GHR		No match	1.77750969	0.960160949
HERC5	No match			
HMOX2	No match			
HOMER2			3.038311293	2.649381728
HS.99472	No match	No match		
HSD11B2	No match	No match		
IL6R	No match	No match		
KBTBD11	No match	No match		
KIAA0040	No match	No match		
KIAA1370	No match	No match		
KLF15			2.021629996	1.311756743
KLF5	No match	No match		
KLF9		No match	1.530696607	1.185931738
KLK3			6.099503364	3.834462507
KLK4			3.284496196	2.285950381
KRT80	No match	No match		
LIN7B			2.011227865	1.367801001
LINCR	No match	No match		
LOC100008588	No match	No match		
LOC100130886		No match	1.579374115	1.39026578
LOC100131392		No match	4.223836585	2.817441331
LOC100134006		No match	9.096026021	4.929293362
LOC340970		No match	9.10688876	4.808123208
LOC346702	No match	No match		
LOC399939		No match	13.86534555	7.790827452
LOC440040		No match	4.767708218	2.932487647
LOC648509	No match	No match		

LOC728431	No match	No match		
LPAR3			6.893218905	3.437555432
MAP3K8	No match	No match		
MBOAT2		No match	1.508600708	1.519063365
MEAF6		No match	1.995188154	1.277304872
MGC87042	No match	No match		
MT1X	No match			
MTMR9			2.958865361	2.141094855
NDRG1			12.28636673	5.270634396
NEDD4L			2.010775392	1.356407928
NFKBIA			2.473432776	1.636273891
NKX3-1			5.587800399	3.692878564
NPC1		No match	1.503981294	0.931045497
NRP1	No match	No match		
PDE9A		No match		
PER1	No match	No match		
PGC		No match	2.345985212	1.614127152
PGLYRP2	No match	No match		
PHLDA1	No match	No match		
PLGLB1	No match	No match		
PNLIP		No match	1.95786479	1.173735831
PPAP2A	No match			
PRKCD	No match	No match		
PRR15L	No match	No match		
PSD	No match	No match		
RASD1		No match	32.46582806	6.442470968
RDH10		No match	4.508463937	1.50798382
RGS2	No match	No match		
RHOB		No match	4.213336184	1.525477243
RHOU			9.374939536	3.643489707
RND3	No match	No match		
RNF160	No match	No match		
S100P		No match	1.85826271	1.691618798
SCNN1G		No match	1.901936023	1.112999245
SGK		No match	6.972653696	7.420656532
SGK1		No match	5.505949329	5.999534669
SIPA1L2		No match	4.192121174	1.899412025
SLC25A18	No match	No match		
SLC26A3	No match	No match		
SLC2A12	No match			
SLC31A2		No match	1.518781327	1.271786442

SLC45A3			9.880929334	6.903293974
SNAI2		No match	2.393726355	1.597350433
SPRYD5		No match	20.65925549	10.88982128
SPSB1		No match	1.657164332	1.18322278
STEAP2	No match	No match		
STK39			3.782399211	3.053446473
SYTL2	No match	No match		
TBC1D8		No match	3.516385962	2.245574986
TMPRSS2			7.44336537	3.282562937
TRIM48			10.49241718	5.886973648
TSKU		No match	4.886237079	2.921684327
TUBA3C		No match	1.904317611	1.252270758
TUBA3D			5.059784869	2.652713618
TUBA3E		No match	3.088542112	1.795690803
ZBTB16			2.488926793	1.751295224
ZC3H12A		No match	1.791360065	1.047353712
ZMIZ1	No match	No match		
ZNF812			3.045436356	1.373163328

Appendix 6C – A list of the 73 enz-induced genes found upregulated in siUTR2 transfected LNCaP-AR$_{F876L}$ cells relative vehicle control (n=3). Highlighted in green are the genes which were also found upregulated in GR signature probe sets >1.6 fold by Dex (FDR<.05). And the comparison of enzalutamide-induced gene fold changes of siT877A and siF876L arm.

8.9 Appendix 6D

GR selective gene set	no match to enz-F876L(1.5 fold FDR<.05)	no match to DHT-laz_ARwt (1.5 fold FDR<.05)	siT877A+enz (fold changes)	siF876L+enz (fold changes)
ABHD2		No match	2.795477	1.612163
ACTA2	No match	No match		
ATAD2			2.963673	2.175572

Gene				
AZGP1			2.452833	1.978209
BCL6		No match	2.375047	1.64314
C1ORF149		No match	2.389371	1.712925
C6ORF85		No match	1.604561	1.09038
C7ORF63	No match	No match		
C9ORF152			1.826755	2.156987
CEBPD		No match	2.138652	1.493145
CGNL1	No match	No match		
CHKA		No match	1.818237	1.404358
CRY2	No match	No match		
DBC1	No match	No match		
DDIT4	No match	No match		
EEF2K		No match	1.945355	1.344368
EMP1	No match	No match		
ERRFI1			7.217317	3.254158
FKBP5			20.10148	11.39908
FLJ22795	No match	No match		
FOXO3		No match	2.077987	1.343096
GADD45B		No match	2.238914	1.01983
GHR		No match	1.77751	0.960161
HERC5	No match			
HOMER2			3.03831129	2.64938173
HSD11B2	No match	No match		
KBTBD11	No match	No match		
KIAA0040	No match	No match		
KLF15			2.02163	1.311757
KLF9		No match	1.530697	1.185932
KRT80	No match	No match		
LIN7B			2.011228	1.367801
LOC100130886		No match	1.579374	1.390266
LOC100131392		No match	4.223837	2.817441
LOC100134006		No match	9.096026	4.929293
LOC340970		No match	9.106889	4.808123
LOC399939		No match	13.86535	7.790827
LOC440040		No match	4.767708	2.932488
LOC728431	No match	No match		
MEAF6		No match	1.995188	1.277305
MT1X	No match			
NPC1		No match	1.503981	0.931045
NRP1	No match	No match		
PGC		No match	2.345985	1.614127

Gene	Col2	Col3	Value1	Value2
PGLYRP2	No match	No match		
PHLDA1	No match	No match		
PNLIP		No match	1.957865	1.173736
PPAP2A	No match			
PRKCD	No match	No match		
PRR15L	No match	No match		
RGS2	No match	No match		
RHOB		No match	4.213336	1.525477
S100P		No match	1.858263	1.691619
SCNN1G		No match	1.901936	1.112999
SGK		No match	6.972654	7.420657
SGK1		No match	5.505949	5.999535
SLC25A18	No match	No match		
SPRYD5		No match	20.65926	10.88982
SPSB1		No match	1.657164	1.183223
STK39			3.782399	3.053446
TRIM48			10.49242	5.886974
TUBA3C		No match	1.904318	1.252271
TUBA3D			5.05978487	2.65271362
TUBA3E		No match	3.088542	1.795691
ZBTB16			2.48892679	1.75129522
ZMIZ1	No match	No match		
ZNF812		No match	3.045436	1.373163

Appendix 6D – A list of the 43 enzalutamide-regulated genes found to be upregulated in siUTR2 transfected LNCaP-AR$_{F876L}$ cells following treatment for 24 hours relative vehicle control (n=3). Highlighted in green are the genes which were also found upregulated in GR selective gene set. And the comparison of enzalutamide-induced gene fold changes of siT877A and siF876L arm.

8.10 Appendix 6E

Sublist	Category	Term	RT	Genes	Count	%	P-Value	Benjamini
☐	KEGG_PATHWAY	Metabolic pathways	RT		79	12.8	5.9E-5	3.6E-3
☐	KEGG_PATHWAY	Protein processing in endoplasmic reticulum	RT		30	4.9	5.8E-11	1.4E-8
☐	KEGG_PATHWAY	Pathways in cancer	RT		24	3.9	6.6E-2	4.6E-1
☐	KEGG_PATHWAY	Biosynthesis of antibiotics	RT		22	3.6	2.1E-4	6.5E-3
☐	KEGG_PATHWAY	Focal adhesion	RT		15	2.4	5.1E-2	4.9E-1
☐	KEGG_PATHWAY	Proteoglycans in cancer	RT		14	2.3	7.9E-2	4.7E-1
☐	KEGG_PATHWAY	Amino sugar and nucleotide sugar metabolism	RT		12	2.0	3.4E-6	4.2E-4
☐	KEGG_PATHWAY	Phagosome	RT		12	2.0	5.8E-2	5.0E-1
☐	KEGG_PATHWAY	Tight junction	RT		11	1.8	6.3E-2	4.9E-1
☐	KEGG_PATHWAY	Valine, leucine and isoleucine degradation	RT		10	1.6	1.2E-4	6.0E-3
☐	KEGG_PATHWAY	Fatty acid metabolism	RT		10	1.6	1.4E-4	5.1E-3
☐	KEGG_PATHWAY	Carbon metabolism	RT		10	1.6	4.8E-2	5.3E-1
☐	KEGG_PATHWAY	Estrogen signaling pathway	RT		9	1.5	5.6E-2	5.1E-1
☐	KEGG_PATHWAY	Protein export	RT		8	1.3	3.0E-5	2.5E-3
☐	KEGG_PATHWAY	Pathogenic Escherichia coli infection	RT		8	1.3	5.1E-3	1.2E-1
☐	KEGG_PATHWAY	Vibrio cholerae infection	RT		8	1.3	6.4E-3	1.3E-1
☐	KEGG_PATHWAY	Peroxisome	RT		8	1.3	6.0E-2	4.8E-1
☐	KEGG_PATHWAY	Insulin secretion	RT		8	1.3	6.6E-2	4.5E-1
☐	KEGG_PATHWAY	Gap junction	RT		8	1.3	7.7E-2	4.7E-1
☐	KEGG_PATHWAY	Steroid biosynthesis	RT		7	1.1	1.2E-4	5.1E-3
☐	KEGG_PATHWAY	Fructose and mannose metabolism	RT		7	1.1	1.9E-3	5.1E-2
☐	KEGG_PATHWAY	Fatty acid degradation	RT		7	1.1	9.7E-3	1.7E-1
☐	KEGG_PATHWAY	Arginine and proline metabolism	RT		7	1.1	1.8E-2	2.7E-1
☐	KEGG_PATHWAY	Thyroid hormone synthesis	RT		7	1.1	7.3E-2	4.6E-1
☐	KEGG_PATHWAY	beta-Alanine metabolism	RT		6	1.0	8.8E-3	1.7E-1
☐	KEGG_PATHWAY	Propanoate metabolism	RT		5	0.8	2.8E-2	3.8E-1
☐	KEGG_PATHWAY	Starch and sucrose metabolism	RT		5	0.8	4.8E-2	5.1E-1
☐	KEGG_PATHWAY	Alanine, aspartate and glutamate metabolism	RT		5	0.8	5.8E-2	4.9E-1
☐	KEGG_PATHWAY	Pentose and glucuronate interconversions	RT		5	0.8	6.3E-2	4.6E-1
☐	KEGG_PATHWAY	Aldosterone-regulated sodium reabsorption	RT		5	0.8	8.0E-2	4.6E-1
☐	KEGG_PATHWAY	Arginine biosynthesis	RT		4	0.7	5.0E-2	5.0E-1
☐	KEGG_PATHWAY	Terpenoid backbone biosynthesis	RT		4	0.7	6.3E-2	4.7E-1
☐	KEGG_PATHWAY	Biosynthesis of unsaturated fatty acids	RT		4	0.7	7.0E-2	4.6E-1

Appendix 6E-Kyoto Encyclopedia of Genes and Genomes (KEGG) pathway analysis summary of enz-AR$_{F876L}$ driven core gene list.

8.11 Appendix 6F

Sublist	Category	Term	RT	Genes	Count	%	P-Value	Benjamini
☐	SP_COMMENT_TYPE	similarity	RT		586	95.3	8.8E-7	4.2E-6
☐	SP_COMMENT_TYPE	subcellular location	RT		490	79.7	6.4E-6	1.9E-5
☐	SP_COMMENT_TYPE	function	RT		471	76.6	3.6E-6	1.2E-5
☐	SP_COMMENT_TYPE	subunit	RT		346	56.3	1.5E-14	3.6E-13
☐	SP_COMMENT_TYPE	tissue specificity	RT		289	47.0	3.3E-2	7.0E-2
☐	SP_COMMENT_TYPE	interaction	RT		172	28.0	6.4E-8	3.8E-7
☐	SP_COMMENT_TYPE	catalytic activity	RT		149	24.2	4.8E-12	3.8E-11
☐	SP_COMMENT_TYPE	online information	RT		129	21.0	7.9E-2	1.2E-1
☐	SP_COMMENT_TYPE	PTM	RT		122	19.8	6.9E-2	1.2E-1
☐	SP_COMMENT_TYPE	disease	RT		103	16.7	3.4E-2	6.6E-2
☐	SP_COMMENT_TYPE	domain	RT		78	12.7	2.0E-2	4.7E-2
☐	SP_COMMENT_TYPE	pathway	RT		73	11.9	2.2E-12	2.6E-11
☐	SP_COMMENT_TYPE	induction	RT		67	10.9	1.0E-6	4.1E-6
☐	SP_COMMENT_TYPE	cofactor	RT		53	8.6	4.9E-2	8.9E-2
☐	SP_COMMENT_TYPE	enzyme regulation	RT		30	4.9	1.5E-2	3.9E-2

Appendix 6F-Functional Annotation Chart of enz-AR$_{F876L}$ driven core gene list.

References

Adams J. The case of scirrhous of the prostate gland with corresponding affliction of the lymphatic glands in the lumbar region and in the pelvis. Lancet. 1853;1:393.

Arany, Z., Sellers, W.R., Livingston, D.M. and Eckner, R. (1994) 'E1A-associated p300 and CREB-associated CBP belong to a conserved family of coactivators', *Cell*, 77(6), pp. 799-800.

Arora, V.K., Schenkein, E., Murali, R., Subudhi, S.K., Wongvipat, J., Balbas, M.D., Shah, N., Cai, L., Efstathiou, E., Logothetis, C., Zheng, D. and Sawyers, C.L. (2013) 'Glucocorticoid receptor confers resistance to antiandrogens by bypassing androgen receptor blockade', *Cell*, 155(6), pp. 1309-22.

Asangani, I.A. and Chinnaiyan, A.M. (2014) 'BETting on a new prostate cancer treatment', *Cell Cycle*, 13(13), pp. 2015-6.

Asangani, I.A., Dommeti, V.L., Wang, X., Malik, R., Cieslik, M., Yang, R., Escara-Wilke, J., Wilder-Romans, K., Dhanireddy, S., Engelke, C., Iyer, M.K., Jing, X., Wu, Y.M., Cao, X., Qin, Z.S., Wang, S., Feng, F.Y. and Chinnaiyan, A.M. (2014) 'Therapeutic targeting of BET bromodomain proteins in castration-resistant prostate cancer', *Nature*, 510(7504), pp. 278-82.

Askew, E.B., Minges, J.T., Hnat, A.T. and Wilson, E.M. (2012) 'Structural features discriminate androgen receptor N/C terminal and coactivator interactions', *Mol Cell Endocrinol*, 348(2), pp. 403-10.

Balbas, M.D., Evans, M.J., Hosfield, D.J., Wongvipat, J., Arora, V.K., Watson, P.A., Chen, Y., Greene, G.L., Shen, Y. and Sawyers, C.L. (2013) 'Overcoming mutation-based resistance to antiandrogens with rational drug design', *Elife*, 2, p. e00499.

Barbieri, I., Cannizzaro, E. and Dawson, M.A. (2013) 'Bromodomains as therapeutic targets in cancer', *Brief Funct Genomics*, 12(3), pp. 219-30.

Bassett, A.R., Tibbit, C., Ponting, C.P. and Liu, J.L. (2013) 'Highly efficient targeted mutagenesis of Drosophila with the CRISPR/Cas9 system', *Cell Rep*, 4(1), pp. 220-8.

Begemann, M.B., Gray, B.N., January, E., Singer, A., Kesler, D.C., He, Y., Liu, H., Guo, H., Jordan, A., Brutnell, T.P., Mockler, T.C. and Oufattole, M. (2017) 'Characterization and Validation of a Novel Group of Type V, Class 2 Nucleases for in vivo Genome Editing', *bioRxiv*.

Beltran, H., Wyatt, A.W., Chedgy, E.C., Donoghue, A., Annala, M., Warner, E.W., Beja, K., Sigouros, M., Mo, F., Fazli, L., Collins, C.C., Eastham, J., Morris, M., Taplin, M.E., Sboner, A., Halabi, S. and

Gleave, M.E. (2017) 'Impact of Therapy on Genomics and Transcriptomics in High-Risk Prostate Cancer Treated with Neoadjuvant Docetaxel and Androgen Deprivation Therapy', *Clin Cancer Res*, 23(22), pp. 6802-6811.

Beumer, K.J. and Carroll, D. (2014) 'Targeted genome engineering techniques in Drosophila', *Methods*, 68(1), pp. 29-37.

Beumer, K.J., Trautman, J.K., Mukherjee, K. and Carroll, D. (2013) 'Donor DNA Utilization During Gene Targeting with Zinc-Finger Nucleases', *G3 (Bethesda)*, 3(4), pp. 657-664.

Bevan, C.L., Hoare, S., Claessens, F., Heery, D.M. and Parker, M.G. (1999) 'The AF1 and AF2 domains of the androgen receptor interact with distinct regions of SRC1', *Mol Cell Biol*, 19(12), pp. 8383-92.

Bibikova, M., Golic, M., Golic, K.G. and Carroll, D. (2002) 'Targeted chromosomal cleavage and mutagenesis in Drosophila using zinc-finger nucleases', *Genetics*, 161(3), pp. 1169-75.

Bikard, D., Jiang, W., Samai, P., Hochschild, A., Zhang, F. and Marraffini, L.A. (2013) 'Programmable repression and activation of bacterial gene expression using an engineered CRISPR-Cas system', *Nucleic Acids Res*, 41(15), pp. 7429-37.

Bogdanove, A.J. and Voytas, D.F. (2011) 'TAL effectors: customizable proteins for DNA targeting', *Science*, 333(6051), pp. 1843-6.

Bohl, C.E., Wu, Z., Miller, D.D., Bell, C.E. and Dalton, J.T. (2007) 'Crystal structure of the T877A human androgen receptor ligand-binding domain complexed to cyproterone acetate provides insight for ligand-induced conformational changes and structure-based drug design', *J Biol Chem*, 282(18), pp. 13648-55.

Bourguet, W., Germain, P. and Gronemeyer, H. (2000) 'Nuclear receptor ligand-binding domains: three-dimensional structures, molecular interactions and pharmacological implications', *Trends Pharmacol Sci*, 21(10), pp. 381-8.

Brinkman, E.K., Chen, T., Amendola, M. and van Steensel, B. (2014) 'Easy quantitative assessment of genome editing by sequence trace decomposition', *Nucleic Acids Res*, 42(22), p. e168.

Brinkmann, A.O. (2011) 'Molecular mechanisms of androgen action--a historical perspective', *Methods Mol Biol*, 776, pp. 3-24.

Brooke, G.N., Parker, M.G. and Bevan, C.L. (2008) 'Mechanisms of androgen receptor activation in advanced prostate cancer: differential co-activator recruitment and gene expression', *Oncogene*, 27(21), pp. 2941-50.

Canalichio, K., Jaber, Y. and Wang, R. (2015) 'Surgery and hormonal treatment for prostate cancer and sexual function', *Translational Andrology and Urology*, 4(2), pp. 103-109.

Carroll, P.R., Parsons, J.K., Andriole, G., Bahnson, R.R., Barocas, D.A., Catalona, W.J., Dahl, D.M., Davis, J.W., Epstein, J.I., Etzioni, R.B., Giri, V.N., Hemstreet, G.P., 3rd, Kawachi, M.H., Lange, P.H., Loughlin, K.R., Lowrance, W., Maroni, P., Mohler, J., Morgan, T.M., Nadler, R.B., Poch, M., Scales, C., Shanefelt, T.M., Vickers, A.J., Wake, R., Shead, D.A. and Ho, M. (2014) 'Prostate cancer early detection, version 1.2014. Featured updates to the NCCN Guidelines', *J Natl Compr Canc Netw*, 12(9), pp. 1211-9; quiz 1219.

Cavanagh, H. and Rogers, K.M. (2015) 'The role of BRCA1 and BRCA2 mutations in prostate, pancreatic and stomach cancers', *Hered Cancer Clin Pract*, 13(1), p. 16.

Chen, B., Gilbert, L.A., Cimini, B.A., Schnitzbauer, J., Zhang, W., Li, G.W., Park, J., Blackburn, E.H., Weissman, J.S., Qi, L.S. and Huang, B. (2013) 'Dynamic imaging of genomic loci in living human cells by an optimized CRISPR/Cas system', *Cell*, 155(7), pp. 1479-91.

Chen, C., Liu, Y., Rappaport, A.R., Kitzing, T., Schultz, N., Zhao, Z., Shroff, A.S., Dickins, R.A., Vakoc, C.R., Bradner, J.E., Stock, W., LeBeau, M.M., Shannon, K.M., Kogan, S., Zuber, J. and Lowe, S.W. (2014a) 'MLL3 is a haploinsufficient 7q tumor suppressor in acute myeloid leukemia', *Cancer Cell*, 25(5), pp. 652-65.

Chen, C.D., Welsbie, D.S., Tran, C., Baek, S.H., Chen, R., Vessella, R., Rosenfeld, M.G. and Sawyers, C.L. (2004) 'Molecular determinants of resistance to antiandrogen therapy', *Nat Med*, 10(1), pp. 33-9.

Chen, F., Pruett-Miller, S.M., Huang, Y., Gjoka, M., Duda, K., Taunton, J., Collingwood, T.N., Frodin, M. and Davis, G.D. (2011) 'High-frequency genome editing using ssDNA oligonucleotides with zinc-finger nucleases', *Nat Methods*, 8(9), pp. 753-5.

Chen, H., Choi, J. and Bailey, S. (2014b) 'Cut site selection by the two nuclease domains of the Cas9 RNA-guided endonuclease', *J Biol Chem*, 289(19), pp. 13284-94.

Chen, J., Ghazawi, F.M. and Li, Q. (2010) 'Interplay of bromodomain and histone acetylation in the regulation of p300-dependent genes', *Epigenetics*, 5(6), pp. 509-15.

Chen, Y., Clegg, N.J. and Scher, H.I. (2009) 'Anti-androgens and androgen-depleting therapies in prostate cancer: new agents for an established target', *Lancet Oncol*, 10(10), pp. 981-91.

Chenouard, V., Brusselle, L., Heslan, J.M., Remy, S., Menoret, S., Usal, C., Ouisse, L.H., TH, N.G., Anegon, I. and Tesson, L. (2016) 'A Rapid and Cost-Effective Method for Genotyping Genome-Edited Animals: A Heteroduplex Mobility Assay Using Microfluidic Capillary Electrophoresis', *J Genet Genomics*, 43(5), pp. 341-8.

Cho, S.W., Kim, S., Kim, J.M. and Kim, J.S. (2013) 'Targeted genome engineering in human cells with the Cas9 RNA-guided endonuclease', *Nat Biotechnol*, 31(3), pp. 230-2.

Choi, P.S. and Meyerson, M. (2014) 'Targeted genomic rearrangements using CRISPR/Cas technology', *Nat Commun*, 5, p. 3728.

Chu, V.T., Weber, T., Wefers, B., Wurst, W., Sander, S., Rajewsky, K. and Kuhn, R. (2015) 'Increasing the efficiency of homology-directed repair for CRISPR-Cas9-induced precise gene editing in mammalian cells', *Nat Biotechnol*, 33(5), pp. 543-8.

Coffey, K., Blackburn, T.J., Cook, S., Golding, B.T., Griffin, R.J., Hardcastle, I.R., Hewitt, L., Huberman, K., McNeill, H.V., Newell, D.R., Roche, C., Ryan-Munden, C.A., Watson, A. and Robson, C.N. (2012) 'Characterisation of a Tip60 specific inhibitor, NU9056, in prostate cancer', *PLoS One*, 7(10), p. e45539.

Comuzzi, B., Lambrinidis, L., Rogatsch, H., Godoy-Tundidor, S., Knezevic, N., Krhen, I., Marekovic, Z., Bartsch, G., Klocker, H., Hobisch, A. and Culig, Z. (2003) 'The transcriptional co-activator cAMP response element-binding protein-binding protein is expressed in prostate cancer and enhances androgen- and anti-androgen-induced androgen receptor function', *Am J Pathol*, 162(1), pp. 233-41.

Comuzzi, B., Nemes, C., Schmidt, S., Jasarevic, Z., Lodde, M., Pycha, A., Bartsch, G., Offner, F., Culig, Z. and Hobisch, A. (2004) 'The androgen receptor co-activator CBP is up-regulated following androgen withdrawal and is highly expressed in advanced prostate cancer', *J Pathol*, 204(2), pp. 159-66.

Cong, L., Ran, F.A., Cox, D., Lin, S., Barretto, R., Habib, N., Hsu, P.D., Wu, X., Jiang, W., Marraffini, L.A. and Zhang, F. (2013) 'Multiplex genome engineering using CRISPR/Cas systems', *Science*, 339(6121), pp. 819-23.

Coutinho, I., Day, T.K., Tilley, W.D. and Selth, L.A. (2016) 'Androgen receptor signaling in castration-resistant prostate cancer: a lesson in persistence', *Endocr Relat Cancer*, 23(12), pp. T179-T197.

Crawford, N.P., Alsarraj, J., Lukes, L., Walker, R.C., Officewala, J.S., Yang, H.H., Lee, M.P., Ozato, K. and Hunter, K.W. (2008) 'Bromodomain 4 activation predicts breast cancer survival', *Proc Natl Acad Sci U S A*, 105(17), pp. 6380-5.

Crona, D.J. and Whang, Y.E. (2017) 'Androgen Receptor-Dependent and -Independent Mechanisms Involved in Prostate Cancer Therapy Resistance', *Cancers (Basel)*, 9(6).

Cucchiara, V., Yang, J.C., Mirone, V., Gao, A.C., Rosenfeld, M.G. and Evans, C.P. (2017) 'Epigenomic Regulation of Androgen Receptor Signaling: Potential Role in Prostate Cancer Therapy', *Cancers (Basel)*, 9(1).

Culig, Z. (2016) 'Androgen Receptor Coactivators in Regulation of Growth and Differentiation in Prostate Cancer', *J Cell Physiol*, 231(2), pp. 270-4.

Cyranoski, D. (2016) 'CRISPR gene-editing tested in a person for the first time', *Nature*, 539(7630), p. 479.

de Bono, J.S., Oudard, S., Ozguroglu, M., Hansen, S., Machiels, J.P., Kocak, I., Gravis, G., Bodrogi, I., Mackenzie, M.J., Shen, L., Roessner, M., Gupta, S. and Sartor, A.O. (2010) 'Prednisone plus cabazitaxel or mitoxantrone for metastatic castration-resistant prostate cancer progressing after docetaxel treatment: a randomised open-label trial', *Lancet*, 376(9747), pp. 1147-54.

de Oliveira Barros, E.G., Palumbo, A., Jr., Mello, P.L., de Mattos, R.M., da Silva, J.H., Pontes, B., Viana, N.B., do Amaral, R.F., Lima, F.R., da Costa, N.M., Palmero, C.Y., Miranda-Alves, L., Takiya, C.M. and Nasciutti, L.E. (2014) 'The reciprocal interactions between astrocytes and prostate cancer cells represent an early event associated with brain metastasis', *Clin Exp Metastasis*.

Debes, J.D., Comuzzi, B., Schmidt, L.J., Dehm, S.M., Culig, Z. and Tindall, D.J. (2005) 'p300 Regulates Androgen Receptor–Independent Expression of Prostate-Specific Antigen in Prostate Cancer Cells Treated Chronically with Interleukin-6', *Cancer Research*, 65(13), pp. 5965-5973.

Debes, J.D., Schmidt, L.J., Huang, H. and Tindall, D.J. (2002) 'p300 Mediates Androgen-independent Transactivation of the Androgen Receptor by Interleukin 6', *Cancer Research*, 62(20), pp. 5632-5636.

Dehm, S.M. and Tindall, D.J. (2011) 'Alternatively spliced androgen receptor variants', *Endocr Relat Cancer*, 18(5), pp. R183-96.

Deltcheva, E., Chylinski, K., Sharma, C.M., Gonzales, K., Chao, Y., Pirzada, Z.A., Eckert, M.R., Vogel, J. and Charpentier, E. (2011) 'CRISPR RNA maturation by trans-encoded small RNA and host factor RNase III', *Nature*, 471(7340), pp. 602-7.

Denmeade, S.R. and Isaacs, J.T. (2002) 'A history of prostate cancer treatment', *Nat Rev Cancer*, 2(5), pp. 389-96.

Dhingra, R., Sharma, T., Singh, S., Sharma, S., Tomar, P., Malhotra, M. and Bhardwaj, T.R. (2013) 'Enzalutamide: a novel anti-androgen with prolonged survival rate in CRPC patients', *Mini Rev Med Chem*, 13(10), pp. 1475-86.

Faivre, E.J., Wilcox, D., Lin, X., Hessler, P., Torrent, M., He, W., Uziel, T., Albert, D.H., McDaniel, K., Kati, W. and Shen, Y. (2017) 'Exploitation of Castration-Resistant Prostate Cancer Transcription Factor Dependencies by the Novel BET Inhibitor ABBV-075', *Mol Cancer Res*, 15(1), pp. 35-44.

Farzadfard, F., Perli, S.D. and Lu, T.K. (2013) 'Tunable and multifunctional eukaryotic transcription factors based on CRISPR/Cas', *ACS Synth Biol*, 2(10), pp. 604-13.

Filippakopoulos, P., Qi, J., Picaud, S., Shen, Y., Smith, W.B., Fedorov, O., Morse, E.M., Keates, T., Hickman, T.T., Felletar, I., Philpott, M., Munro, S., McKeown, M.R., Wang, Y., Christie, A.L., West, N., Cameron, M.J., Schwartz, B., Heightman, T.D., La Thangue, N., French, C.A., Wiest, O., Kung, A.L., Knapp, S. and Bradner, J.E. (2010) 'Selective inhibition of BET bromodomains', *Nature*, 468(7327), pp. 1067-73.

Fu, M., Rao, M., Wang, C., Sakamaki, T., Wang, J., Di Vizio, D., Zhang, X., Albanese, C., Balk, S., Chang, C., Fan, S., Rosen, E., Palvimo, J.J., Janne, O.A., Muratoglu, S., Avantaggiati, M.L. and Pestell, R.G. (2003) 'Acetylation of androgen receptor enhances coactivator binding and promotes prostate cancer cell growth', *Mol Cell Biol*, 23(23), pp. 8563-75.

Fu, M., Wang, C., Reutens, A.T., Wang, J., Angeletti, R.H., Siconolfi-Baez, L., Ogryzko, V., Avantaggiati, M.L. and Pestell, R.G. (2000) 'p300 and p300/cAMP-response element-binding

protein-associated factor acetylate the androgen receptor at sites governing hormone-dependent transactivation', *J Biol Chem*, 275(27), pp. 20853-60.

Fuguo, J. and Jennifer, A.D. (2017) 'CRISPR–Cas9 Structures and Mechanisms', *Annual Review of Biophysics*, 46(1), pp. 505-529.

Gaj, T., Gersbach, C.A. and Barbas, C.F., 3rd (2013) 'ZFN, TALEN, and CRISPR/Cas-based methods for genome engineering', *Trends Biotechnol*, 31(7), pp. 397-405.

Gann, P.H. (2002) 'Risk factors for prostate cancer', *Rev Urol*, 4 Suppl 5, pp. S3-s10.

Gao, X.N., Lin, J., Ning, Q.Y., Gao, L., Yao, Y.S., Zhou, J.H., Li, Y.H., Wang, L.L. and Yu, L. (2013) 'A histone acetyltransferase p300 inhibitor C646 induces cell cycle arrest and apoptosis selectively in AML1-ETO-positive AML cells', *PLoS One*, 8(2), p. e55481.

Gaughan, L., Logan, I.R., Cook, S., Neal, D.E. and Robson, C.N. (2002) 'Tip60 and histone deacetylase 1 regulate androgen receptor activity through changes to the acetylation status of the receptor', *J Biol Chem*, 277(29), pp. 25904-13.

Gilbert, L.A., Larson, M.H., Morsut, L., Liu, Z., Brar, G.A., Torres, S.E., Stern-Ginossar, N., Brandman, O., Whitehead, E.H., Doudna, J.A., Lim, W.A., Weissman, J.S. and Qi, L.S. (2013) 'CRISPR-mediated modular RNA-guided regulation of transcription in eukaryotes', *Cell*, 154(2), pp. 442-51.

Gomella, L.G. (2009) 'Effective testosterone suppression for prostate cancer: is there a best castration therapy?', *Rev Urol*, 11(2), pp. 52-60.

Gottlieb, B., Beitel, L.K., Nadarajah, A., Paliouras, M. and Trifiro, M. (2012) 'The androgen receptor gene mutations database: 2012 update', *Hum Mutat*, 33(5), pp. 887-94.

Gratz, S.J., Cummings, A.M., Nguyen, J.N., Hamm, D.C., Donohue, L.K., Harrison, M.M., Wildonger, J. and O'Connor-Giles, K.M. (2013) 'Genome engineering of Drosophila with the CRISPR RNA-guided Cas9 nuclease', *Genetics*, 194(4), pp. 1029-35.

Gravina, G.L., Festuccia, C., Marampon, F., Popov, V.M., Pestell, R.G., Zani, B.M. and Tombolini, V. (2010) 'Biological rationale for the use of DNA methyltransferase inhibitors as new strategy for modulation of tumor response to chemotherapy and radiation', *Mol Cancer*, 9, p. 305.

Greschik, H. and Moras, D. (2003) 'Structure-activity relationship of nuclear receptor-ligand interactions', *Curr Top Med Chem*, 3(14), pp. 1573-99.

Guerrero, J., Alfaro, I.E., Gomez, F., Protter, A.A. and Bernales, S. (2013) 'Enzalutamide, an androgen receptor signaling inhibitor, induces tumor regression in a mouse model of castration-resistant prostate cancer', *Prostate*, 73(12), pp. 1291-305.

Guschin, D.Y., Waite, A.J., Katibah, G.E., Miller, J.C., Holmes, M.C. and Rebar, E.J. (2010) 'A rapid and general assay for monitoring endogenous gene modification', *Methods Mol Biol*, 649, pp. 247-56.

Gwiazda, K.S., Grier, A.E., Sahni, J., Burleigh, S.M., Martin, U., Yang, J.G., Popp, N.A., Krutein, M.C., Khan, I.F., Jacoby, K., Jensen, M.C., Rawlings, D.J. and Scharenberg, A.M. (2016) 'High Efficiency CRISPR/Cas9-mediated Gene Editing in Primary Human T-cells Using Mutant Adenoviral E4orf6/E1b55k "Helper" Proteins', *Mol Ther*, 24(9), pp. 1570-80.

Han, H.S., Shim, Y.K., Kim, J.E., Jeon, H.J., Lim, S.N., Oh, T.K., Lee, K.H. and Kim, S.T. (2012) 'A pilot study of adrenal suppression after dexamethasone therapy as an antiemetic in cancer patients', *Support Care Cancer*, 20(7), pp. 1565-72.

Hassanipour-Azgomi, S., Mohammadian-Hafshejani, A., Ghoncheh, M., Towhidi, F., Jamehshorani, S. and Salehiniya, H. (2016) 'Incidence and mortality of prostate cancer and their relationship with the Human Development Index worldwide', *Prostate Int*, 4(3), pp. 118-24.

Heck, M.M., Gschwend, J.E. and Retz, M. (2012) 'Enzalutamide (formerly MDV3100) prolongs survival in docetaxel-pretreated castration-resistant prostate cancer patients', *Translational Andrology and Urology*, 2(2), pp. 92-93.

Heckl, D., Kowalczyk, M.S., Yudovich, D., Belizaire, R., Puram, R.V., McConkey, M.E., Thielke, A., Aster, J.C., Regev, A. and Ebert, B.L. (2014) 'Generation of mouse models of myeloid malignancy with combinatorial genetic lesions using CRISPR-Cas9 genome editing', *Nature Biotechnology*, 32, p. 941.

Heemers, H.V., Debes, J.D. and Tindall, D.J. (2008) 'The role of the transcriptional coactivator p300 in prostate cancer progression', *Adv Exp Med Biol*, 617, pp. 535-40.

Heemers, H.V., Sebo, T.J., Debes, J.D., Regan, K.M., Raclaw, K.A., Murphy, L.M., Hobisch, A., Culig, Z. and Tindall, D.J. (2007) 'Androgen deprivation increases p300 expression in prostate cancer cells', *Cancer Res*, 67(7), pp. 3422-30.

Heintze, J., Luft, C. and Ketteler, R. (2013) 'A CRISPR CASe for high-throughput silencing', *Front Genet*, 4, p. 193.

Holkers, M., Maggio, I., Liu, J., Janssen, J.M., Miselli, F., Mussolino, C., Recchia, A., Cathomen, T. and Goncalves, M.A. (2013) 'Differential integrity of TALE nuclease genes following adenoviral and lentiviral vector gene transfer into human cells', *Nucleic Acids Res*, 41(5), p. e63.

Hongmao, S. (2016) 'Chapter 3 - Structure-Based Ligand Design II: With Structure of Protein/Lead Compound Complex Unavailable', in *A Practical Guide to Rational Drug Design*. Woodhead Publishing, pp. 61-108.

Horii, T., Tamura, D., Morita, S., Kimura, M. and Hatada, I. (2013) 'Generation of an ICF syndrome model by efficient genome editing of human induced pluripotent stem cells using the CRISPR system', *Int J Mol Sci*, 14(10), pp. 19774-81.

Horoszewicz, J.S., Leong, S.S., Chu, T.M., Wajsman, Z.L., Friedman, M., Papsidero, L., Kim, U., Chai, L.S., Kakati, S., Arya, S.K. and Sandberg, A.A. (1980) 'The LNCaP cell line--a new model for studies on human prostatic carcinoma', *Prog Clin Biol Res*, 37, pp. 115-32.

Hsu, P.D., Lander, E.S. and Zhang, F. (2014) 'Development and applications of CRISPR-Cas9 for genome engineering', *Cell*, 157(6), pp. 1262-78.

Hu, R., Dunn, T.A., Wei, S., Isharwal, S., Veltri, R.W., Humphreys, E., Han, M., Partin, A.W., Vessella, R.L., Isaacs, W.B., Bova, G.S. and Luo, J. (2009) 'Ligand-independent androgen receptor variants derived from splicing of cryptic exons signify hormone-refractory prostate cancer', *Cancer Res*, 69(1), pp. 16-22.

Hu, R., Wallace, J., Dahlem, T.J., Grunwald, D.J. and O'Connell, R.M. (2013) 'Targeting human microRNA genes using engineered Tal-effector nucleases (TALENs)', *PLoS One*, 8(5), p. e63074.

Huggins, C. and Clark, P.J. (1940) 'QUANTITATIVE STUDIES OF PROSTATIC SECRETION : II. THE EFFECT OF CASTRATION AND OF ESTROGEN INJECTION ON THE NORMAL AND ON THE HYPERPLASTIC PROSTATE GLANDS OF DOGS', *J Exp Med*, 72(6), pp. 747-62.

Huggins, C. and Hodges, C.V. (1972) 'Studies on prostatic cancer. I. The effect of castration, of estrogen and androgen injection on serum phosphatases in metastatic carcinoma of the prostate', *CA Cancer J Clin*, 22(4), pp. 232-40.

Huggins, C. and Hodges, C.V. (2002) 'Studies on prostatic cancer. I. The effect of castration, of estrogen and of androgen injection on serum phosphatases in metastatic carcinoma of the prostate. 1941', *J Urol*, 167(2 Pt 2), pp. 948-51; discussion 952.

Hwang, W.Y., Fu, Y., Reyon, D., Maeder, M.L., Tsai, S.Q., Sander, J.D., Peterson, R.T., Yeh, J.R. and Joung, J.K. (2013) 'Efficient genome editing in zebrafish using a CRISPR-Cas system', *Nat Biotechnol*, 31(3), pp. 227-9.

Isikbay, M., Otto, K., Kregel, S., Kach, J., Cai, Y., Vander Griend, D.J., Conzen, S.D. and Szmulewitz, R.Z. (2014) 'Glucocorticoid receptor activity contributes to resistance to androgen-targeted therapy in prostate cancer', *Horm Cancer*, 5(2), pp. 72-89.

Jiang, W., Bikard, D., Cox, D., Zhang, F. and Marraffini, L.A. (2013) 'RNA-guided editing of bacterial genomes using CRISPR-Cas systems', *Nat Biotechnol*, 31(3), pp. 233-9.

Jin, L., Garcia, J., Chan, E., de la Cruz, C., Segal, E., Merchant, M., Kharbanda, S., Raisner, R., Haverty, P.M., Modrusan, Z., Ly, J., Choo, E., Kaufman, S., Beresini, M.H., Romero, F.A., Magnuson, S. and Gascoigne, K.E. (2017) 'Therapeutic Targeting of the CBP/p300 Bromodomain Blocks the Growth of Castration-Resistant Prostate Cancer', *Cancer Res*, 77(20), pp. 5564-5575.

Jinek, M., Chylinski, K., Fonfara, I., Hauer, M., Doudna, J.A. and Charpentier, E. (2012) 'A programmable dual-RNA-guided DNA endonuclease in adaptive bacterial immunity', *Science*, 337(6096), pp. 816-21.

Jinek, M., East, A., Cheng, A., Lin, S., Ma, E. and Doudna, J. (2013) 'RNA-programmed genome editing in human cells', *Elife*, 2, p. e00471.

Joseph, J.D., Lu, N., Qian, J., Sensintaffar, J., Shao, G., Brigham, D., Moon, M., Maneval, E.C., Chen, I., Darimont, B. and Hager, J.H. (2013) 'A clinically relevant androgen receptor mutation confers resistance to second-generation antiandrogens enzalutamide and ARN-509', *Cancer Discov*, 3(9), pp. 1020-9.

Josling, G.A., Selvarajah, S.A., Petter, M. and Duffy, M.F. (2012) 'The role of bromodomain proteins in regulating gene expression', *Genes (Basel)*, 3(2), pp. 320-43.

Jubair, L. and McMillan, N.A.J. (2017) 'The Therapeutic Potential of CRISPR/Cas9 Systems in Oncogene-Addicted Cancer Types: Virally Driven Cancers as a Model System', *Mol Ther Nucleic Acids*, 8, pp. 56-63.

Kach, J., Conzen, S.D. and Szmulewitz, R.Z. (2015) 'Targeting the glucocorticoid receptor in breast and prostate cancers', *Sci Transl Med*, 7(305), p. 305ps19.

Kach, J., Long, T.M., Selman, P., Tonsing-Carter, E.Y., Bacalao, M.A., Lastra, R.R., de Wet, L., Comiskey, S., Gillard, M., VanOpstall, C., West, D.C., Chan, W.C., Griend, D.V., Conzen, S.D. and Szmulewitz, R.Z. (2017) 'Selective Glucocorticoid Receptor Modulators (SGRMs) Delay Castrate-Resistant Prostate Cancer Growth', *Mol Cancer Ther*, 16(8), pp. 1680-1692.

Kalkhoven, E. (2004) 'CBP and p300: HATs for different occasions', *Biochem Pharmacol*, 68(6), pp. 1145-55.

Kang, Z., Janne, O.A. and Palvimo, J.J. (2004) 'Coregulator recruitment and histone modifications in transcriptional regulation by the androgen receptor', *Mol Endocrinol*, 18(11), pp. 2633-48.

Karantanos, T., Corn, P.G. and Thompson, T.C. (2013) 'Prostate cancer progression after androgen deprivation therapy: mechanisms of castrate resistance and novel therapeutic approaches', *Oncogene*, 32(49), pp. 5501-11.

Kc, R., Srivastava, A., Wilkowski, J.M., Richter, C.E., Shavit, J.A., Burke, D.T. and Bielas, S.L. (2016) 'Detection of nucleotide-specific CRISPR/Cas9 modified alleles using multiplex ligation detection', *Sci Rep*, 6, p. 32048.

Kim, S. and Kim, J.S. (2011) 'Targeted genome engineering via zinc finger nucleases', *Plant Biotechnol Rep*, 5(1), pp. 9-17.

Kim, Y.G., Cha, J. and Chandrasegaran, S. (1996) 'Hybrid restriction enzymes: zinc finger fusions to Fok I cleavage domain', *Proc Natl Acad Sci U S A*, 93(3), pp. 1156-60.

Kobayashi, T., Inoue, T., Kamba, T. and Ogawa, O. (2013) 'Experimental Evidence of Persistent Androgen-Receptor-Dependency in Castration-Resistant Prostate Cancer', *International Journal of Molecular Sciences*, 14(8), pp. 15615-15635.

Kondo, S. and Ueda, R. (2013) 'Highly improved gene targeting by germline-specific Cas9 expression in Drosophila', *Genetics*, 195(3), pp. 715-21.

Koochekpour, S. (2010) 'Androgen receptor signaling and mutations in prostate cancer', *Asian J Androl*, 12(5), pp. 639-57.

Korpal, M., Korn, J.M., Gao, X., Rakiec, D.P., Ruddy, D.A., Doshi, S., Yuan, J., Kovats, S.G., Kim, S., Cooke, V.G., Monahan, J.E., Stegmeier, F., Roberts, T.M., Sellers, W.R., Zhou, W. and Zhu, P.

(2013a) 'An F876L Mutation in Androgen Receptor Confers Genetic and Phenotypic Resistance to MDV3100 (Enzalutamide)', *Cancer Discovery*.

Korpal, M., Korn, J.M., Gao, X., Rakiec, D.P., Ruddy, D.A., Doshi, S., Yuan, J., Kovats, S.G., Kim, S., Cooke, V.G., Monahan, J.E., Stegmeier, F., Roberts, T.M., Sellers, W.R., Zhou, W. and Zhu, P. (2013b) 'An F876L mutation in androgen receptor confers genetic and phenotypic resistance to MDV3100 (enzalutamide)', *Cancer Discov*, 3(9), pp. 1030-43.

Kroon, J., Puhr, M., Buijs, J.T., van der Horst, G., Hemmer, D.M., Marijt, K.A., Hwang, M.S., Masood, M., Grimm, S., Storm, G., Metselaar, J.M., Meijer, O.C., Culig, Z. and van der Pluijm, G. (2016) 'Glucocorticoid receptor antagonism reverts docetaxel resistance in human prostate cancer', *Endocr Relat Cancer*, 23(1), pp. 35-45.

LaFountaine, J.S., Fathe, K. and Smyth, H.D. (2015) 'Delivery and therapeutic applications of gene editing technologies ZFNs, TALENs, and CRISPR/Cas9', *Int J Pharm*, 494(1), pp. 180-94.

Lamb, B.M., Mercer, A.C. and Barbas, C.F., 3rd (2013) 'Directed evolution of the TALE N-terminal domain for recognition of all 5' bases', *Nucleic Acids Res*, 41(21), pp. 9779-85.

Lamoureux, F., Baud'huin, M., Rodriguez Calleja, L., Jacques, C., Berreur, M., Redini, F., Lecanda, F., Bradner, J.E., Heymann, D. and Ory, B. (2014) 'Selective inhibition of BET bromodomain epigenetic signalling interferes with the bone-associated tumour vicious cycle', *Nat Commun*, 5, p. 3511.

Lange, A., Mills, R.E., Lange, C.J., Stewart, M., Devine, S.E. and Corbett, A.H. (2007) 'Classical nuclear localization signals: definition, function, and interaction with importin alpha', *J Biol Chem*, 282(8), pp. 5101-5.

Legube, G. and Trouche, D. (2003) 'Regulating histone acetyltransferases and deacetylases', *EMBO Rep*, 4(10), pp. 944-7.

Li, H., Haurigot, V., Doyon, Y., Li, T., Wong, S.Y., Bhagwat, A.S., Malani, N., Anguela, X.M., Sharma, R., Ivanciu, L., Murphy, S.L., Finn, J.D., Khazi, F.R., Zhou, S., Paschon, D.E., Rebar, E.J., Bushman, F.D., Gregory, P.D., Holmes, M.C. and High, K.A. (2011) 'In vivo genome editing restores haemostasis in a mouse model of haemophilia', *Nature*, 475(7355), pp. 217-21.

Li, K., Wang, G., Andersen, T., Zhou, P. and Pu, W.T. (2014) 'Optimization of genome engineering approaches with the CRISPR/Cas9 system', *PLoS One*, 9(8), p. e105779.

Li, Z., Alyamani, M., Li, J., Rogacki, K., Abazeed, M., Upadhyay, S.K., Balk, S.P., Taplin, M.E., Auchus, R.J. and Sharifi, N. (2016) 'Redirecting abiraterone metabolism to fine-tune prostate cancer anti-androgen therapy', *Nature*, 533(7604), pp. 547-51.

Lin, S., Staahl, B.T., Alla, R.K. and Doudna, J.A. (2014) 'Enhanced homology-directed human genome engineering by controlled timing of CRISPR/Cas9 delivery', *Elife*, 3, p. e04766.

Lino, C.A., Harper, J.C., Carney, J.P. and Timlin, J.A. (2018) 'Delivering CRISPR: a review of the challenges and approaches', *Drug Deliv*, 25(1), pp. 1234-1257.

Lochrin, S.E., Price, D.K. and Figg, W.D. (2014) 'BET bromodomain inhibitors--a novel epigenetic approach in castration-resistant prostate cancer', *Cancer Biol Ther*, 15(12), pp. 1583-5.

Lorente, D. and De Bono, J.S. (2014) 'Molecular alterations and emerging targets in castration resistant prostate cancer', *Eur J Cancer*, 50(4), pp. 753-64.

Louie, M.C., Yang, H.Q., Ma, A.H., Xu, W., Zou, J.X., Kung, H.J. and Chen, H.W. (2003) 'Androgen-induced recruitment of RNA polymerase II to a nuclear receptor-p160 coactivator complex', *Proc Natl Acad Sci U S A*, 100(5), pp. 2226-30.

Mahfouz, M.M., Piatek, A. and Stewart, C.N., Jr. (2014) 'Genome engineering via TALENs and CRISPR/Cas9 systems: challenges and perspectives', *Plant Biotechnol J*, 12(8), pp. 1006-14.

Makarova, K.S., Haft, D.H., Barrangou, R., Brouns, S.J., Charpentier, E., Horvath, P., Moineau, S., Mojica, F.J., Wolf, Y.I., Yakunin, A.F., van der Oost, J. and Koonin, E.V. (2011) 'Evolution and classification of the CRISPR-Cas systems', *Nat Rev Microbiol*, 9(6), pp. 467-77.

Makarova, K.S., Wolf, Y.I., Alkhnbashi, O.S., Costa, F., Shah, S.A., Saunders, S.J., Barrangou, R., Brouns, S.J., Charpentier, E., Haft, D.H., Horvath, P., Moineau, S., Mojica, F.J., Terns, R.M., Terns, M.P., White, M.F., Yakunin, A.F., Garrett, R.A., van der Oost, J., Backofen, R. and Koonin, E.V. (2015) 'An updated evolutionary classification of CRISPR-Cas systems', *Nat Rev Microbiol*, 13(11), pp. 722-36.

Mali, P., Aach, J., Stranges, P.B., Esvelt, K.M., Moosburner, M., Kosuri, S., Yang, L. and Church, G.M. (2013a) 'CAS9 transcriptional activators for target specificity screening and paired nickases for cooperative genome engineering', *Nat Biotechnol*, 31(9), pp. 833-8.

Mali, P., Yang, L., Esvelt, K.M., Aach, J., Guell, M., DiCarlo, J.E., Norville, J.E. and Church, G.M. (2013b) 'RNA-guided human genome engineering via Cas9', *Science*, 339(6121), pp. 823-6.

Mao, Z., Bozzella, M., Seluanov, A. and Gorbunova, V. (2008) 'DNA repair by nonhomologous end joining and homologous recombination during cell cycle in human cells', *Cell Cycle*, 7(18), pp. 2902-6.

Mateo, J., Smith, A., Ong, M. and de Bono, J.S. (2014) 'Novel drugs targeting the androgen receptor pathway in prostate cancer', *Cancer Metastasis Rev*, 33(2-3), pp. 567-79.

McEwan, I.J. (2004) 'Molecular mechanisms of androgen receptor-mediated gene regulation: structure-function analysis of the AF-1 domain', *Endocrine-Related Cancer*, 11(2), pp. 281-293.

'Method of the Year 2011', (2012) *Nat Methods*, 9(1), p. 1.

Miller, J.C., Holmes, M.C., Wang, J., Guschin, D.Y., Lee, Y.L., Rupniewski, I., Beausejour, C.M., Waite, A.J., Wang, N.S., Kim, K.A., Gregory, P.D., Pabo, C.O. and Rebar, E.J. (2007) 'An improved zinc-finger nuclease architecture for highly specific genome editing', *Nat Biotechnol*, 25(7), pp. 778-85.

Mohler, J.L., Kantoff, P.W., Armstrong, A.J., Bahnson, R.R., Cohen, M., D'Amico, A.V., Eastham, J.A., Enke, C.A., Farrington, T.A., Higano, C.S., Horwitz, E.M., Kane, C.J., Kawachi, M.H., Kuettel, M., Kuzel, T.M., Lee, R.J., Malcolm, A.W., Miller, D., Plimack, E.R., Pow-Sang, J.M., Raben, D., Richey, S., Roach, M., 3rd, Rohren, E., Rosenfeld, S., Schaeffer, E., Small, E.J., Sonpavde, G., Srinivas, S., Stein, C., Strope, S.A., Tward, J., Shead, D.A. and Ho, M. (2014) 'Prostate cancer, version 2.2014', *J Natl Compr Canc Netw*, 12(5), pp. 686-718.

Monge, A., Jagla, M., Lapouge, G., Sasorith, S., Cruchant, M., Wurtz, J.M., Jacqmin, D., Bergerat, J.P. and Ceraline, J. (2006) 'Unfaithfulness and promiscuity of a mutant androgen receptor in a hormone-refractory prostate cancer', *Cell Mol Life Sci*, 63(4), pp. 487-97.

Moran, E. (1993) 'DNA tumor virus transforming proteins and the cell cycle', *Curr Opin Genet Dev*, 3(1), pp. 63-70.

Nadal, R. and Bellmunt, J. (2016) 'The evolving role of enzalutamide on the treatment of prostate cancer', *Future Oncol*, 12(5), pp. 607-16.

Nelson, P.S., Clegg, N., Arnold, H., Ferguson, C., Bonham, M., White, J., Hood, L. and Lin, B. (2002) 'The program of androgen-responsive genes in neoplastic prostate epithelium', *Proc Natl Acad Sci U S A*, 99(18), pp. 11890-5.

Nelson, W.G. and Yegnasubramanian, S. (2013) 'Resistance emerges to second-generation antiandrogens in prostate cancer', *Cancer Discov*, 3(9), pp. 971-4.

Nemudryi, A.A., Valetdinova, K.R., Medvedev, S.P. and Zakian, S.M. (2014) 'TALEN and CRISPR/Cas Genome Editing Systems: Tools of Discovery', *Acta Naturae*, 6(3), pp. 19-40.

Niu, Y., Shen, B., Cui, Y., Chen, Y., Wang, J., Wang, L., Kang, Y., Zhao, X., Si, W., Li, W., Xiang, A.P., Zhou, J., Guo, X., Bi, Y., Si, C., Hu, B., Dong, G., Wang, H., Zhou, Z., Li, T., Tan, T., Pu, X., Wang, F., Ji, S., Zhou, Q., Huang, X., Ji, W. and Sha, J. (2014) 'Generation of gene-modified cynomolgus monkey via Cas9/RNA-mediated gene targeting in one-cell embryos', *Cell*, 156(4), pp. 836-43.

Nyquist, M.D., Li, Y., Hwang, T.H., Manlove, L.S., Vessella, R.L., Silverstein, K.A., Voytas, D.F. and Dehm, S.M. (2013) 'TALEN-engineered AR gene rearrangements reveal endocrine uncoupling of androgen receptor in prostate cancer', *Proc Natl Acad Sci U S A*, 110(43), pp. 17492-7.

O'Neill, D., Jones, D., Wade, M., Grey, J., Nakjang, S., Guo, W., Cork, D., Davies, B.R., Wedge, S.R., Robson, C.N. and Gaughan, L. (2015) 'Development and exploitation of a novel mutant androgen receptor modelling strategy to identify new targets for advanced prostate cancer therapy', *Oncotarget*.

Owens, J.B., Urschitz, J., Stoytchev, I., Dang, N.C., Stoytcheva, Z., Belcaid, M., Maragathavally, K.J., Coates, C.J., Segal, D.J. and Moisyadi, S. (2012) 'Chimeric piggyBac transposases for genomic targeting in human cells', *Nucleic Acids Res*, 40(14), pp. 6978-91.

Paquet, D., Kwart, D., Chen, A., Sproul, A., Jacob, S., Teo, S., Olsen, K.M., Gregg, A., Noggle, S. and Tessier-Lavigne, M. (2016) 'Efficient introduction of specific homozygous and heterozygous mutations using CRISPR/Cas9', *Nature*, 533(7601), pp. 125-9.

Paul, R. and Breul, J. (2000) 'Antiandrogen withdrawal syndrome associated with prostate cancer therapies: incidence and clinical significance', *Drug Saf*, 23(5), pp. 381-90.

Pawar, A., Gollavilli, P.N., Wang, S. and Asangani, I.A. (2018) 'Resistance to BET Inhibitor Leads to Alternative Therapeutic Vulnerabilities in Castration-Resistant Prostate Cancer', *Cell Rep*, 22(9), pp. 2236-2245.

Perez-Pinera, P., Kocak, D.D., Vockley, C.M., Adler, A.F., Kabadi, A.M., Polstein, L.R., Thakore, P.I., Glass, K.A., Ousterout, D.G., Leong, K.W., Guilak, F., Crawford, G.E., Reddy, T.E. and Gersbach,

C.A. (2013) 'RNA-guided gene activation by CRISPR-Cas9-based transcription factors', *Nat Methods*, 10(10), pp. 973-6.

Perez-Salvia, M. and Esteller, M. (2017) 'Bromodomain inhibitors and cancer therapy: From structures to applications', *Epigenetics*, 12(5), pp. 323-339.

Perez, E.E., Wang, J., Miller, J.C., Jouvenot, Y., Kim, K.A., Liu, O., Wang, N., Lee, G., Bartsevich, V.V., Lee, Y.L., Guschin, D.Y., Rupniewski, I., Waite, A.J., Carpenito, C., Carroll, R.G., Orange, J.S., Urnov, F.D., Rebar, E.J., Ando, D., Gregory, P.D., Riley, J.L., Holmes, M.C. and June, C.H. (2008) 'Establishment of HIV-1 resistance in CD4+ T cells by genome editing using zinc-finger nucleases', *Nat Biotechnol*, 26(7), pp. 808-16.

Petrylak, D.P. (2013) 'Current state of castration-resistant prostate cancer', *Am J Manag Care*, 19(18 Suppl), pp. s358-65.

Polkinghorn, W.R., Parker, J.S., Lee, M.X., Kass, E.M., Spratt, D.E., Iaquinta, P.J., Arora, V.K., Yen, W.F., Cai, L., Zheng, D., Carver, B.S., Chen, Y., Watson, P.A., Shah, N.P., Fujisawa, S., Goglia, A.G., Gopalan, A., Hieronymus, H., Wongvipat, J., Scardino, P.T., Zelefsky, M.J., Jasin, M., Chaudhuri, J., Powell, S.N. and Sawyers, C.L. (2013) 'Androgen receptor signaling regulates DNA repair in prostate cancers', *Cancer Discov*, 3(11), pp. 1245-53.

Poujol, N., Wurtz, J.M., Tahiri, B., Lumbroso, S., Nicolas, J.C., Moras, D. and Sultan, C. (2000) 'Specific recognition of androgens by their nuclear receptor. A structure-function study', *J Biol Chem*, 275(31), pp. 24022-31.

Prykhozhij, S.V., Fuller, C., Steele, S.L., Veinotte, C.J., Razaghi, B., McMaster, C., Shlien, A., Malkin, D. and Berman, J.N. (2017) 'Successful optimization of CRISPR/Cas9-mediated defined point mutation knock-in using allele-specific PCR assays in zebrafish', *bioRxiv*.

Prykhozhij, S.V., Fuller, C., Steele, S.L., Veinotte, C.J., Razaghi, B., Robitaille, J.M., McMaster, C.R., Shlien, A., Malkin, D. and Berman, J.N. (2018) 'Optimized knock-in of point mutations in zebrafish using CRISPR/Cas9', *Nucleic Acids Res*.

Raina, K., Lu, J., Qian, Y., Altieri, M., Gordon, D., Rossi, A.M., Wang, J., Chen, X., Dong, H., Siu, K., Winkler, J.D., Crew, A.P., Crews, C.M. and Coleman, K.G. (2016) 'PROTAC-induced BET protein degradation as a therapy for castration-resistant prostate cancer', *Proc Natl Acad Sci U S A*, 113(26), pp. 7124-9.

Ramlee, M.K., Yan, T., Cheung, A.M.S., Chuah, C.T.H. and Li, S. (2015) 'High-throughput genotyping of CRISPR/Cas9-mediated mutants using fluorescent PCR-capillary gel electrophoresis', *Scientific Reports*, 5, p. 15587.

Ran, F.A., Hsu, P.D., Lin, C.Y., Gootenberg, J.S., Konermann, S., Trevino, A.E., Scott, D.A., Inoue, A., Matoba, S., Zhang, Y. and Zhang, F. (2013) 'Double nicking by RNA-guided CRISPR Cas9 for enhanced genome editing specificity', *Cell*, 154(6), pp. 1380-9.

Ren, X., Sun, J., Housden, B.E., Hu, Y., Roesel, C., Lin, S., Liu, L.P., Yang, Z., Mao, D., Sun, L., Wu, Q., Ji, J.Y., Xi, J., Mohr, S.E., Xu, J., Perrimon, N. and Ni, J.Q. (2013) 'Optimized gene editing technology for Drosophila melanogaster using germ line-specific Cas9', *Proc Natl Acad Sci U S A*, 110(47), pp. 19012-7.

Richardson, C.D., Ray, G.J., DeWitt, M.A., Curie, G.L. and Corn, J.E. (2016) 'Enhancing homology-directed genome editing by catalytically active and inactive CRISPR-Cas9 using asymmetric donor DNA', *Nat Biotechnol*, 34(3), pp. 339-44.

Robert, F., Barbeau, M., Ethier, S., Dostie, J. and Pelletier, J. (2015) 'Pharmacological inhibition of DNA-PK stimulates Cas9-mediated genome editing', *Genome Med*, 7, p. 93.

Rodriguez-Vida, A., Bianchini, D., Van Hemelrijck, M., Hughes, S., Malik, Z., Powles, T., Bahl, A., Rudman, S., Payne, H., de Bono, J. and Chowdhury, S. (2015) 'Is there an antiandrogen withdrawal syndrome with enzalutamide?', *BJU Int*, 115(3), pp. 373-80.

Romanel, A., Gasi Tandefelt, D., Conteduca, V., Jayaram, A., Casiraghi, N., Wetterskog, D., Salvi, S., Amadori, D., Zafeiriou, Z., Rescigno, P., Bianchini, D., Gurioli, G., Casadio, V., Carreira, S., Goodall, J., Wingate, A., Ferraldeschi, R., Tunariu, N., Flohr, P., De Giorgi, U., de Bono, J.S., Demichelis, F. and Attard, G. (2015) 'Plasma AR and abiraterone-resistant prostate cancer', *Sci Transl Med*, 7(312), p. 312re10.

Ruggero, K., Farran-Matas, S., Martinez-Tebar, A. and Aytes, A. (2018) 'Epigenetic Regulation in Prostate Cancer Progression', *Curr Mol Biol Rep*, 4(2), pp. 101-115.

Sanchez, R. and Zhou, M.M. (2009) 'The role of human bromodomains in chromatin biology and gene transcription', *Curr Opin Drug Discov Devel*, 12(5), pp. 659-65.

Sanjana, N.E., Cong, L., Zhou, Y., Cunniff, M.M., Feng, G. and Zhang, F. (2012) 'A transcription activator-like effector toolbox for genome engineering', *Nat Protoc*, 7(1), pp. 171-92.

Santer, F.R., Hoschele, P.P., Oh, S.J., Erb, H.H., Bouchal, J., Cavarretta, I.T., Parson, W., Meyers, D.J., Cole, P.A. and Culig, Z. (2011) 'Inhibition of the acetyltransferases p300 and CBP reveals a targetable function for p300 in the survival and invasion pathways of prostate cancer cell lines', *Mol Cancer Ther*, 10(9), pp. 1644-55.

Sapranauskas, R., Gasiunas, G., Fremaux, C., Barrangou, R., Horvath, P. and Siksnys, V. (2011) 'The Streptococcus thermophilus CRISPR/Cas system provides immunity in Escherichia coli', *Nucleic Acids Res*, 39(21), pp. 9275-82.

Sartor, A.O., Hricak, H., Wheeler, T.M., Coleman, J., Penson, D.F., Carroll, P.R., Rubin, M.A. and Scardino, P.T. (2008) 'Evaluating localized prostate cancer and identifying candidates for focal therapy', *Urology*, 72(6 Suppl), pp. S12-24.

Schornack, S., Meyer, A., Romer, P., Jordan, T. and Lahaye, T. (2006) 'Gene-for-gene-mediated recognition of nuclear-targeted AvrBs3-like bacterial effector proteins', *J Plant Physiol*, 163(3), pp. 256-72.

Schumann, K., Lin, S., Boyer, E., Simeonov, D.R., Subramaniam, M., Gate, R.E., Haliburton, G.E., Ye, C.J., Bluestone, J.A., Doudna, J.A. and Marson, A. (2015) 'Generation of knock-in primary human T cells using Cas9 ribonucleoproteins', *Proceedings of the National Academy of Sciences*, 112(33), pp. 10437-10442.

Schwank, G., Koo, B.K., Sasselli, V., Dekkers, J.F., Heo, I., Demircan, T., Sasaki, N., Boymans, S., Cuppen, E., van der Ent, C.K., Nieuwenhuis, E.E., Beekman, J.M. and Clevers, H. (2013) 'Functional repair of CFTR by CRISPR/Cas9 in intestinal stem cell organoids of cystic fibrosis patients', *Cell Stem Cell*, 13(6), pp. 653-8.

Schweizer, M.T. and Antonarakis, E.S. (2012) 'Abiraterone and other novel androgen-directed strategies for the treatment of prostate cancer: a new era of hormonal therapies is born', *Therapeutic Advances in Urology*, 4(4), pp. 167-178.

Sebo, Z.L., Lee, H.B., Peng, Y. and Guo, Y. (2014) 'A simplified and efficient germline-specific CRISPR/Cas9 system for Drosophila genomic engineering', *Fly (Austin)*, 8(1), pp. 52-7.

Segura, M.F., Fontanals-Cirera, B., Gaziel-Sovran, A., Guijarro, M.V., Hanniford, D., Zhang, G., Gonzalez-Gomez, P., Morante, M., Jubierre, L., Zhang, W., Darvishian, F., Ohlmeyer, M., Osman,

I., Zhou, M.M. and Hernando, E. (2013) 'BRD4 sustains melanoma proliferation and represents a new target for epigenetic therapy', *Cancer Res*, 73(20), pp. 6264-76.

Semenas, J., Dizeyi, N. and Persson, J.L. (2013) 'Enzalutamide as a second generation antiandrogen for treatment of advanced prostate cancer', *Drug Des Devel Ther*, 7, pp. 875-81.

Shalem, O., Sanjana, N.E., Hartenian, E., Shi, X., Scott, D.A., Mikkelson, T., Heckl, D., Ebert, B.L., Root, D.E., Doench, J.G. and Zhang, F. (2014) 'Genome-scale CRISPR-Cas9 knockout screening in human cells', *Science*, 343(6166), pp. 84-87.

Shimamura, T., Chen, Z., Soucheray, M., Carretero, J., Kikuchi, E., Tchaicha, J.H., Gao, Y., Cheng, K.A., Cohoon, T.J., Qi, J., Akbay, E., Kimmelman, A.C., Kung, A.L., Bradner, J.E. and Wong, K.K. (2013) 'Efficacy of BET bromodomain inhibition in Kras-mutant non-small cell lung cancer', *Clin Cancer Res*, 19(22), pp. 6183-92.

Shmakov, S., Abudayyeh, O.O., Makarova, K.S., Wolf, Y.I., Gootenberg, J.S., Semenova, E., Minakhin, L., Joung, J., Konermann, S., Severinov, K., Zhang, F. and Koonin, E.V. (2015) 'Discovery and Functional Characterization of Diverse Class 2 CRISPR-Cas Systems', *Mol Cell*, 60(3), pp. 385-97.

Shtraizent, N., Matsui, H., Polotskaia, A. and Bargonetti, J. (2015) 'Hot Spot Mutation in TP53 (R248Q) Causes Oncogenic Gain-of-Function Phenotypes in a Breast Cancer Cell Line Derived from an African American patient', *Int J Environ Res Public Health*, 13(1), p. ijerph13010022.

Silberstein, J.L., Pal, S.K., Lewis, B. and Sartor, O. (2013) 'Current clinical challenges in prostate cancer', *Transl Androl Urol*, 2(3), pp. 122-36.

Song, L.N., Coghlan, M. and Gelmann, E.P. (2004) 'Antiandrogen effects of mifepristone on coactivator and corepressor interactions with the androgen receptor', *Mol Endocrinol*, 18(1), pp. 70-85.

Sramkoski, R.M., Pretlow, T.G., 2nd, Giaconia, J.M., Pretlow, T.P., Schwartz, S., Sy, M.S., Marengo, S.R., Rhim, J.S., Zhang, D. and Jacobberger, J.W. (1999) 'A new human prostate carcinoma cell line, 22Rv1', *In Vitro Cell Dev Biol Anim*, 35(7), pp. 403-9.

Srivastava, M., Nambiar, M., Sharma, S., Karki, S.S., Goldsmith, G., Hegde, M., Kumar, S., Pandey, M., Singh, R.K., Ray, P., Natarajan, R., Kelkar, M., De, A., Choudhary, B. and Raghavan, S.C. (2012)

'An inhibitor of nonhomologous end-joining abrogates double-strand break repair and impedes cancer progression', *Cell*, 151(7), pp. 1474-87.

Steketee, K., Timmerman, L., Ziel-van der Made, A.C., Doesburg, P., Brinkmann, A.O. and Trapman, J. (2002) 'Broadened ligand responsiveness of androgen receptor mutants obtained by random amino acid substitution of H874 and mutation hot spot T877 in prostate cancer', *Int J Cancer*, 100(3), pp. 309-17.

Sung, Y.H., Jin, Y., Kim, S. and Lee, H.W. (2014) 'Generation of knockout mice using engineered nucleases', *Methods*, 69(1), pp. 85-93.

Suzman, D.L. and Antonarakis, E.S. (2014) 'Castration-resistant prostate cancer: latest evidence and therapeutic implications', *Ther Adv Med Oncol*, 6(4), pp. 167-79.

Suzuki, H., Akakura, K., Komiya, A., Aida, S., Akimoto, S. and Shimazaki, J. (1996) 'Codon 877 mutation in the androgen receptor gene in advanced prostate cancer: relation to antiandrogen withdrawal syndrome', *Prostate*, 29(3), pp. 153-8.

Takayama, K. and Inoue, S. (2013) 'Transcriptional network of androgen receptor in prostate cancer progression', *Int J Urol*, 20(8), pp. 756-68.

Tan, J., Sharief, Y., Hamil, K.G., Gregory, C.W., Zang, D.Y., Sar, M., Gumerlock, P.H., deVere White, R.W., Pretlow, T.G., Harris, S.E., Wilson, E.M., Mohler, J.L. and French, F.S. (1997) 'Dehydroepiandrosterone activates mutant androgen receptors expressed in the androgen-dependent human prostate cancer xenograft CWR22 and LNCaP cells', *Mol Endocrinol*, 11(4), pp. 450-9.

Tan, M.H., Li, J., Xu, H.E., Melcher, K. and Yong, E.L. (2015a) 'Androgen receptor: structure, role in prostate cancer and drug discovery', *Acta Pharmacol Sin*, 36(1), pp. 3-23.

Tan, M.H.E., Li, J., Xu, H.E., Melcher, K. and Yong, E.-l. (2015b) 'Androgen receptor: structure, role in prostate cancer and drug discovery', *Acta Pharmacol Sin*, 36(1), pp. 3-23.

Taniguchi, Y. (2016) 'The Bromodomain and Extra-Terminal Domain (BET) Family: Functional Anatomy of BET Paralogous Proteins', *Int J Mol Sci*, 17(11).

Taplin, M.E., Bubley, G.J., Ko, Y.J., Small, E.J., Upton, M., Rajeshkumar, B. and Balk, S.P. (1999) 'Selection for androgen receptor mutations in prostate cancers treated with androgen antagonist', *Cancer Res*, 59(11), pp. 2511-5.

Tepper, C.G., Boucher, D.L., Ryan, P.E., Ma, A.H., Xia, L., Lee, L.F., Pretlow, T.G. and Kung, H.J. (2002) 'Characterization of a novel androgen receptor mutation in a relapsed CWR22 prostate cancer xenograft and cell line', *Cancer Res*, 62(22), pp. 6606-14.

Thomas, P. and Smart, T.G. (2005) 'HEK293 cell line: a vehicle for the expression of recombinant proteins', *J Pharmacol Toxicol Methods*, 51(3), pp. 187-200.

Tomkinson, A.E., Howes, T.R. and Wiest, N.E. (2013) 'DNA ligases as therapeutic targets', *Transl Cancer Res*, 2(3).

Torres, R., Martin, M.C., Garcia, A., Cigudosa, J.C., Ramirez, J.C. and Rodriguez-Perales, S. (2014) 'Engineering human tumour-associated chromosomal translocations with the RNA-guided CRISPR-Cas9 system', *Nat Commun*, 5, p. 3964.

Townsend, J.A., Wright, D.A., Winfrey, R.J., Fu, F., Maeder, M.L., Joung, J.K. and Voytas, D.F. (2009) 'High-frequency modification of plant genes using engineered zinc-finger nucleases', *Nature*, 459(7245), pp. 442-5.

Tran, C., Ouk, S., Clegg, N.J., Chen, Y., Watson, P.A., Arora, V., Wongvipat, J., Smith-Jones, P.M., Yoo, D., Kwon, A., Wasielewska, T., Welsbie, D., Chen, C.D., Higano, C.S., Beer, T.M., Hung, D.T., Scher, H.I., Jung, M.E. and Sawyers, C.L. (2009) 'Development of a second-generation antiandrogen for treatment of advanced prostate cancer', *Science*, 324(5928), pp. 787-90.

Tsao, C.K., Galsky, M.D., Small, A.C., Yee, T. and Oh, W.K. (2012) 'Targeting the androgen receptor signalling axis in castration-resistant prostate cancer (CRPC)', *BJU Int*, 110(11), pp. 1580-8.

Urbanucci, A., Barfeld, S.J., Kytola, V., Itkonen, H.M., Coleman, I.M., Vodak, D., Sjoblom, L., Sheng, X., Tolonen, T., Minner, S., Burdelski, C., Kivinummi, K.K., Kohvakka, A., Kregel, S., Takhar, M., Alshalalfa, M., Davicioni, E., Erho, N., Lloyd, P., Karnes, R.J., Ross, A.E., Schaeffer, E.M., Vander Griend, D.J., Knapp, S., Corey, E., Feng, F.Y., Nelson, P.S., Saatcioglu, F., Knudsen, K.E., Tammela, T.L.J., Sauter, G., Schlomm, T., Nykter, M., Visakorpi, T. and Mills, I.G. (2017) 'Androgen Receptor Deregulation Drives Bromodomain-Mediated Chromatin Alterations in Prostate Cancer', *Cell Rep*, 19(10), pp. 2045-2059.

Valetdinova, K.R., Medvedev, S.P. and Zakian, S.M. (2015) 'Model systems of motor neuron diseases as a platform for studying pathogenic mechanisms and searching for therapeutic agents', *Acta Naturae*, 7(1), pp. 19-36.

van de Wijngaart, D.J., Dubbink, H.J., van Royen, M.E., Trapman, J. and Jenster, G. (2012) 'Androgen receptor coregulators: recruitment via the coactivator binding groove', *Mol Cell Endocrinol*, 352(1-2), pp. 57-69.

Vartak, S.V. and Raghavan, S.C. (2015) 'Inhibition of nonhomologous end joining to increase the specificity of CRISPR/Cas9 genome editing', *FEBS J*, 282(22), pp. 4289-94.

Vassena, R., Heindryckx, B., Peco, R., Pennings, G., Raya, A., Sermon, K. and Veiga, A. (2016) 'Genome engineering through CRISPR/Cas9 technology in the human germline and pluripotent stem cells', *Hum Reprod Update*, 22(4), pp. 411-9.

Vasudevamurthy, A.K., Ledet, E., Garvey, C., Lewis, B.E. and Sartor, O. (2017) 'Estrogen-Mediated Activation of H875Y Androgen Receptor Mutation in a Prostate Cancer Patient', *Clin Genitourin Cancer*, 15(1), pp. e111-e113.

Veldscholte, J., Ris-Stalpers, C., Kuiper, G.G., Jenster, G., Berrevoets, C., Claassen, E., van Rooij, H.C., Trapman, J., Brinkmann, A.O. and Mulder, E. (1990) 'A mutation in the ligand binding domain of the androgen receptor of human LNCaP cells affects steroid binding characteristics and response to anti-androgens', *Biochem Biophys Res Commun*, 173(2), pp. 534-40.

Wadosky, K.M. and Koochekpour, S. (2016) 'Molecular mechanisms underlying resistance to androgen deprivation therapy in prostate cancer', *Oncotarget*, 7(39), pp. 64447-64470.

Waltering, K.K., Helenius, M.A., Sahu, B., Manni, V., Linja, M.J., Janne, O.A. and Visakorpi, T. (2009) 'Increased expression of androgen receptor sensitizes prostate cancer cells to low levels of androgens', *Cancer Res*, 69(20), pp. 8141-9.

Wang, H., Yang, H., Shivalila, C.S., Dawlaty, M.M., Cheng, A.W., Zhang, F. and Jaenisch, R. (2013) 'One-step generation of mice carrying mutations in multiple genes by CRISPR/Cas-mediated genome engineering', *Cell*, 153(4), pp. 910-8.

Wang, K., Tang, X., Liu, Y., Xie, Z., Zou, X., Li, M., Yuan, H., Ouyang, H., Jiao, H. and Pang, D. (2016) 'Efficient Generation of Orthologous Point Mutations in Pigs via CRISPR-assisted ssODN-mediated Homology-directed Repair', *Mol Ther Nucleic Acids*, 5(11), p. e396.

Wang, T., Wei, J.J., Sabatini, D.M. and Lander, E.S. (2014) 'Genetic screens in human cells using the CRISPR-Cas9 system', *Science*, 343(6166), pp. 80-4.

Watson, P.A., Chen, Y.F., Balbas, M.D., Wongvipat, J., Socci, N.D., Viale, A., Kim, K. and Sawyers, C.L. (2010) 'Constitutively active androgen receptor splice variants expressed in castration-resistant prostate cancer require full-length androgen receptor', *Proc Natl Acad Sci U S A*, 107(39), pp. 16759-65.

Wiench, M., Miranda, T.B. and Hager, G.L. (2011) 'Control of nuclear receptor function by local chromatin structure', *Febs j*, 278(13), pp. 2211-30.

Wright, A.V., Nunez, J.K. and Doudna, J.A. (2016) 'Biology and Applications of CRISPR Systems: Harnessing Nature's Toolbox for Genome Engineering', *Cell*, 164(1-2), pp. 29-44.

Wu, X., Kriz, A.J. and Sharp, P.A. (2014) 'Target specificity of the CRISPR-Cas9 system', *Quant Biol*, 2(2), pp. 59-70.

Wyatt, A.W. and Gleave, M.E. (2015) 'Targeting the adaptive molecular landscape of castration-resistant prostate cancer', *EMBO Mol Med*, 7(7), pp. 878-94.

Xiao, A., Wang, Z., Hu, Y., Wu, Y., Luo, Z., Yang, Z., Zu, Y., Li, W., Huang, P., Tong, X., Zhu, Z., Lin, S. and Zhang, B. (2013) 'Chromosomal deletions and inversions mediated by TALENs and CRISPR/Cas in zebrafish', *Nucleic Acids Res*, 41(14), p. e141.

Xie, N., Cheng, H., Lin, D., Liu, L., Yang, O., Jia, L., Fazli, L., Gleave, M.E., Wang, Y., Rennie, P. and Dong, X. (2015) 'The expression of glucocorticoid receptor is negatively regulated by active androgen receptor signaling in prostate tumors', *Int J Cancer*, 136(4), pp. E27-38.

Xue, W., Chen, S., Yin, H., Tammela, T., Papagiannakopoulos, T., Joshi, N.S., Cai, W., Yang, G., Bronson, R., Crowley, D.G., Zhang, F., Anderson, D.G., Sharp, P.A. and Jacks, T. (2014) 'CRISPR-mediated direct mutation of cancer genes in the mouse liver', *Nature*, 514(7522), pp. 380-4.

Yang, H., Wang, H., Shivalila, C.S., Cheng, A.W., Shi, L. and Jaenisch, R. (2013a) 'One-step generation of mice carrying reporter and conditional alleles by CRISPR/Cas-mediated genome engineering', *Cell*, 154(6), pp. 1370-9.

Yang, L., Guell, M., Byrne, S., Yang, J.L., De Los Angeles, A., Mali, P., Aach, J., Kim-Kiselak, C., Briggs, A.W., Rios, X., Huang, P.Y., Daley, G. and Church, G. (2013b) 'Optimization of scarless human stem cell genome editing', *Nucleic Acids Res*, 41(19), pp. 9049-61.

Yang, Y.A. and Yu, J. (2015) 'Current perspectives on FOXA1 regulation of androgen receptor signaling and prostate cancer', *Genes Dis*, 2(2), pp. 144-151.

Yang, Z., Yik, J.H., Chen, R., He, N., Jang, M.K., Ozato, K. and Zhou, Q. (2005) 'Recruitment of P-TEFb for stimulation of transcriptional elongation by the bromodomain protein Brd4', *Mol Cell*, 19(4), pp. 535-45.

Yap, T.A., Zivi, A., Omlin, A. and de Bono, J.S. (2011) 'The changing therapeutic landscape of castration-resistant prostate cancer', *Nature Reviews Clinical Oncology*, 8, p. 597.

Yoshida, T., Kinoshita, H., Segawa, T., Nakamura, E., Inoue, T., Shimizu, Y., Kamoto, T. and Ogawa, O. (2005) 'Antiandrogen bicalutamide promotes tumor growth in a novel androgen-dependent prostate cancer xenograft model derived from a bicalutamide-treated patient', *Cancer Res*, 65(21), pp. 9611-6.

Yoshimi, K., Kunihiro, Y., Kaneko, T., Nagahora, H., Voigt, B. and Mashimo, T. (2016) 'ssODN-mediated knock-in with CRISPR-Cas for large genomic regions in zygotes', *Nat Commun*, 7, p. 10431.

Yu, C., Liu, Y., Ma, T., Liu, K., Xu, S., Zhang, Y., Liu, H., La Russa, M., Xie, M., Ding, S. and Qi, L.S. (2015) 'Small molecules enhance CRISPR genome editing in pluripotent stem cells', *Cell Stem Cell*, 16(2), pp. 142-7.

Yu, Z., Ren, M., Wang, Z., Zhang, B., Rong, Y.S., Jiao, R. and Gao, G. (2013) 'Highly efficient genome modifications mediated by CRISPR/Cas9 in Drosophila', *Genetics*, 195(1), pp. 289-91.

Zhan, T., Rindtorff, N., Betge, J., Ebert, M.P. and Boutros, M. (2018) 'CRISPR/Cas9 for cancer research and therapy', *Semin Cancer Biol*.

Zhang, J.P., Li, X.L., Li, G.H., Chen, W., Arakaki, C., Botimer, G.D., Baylink, D., Zhang, L., Wen, W., Fu, Y.W., Xu, J., Chun, N., Yuan, W., Cheng, T. and Zhang, X.B. (2017a) 'Efficient precise knockin with a double cut HDR donor after CRISPR/Cas9-mediated double-stranded DNA cleavage', *Genome Biol*, 18(1), p. 35.

Zhang, L., Wang, P., Feng, Q., Wang, N., Chen, Z., Huang, Y., Zheng, W. and Jiang, X. (2017b) 'Lipid nanoparticle-mediated efficient delivery of CRISPR/Cas9 for tumor therapy', *Npg Asia Materials*, 9, p. e441.

Zhang, X., Morrissey, C., Sun, S., Ketchandji, M., Nelson, P.S., True, L.D., Vakar-Lopez, F., Vessella, R.L. and Plymate, S.R. (2011) 'Androgen receptor variants occur frequently in castration resistant prostate cancer metastases', *PLoS One*, 6(11), p. e27970.

Zhau, H.Y., Chang, S.M., Chen, B.Q., Wang, Y., Zhang, H., Kao, C., Sang, Q.A., Pathak, S.J. and Chung, L.W. (1996) 'Androgen-repressed phenotype in human prostate cancer', *Proc Natl Acad Sci U S A*, 93(26), pp. 15152-7.

Zhong, J., Ding, L., Bohrer, L.R., Pan, Y., Liu, P., Zhang, J., Sebo, T.J., Karnes, R.J., Tindall, D.J., van Deursen, J. and Huang, H. (2014) 'p300 acetyltransferase regulates androgen receptor degradation and PTEN-deficient prostate tumorigenesis', *Cancer Res*, 74(6), pp. 1870-1880.

Zhu, X., Xu, Y., Yu, S., Lu, L., Ding, M., Cheng, J., Song, G., Gao, X., Yao, L., Fan, D., Meng, S., Zhang, X., Hu, S. and Tian, Y. (2014) 'An efficient genotyping method for genome-modified animals and human cells generated with CRISPR/Cas9 system', *Sci Rep*, 4, p. 6420.

Zuber, V., Bettella, F., Witoelar, A., Andreassen, O.A., Mills, I.G. and Urbanucci, A. (2017) 'Bromodomain protein 4 discriminates tissue-specific super-enhancers containing disease-specific susceptibility loci in prostate and breast cancer', *BMC Genomics*, 18(1), p. 270.